ABSTRACT

CORBIN, NICOLE A. Northern California's Central Valley Spatial Precipitation Patterns Associated with Atmospheric Rivers Under Different Environmental Conditions. (Under the direction of Sandra Yuter.)

The supply of fresh water to California is dependent on infrequent, but long-lasting storms. These storms are associated with atmospheric rivers, which are narrow plumes of strong horizontal water vapor flux. The details of where and how much precipitation this region receives are important for short-term flood forecasting and long-term water resource management. In this study, radar-derived precipitation frequency is used to characterize the spatial distribution and variability of precipitation from 64 high-impact events in the Central Valley of northern California and the interior mountain slopes between 2005 and 2010.

Atmospheric river events produce a range of spatial patterns of precipitation frequency from event to event. A composite of all events shows three locations in the radar domain that commonly experience locally higher precipitation frequencies: the lee slopes of the Coastal Mountains, the northern end of the Central Valley, and the windward slopes of the northern Sierra Nevada Mountains.

Events with southerly winds at the onset of atmospheric river conditions produce greater values of precipitation frequency throughout the radar domain compared to westerly events. The change of precipitation frequency with elevation shows little difference between southerly and westerly events. We also document a number of covariations among wind direction at the onset of atmospheric river conditions and other environmental variables. Southerly wind events are associated with longer durations of atmospheric river conditions, higher altitude Sierra barrier jets over the valley, larger magnitudes of upslope wind (from 230 degrees) and storm total IWV flux compared to atmospheric river conditions with westerly winds. Longer storm durations, stronger upslope flow, and high integrated water vapor flux would each independently produce greater values of precipitation frequency, though the slight co-variation among these environmental variables makes the attribution of precipitation frequency patterns to solely one variable more difficult.

Our radar-derived precipitation frequency change with altitude on the Sierra Nevada slopes indicates an increase of precipitation frequency from the valley to 1 km MSL, and

decreasing precipitation frequency above 1 km MSL. This generally concurs with a linear model average from Lundquist et al. (2010).

Northern California's Central Valley Spatial Precipitation Patterns Associated with Atmospheric Rivers Under Different Environmental Conditions

by
Nicole A. Corbin

A thesis submitted to the Graduate Faculty of
North Carolina State University
in partial fulfillment of the
requirements for the degree of
Master of Science

Marine, Earth, and Atmospheric Sciences

Raleigh, North Carolina
2016

APPROVED BY:

_____	_____
Sandra Yuter Committee Chair	David Kingsmill
_____	
Matthew Parker	

ACKNOWLEDGMENTS

I would like to acknowledge my adviser, Dr. Sandra Yuter, for her continued support and guidance, and for shaping me into a real scientist. I would also like to thank my lab mates past and present for their technical assistance and for being genuinely great people to work with. I thank Dr. David Kingsmill for his years of guidance on this project from day one, and Dr. Matthew Parker, for providing invaluable insight. I also acknowledge my many friends that have supported me throughout this entire process. Last, I would like to thank the many coffee shops in the Raleigh area, especially Cup A Joe Mission Valley, for providing me with space to work and much needed caffeine.

TABLE OF CONTENTS

LIST OF TABLES

LIST OF FIGURES

CHAPTER I - Introduction

California is a large, populous state with high demands on fresh water for agriculture, human consumption, and hydroelectricity. Much of California's annual precipitation comes in a few multi-day events where several centimeters or more of rainfall a day can increase the risk for flooding (Dettinger et al. 2011). Sacramento, located in the north Central Valley, is one of the most at-risk urban cities in the United States for devastating flooding, second only to New Orleans (Lund 2007). Better information on where high precipitation accumulations are likely to occur within and among the watersheds in the northern Central Valley adjacent to Sacramento is important for short-term flood warnings as well as long-term water resource planning. Precipitation falling over the low elevations of the Central Valley of California poses an immediate risk of contributing to potential flooding as compared to the longer latency between precipitation falling on high elevations and when it reaches the valley.

Previous work has shown that most west coast U.S. storms that produce heavy rainfall are associated with an atmospheric river (Ralph et al. 2006; Lund 2007; Smith et al. 2010; Yuter et al. 2011; Ralph et al. 2013). An atmospheric river is defined as a narrow (<1000 km width) filament of contiguous water vapor flux associated with the pre-frontal low level jet (Zhu and Newell 1998, Ralph et al. 2004). The atmospheric river often lies within the warm conveyor belt near the leading edge of the cold front and within the lowest 3-4 km of the atmosphere (Ralph et al. 2004, 2005). Usually, the plume of enhanced water vapor flux is primarily the result of local moisture convergence (Bao et al. 2006). In some atmospheric river cases, there is net transport of water vapor from the tropics to the coast of California (Lackmann and Gyakum 1999; Bao et al. 2006). Atmospheric rivers account for 40% of California's annual precipitation (Dettinger et al. 2011).

Neiman et al. (2002) concluded that the component of the wind directed normal to the Coastal Mountains of California at 1 km above mean sea level produced the highest correlation with rain rates at higher terrain downstream of the coastal profilers. Ralph et al. (2013) developed a set of criteria for forecasting the top 10% of precipitation events in

coastal California consisting of a duration of 32 hours or longer of conditions with IWV > 2 cm and integrated water vapor flux > 15 cm m s^{-1}.

There is a close relationship among the stage of the cyclone, the frontal orientations, and the direction of the wind at the coast at the onset of atmospheric river landfall. We document variability of the synoptic setting in terms of both composite maps and analyses for individual storms. The Norwegian cyclone model (Bjerknes and Solberg 1922) depicts the evolution of a cyclone from development to maturation. In the developing stage (stage 1), a west-east oriented cold front extends to the west from the low pressure center and a west-east oriented warm front extends to the east from the low pressure center. Winds in the warm sector (east of the cold front and west of the warm front) are predominantly westerly. As the cyclone matures and the pressure minimum deepens (stages 2 and 3), the cold front progresses eastward consistent with the westerly winds behind it. This begins a "wrapping-up" of the isotherms around the central low. In the mature stage (stage 4), the warm sector narrows and an occluded front forms near the low pressure center (Scultz and Vaughn 2011). At the terminus of the occluded front, the north-south oriented cold front and northwest-southeast oriented warm front branch off, leading to a warm sector that is removed from the central low pressure center (Fig. 1.1).

Based on eight years of satellite data and reanalysis output, Neiman et al. (2008) found seasonal contrasts in atmospheric river geometries over the ocean and the associated precipitation in the western United States. Since stronger winds are more likely in December, January, and February as compared to June, July, and August, winter atmospheric rivers are likely to have higher integrated water vapor transport and higher precipitation accumulation. Seasonal composites derived from reanalysis moisture, wind and pressure fields indicated that winter atmospheric rivers are typically located within warm, moist pre-cold frontal air mass (Neiman et al. 2008). In summer, the composites showed that the horizontal moisture transport was weaker and located in the post-cold frontal air mass (Neiman et al. 2008).

The terrain-parallel southerly barrier jet at the base of the windward slopes of the Sierra Nevada mountains (Parish 1982; Marwitz 1983; 1986; 1987; Reynolds and Dennis 1986) forms in a stable layer and redistributes low-level moisture within the northern Central

Valley (Galewsky and Sobel 2005; Reeves and Lin 2007; Reeves et al. 2008, Smith et al. 2010). The atmospheric river glides up and over the stable, blocked flow at the base of terrain, in effect shifting the western edge of the orographic enhancement of precipitation from the foothills into the valley (Kingsmill et al. 2013, Neiman et al. 2013).

We build and expand upon previous studies by examining the variability of the spatial distribution of precipitation within the northern Central Valley for 64 atmospheric river events from March 2005 to April 2010. The same events were analyzed in Ralph et al. (2013) but they focused on gauge-estimated precipitation in the Coastal Mountain range, whereas this study will quantify precipitation frequency from weather radars. Orographic precipitation analyses using regional radar data for the Alps and the Cascades have documented that the spatial pattern of precipitation accumulation over terrain is primarily controlled by wind direction and the wind speed with other variables such has stability and the height of the freezing level having secondary roles (Panziera and Germann 2010; Yuter et al. 2011). While idealized model studies and observational case studies have demonstrated the importance of blocked versus unblocked flow in orographic precipitation patterns (Colle 2004; Medina et al. 2007), real-world studies utilizing large sample sizes of orographic storms demonstrate that neutral-to-stable conditions are the norm (Panziera and Germann 2010; Yuter et al. 2011). The occasional storm with unstable low-level flow will yield a markedly different spatial pattern of precipitation, however this occurs infrequently enough to not change long-term precipitation patterns in many regions. Based on this precedent, we first categorize storms by wind direction and then examine the co-variation and roles of other environmental variables. We examine both the frequency of near surface precipitation and the change in the frequency with altitude as both relevant for nowcasting and forecasting regional precipitation.

The windward slopes of the Sierra Nevada contain multiple reservoirs and the precipitation that falls over the Sierra as rain and snow is a primary fresh water resource for California (Jeton et al. 1996). Several studies have examined how precipitation changes with altitude along the Sierra Nevada windward slope. Lundquist et al. (2010) used a combination of multi-year rain gauge data sets to quantify precipitation and wind profiler data to examine

characteristics of the Sierra barrier jet. In the long-term average for the Yuba river basin, a linear model (based on Smith and Barstad, 2004) indicated that precipitation increased with increasing altitude from the valley to 1 km elevation and then decreased with increasing altitude at higher elevations (Fig. 1.2). From the same study, a 27-year average of annual precipitation accumulation from the Parameter-Elevation Regression on Independent Slopes Model (PRISM; Daly et al. 1994) also indicated a doubling of precipitation from 250 - 1000 m MSL, and constant precipitation above 1000 m MSL for the Yuba watershed. Long-term rain gauge annual precipitation accumulation observations for elevations below 1 km on the Yuba basin slopes also showed in increase in precipitation from the base of the valley to 1 km elevation (Lundquist et al. 2010). This is not surprising, as the PRISM uses a few regionally representative rain gauges as an input (Daly et al. 1994). At elevations above 1 km, rain gauge observations did not show a clear trend with precipitation accumulation with elevation. This may be related to the potential for overexposure or obstruction of rain gauges at high elevations on the Sierra Nevada Mountains, which are densely forested. Lundquist et al. (2010) also found that higher Sierra barrier jet height corresponds to a decreasing gradient in precipitation with altitude (Lundquist et al. 2010, their Figs. 8 and 9).

This study builds upon the work of Lundquist et al. (2010) by utilizing weather radar data to gain a wider spatial coverage of precipitation in the area, especially over the low elevations of the Central Valley. We examine precipitation spatial characteristics in the context of several environmental conditions within twelve watersheds encircling the northern Central Valley. The following are specific goals of the present study.

- Quantify the long-term baseline spatial pattern and inter-storm variability of precipitation in the northern Central Valley and adjacent mountainous terrain for atmospheric river storm events.
- Document the co-variation of wind direction, upslope wind speed, storm total upslope integrated water vapor flux, Sierra Barrier Jet height, and the parent mid-latitude cyclone and how these contribute to the spatial pattern of precipitation

- Determine the observed change of precipitation frequency with increasing elevation above and below 1 km and how these vary with environmental conditions and baseline precipitation frequency.

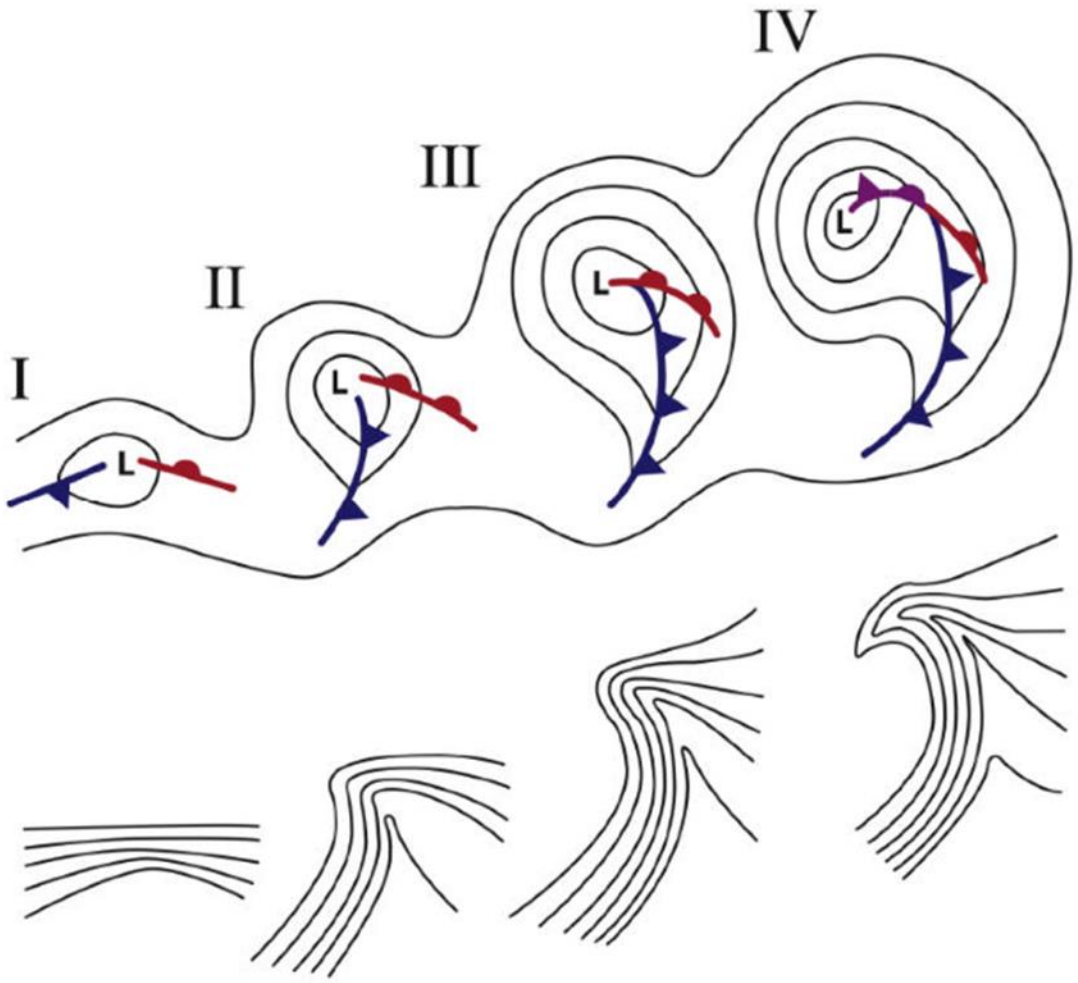

Figure 1.1 Conceptual model of a Norwegian cyclone reproduced from Fig. 15a in Schultz et al. (2011). Top shows 850 mb geopotential heights and fronts. Bottom shows 850 mb potential temperature contours. Cyclone stages are labelled with roman numerals and are approximately 6-24 hours apart. Frontal symbols are conventional. The distance from the cyclone center (denoted by L) to the outermost geopotential height contour in stage IV is 1000 km.

Figure 1.2 Figure 3 from Lundquist et al. (2010) showing the mean annual precipitation (cm) for water years from 2001 to 2007 from the linear model (Smith and Barstad 2004, panel a), the PRISM (Daly et al. 1994, panel b), and rain gauges (panel c). Basins shown are the Feather, Yuba, and American River basin from north to south. Black box in panel c shows domain for calculation of precipitation frequency gradient in Fig. 3.15 in the current study. Box and whisker plots of mean annual precipitation in centimeters for each 100-m elevation band within the Yuba basin for the linear model (panel d), PRISM (panel e), and rain gauges (panel f). Red circled dots in panel f are stations within the Yuba basin, and black dots are stations in neighboring basins. In (d) and (e), the left and right edges of each blue box are the 25th and 75th percentiles of the MAP, respectively, and the width of the box is the interquartile range. The red line is the median. The horizontal black dashed lines or "whiskers" illustrate the extent of other values, except for those that are more than 1.5 times the interquartile range away from the edges of the blue box, which are displayed with a red +. The black dash–dot lines indicate the approximate 1980 to 2007 PRISM average for the region: an increase of precipitation from 100 to 200 cm between 250- and 1000-m elevation, with constant 200 cm precipitation above, for reference. Caption adapted from Figure 3 of Lundquist et al. (2010).

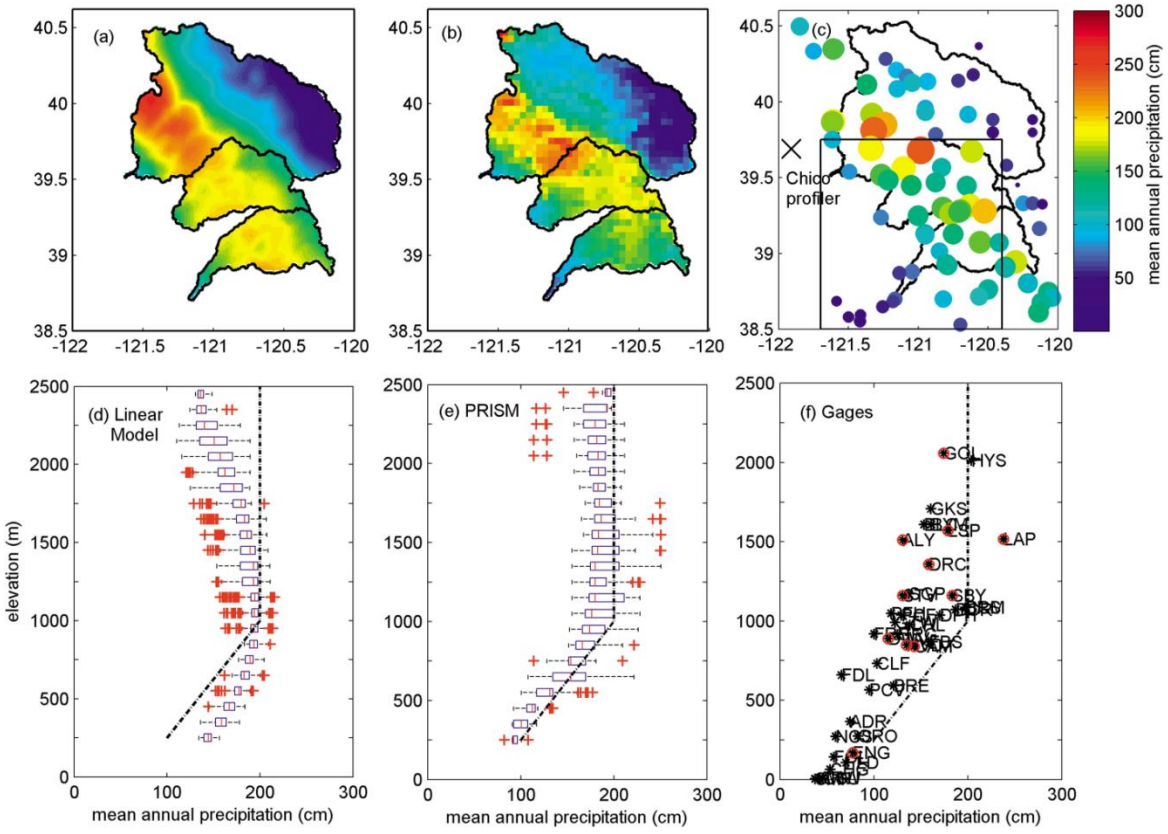
(a)
(b)
(c)
Chico profiler
mean annual precipitation (cm)
(d) Linear Model
(e) PRISM
(f) Gages
elevation (m)
mean annual precipitation (cm)
mean annual precipitation (cm)
mean annual precipitation (cm)
HYS
GKS
LAP
ALY
ORC
CLF
FDL
ORE
ADR

CHAPTER II - Data and methods

The area of interest for this study spans the northern Central Valley from the lee of the Coastal Range to the windward side of the Sierra Nevada Mountains with particular focus on precipitation distribution within the Sacramento River hydrologic region (Fig. 2.1). Due to limited high-quality rain gauge observations in these mountainous regions, precipitation frequency data were obtained from two National Weather Service (NWS) Weather Surveillance Radars-1988 Doppler (WSR-88D), one located at the Beale Air Force Base (KBBX) and the other located near Sacramento, California (KDAX). The radar data processing follows methods used by Yuter et al. (2011) and Cunningham and Yuter (2014), who also studied relationships among radar-estimated precipitation, terrain, and environmental variables on the Cascade Mountain Range in Oregon.

2.1 Atmospheric river definition

We use the atmospheric river start and end times from Ralph et al. (2013; Appendix A). Ralph et al.'s (2013) analysis focused on maximum values of wind speed and water vapor variables, which may not be representative of the full atmospheric river period. This study will focus instead on mean values and time-integrated values.

An atmospheric river event in Ralph et al. (2013) was identified by meeting two criteria for 8 or more consecutive hours: 1) integrated water vapor (IWV) of at least 2 cm, and 2) maximum upslope IWV flux of at least 15 cm m s^{-1} at the coastal wind profiler in Bodega Bay, CA. Ninety-one atmospheric river events were identified using these criteria. One hour of data or more were missing in the National Center for Environmental Information Level II archive for one or both radars for 27 of the 91 cases and are not included in this study. The remaining 64 atmospheric river cases with uninterrupted data coverage range in duration from 8 to 44 hours, and all but 12 storms occurred in the cool season (October through March). The 64 cases total 971 hours of data. A table detailing relevant environmental conditions of each atmospheric river event is provided in Appendix A.

2.2 Wind profiler data

Two vertically-pointing 915 MHz wind profilers were used in this study: a coastal profiler at Bodega Bay, CA (BBY) and an inland profiler at Chico, CA (CCO) near the base of the Sierra Nevada Mountains (Fig. 2.1). Both Chico and Bodega Bay profilers collected data during the cool season as part of the National Oceanic and Atmospheric Administration's (NOAA) Hydrometeorology Testbed program (Ralph et al. 2005; http://hmt.noaa.gov). The wind direction for each event is defined as the layer mean wind direction from 0.75 - 1.25 km above mean sea level (MSL) at Bodega Bay, the layer in which the vertical center of the atmospheric river is most commonly located. This layer has been termed the "atmospheric river-controlling layer" in previous studies (Neiman et al. 2002, 2013).

2.2.1 Wind speed and direction variables

The wind direction at the onset of the atmospheric river conditions at Bodega Bay was examined for a relationship with precipitation frequency. Wind profiles were available for 60 of the 64 atmospheric river events. The wind direction at the onset of atmospheric river conditions was chosen instead of the mean wind direction since the wind direction at Bodega Bay can change substantially as the extratropical cyclone moves along its track (Fig. 2.2). Three categories of wind direction at the onset of atmospheric river conditions are defined based upon the 33rd and 66th percentiles of all values in the dataset: southerly (154.5 – 186.0^{o}; 20 events; 26% of 971 atmospheric river hours), southwesterly (186.0 – 230.5^{o}; 20 events; 33% of 971 atmospheric river hours), and westerly (230.5 – 287.5^{o}; 20 events; 37% of 971 atmospheric river hours).

Additionally, the component of the speed of the wind in the 0.75 - 1.25 km MSL layer normal to the Coastal mountain crest (from 230^{o} as in Neiman et al. 2008) was examined. Three categories of storm mean upslope wind speed are defined based on the 33rd and 66th percentiles of values in the 64 storm dataset: low upslope speed (4 m s^{-1} – 10 m s^{-1}; 20 events; 25% of 971 atmospheric river hours), middle upslope wind speed (10 m s^{-1} –

12.75 m s^{-1}; 20 events; 20 events; 33% of 971 atmospheric river hours), high upslope wind speed (12.75 m s^{-1} – 19 m s^{-1}; 20 events; 38% of 971 atmospheric river hours).

2.2.2 Sierra barrier jet altitude

The Chico profiler in the Central Valley detected the presence and characteristics of the Sierra barrier jet during the 52 cool season atmospheric river events. Previous studies have used wind profiler data from Sloughhouse, CA for Sierra barrier jet detection. Sloughhouse had Sierra barrier jet information available for only 13 of the 52 cool season atmospheric river events. Thirty-nine of the 52 cool season atmospheric river events had Sierra barrier jet information from Chico, so Chico was chosen for this study. As in Neiman et al. (2010), the criteria for defining an Sierra barrier jet are 1) the maximum speed of at least 12 ms-1, 2) the valley parallel component of the wind maximum decreases by at least 2 ms-1 in the layer above the speed maximum and below 3 km MSL, 3) the maximum speed must be at least 200 m above the ground to eliminate shallow flows. The magnitude of the Sierra barrier jet is defined as the maximum speed of the valley parallel component of the flow during the duration of the Sierra barrier jet, and the altitude of the Sierra barrier jet is the height above sea level at which the speed maximum occurs. If there is more than one jet in the profile that satisfies these criteria, the jet with the largest magnitude is chosen as the Sierra barrier jet.

This commonly-used set of criteria for defining a Sierra barrier jet has weaknesses in not including any thermodynamic constraints to assess the degree of blocking. This means that using these criteria, a jet may be identified in a wind profile, but may not be associated with the characteristic blocked flow of the Sierra Barrier jet. However, no thermodynamic information is provided at the Chico profiler observation site for this time period, and thus the Sierra barrier jet is only constrained by kinematic traits in this study.

The Sierra barrier jet is not a steady state phenomenon and does not always co-occur with an atmospheric river. Because of this, the time periods in which the occurrence or non-occurrence of a Sierra barrier jet overlaps with an atmospheric river event are referred to as a sub-atmospheric river period (Fig. 2.3). Sierra barrier jet information from Chico was

available only during the cool season. For the 52 cool season atmospheric river events, 78 sub-atmospheric river periods were identified, totaling 789 hours. The length of the sub-atmospheric river periods varied from 1 to 43 hours.

The 78 sub-atmospheric river periods were divided into categories based on Sierra barrier jet altitude. Sierra barrier jet altitude categories were defined in the same manner as Lundquist et al. (2010), where high altitude corresponds to an altitude >1200 m (11 periods; 17% of sub-atmospheric river period hours), low altitude corresponds to an altitude <700 m (9 events; 15% of sub-atmospheric river period hours), and middle altitude is everything in between (16 periods; 31% of sub-atmospheric river period hours). Additionally, we define a fourth category, no Sierra barrier jet, for the sub-atmospheric river periods in which no Sierra barrier jet was detected at Chico (38% of sub-atmospheric river period hours). The "no Sierra barrier jet" periods are only defined for events in which the Chico profiler was recording data, such that a distinction between "no Sierra barrier jet" and "no data" is made.

2.3 Storm total upslope integrated water vapor flux

Hourly-averaged GPS-Met-derived IWV data (Duan et al. 1996; Mattioli et al. 2007) for 56 of the 64 atmospheric river events were obtained from the Bodega Bay site. IWV is calculated based on the apparent delay in transmitted signals from GPS satellites to a GPS receiver at Bodega Bay (Bevis et al. 1992, Duan et al. 1996). These measurements are obtained every 30 minutes and are averaged every hour (see Neiman et al. 2009 for calculation). A combination of wind profiler and IWV measurements were used to calculate the storm total upslope IWV flux. As in Ralph et al. (2013), hourly IWV values were multiplied by the component of the wind in the 0.75 - 1.25 km MSL layer directed normal to the Coastal mountain crest (230°). The storm total upslope IWV flux is the sum of the observations over the duration of the atmospheric river event, resulting in units of cm m s^{-1}. As 75% of the water vapor flux in atmospheric river events occurs in the lowest 2.25 km of the atmosphere (Ralph et al. 2005), using the full-column integrated water vapor and the layer mean wind at 1 km in the calculation of integrated water vapor flux is reasonable. IWV data were available for 56 atmospheric river events.

The atmospheric river events are grouped into three categories separated by the 33rd and 66th percentiles of all storm total upslope IWV flux values in the 56 observations available in the dataset. Low storm total upslope IWV flux events are those with values between 137 and 289 cm m s^{-1} (18 events; 18% of 971 atmospheric river hours); middle storm total upslope IWV flux events are those with values between 289 and 446 cm m s^{-1} (19 events; 25% of atmospheric river hours); high storm total upslope IWV flux events are those with values between 446 and 1900 cm m s^{-1} (19 events; 47% of atmospheric river hours). As a consequence, the longest lasting atmospheric river events are also those with the largest values of storm total upslope IWV flux. A table detailing all environmental variable categories and their sample sizes is in Table 2.1.

2.4 Radar data

The NWS WSR-88D radars, KDAX (38.5 °N, 121.7 °W, 9 m MSL) and KBBX (39.5 °N, 121.6 °W, 53 m MSL), are located at low elevations of California's Central Valley (Fig. 2.1). KBBX is situated roughly 110 km due north of KDAX. These radars have a wide view of Northern California's interior mountain slopes and Central Valley. It is important to note that KDAX and KBBX cannot obtain data on the windward side of the Coastal range and the lee side of the Sierra Nevadas due to beam blockage, and this study will focus only on precipitation falling over the northern Central Valley and neighboring interior mountain slopes. Archived Level II data were obtained from the NCEI Next Generation Radar (NEXRAD) Data Inventory (NOAA 1991) for the 64 atmospheric river events. The period of study is primarily prior to the NWS radar data dual polarization upgrade, so no polarimetric data were used. KDAX underwent the NWS dual polarization upgrade in mid-2008, and KBBX did not receive the upgrade until after the period of study.

2.4.1 Quality control

Level II polar volumetric radar data from individual radars were quality controlled using the same methods as Cunningham and Yuter (2014). The quality control algorithm removes instances of anomalous propagation and ground clutter. Additionally, a clutter map

for each radar was designed to remove data from locations that consistently return high reflectivity values, even in clear conditions. The cluttermap also removes all data within 25 km of KBBX and 30 km of KDAX due to the high frequency of non-meteorological echo there (Figure 2.4; see appendix B for clutter map algorithm). Due to the close proximity of the radars to each other, these data holes are filled by the neighboring radar.

A relative reflectivity calibration was performed on the raw Level II data for the 64 atmospheric river events. A vertical curtain 38 km long, equidistant from both radars, and perpendicular to a line connecting them was taken through radar volumes for each atmospheric river event. At half-hour intervals, the return from KDAX was subtracted from the return from KBBX for gates that intersected the curtain. The median value of all differences during each storm was taken as the relative calibration factor, which was applied to KBBX. Details of the radar calibration methodology are included in Appendix C.

2.4.2 Precipitation frequency

As in Cunningham and Yuter (2014), radar data from the two lowest elevation angles (0.5 and 1.5°) were each separately interpolated to two-dimensional Cartesian maps using the National Center for Atmospheric Research (NCAR) REORDER software (Mohr et al. 1986, Oye and Case 1995, NCAR Field Observing Facility, Boulder, CO, 33 pp. Available online from http://www.eol.ucar.edu/rsf/UserGuides/ELDORA/DataAnalysis/reorder/unixreorder.ps., technical guide, 1994). The 0.5° tilt experiences frequent partial and total beam blockage from the surrounding mountains (Fig. 2.5). The 1.5° tilt clears the tallest mountain peaks in the radar domain under typical atmospheric conditions.

Data from each radar were re-gridded from their initial volumetric-polar coordinate system to a Cartesian grid with dimensions 402 km × 402 km × 1 km. The grid has a single vertical level 1 km deep and a horizontal grid spacing of 2 km. The re-gridding was performed using a Cressman weighting scheme with an azimuthal radius of 1.1°. The 0.5 and 1.5° tilts were re-gridded separately to minimize artifacts of the Cressman weighting scheme when a bright band is present.

Using the methods of Yuter et al. (2011) and Cunningham and Yuter (2014), we created precipitation frequency maps for each atmospheric river event and sub-atmospheric river period and for the 0.5 and 1.5° tilts separately. A precipitation frequency map describes the frequency that a grid cell reports a reflectivity value greater than a threshold value relative to the number of volumes in the event. A threshold of 13 dBZ is used in the calculation of precipitation frequency in this study. Hagen and Yuter (2003) found that 13 dBZ roughly corresponds to a rain rate of 0.2 mm hr^{-1}, which is the approximate lower limit on precipitation intensity that a rain gauge would be able to detect. The equation for calculating precipitation frequency is:

$$precipitation\ frequency = \frac{number\ of\ times\ a\ grid\ cell\ reports\ dBZ > 13}{number\ of\ volumes\ in\ event}$$

The 2D precipitation frequency maps for each of the 64 storms and both radars were created for the 0.5° and 1.5° tilts separately and were subsequently merged by taking the largest precipitation frequency value at each grid location. By combining data from both tilts, we gain information about precipitation at high elevations near mountain slopes that may be blocked by the terrain in the 0.5° tilt.

Precipitation frequency maps from each radar were stitched together and regridded to a common 1602 km by 1602 km regional precipitation frequency map with horizontal grid spacing of 2 km. Overlapping data points were assigned the largest precipitation frequency value that intersected that grid location. In the final step, a data quality mask was applied to the regional precipitation frequency maps to mask areas frequently subjected to beam blockage from the mountains from being included in later statistics (Fig. 2.1). This mask was drawn by hand using a terrain map and several representative precipitation frequency maps for reference.

Precipitation frequency is presented in two ways depending on the particular aspect of the analysis. Precipitation frequency in units of hours is more are useful when comparing individual storm maps, as they demonstrate the duration as well as the spatial distribution of precipitation. Precipitation frequency in units of hours is obtained by multiplying the unitless precipitation frequency value by the number of hours the atmospheric river event lasted.

When aggregating multiple precipitation frequency maps as a function of environmental conditions, it is more useful to present precipitation frequency in normalized units of a fraction to mitigate sample size discrepancies among groupings. We aggregate the precipitation frequency maps into groups based on the based on the environmental variable subsets (defined in sections 2.2.1, 2.2.2, and 2.3). We also aggregate all 64 atmospheric river precipitation frequency maps into one grand precipitation frequency composite (Fig. 2.6).

Hourly wind data were available for 60 of the 64 atmospheric river events in the dataset, so environmental variable composites based on wind information include only those 60 precipitation frequency maps. Hourly averaged GPS-Met derived IWV were available for 56 of the 64 atmospheric river events, so storm total upslope IWV flux composites include only 56 of the precipitation frequency maps.

Precipitation frequency is a reasonable proxy for precipitation accumulation (Doneaud et al. 1988; Biasutti et al. 2011). It should also be emphasized that precipitation frequency maps do not show instantaneous precipitation intensity or accumulation, but rather a frequency of precipitation occurrence. The use of a proxy is necessary to minimize any misinterpretation of the bright band.

2.5 Synoptic context

Three-dimensional gridded data from the Climate Forecast System Reanalysis (CFSR) dataset at a horizontal resolution of 0.5° latitude × 0.5° longitude (Saha et al. 2010; http://cfs.ncep.noaa.gov/cfsr/) were used to examine the synoptic-scale context of the 64 atmospheric river events. Reanalysis data are available every 6 hours, and the analysis time closest to the start of the onset of atmospheric river conditions was examined. If the start time was exactly between two analysis times, the earlier time was chosen.

We computed the integrated water vapor transport (IVT) from the reanalysis for the time closest to atmospheric river landfall. IVT magnitude is defined as:

$$IVT = \frac{1}{g}\int_{p_1}^{p_2} q(p)\ \overrightarrow{V_h}(p) \quad dp$$

where g is Earth's gravitational acceleration, q(p) is the vapor mixing ratio at pressure level p, $\overrightarrow{V_h}(p)$ is the horizontal wind vector at p, and has units of kg m^{-1} s^{-1}. IVT was vertically integrated from 1000 hPa - 300 hPa.

The position of the low center was manually located by visual inspection of the 850 hPa field over the northeastern Pacific. The 850 hPa field was chosen over the mean sea level pressure field as low pressure centers at 850 hPa were more coherent in shape and more distinguishable from noise. The 850 hPa low pressure center that was in closest proximity to the atmospheric river interacting with the California coast was selected as the cyclone of primary importance for each case. Additionally, each cyclone low was assigned a subjective clarity parameter on a scale of 1 to 5. A low clarity parameter (1 or 2) was assigned when the position of the low center was not well defined in the 850 hPa maps. A high clarity parameter (4 or 5) was assigned when the position of the 850 hPa low was well defined. For the 14 most well-defined cyclones at the onset of atmospheric river conditions, 6-hourly analyses were obtained to track the position of the cyclone through the duration of the event.

Additionally, surface analyses from the NWS/NCEP Ocean Prediction Center (http://nomads.ncdc.noaa.gov/ncep/NCEP) are used to assess the general position of the surface cyclone, the 24-hour track forecast, and the location and orientation of frontal boundaries in the context of the Norwegian cyclone model. Surface analyses were available for 63 of the 64 atmospheric river events. As in the CFSR reanalysis dataset, the time closest to the start of the atmospheric river event was examined.

2.6 Precipitation frequency gradient with altitude

The precipitation frequency gradient is an analog to the orographic precipitation gradient used in Lundquist et al. (2010). We extend the results of the 27-year PRISM, linear model, and rain gauge averages from Lundquist et al. (2010) to a larger domain using radar data to determine the change of precipitation frequency with elevation within 12 watersheds in northern California for the 64 atmospheric river events and 84 sub-atmospheric river periods in our dataset. The change of precipitation frequency with elevation is examined above and below 1 km MSL separately. The advantage of using radar data to assess the

change in precipitation with elevation is the increased number of observations over the valley, where rain gauge coverage is sparse. This is highly relevant since the gradient in precipitation along mountain slopes is a function of precipitation over both the valley and high elevations.

For each watershed in the 64 atmospheric river storm regional precipitation frequency composite (Fig. 2.6), precipitation frequency observations are sectioned into 200 m surface elevation bins from 0 - 2400 m MSL. Elevation bins containing less than 5 observations were neglected in further calculations. A best fit (least squares) line is calculated through the 50th percentiles of the distributions within elevation bins above and below 1 km MSL altitude separately. The slope of the best fit line has units of km^{-1} and is termed the precipitation frequency gradient.

A visual workflow for computing the precipitation frequency gradient is shown in Figure 2.7 using the 64 atmospheric river event precipitation frequency composite and the American River basin as an example. The 1.2 km MSL elevation bin is used to demonstrate the distribution of precipitation frequency values in one of 12 elevation bins for the American River basin. In this basin, the elevations below 1 km MSL have a precipitation frequency gradient value of 0.06 km^{-1}, indicated by the light red shading. The elevations above 1 km MSL have a precipitation frequency gradient of -0.07 km^{-1} indicated by the light blue shading.

A large positive value of precipitation frequency gradient corresponds to a large increase in precipitation frequency with altitude, and a large negative value implies a large decrease in precipitation frequency with altitude. A precipitation frequency gradient near zero represents nearly constant precipitation frequency with altitude. This quantity is calculated in all basins. The Redding and Tehama basins lie entirely below 1 km MSL, so the precipitation frequency gradient was calculated below 1 km only in these watersheds.

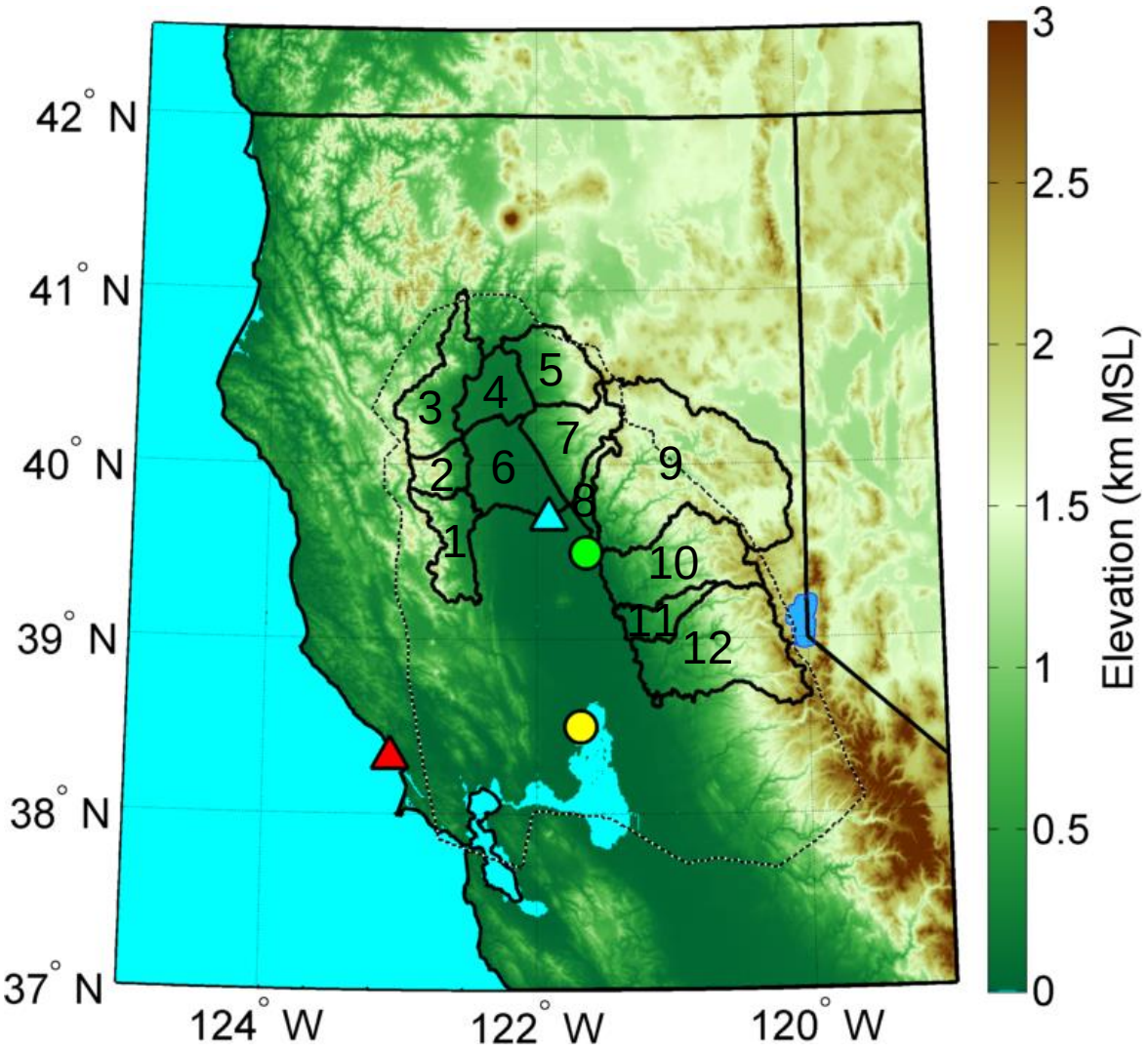

Figure 2.1 Topography of northern California showing locations of 915-MHz wind profilers (triangles; red Bodega Bay, BBY; blue Chico, CCO), WSR-88Ds (circles; yellow KDAX; green KBBX), radar data quality mask (black and white dashed line), and watershed boundaries (solid black lines). The basins are labelled numerically as follows: Stony Creek (1), Ball Mountain (2), Shasta Bally (3), Redding (4), Whitmore (5), Tehama (6), Eastern Tehama (7), Butte Creek (8), Feather River (9), Yuba River (10), Bear River (11), and American River (12). Watershed shapefile provided by atlas.ca.gov.

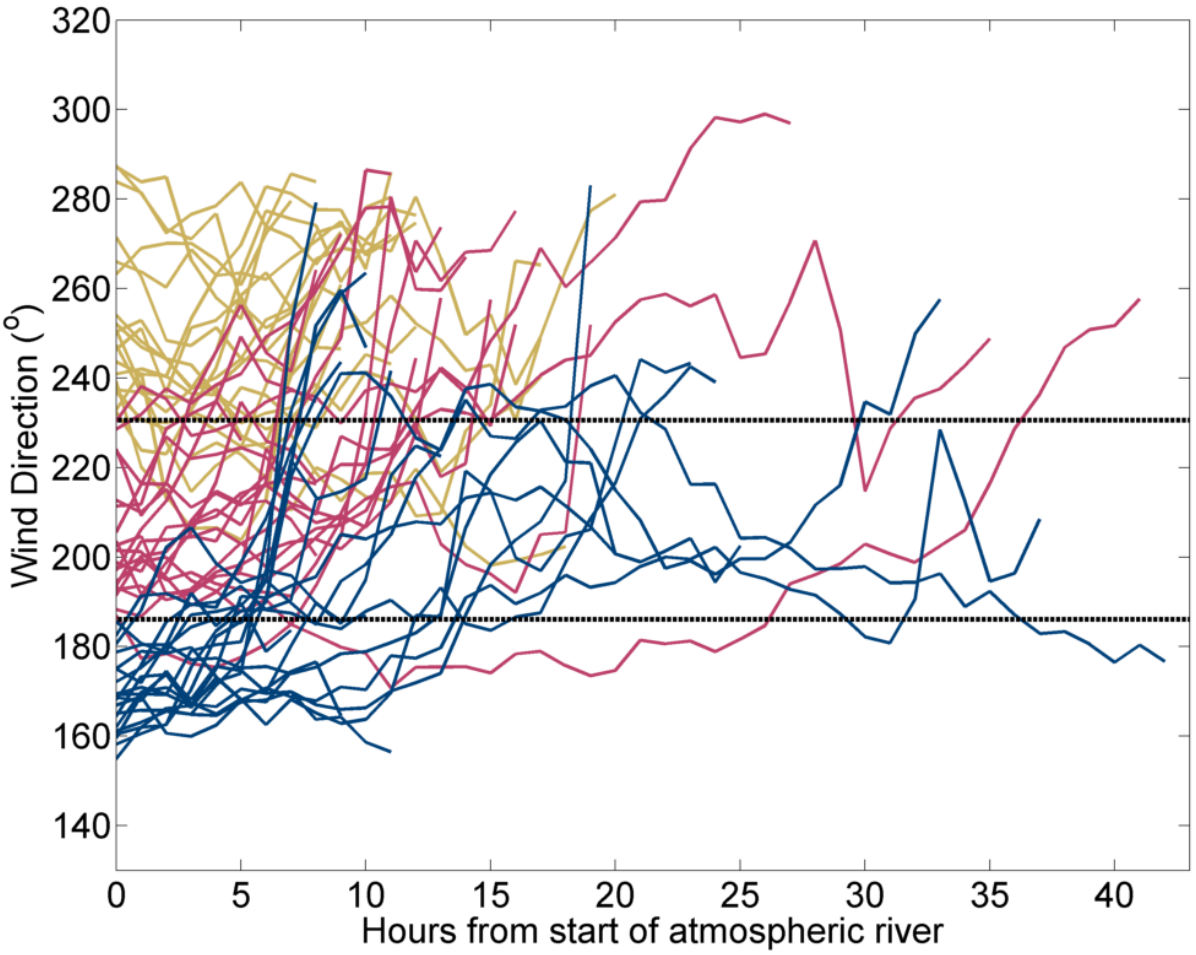

Figure 2.2 Wind direction time series of 60 cool season atmospheric river events. Gold, magenta, and navy blue lines correspond to atmospheric river conditions that begin with westerly, southwesterly, and southerly wind directions, respectively, as defined in section 2.2.1. Black dashed lines indicate the boundaries between wind direction categories.

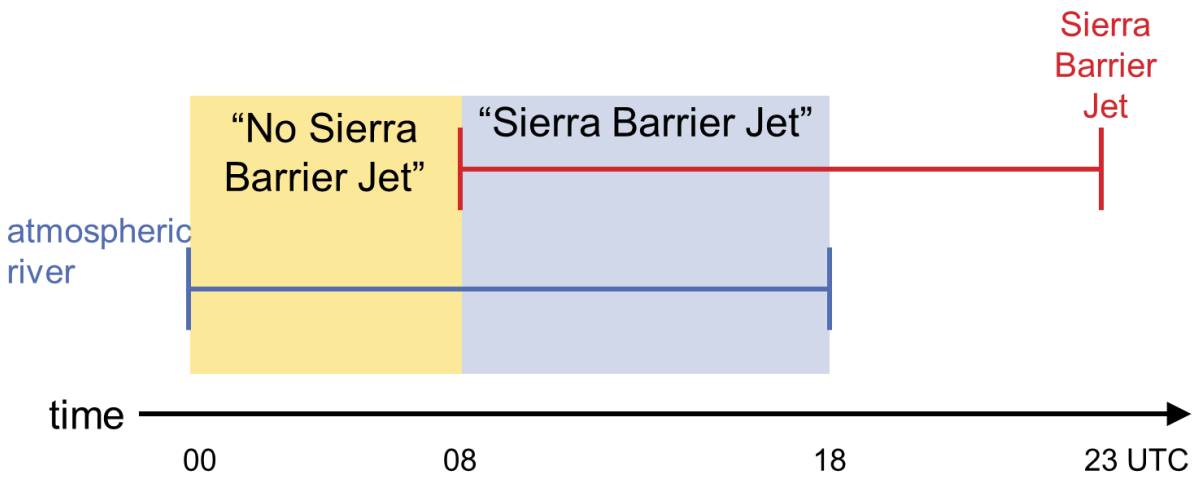

Figure 2.3 A hypothetical example of how a sub-atmospheric river period is defined. An atmospheric river event lasts from 00 – 18 UTC (18 hours) and a Sierra barrier jet lasts from 08 – 23 UTC (15 hours). This is considered 1 atmospheric river event and two sub-atmospheric river periods. One "No Sierra barrier jet" sub-atmospheric river period for 8 hours (00 – 08 UTC) and one "Sierra barrier jet" for 10 hours (08 – 18 UTC). The portion of the Sierra barrier jet after the end of the atmospheric river event at 18 UTC is not considered a sub-atmospheric river period.

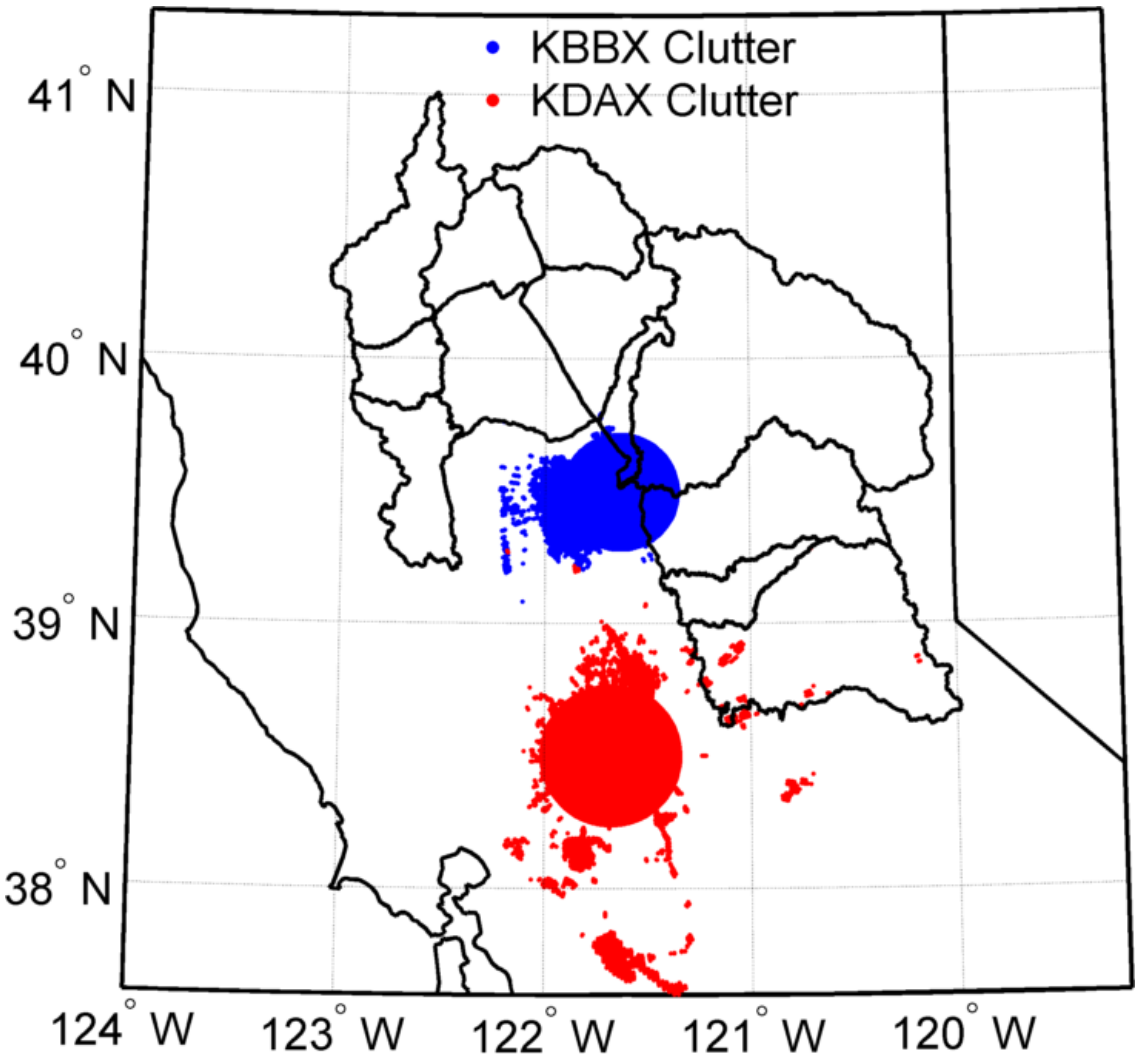

Figure 2.4 Shaded areas denote locations where radar data are removed from the KBBX (blue) and KDAX (red) radars due to persistent non-meteorological echo. Thick black lines indicate the state boundary of California as well as the 12 watershed basins used in this study.

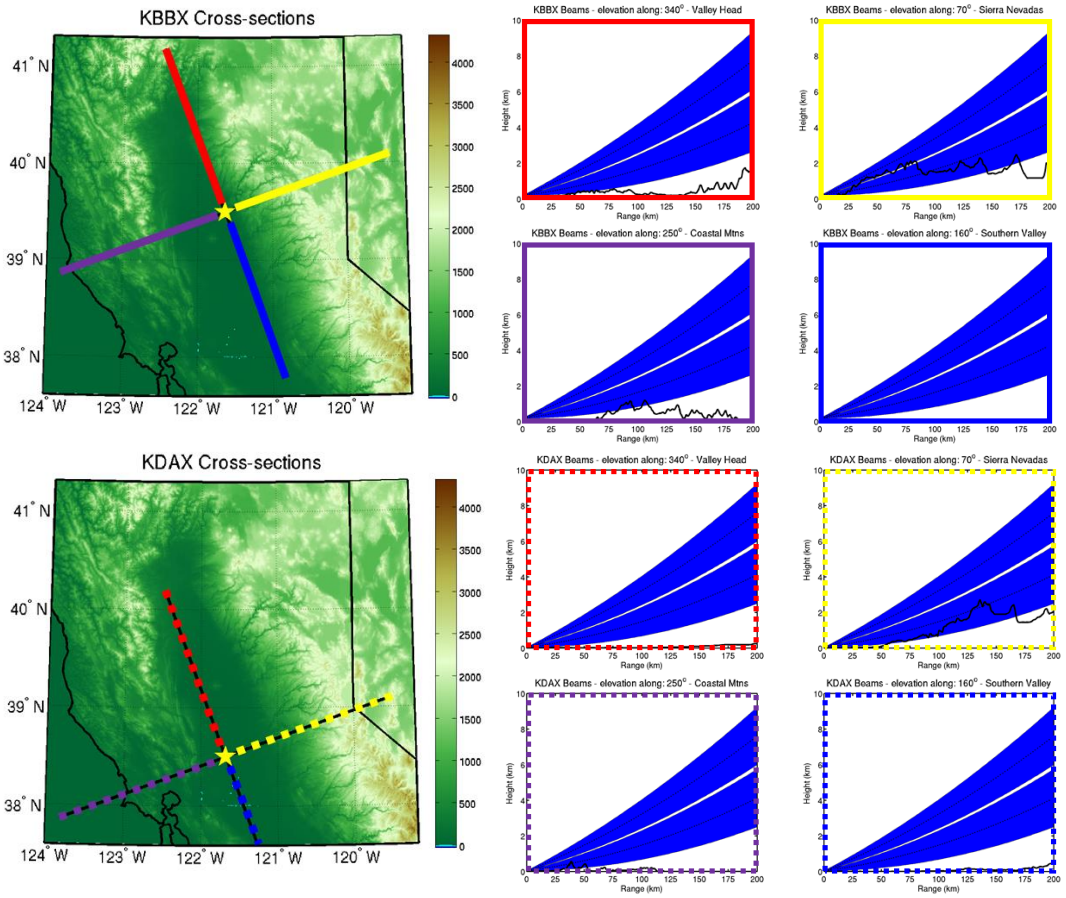

Figure 2.5 Profiles of topography along select radar beam azimuths. Left panels show a plan view of topography and the selected azimuthal profiles for both radars in this study. Colors and line dashes correspond to colors and line dashes surrounding the right panels. Right panels display terrain profiles as a function of range from radar and elevation (solid black lines) and the half power beam width of the 0.5 and 1.5 degree tilts from the radar (blue shading). Beam centers are shown in black dotted line through the center of the blue shading.

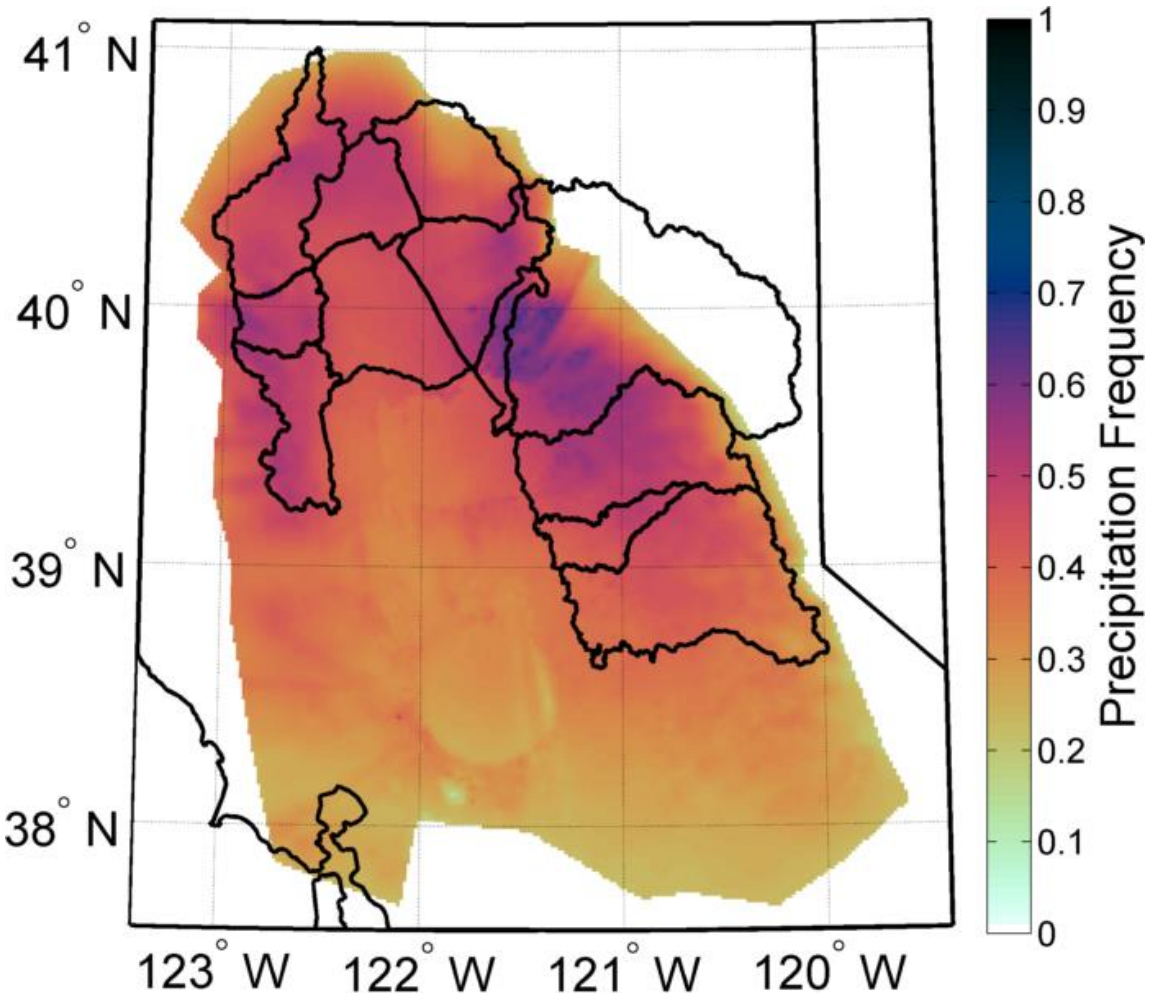

Figure 2.6 Precipitation frequency composite of all 64 atmospheric river events, only within the radar data quality mask. Shading represents the percent of 971 hours of atmospheric river conditions that a grid location reports reflectivity 13 dBZ or greater (precipitation frequency). Thick, black lines indicate the 12 watershed boundaries. Data are only displayed for locations within the data quality mask.

Figure 2.7 Methods used to calculate the precipitation frequency gradient using the 64 atmospheric river event precipitation frequency composite in units of hours and the American River basin as an example. a) Composite precipitation frequency in units of fraction. Thin gray contours denote every 200 m MSL. Thin blue contour denotes 1 km MSL. Thicker black line shows the boundary of the American River basin. b) As in a), but showing only the data that lie within the 200 m elevation bin centered on 1.2 km MSL. c) The distribution of values of precipitation frequency within the 1.2 km MSL elevation bin. The parameter of interest for the final calculation of the precipitation frequency gradient is the 50^{th} percentile of the distribution (dark blue line). The 25^{th} (red line) and 75^{th} (green line) percentiles of the distribution are also shown. d) The 50^{th} (hollow blue circles) and 25^{th} and 75^{th} (small black dots connected by thin black lines) percentiles of the precipitation frequency distribution in all twelve elevation bins, including the example 1.2 km elevation bin shown in panels b and c, as a function of elevation. Thick blue lines denote the linear best fit through the 50^{th} percentiles of the distribution of precipitation frequencies. The thin black dashed line denotes the 1 km MSL elevation split, where the precipitation frequency gradient is computed separately above and below 1 km. The slope is termed the precipitation frequency gradient. e) Figure shows the two areas above and below 1 km MSL shaded by the precipitation frequency gradient value.

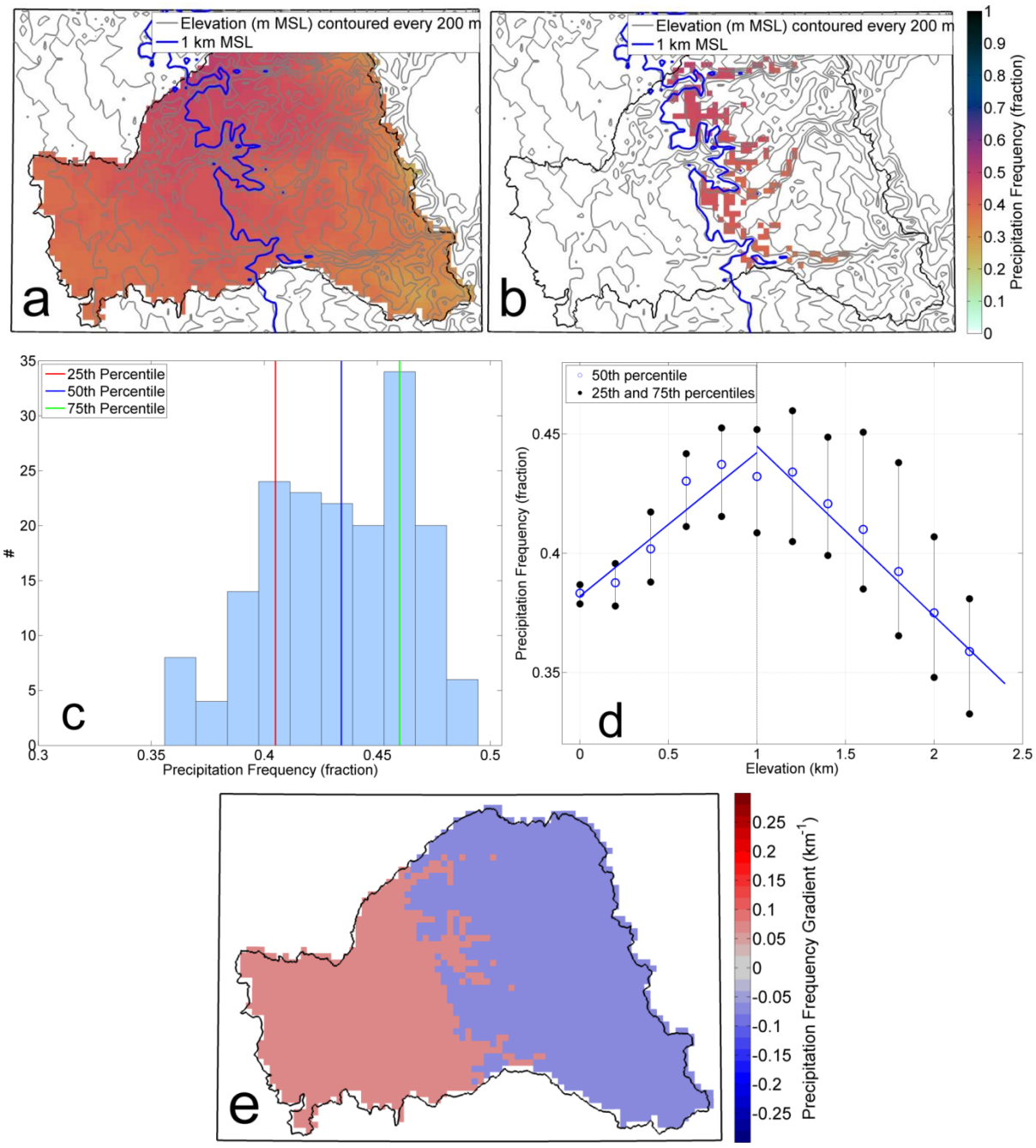
Elevation (m MSL) contoured every 200 m
1 km MSL
a
b
Precipitation Frequency (fraction)
25th Percentile
50th Percentile
75th Percentile
#
Precipitation Frequency (fraction)
c
50th percentile
25th and 75th percentiles
Precipitation Frequency (fraction)
Elevation (km)
d
e
Precipitation Frequency Gradient (km-1)

Table 2.1 Environmental variable categories. The min value column describes the minimum value for all atmospheric river events or sub-atmospheric periods. The max value column describes the maximum value for all atmospheric river events or sub-atmospheric periods. The duration column is the sum of the duration of all atmospheric river events or sub-atmospheric river period subset.

Wind Direction	Min Value (degrees)	Max value (degrees)	Duration (hours)
Westerly	232.386	287.499	253
Southwesterly	186.917	230.332	324
Southerly	154.894	185.648	356

SBJ Altitude	Min value (m)	Max value (m)	Duration (hours)
High Altitude	1200	1700	134
Middle Altitude	700	1200	245
Low Altitude	0	700	118
No SBJ			300

Upslope Speed	Min value (m/s)	Max value (m/s)	Duration (hours)
High Upslope Speed	12.783	18.155	369
Middle Upslope Speed	10.171	12.711	318
Low Upslope Speed	4.282	9.727	246

Upslope IWV Flux	Min Value (cm m/s)	Max value (cm m/s)	Duration (hours)
High Upslope Flux	427.457	1894.142	507
Middle Upslope Flux	232.153	411.373	252
Low Upslope Flux	137.739	222.731	212

CHAPTER III - Results

3.1 Synoptic overview

At the time of atmospheric river landfall at Bodega Bay, most of the extratropical cyclones associated with the 64 atmospheric river events contained occluded and cold fronts (Fig. 3.1a). Based on the NWS/NCEP marine surface analyses, 35 (56%) of the cyclones are in the mature stage (stage 4). Twelve (19%) of the cyclones do not clearly conform to any stage of the Norwegian cyclone model (Fig. 3.1a). These cyclones have attendant occluded and cold fronts, but no warm front is present. Seven of the 12 non-classifiable cyclones occurred in the warm season.

3.1.1 Cyclone tracks

The most common 24-hour cyclone forecast track direction from the NWS/NCEP Ocean Prediction Center marine surface analyses is towards the northeast (Fig. 3.1b). Examination of NWS/NCEP cyclone tracks (Fig. 3.2) indicates atmospheric river conditions that begin with a westerly wind direction at Bodega Bay tend to be associated with cyclone centers at relatively higher latitudes (>45 ^{0}N) and a range of longitudes between 120 and 140 °W in the northeast Pacific. Atmospheric river conditions that begin with a southerly wind direction tend to be associated with cyclone centers at relatively lower latitudes (<45 ^{0}N) and locations typically west of 130 °W. The correlations among wind direction at the onset of atmospheric river conditions and latitude of the cyclones identified in both the NWS/NCEP and CFSR datasets are very weak (r^2 = 0.1626 for NWS/NCEP dataset and r^2 = 0.3038 for CFSR dataset when using only cyclone lows with a clarity parameters greater than 3).

The progression of the 6-hourly cyclone center tracks from 14 of the most-well-defined cyclones at the onset of atmospheric river conditions (using the CFSR dataset) shows very little correlation among cyclone track, wind direction at Bodega Bay, and duration of atmospheric river conditions at Bodega Bay (Fig. 3.3). Some cyclones, especially those closely associated with the semi-permanent Aleutian low, do not change position very much throughout the duration of atmospheric river conditions over Bodega Bay. Additionally,

some cyclones dissipate or merge with other cyclones while the atmospheric river conditions persist over Bodega Bay.

3.1.2 Frontal geometry

It is not surprising that visual inspection of frontal geometry from the NWS/NCEP surface analyses shows that the orientation of the cold front is related to the wind direction at Bodega Bay at the onset of atmospheric river conditions. Figure 3.4a shows a cyclone that produces southerly winds at Bodega Bay and has a nearly north-south oriented cold front. Figure 3.4b shows a cyclone with southwesterly winds at Bodega Bay and a cold front with a more northeast-southwest orientation. Figure 3.4c shows a cyclone with westerly winds at Bodega Bay and a northeast-southwest oriented cold front that tilts nearly west-east at the terminus of the cold front. Since the winds within the atmospheric river on the warm side of the cold front are typically parallel to the cold front, the shift in cold front orientation from more north-south to more east-west with increasingly westerly winds is consistent.

The common northeastward track and the tendency for increasingly westerly winds to be associated with higher latitude cyclones helps explain the finding that atmospheric river conditions with initial southerly or southwesterly winds at Bodega Bay tend to have longer durations than events initiating with westerly winds. A cyclone with a north-south oriented cold front tracking northeastward will allow for more of the length (rather than the narrow width) of the atmospheric river to track over Bodega Bay. A cyclone with a west-east oriented cold front tracking northeastward is more likely to lift northward away from Bodega Bay and yield shorter durations of atmospheric river conditions there.

3.1.3 Composite synoptic conditions

Among the 64 cases, there is large variability in the geometry of the atmospheric river relative to the position of the cyclone 850 hPa low for atmospheric rivers initiating with southerly, southwesterly and westerly wind direction (Appendix E). While the atmospheric river is generally located within the warm sector of the cyclone, some atmospheric rivers wrap around the low along the leading edge of the occluded front and some atmospheric

rivers extend eastward from the low over the warm front. Hence the composites of IVT and 850 hPa height do not represent well any individual event. Keeping this caveat in mind, as wind direction shifts from more southerly to more westerly at atmospheric river onset at Bodega Bay, the composites show a deepening of the semi-permanent Aleutian low (approximately 57 °N, 150 °W), increasingly zonal isoheights, and a turning from north-south to west-east orientation of the band of high IVT near the California coast (Fig. 3.5). The band of high IVT in these composites is much wider than that of a typical atmospheric river with a width dimension of < 1000 km due to the combining of atmospheric rivers with slightly different positions and orientations in the composite. The magnitude of the maximum band of IVT near the California coast and the magnitudes of the inter-quartile range of IVT do not vary much with wind direction at atmospheric river onset. The orientation of locally higher values in inter-quartile range of IVT follows the change in the composite IVT band orientation. Especially in the vicinity of the semi-permanent Aleutian low, the inter-quartile range of 850 hPa heights is narrower for westerly as compared to southerly wind conditions at atmospheric river onset indicating less consistency in the low position among the set of southerly storms.

3.2 Covariation of environmental variables

We found a number of covariations among environmental variables and wind direction at the onset of atmospheric river conditions at Bodega Bay. For example, there is a weak linear relationship between the wind direction at the onset of atmospheric river conditions at Bodega Bay and the altitude of the Sierra barrier jet such that southerly winds are associated with higher altitude Sierra barrier jets (Fig. 3.6). We also note that there is no preferential wind direction (within the range of wind direction values explored in this study) for the presence of a Sierra barrier jet.

The physical reasoning as to why this is the case is ambiguous, and has yet to be quantified in the Sierra barrier jet literature. The Sierra barrier jet is located at altitudes in the atmosphere lower than the atmospheric river, and the atmospheric river flow will override the stable barrier jet (Kingsmill et al. 2013, their Fig. 15). This is easy to interpret for

atmospheric rivers that intersect the coast from a westerly direction. The valley-parallel component of the winds within the atmospheric river is very small compared to the Sierra Barrier jet, and the wind profiler can easily distinguish both features. The distinction between the atmospheric river within the pre-frontal low-level jet and the Sierra Barrier jet when both features have a southerly component becomes ambiguous without information regarding the thermodynamics of the environment. The wind profiler only detects wind speed and direction, and does not distinguish between a jet within a stable layer, and a jet within an atmospheric river. This means that the relationship between the Sierra Barrier jet using the commonly used Neiman et al. (2010, 2013) definition and wind direction may be an artifact of the weaknesses in the Sierra Barrier jet definition. A vertically broad region of strong, southerly winds may be flagged as a Sierra barrier jet while not necessarily exhibiting a narrow, jet-like speed maximum. Figure 3.7 shows an example of a vertical wind profile which was flagged as a high altitude Sierra barrier jet while the environment is experiencing overwhelming strong southerly winds from near the surface to 3 km MSL and above. This is a case in which the criteria provided in previous studies are not capable of distinguishing a Sierra barrier jet from a broad vertical area of southerly winds. Time-height profiles of wind speed and direction from the Chico, CA wind profiler are publicly available from NOAA/ESRL/PSD (www.esrl.noaa.gov/psd/data/obs/datadisplay/).

In this study, atmospheric river conditions that begin with southerly winds have the highest mean upslope wind speeds (Fig. 3.8). While it may seem that the southwesterly and westerly events would have a larger component of the wind from 230° (the upslope direction) than the southerly events, the southerly events have stronger wind speeds overall. On average, southerly events have full wind speeds approximately 4.6 and 7.4 m s^{-1} higher than southwesterly and westerly events, respectively. Upslope wind speeds in southerly events are on average approximately 2.0 and 5.8 m s^{-1} higher than for southwesterly and westerly events, respectively.

The storm total upslope IWV flux is also directly related to the duration of atmospheric river conditions at Bodega Bay. Since atmospheric river conditions at Bodega Bay that begin with a southerly or southwesterly direction are more likely to persist longer

(>20 hours) than those with westerly winds (Fig. 2.2), high values of storm total upslope IWV flux are also more likely to be associated with southerly winds (Fig. 3.8).

The interrelations among all variables examined in this study demonstrates the complexity of attributing precipitation patterns in this portion of northern California's Central Valley to solely one variable. A table summarizing the covariations is shown in table 3.1. This table excludes southwesterly event comparisons as the southwesterly events tend to share characteristics of either westerly or southerly events.

3.3 Spatial patterns of precipitation frequency

Precipitation frequency maps and environmental information for each of the 64 atmospheric river events are included Appendix D. Figure 3.9 (a-c) illustrates the striking differences in the precipitation distribution and frequency among atmospheric river events. Each of these precipitation frequency maps have been multiplied by the duration of the atmospheric river event, such that each map shows how long precipitation above the 13 dBZ threshold was occurring in hours. The 8 November 2006 (Fig. 3.9a) event was a westerly event that lasted only 12 hours and had low precipitation frequency values throughout the region, except for larger values at high elevations in the Feather and Yuba basins. The 7 November 2005 (Fig. 3.9b) event was a southwesterly event had a maximum in precipitation frequency at the northern end of the Central Valley, and relatively low values of precipitation frequency (<7 hours out of 20 total atmospheric river hours) along the Sierra Nevada slopes. The 18 December 2005 (Fig. 3.9c) event was a southerly event that lasted 43 hours and produced some of the greatest precipitation frequency values (> 35 hours).

3.3.1 Composite precipitation frequency

A composite of all 64 atmospheric river event regional precipitation frequency maps (Fig. 2.6) shows that as expected, precipitation with radar reflectivity > 13 dBZ fell less frequently over the low elevations of the Central Valley as compared to the surrounding mountain slopes. There are three major hotspots for frequent precipitation in the radar domain: the northern lee Coastal Range, the northern end of the central valley, and the

northern windward Sierra Nevada Mountain slopes, especially in the vicinity of the Plumas National Forest (centered at 40.0 °N, 120.7 °W). The maximum in precipitation frequency at the Plumas National Forest conforms to the model results in Reeves et al. (2008), which found increased precipitation accumulation there associated with localized convergence.

The inter-storm variability of precipitation frequency values in this composite can be quantified by computing the inter-quartile range of precipitation frequencies at each grid location. The inter-quartile range is calculated by subtracting the 25th percentile from the 75th percentile of precipitation frequency values that make up the composite (64 values, one per atmospheric river event precipitation frequency map). The inter-quartile range of precipitation frequencies in the 64 event atmospheric river composite shows the largest variability over the leeward Coastal Mountain slopes and high elevations of the Sierra Nevada Mountains (Fig. 3.10). The lee of the Coastal Mountains often experiences downslope winds due to the predominantly westerly winds in the northern hemisphere middle latitudes. Downslope winds tend to suppress condensation rates and precipitation. Only under a specific set of wind directions (those with an easterly component) will the lee of the Coastal Mountains experience upslope winds that favor enhanced condensation rates and precipitation. The higher variability in precipitation frequency along the lee of the Coastal Mountains may be because easterly wind directions are less common to this region. At the high elevations of the Sierra Nevadas, there may be some intermittent ducting and blocking of the radar beam with varying environmental stabilities storm-to-storm that is contributing to the higher variability. The variability at high elevations of the Sierra Nevada slopes may also be due to differential fall speeds of frozen versus liquid hydrometeors. The heavier, liquid particles will fall out of the cloud and reach the surface at a faster rate than lighter, ice particles. These ice particles are more likely to be advected further downstream than their liquid counterparts, especially at high elevations above the freezing level (average freezing level in this study on the coast is 2.9 km MSL, ranging from 1.4 to 4.6 km MSL). Other areas such as over the low elevations of the Central Valley and along the low and middle Sierra Nevada slopes show generally less variability with small, localized patches of higher variability.

3.3.2 Wind direction and Sierra barrier jet composites

Atmospheric river conditions over Bodega Bay that begin with southerly winds have greater precipitation frequency values (in units of fraction) throughout the radar domain compared to westerly events. This implies that in southerly storms, the precipitation area is more widespread throughout the duration of atmospheric river conditions as compared to the westerly cases. Southerly events are especially more likely to have greater precipitation frequencies in the low elevations of the valley compared to those with westerly winds, which are more likely to have precipitation frequencies concentrated in the three main hotspots (northern lee Coastal Range, northern end of the valley, and northern windward Sierra Nevadas; Fig. 3.11a-c).

A Sierra barrier jet is present for 489 of the 789 hours (62%) of sub-atmospheric river periods examined. A high altitude Sierra barrier jet period is more likely to have a greater precipitation frequencies overall compared to middle and low altitude Sierra barrier jet periods. The periods with a low altitude Sierra barrier jet or without a Sierra barrier jet have lower precipitation frequencies in general, but still have a maximum at the Plumas National Forest in the western portion of the Feather River watershed (centered at 40.0 °N, 120.7 °W). Precipitation frequency over the low elevations of the Central Valley decreases substantially (~40%) from high altitude Sierra barrier jet sub-atmospheric river periods to low altitude Sierra barrier jet sub-atmospheric river periods (Fig. 3.11d-g). It is unsurprising that the high altitude Sierra Barrier jet composite precipitation frequency map is similar to the southerly wind direction composite precipitation frequency map given the relationship between the two variables determined in section 3.2, Figure 3.6, and Table 2.

3.3.3 Mean upslope wind speed and storm total upslope IWV flux composites

Atmospheric river events with high magnitude mean upslope (from 230°) wind speeds yield high precipitation frequencies throughout the domain as compared to the middle and low mean upslope speed events (Fig. 3.12a-c). This is consistent with previous studies

(Neiman et al. 2002, Colle 2004, Smith and Barstad 2004, James and Houze 2005, Yuter et al. 2011).

The high and middle storm total upslope IWV flux composite subsets produce higher precipitation frequencies across the domain compared to low storm total upslope IWV flux events (Fig. 3.12d-f). This is expected, as greater input water vapor to the system should result in greater precipitation frequency over the domain. The high and middle storm total upslope IWV flux composites are also those with the longest durations of atmospheric river conditions at Bodega Bay. Since this variable is time-integrated, it follows that the longer duration events would also have the highest values of precipitation frequency across the domain.

The differences among high, middle, and low categories of time-integrated upslope IWV flux are not as striking as the differences in mean upslope wind speed (Fig. 3.12d-f). This suggests that the inclusion of IWV to upslope wind speed may not add additional skill in distinguishing precipitation patterns in atmospheric river events.

Given the relationship both mean upslope wind speed and time-integrated upslope IWV flux have with wind direction (Table 2), it is unsurprising that the "high" precipitation frequency composites of both categories appear similar to the southerly wind direction precipitation frequency composites.

3.4 Precipitation frequency gradient with altitude

The precipitation frequency gradient within each of the 12 the watersheds in the 64 storm composite above and below 1 km is shown in Figure 3.13. In general, precipitation frequency during atmospheric river events will tend to increase with elevation up to 1 km, and decrease above 1 km along the Sierra Nevada slopes. Along the Sierra Nevadas, the precipitation frequency gradient tends to increase in magnitude up to the Butte Creek basin (basin number 8). Basins at northern end of the central valley and along the Coastal Mountains have relatively weak precipitation frequency gradients.

3.4.1 Confidence in the mean of 64 atmospheric river event precipitation frequency gradients

We test whether the mean precipitation frequency gradient produced by the 64 event composite would be changed substantially by increasing our sample size. The test is performed by comparing the composite precipitation frequency gradients shown in Figure 3.13 to the 95% confidence interval in the mean of the distribution of precipitation frequency gradients of single-storm radar composites (see appendix D for single-storm radar composites). The precipitation frequency gradient calculations as in section 2.4.2 are computed using single-storm radar composites. This produces two sets of 64 precipitation frequency gradient values within one basin, one set above 1 km MSL and one set below 1 km MSL. The 95% confidence interval in the mean of the distribution of the aforementioned sets of precipitation frequency gradients above and below 1 km is computed assuming a normal distribution. The 95% confidence interval in the mean is compared to the precipitation frequency gradient of the 64 event composite shown in Figure 3.13.

For all basins and elevations, we are 95% confident that the true value of the mean of the distribution of single-storm precipitation frequency gradient lies within in the confidence interval shown in Figure 3.14. The precipitation frequency gradient produced by the 64 event composite also lies within the 95% confidence interval in the mean of the single-storm precipitation frequency gradients. This suggests that the 64 event composite is generally representative of the mean of all single-storm events, and any additional single-storm precipitation frequency composites will not skew the mean of the distribution very much from the 64 event composite precipitation frequency gradient.

3.4.2 Precipitation frequency gradient in wind direction and Sierra barrier jet altitude subsets

As a more direct comparison to Lundquist et al.'s analysis (2010; Fig. 1.2), we compute the change of precipitation frequency with height for the portion of the radar domain that overlaps with Lundquist et al.'s domain (see black box in Fig. 1.2c). Fig. 3.15 shows the precipitation frequency gradients for the subsets based on the wind direction at the onset of atmospheric river conditions and the Sierra barrier jet altitude. The precipitation

frequency gradients below 1 km in the wind direction subsets are similar for the southerly, southwesterly, and westerly composites (0.10 km^{-1}, 0.15 km^{-1}, 0.12 km^{-1}, respectively), but the median precipitation frequency at any elevation bin is greater for southerly storms than westerly storms. This implies that the baseline precipitation is greater for southerly storms compared to westerly storms, and that the orographic enhancement (change in precipitation with elevation) is roughly similar among the wind direction subsets.

The low altitude Sierra barrier jet subset has a much greater precipitation frequency gradient below 1 km (0.20 km^{-1}) compared to high altitude Sierra barrier jet subset (0.09 km^{-1}). The precipitation frequency in the 1 km elevation bin is higher for the high altitude Sierra barrier jet subset than for the low altitude Sierra barrier jet subset, but the difference in precipitation frequency at the lowest elevation bin (0 km MSL) is much greater between the two subsets. This suggests that the primary control of the increased precipitation frequency gradient in low altitude Sierra barrier jet periods is primarily due to decreased precipitation frequency at low elevations. The trends in the magnitude of precipitation frequency gradient in this study are consistent with the rain gauge determined daily precipitation accumulation change with height of Lundquist et al. (2010). However, Lundquist et al. (2010) attributed the increase in precipitation with elevation to changes in precipitation at higher elevations (near 1 km MSL) rather than precipitation at low elevations. A further discussion of the comparison of the radar-derived precipitation frequency gradient from this study and the orographic precipitation gradient from Lundquist et al. (2010) is in section 3.4.3. Additionally, given the covariation of variables (3.2, Table 3.1), it is difficult to attribute the precipitation frequency gradients produced by these composites solely to the wind direction or Sierra barrier jet altitude.

3.4.3 The importance of precipitation at low elevations in the Central Valley

Lundquist et al. (2010) used eight rain gauges near the base of the Feather, Yuba, and American River basins to characterize precipitation in the valley. Their analysis did not detect a change in valley precipitation from those 8 gauges as a function of Sierra barrier jet height. Because of this, their subsequent calculations to quantify the precipitation gradient on

the Sierra Nevada slopes were normalized by precipitation in the valley (elevations below 200 m MSL). This method of normalization essentially erases the potential for changes in valley precipitation to dictate the gradient in precipitation with elevation.

Thermodynamic profiles were not available during this study period, and we cannot assess the depth or width of the stable barrier at the foothills of the Sierra Nevadas. In theory, a higher altitude Sierra barrier jet could only occur within a deeper stable layer, and a deeper stable layer would support a wider area of the valley affected by blocking (Pierrehumbert and Wyman, 1985). As shown in Kingsmill et al. (2013), an atmospheric river will tend to glide over the stably stratified Sierra barrier jet (see their Figure 15). The extra lifting of the atmospheric river over the Sierra barrier jet at low elevations of the Central Valley will increase condensation rates and precipitation accumulation further west of the Sierra Nevada foothills than if the Sierra barrier jet were not present. A stable barrier that extends further west into the central valley would additionally support increased precipitation at low elevations. This theory suggests that a higher altitude Sierra barrier jet would be associated with increased precipitation over low elevations in the valley, much like is shown with the radar observations in this study (Figure 3.11d-g). The radar observations in this study show similar precipitation at elevations near 1 km MSL on the Sierra Nevada slopes for changes in Sierra barrier jet altitude (precipitation frequency of roughly 0.6, Figure 3.11d-g).

The gradient of precipitation frequency with elevation is dependent on precipitation amounts at high elevations and low elevations on mountain slopes equally. Given that the radar observations of precipitation frequency at elevations near 1 km MSL are roughly similar for all categories of Sierra barrier jet altitude, a high altitude Sierra barrier jet will decrease the magnitude of the precipitation gradient (evaluated from 0 - 1 km MSL) by increasing the precipitation in the valley (Figure 3.15).

The decrease in precipitation with elevation for increasing Sierra barrier jet altitude is consistent with the results of Lundquist et al. (2010), but for a different reason. Lundquist et al. (2010) determined that the change in precipitation gradient for changing Sierra barrier jet altitude was due to changes in precipitation at higher elevations along the Sierra Nevada slopes. This was further emphasized by normalizing all calculations of precipitation gradients

by valley precipitation. Our greater spatial coverage of precipitation at low elevations in the central valley (compared to Lundquist et al. (2010)'s eight rain gauge observations) has shown that precipitation at low elevations is the primary driver of changes in the precipitation frequency gradient among Sierra barrier jet altitude categories.

3.4.4 Evaluation of 1 km MSL inflection in precipitation frequency gradient

Lundquist et al. (2010) found an inflection point in precipitation accumulation with increasing elevation at 1 km MSL such that precipitation increases on the portion of the Sierras below 1 km and is constant above 1 km. We test in this study whether the difference in precipitation frequency gradient above 1 km and below 1 km are statistically different in each basin in the domain. To test if the 1 km altitude inflection could have happened by random chance, a variant of a Monte Carlo test was performed. For this test, we assume that if an inflection point exists, it will be at 1 km MSL. The Monte Carlo test determines whether the inflection is statistically significant or a product of random chance.

As in section 3.4.1, we calculate the gradient for each storm separately yielding two sets of 64 individual storm precipitation frequency gradients. The means of these sets are subtracted (mean above 1 km minus mean below 1 km) to yield one "true" precipitation frequency gradient difference for each basin.

We then test if the "true" difference in the means could have been found purely by random chance. Within one basin, a random selection of precipitation frequency gradients are chosen to be the "random above" and "random below" 1 km sets. The means of these "random" sets are computed and subtracted in the same manner as the "true" difference calculation from above. This process of randomly selecting "random" precipitation frequency gradient differences is repeated 10,000 times.

The 90th and 99th percentiles of the "random" precipitation frequency gradient difference distribution are computed, and the "true" precipitation frequency gradient is compared to the "random" distribution. If the "true" precipitation frequency gradient difference lies outside the middle 99% of the "random" distribution, there is a significant

chance that the "true" precipitation frequency gradient difference was not due to random chance.

This analysis shows that the difference between the precipitation frequency gradient above and below 1 km is significant in basins number 1 (Stony Creek), 3 (Shasta Bally), 5 (Whitmore), 8 (Butte Creek), 9 (Feather River), 10 (Yuba River), 11 (Bear River), and 12 (American River), though basins 1, 11, and 12 do overlap with the outliers of the distributions (Fig. 3.16).

Previous studies of precipitation climatologies near the U.S. West Coast have also noted an inflection point in precipitation accumulation at middle elevations of mountain slopes associated with low-level blocking independent of the presence of a barrier jet (James and Houze 2005, Yuter et al. 2011). Low-level blocking can also occur with down valley flow, where denser air flows down the mountain slopes, and stable blocked flow, where winds impinging on mountain slopes are forced down mountain slopes (Steiner et al. 2003, Yuter et al. 2011). James and Houze (2005) also noted that precipitation is typically enhanced over the lower windward slopes of the Coastal Range near Eureka, CA. We infer that a similar phenomenon is occurring on the windward slopes of the Sierra range. Additionally, some atmospheric river cases could also contain snow above 1 km. While the change in reflectivity due to the change of the complex index of refraction of ice may decrease the precipitation frequency, the 13 dBZ threshold is low enough that it would encompass moderate to heavy snow conditions at this altitude. The lee-side of the Coastal Range in this study likely is not producing a 1 km inflection point in precipitation frequency since winds in these events are largely westerly and downslope in that region.

3.4.5 Comparison of precipitation frequency gradient to model output from previous studies

The radar-derived precipitation frequency maps are independent of rain gauges and provide another constraint on the actual change of precipitation with height along the windward Sierra Nevada slopes. For altitudes less than 1 km, our results, Lundquist et al. (2010) rain gauge analysis, PRISM (Daley et al. 1994), and linear model (Smith and Barstad, 2004) all agree. However, above 1 km altitude, there is disagreement. Our radar derived

analysis shows a decrease in precipitation within increasing height in concurrence with the Smith and Barstad (2004) linear model as analyzed by Lundquist et al. (2010). Above 1 km altitude, PRISM indicates nearly constant precipitation with height. The rain gauges at high elevations on the Sierras Nevadas that PRISM uses as an input are at risk of overexposure or obstruction by the densely forested surroundings. This may be degrading the accuracy of the PRISM output. As PRISM uses only a few representative rain gauges as input (Daly et al. 1994), we are confident that the spatial precipitation patterns observed by the radars in this study are more representative of the true precipitation patterns than PRISM. It is likely that PRISM will over-predict precipitation at elevations above 1 km the Sierra Nevadas. This has direct implications for water resource management in reservoirs located above 1 km MSL on the Sierra Nevada slopes.

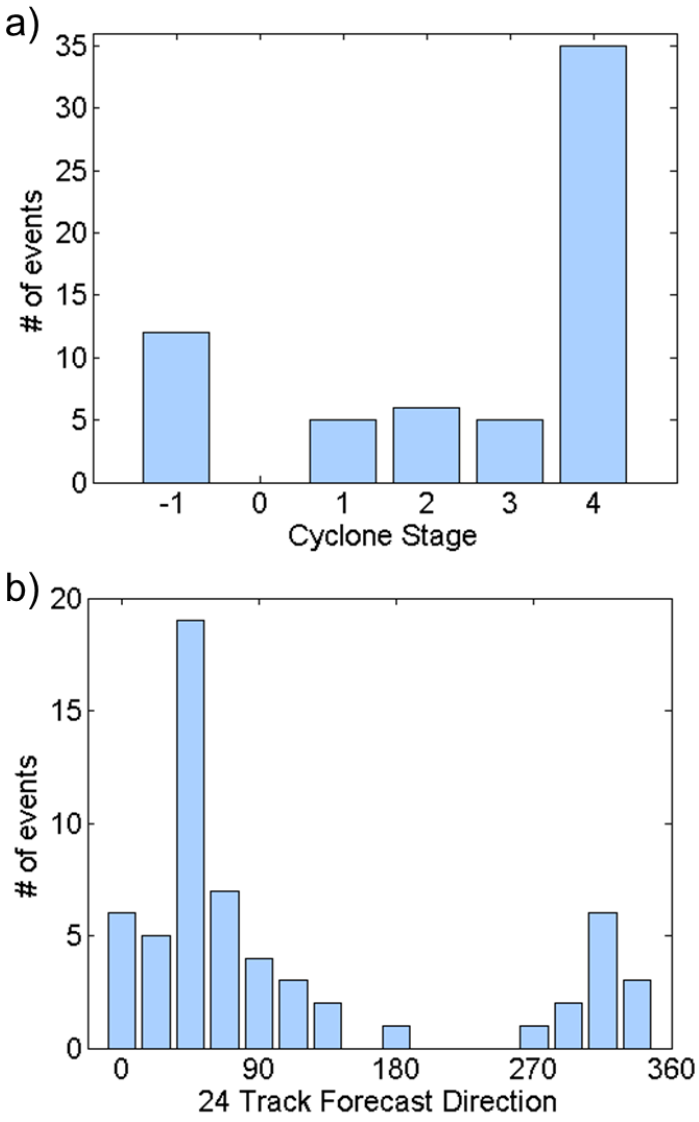

Figure 3.1 a) Histogram of cyclone stage as determined from the 63 NWS/NCEP marine surface analyses. Stage numbers 1-4 correspond to stages 1-4 of the Norwegian cyclone model as in Fig. 1.1. A stage of -1 indicates a cyclone that is unclassifiable by the Norwegian cyclone model. b) Histogram of the direction of the 24 hour forecasted cyclone track from the 63 NWS/NCEP marine surface analyses. Zero degrees refers to due north.

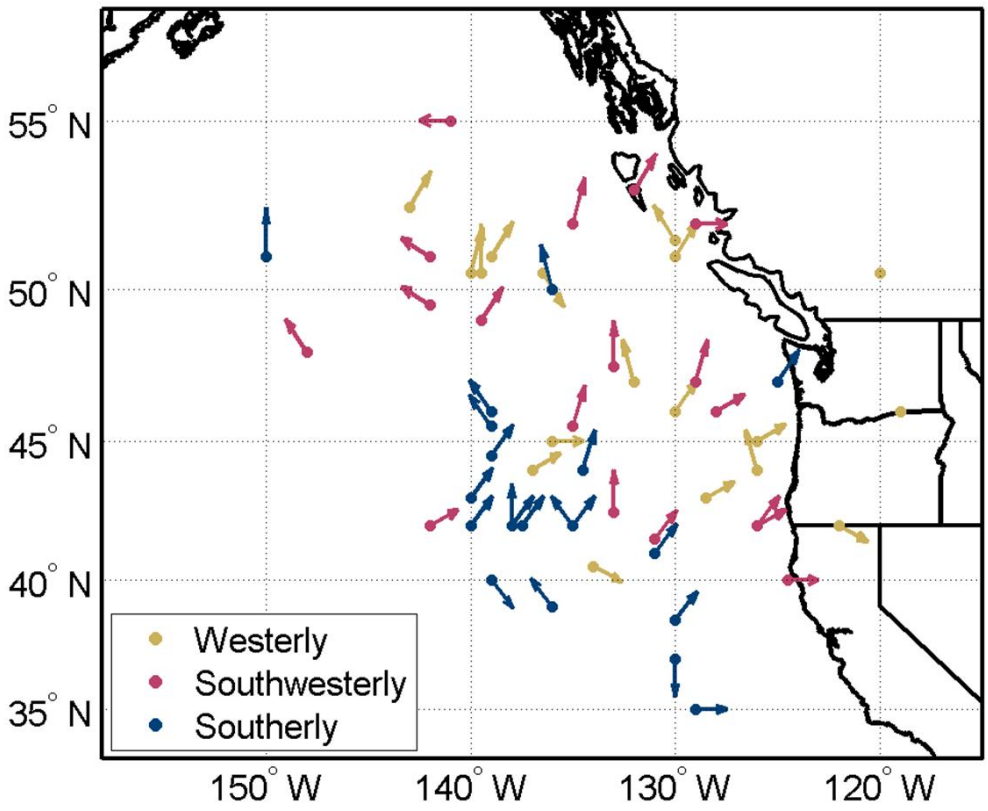

Figure 3.2 Position of the center of the cyclone associated with atmospheric river conditions at BBY as located visually by the NWS/NCEP Ocean Prediction Center surface analysis maps are denoted by filled circles. Gold, magenta, and navy blue circles correspond to westerly, southwesterly, and southerly winds at the onset of atmospheric river conditions as defined in section 2b. The direction of the 24 hour forecast track is shown by the arrows. Circles without an arrow were described as "dissipating" by the Ocean Prediction Center, and did not have a 24-hour cyclone track.

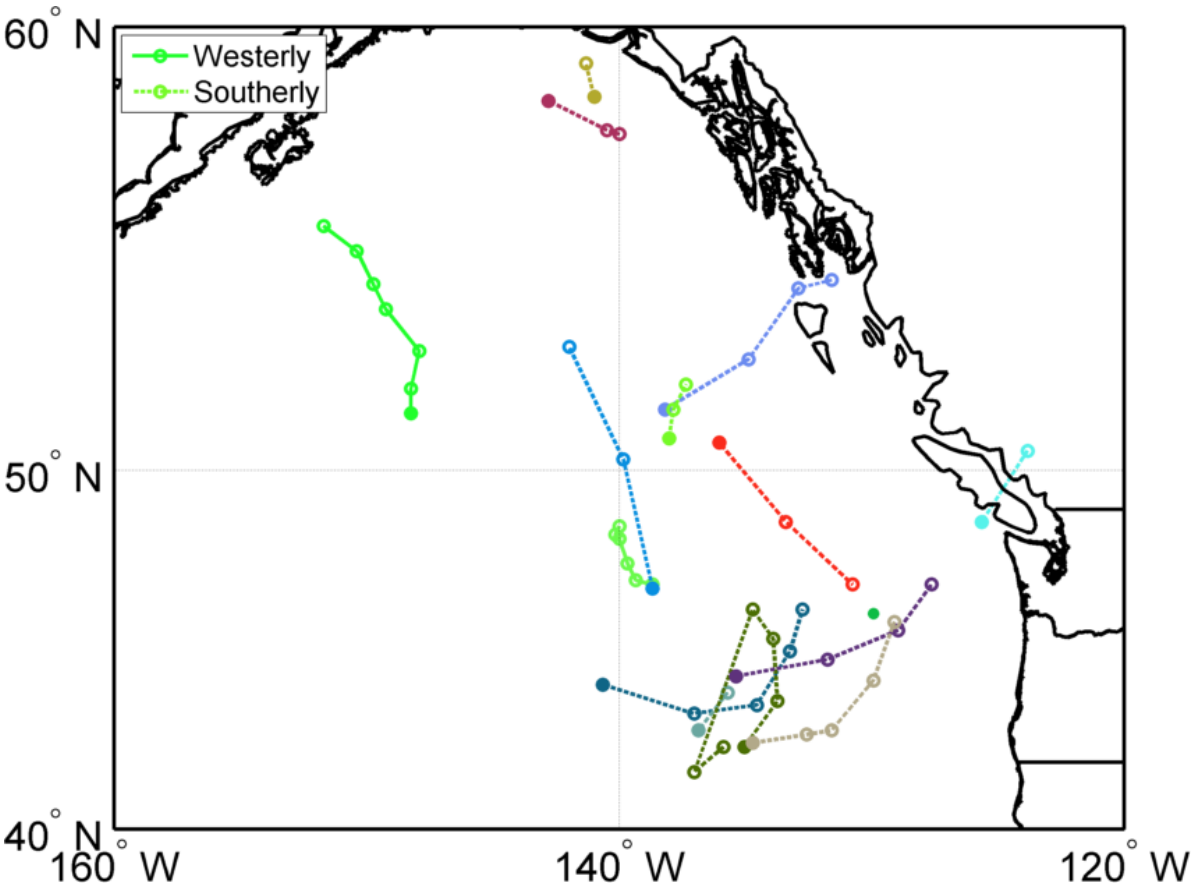

Figure 3.3 850 hPa cyclone center tracks for 17 atmospheric river events using 6-hourly analyses of Climate Forecast System Reanalysis data. The filled circle on each track indicates the cyclone position at the onset of atmospheric conditions at Bodega Bay. Hollow circles indicate the position of the cyclone at subsequent analysis times in chronological order. Westerly atmospheric river events are denoted by solid lines through points. Southerly atmospheric river events are denoted by dashed lines through points.

Figure 3.4 Example surface analysis for events with a) southerly (valid 12 UTC 20 Dec 2009), b) southwesterly (valid 18 UTC 17 Jan 2010), c) westerly (valid 06 UTC 01 Feb 2006) winds at the onset of atmospheric river conditions at Bodega Bay prepared by NWS/NCEP Ocean Prediction center. Contours of sea level pressure are displayed in green lines. Low and high pressure centers are indicated by red Ls and blue Hs, respectively. Fronts and available surface observations are denoted following standards. The red arrows extending from the centers of low pressure indicate the 24-hour cyclone forecast track. Red Xs indicate the 24-hour cyclone position forecast.

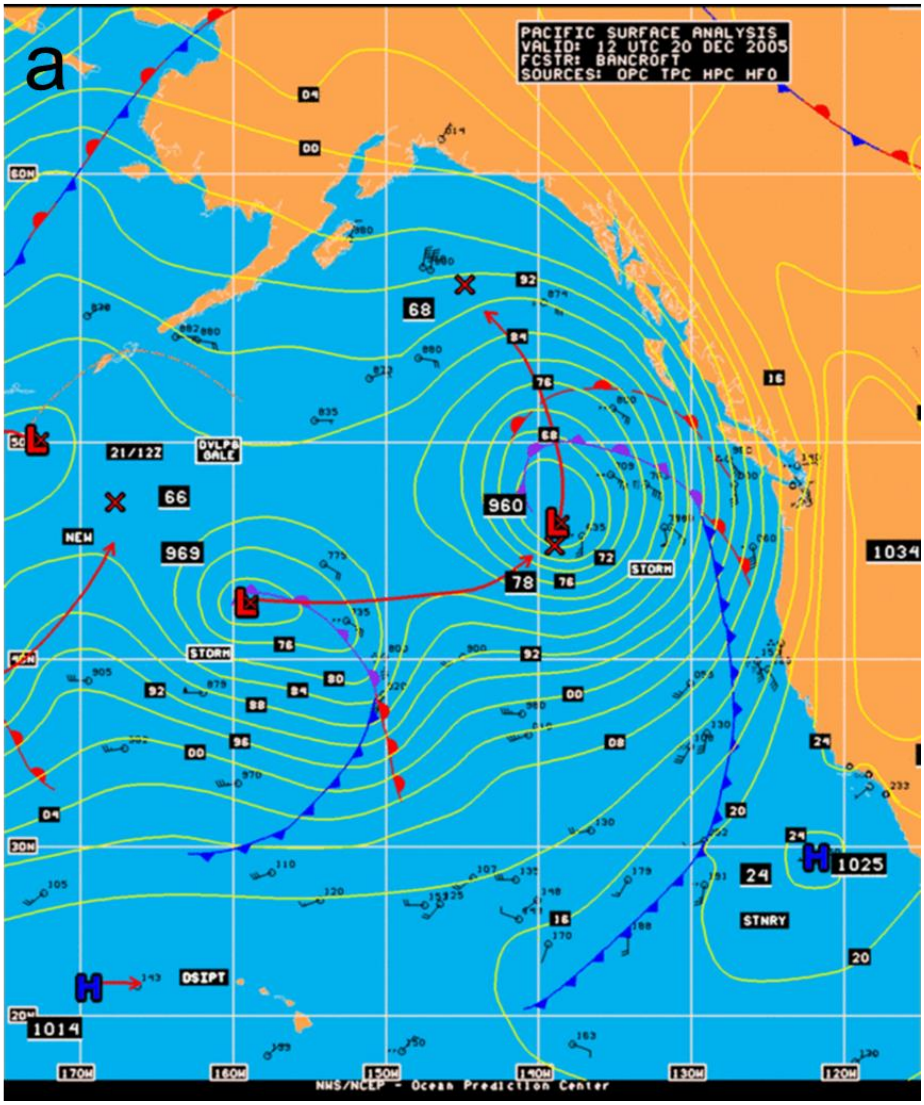
a
PACIFIC SURFACE ANALYSIS
VALID: 12 UTC 20 DEC 2005
FCSTR: BANCROFT
SOURCES: OPC TPC HPC HFO
68
66
969
960
1034
1025
1014
24
21/12Z
DVLPD GALE
NEW
STORM
STNRY
DSIPT
NWS/NCEP - Ocean Prediction Center

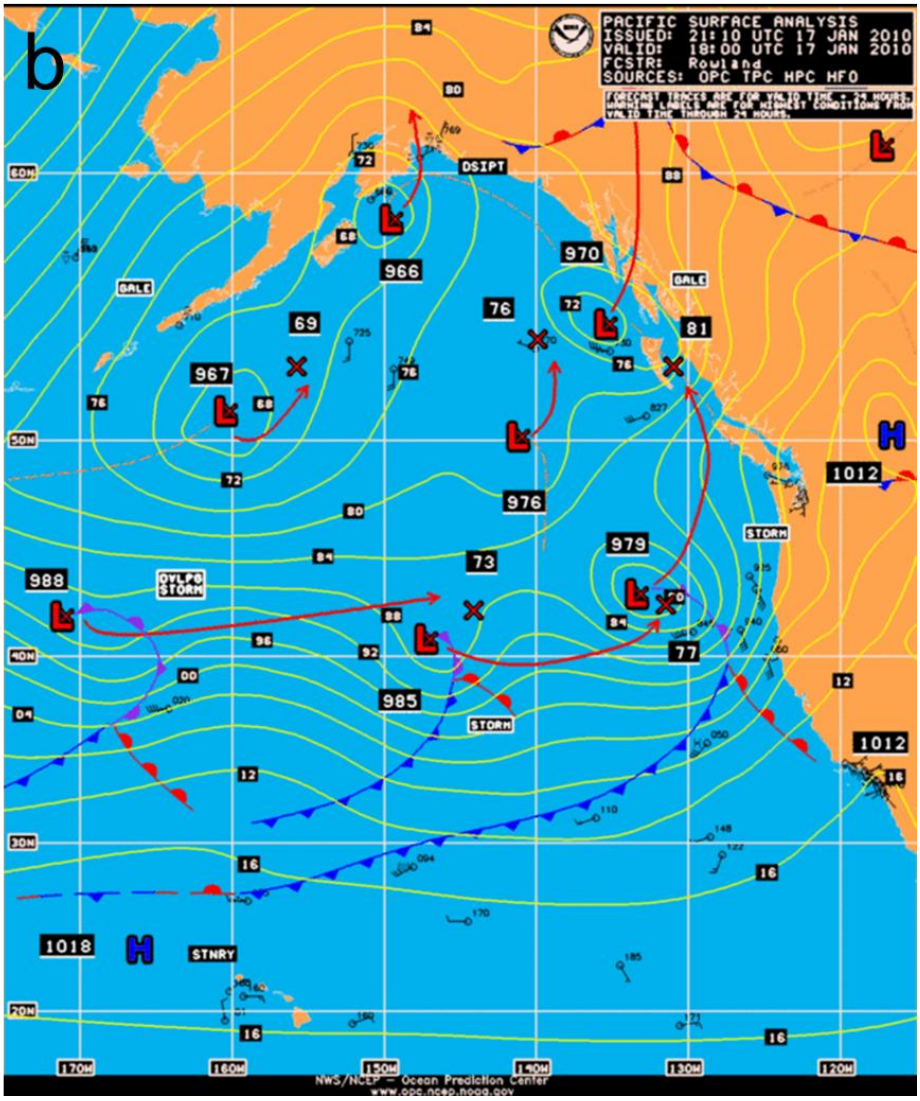
b
PACIFIC SURFACE ANALYSIS
ISSUED: 21:10 UTC 17 JAN 2010
VALID: 18:00 UTC 17 JAN 2010
FCSTR: Rowland
SOURCES: OPC TPC HPC HFO
DSIPT
966
970
976
979
985
988
967
1012
1018
GALE
STORM
STNRY
OVLPG STORM
NWS/NCEP - Ocean Prediction Center
www.opc.ncep.noaa.gov

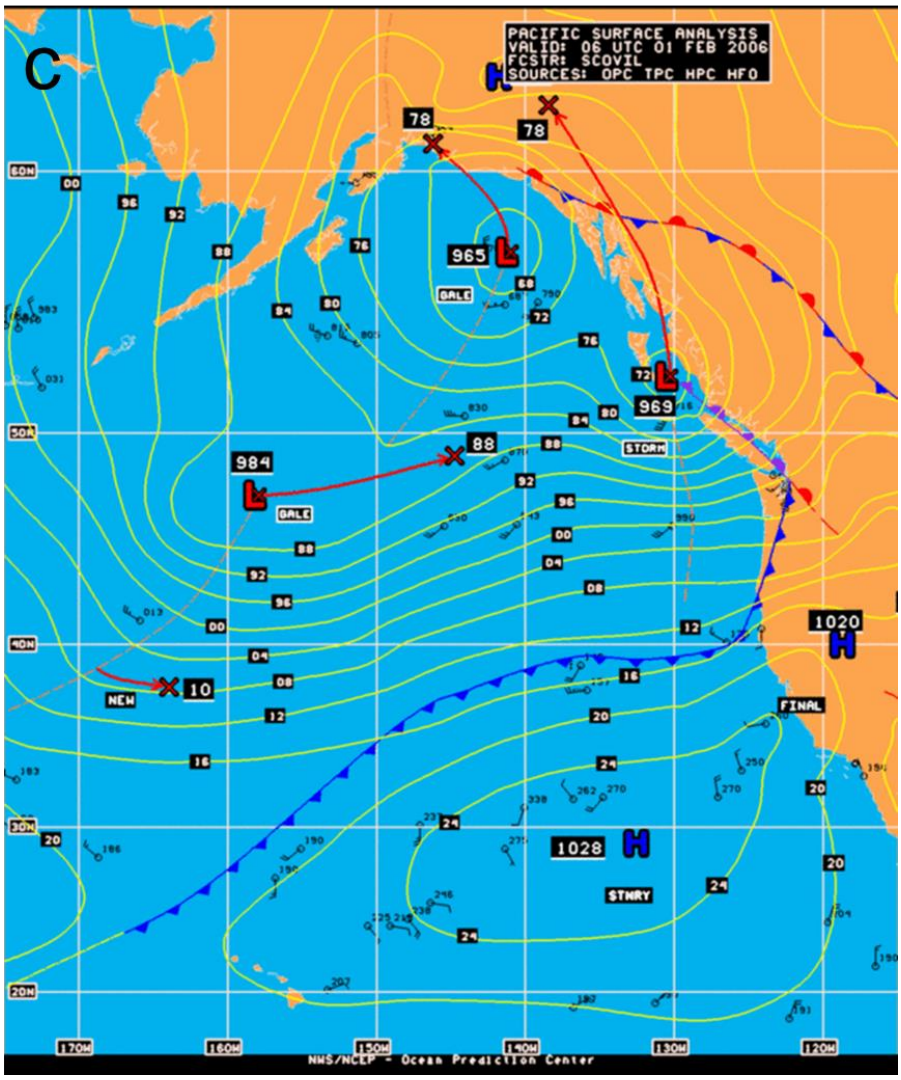
C
PACIFIC SURFACE ANALYSIS
VALID: 06 UTC 01 FEB 2006
FCSTR: SCOVIL
SOURCES: OPC TPC HPC HFO
78
78
965
GALE
969
STORM
984
GALE
88
NEW
10
1020
FINAL
1028
STNRY
60N
50N
40N
30N
20N
170W
160W
150W
140W
130W
120W
NWS/NCEP - Ocean Prediction Center

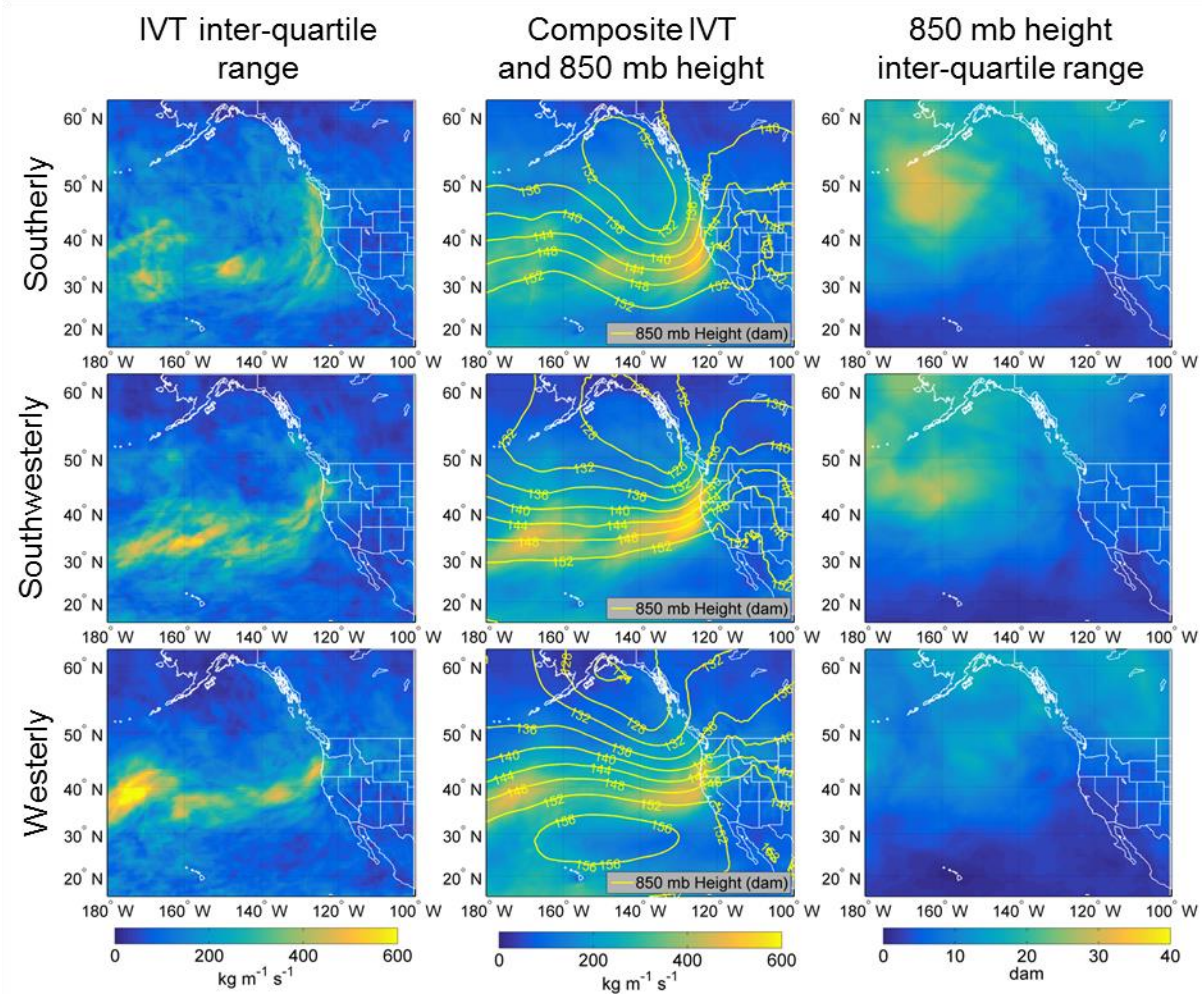

Figure 3.5 Middle column: composite mean of IVT (shading, kg m^{-1} s^{-1}) and 850 mb height (contoured, dam). Left column: inter-quartile range (75^{th} percentile minus 25^{th} percentile of values) of IVT in the composite mean (units of kg m^{-1} s^{-1}). Right column: inter-quartile range (75^{th} percentile minus 25^{th} percentile of values) of 850 mb height in the composite mean (units of dam). Top row: set of events with southerly winds at the onset of atmospheric river conditions. Middle row: set of events with southwesterly winds at the onset of atmospheric river conditions. Bottom row: set of events with westerly winds at the onset of atmospheric river conditions.

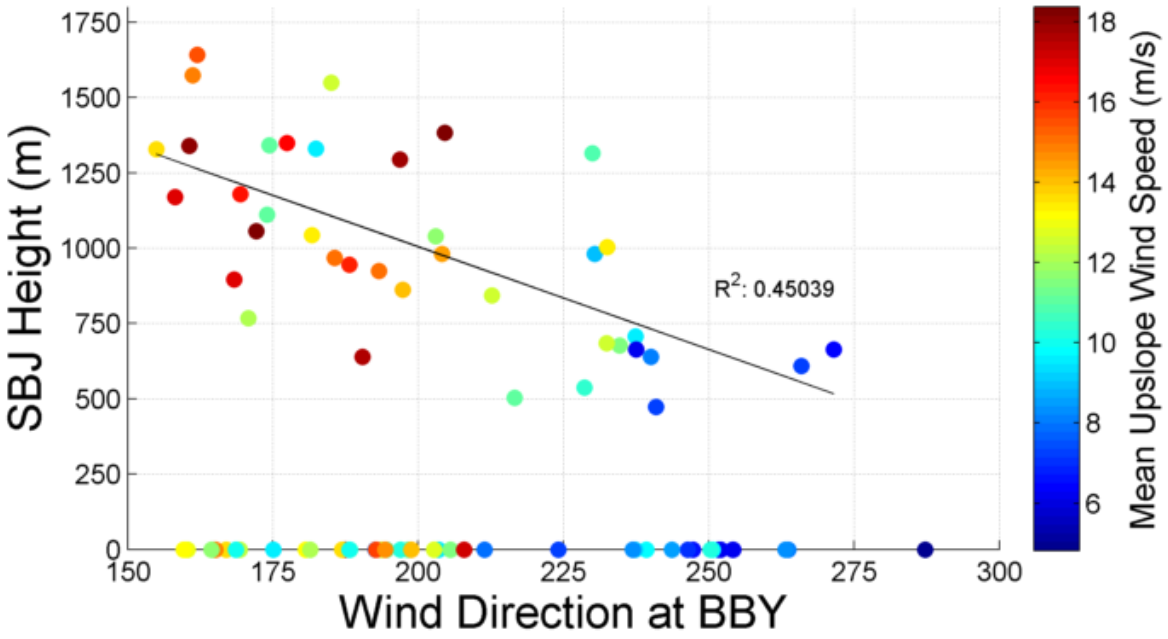

Figure 3.6 Wind direction at the onset of atmospheric river conditions at Bodega Bay (BBY) versus the altitude of the Sierra barrier jet (SBJ). A Sierra barrier jet altitude of 0 m indicates a "no Sierra barrier jet" sub-atmospheric river period. Dots are shaded based on the mean upslope wind speed at Bodega Bay. The linear trend line through only the data points where a Sierra barrier jet is present is indicated in the solid black line, and the r^2 value of the relationship is also indicated on the graph.

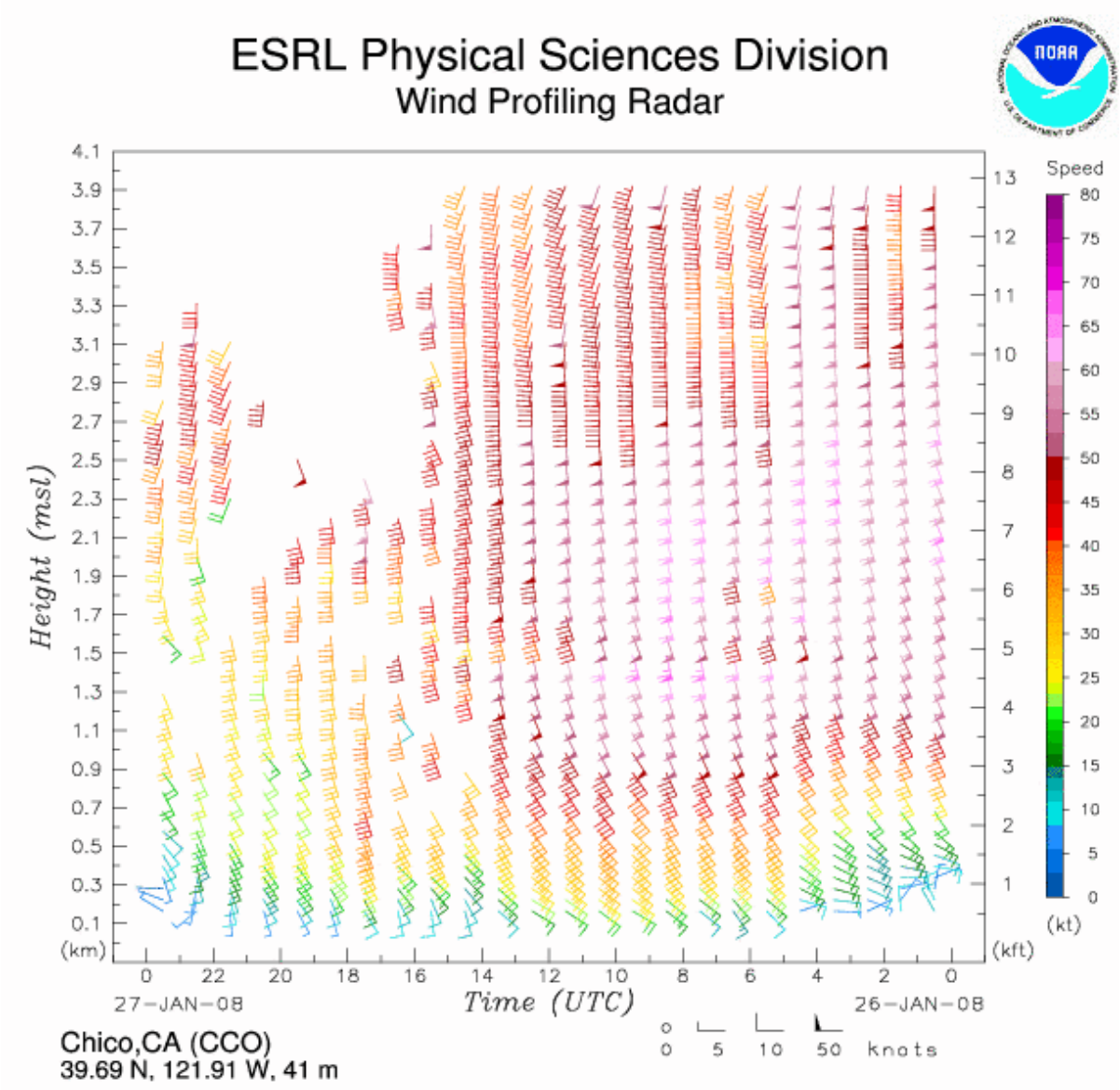

Figure 3.7 Time-height profile of wind speed and direction from the valley wind profiler (Chico, CA) for the high altitude Sierra barrier jet case on 26 Jan 2008 that overlapped temporally with the atmospheric river event that began on 26 Jan 2008 at 0200 UTC. A broad vertical column of strong southerly winds is present during the entirety of the atmospheric river event (0200 UTC - 1400 UTC on 26 Jan 2008).Wind barbs use standard notation for speed and direction and are color coded by wind speed in knots.

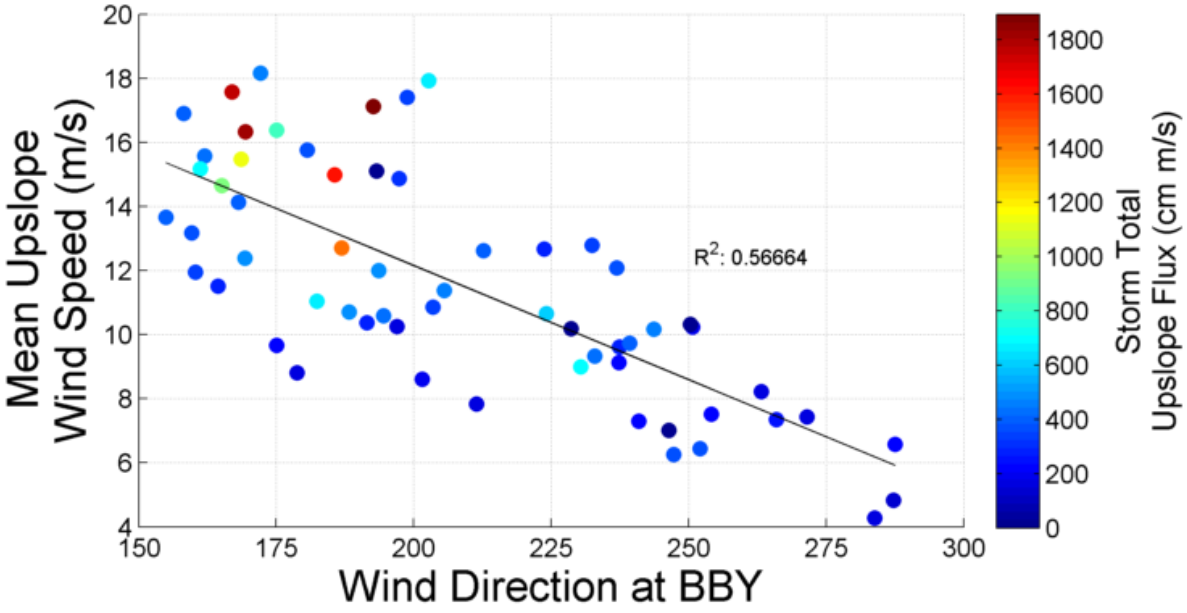

Figure 3.8 Wind direction at the onset of atmospheric river conditions at Bodega Bay (BBY) versus the storm mean upslope (from 230 degrees) wind speed. Dots are shaded based on the storm total upslope IWV flux at Bodega Bay. The linear trend line is present is indicated in the solid black line, and the r^2 value of the relationship is also indicated on the graph.

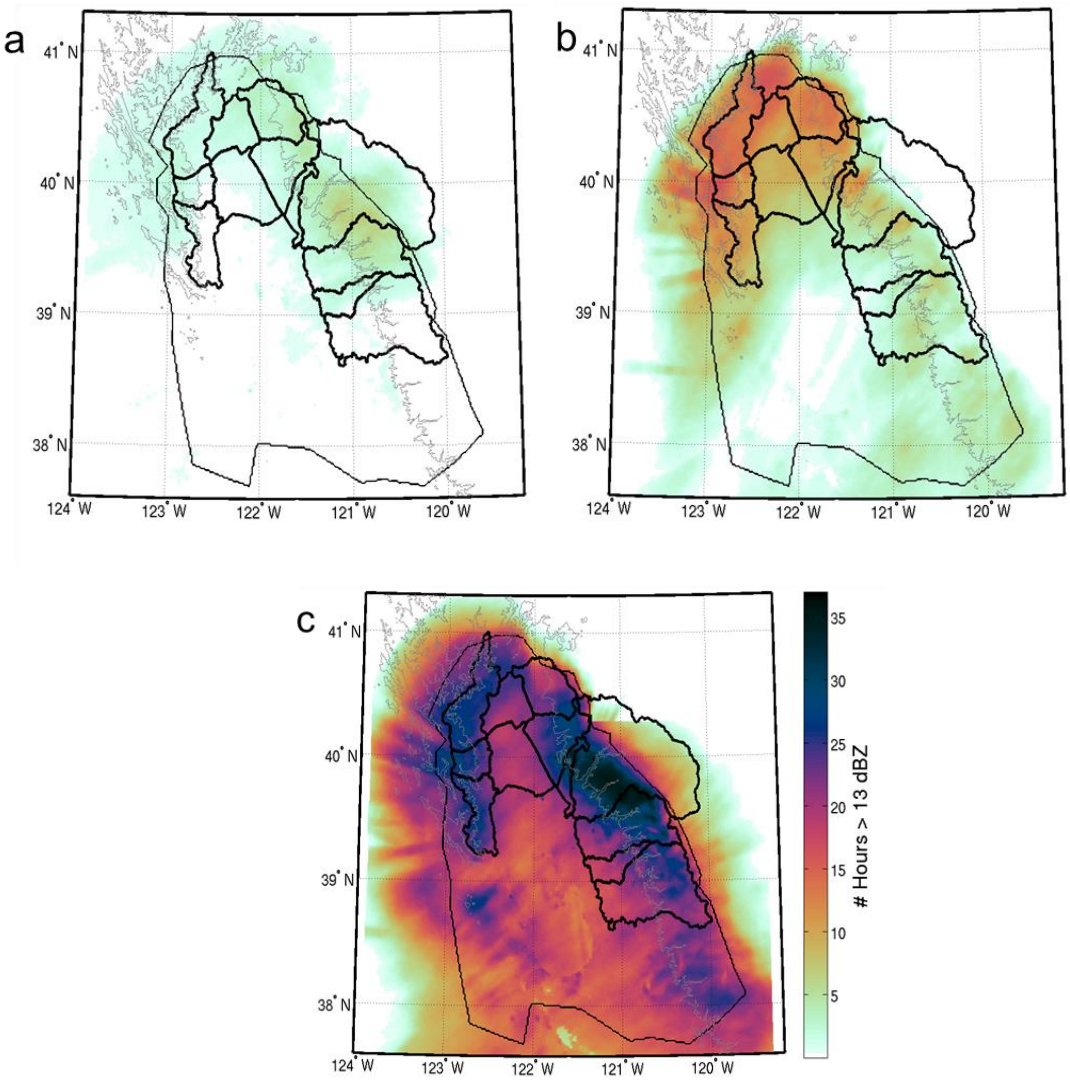

Figure 3.9 Three examples of regional precipitation frequency composites for atmospheric river events beginning on a) 8 Nov 2006, b) 7 Nov 2005, and c) 18 Dec 2005. Panel a) is a westerly event. Panel b) is a southwesterly event. Panel c) is a southerly event. These precipitation frequency maps have been multiplied by the duration of atmospheric river conditions such that darker colors represent longer durations of precipitation versus lighter colors. The thin, black line indicates the radar data quality mask extent. The thin gray line indicates 1 km MSL altitude. The thick, black lines indicate the 12 watershed boundaries.

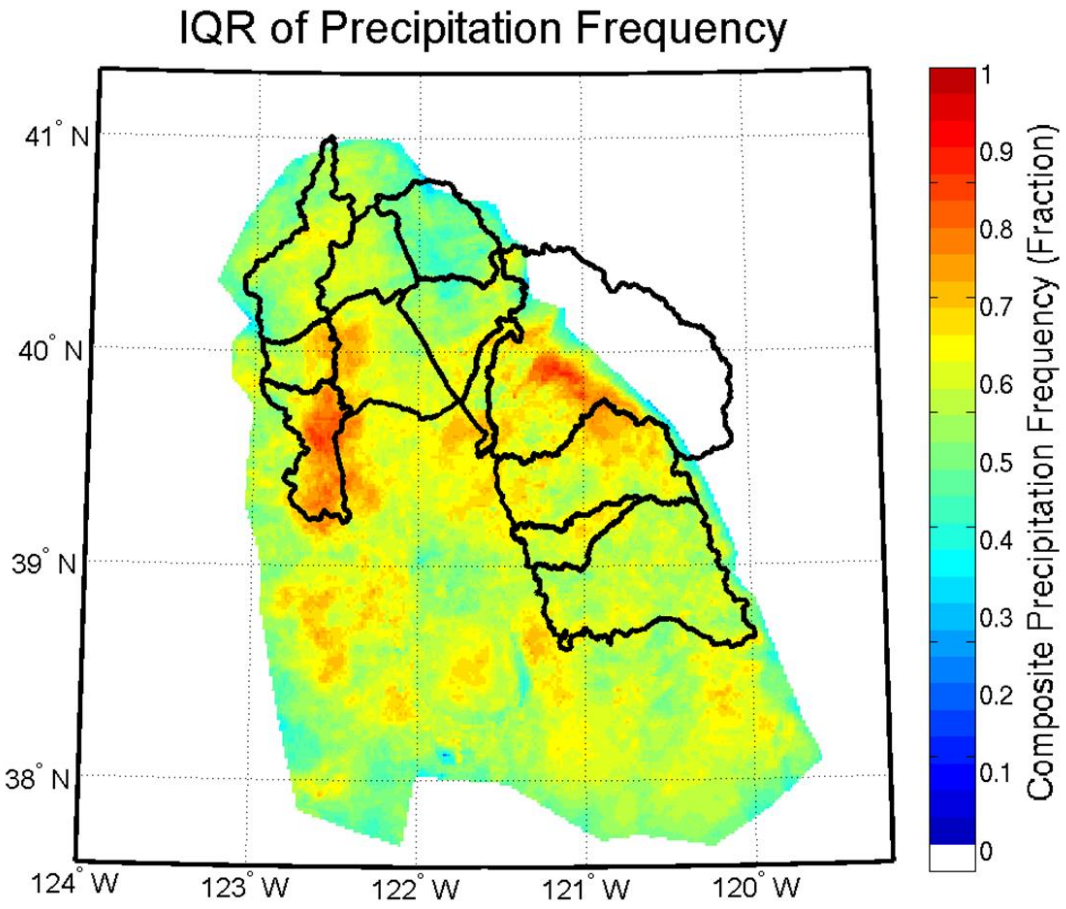

Figure 3.10 The inter-quartile range (75th minus the 25th percentile) of precipitation frequency values in units of fraction in the 64 atmospheric river event precipitation frequency composite. Thick, black lines indicate the 12 watershed boundaries. Data are only displayed for locations within the data quality mask.

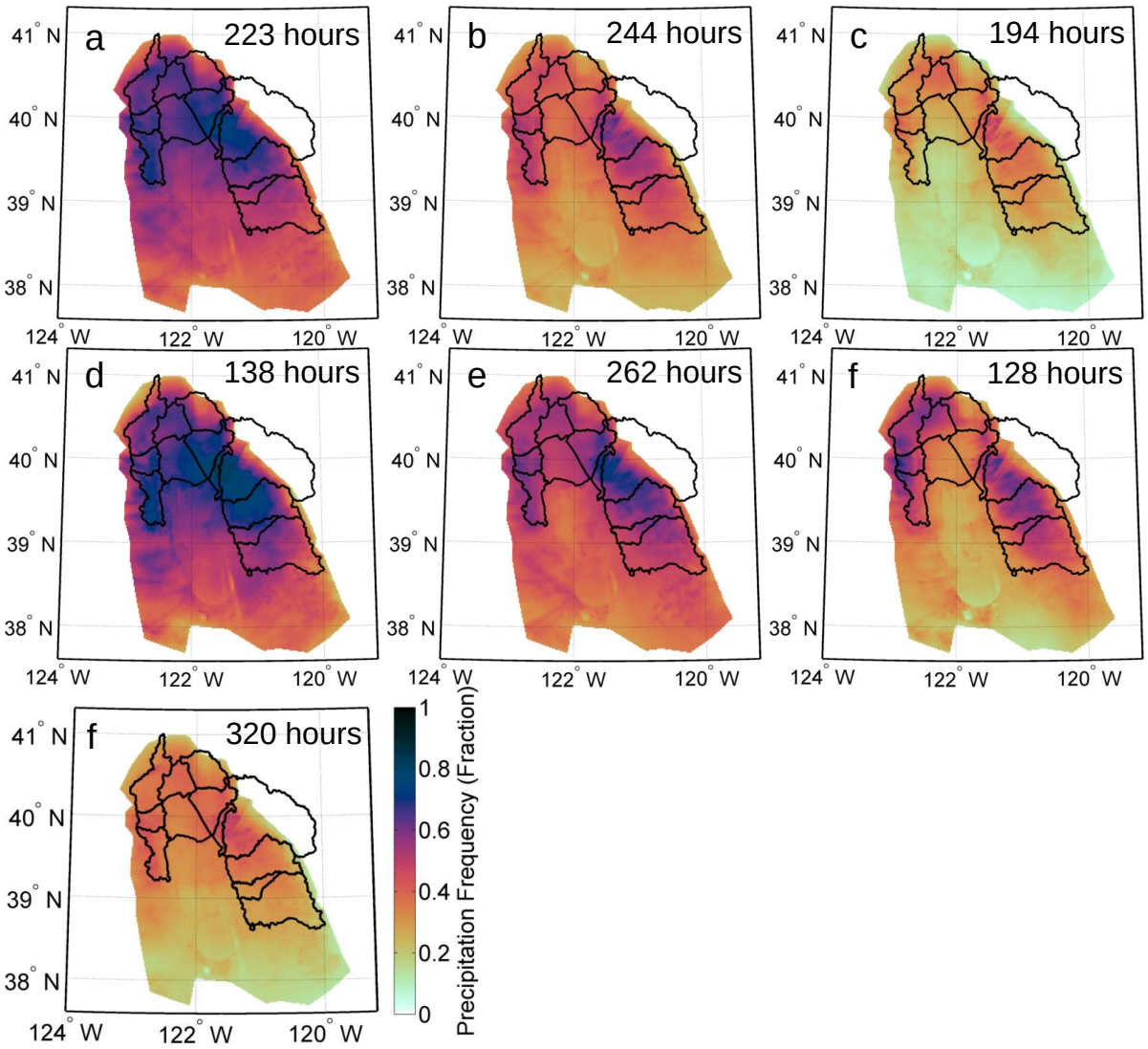

Figure 3.11 Composite precipitation frequency maps in units of fraction for southerly, southwesterly, and westerly wind directions at the onset of atmospheric river conditions (a-c, respectively), high, middle, and low altitude Sierra barrier jet sub-atmospheric river periods (d-f, respectively), and sub-atmospheric river periods without a Sierra barrier jet (g). The thin gray line indicates 1 km MSL altitude. The thick, black lines indicate the 12 watershed boundaries. The total duration of atmospheric river events and sub-atmospheric river periods is indicated in the top right of each frame. Data outside the data quality mask are not displayed.

Figure 3.12 Composite precipitation frequency maps in units of fraction for high, middle, and low mean upslope wind categories (a-c, respectively) and high, middle, and low upslope IWV flux categories (bottom panel, respectively). The thin gray line indicates 1 km MSL altitude. The thick, black lines indicate the 12 watershed boundaries. The total duration of atmospheric river events and sub-atmospheric river periods is indicated in the top right of each frame. Data outside the data quality mask are not displayed. Color scale is the same as in figure 3.11.

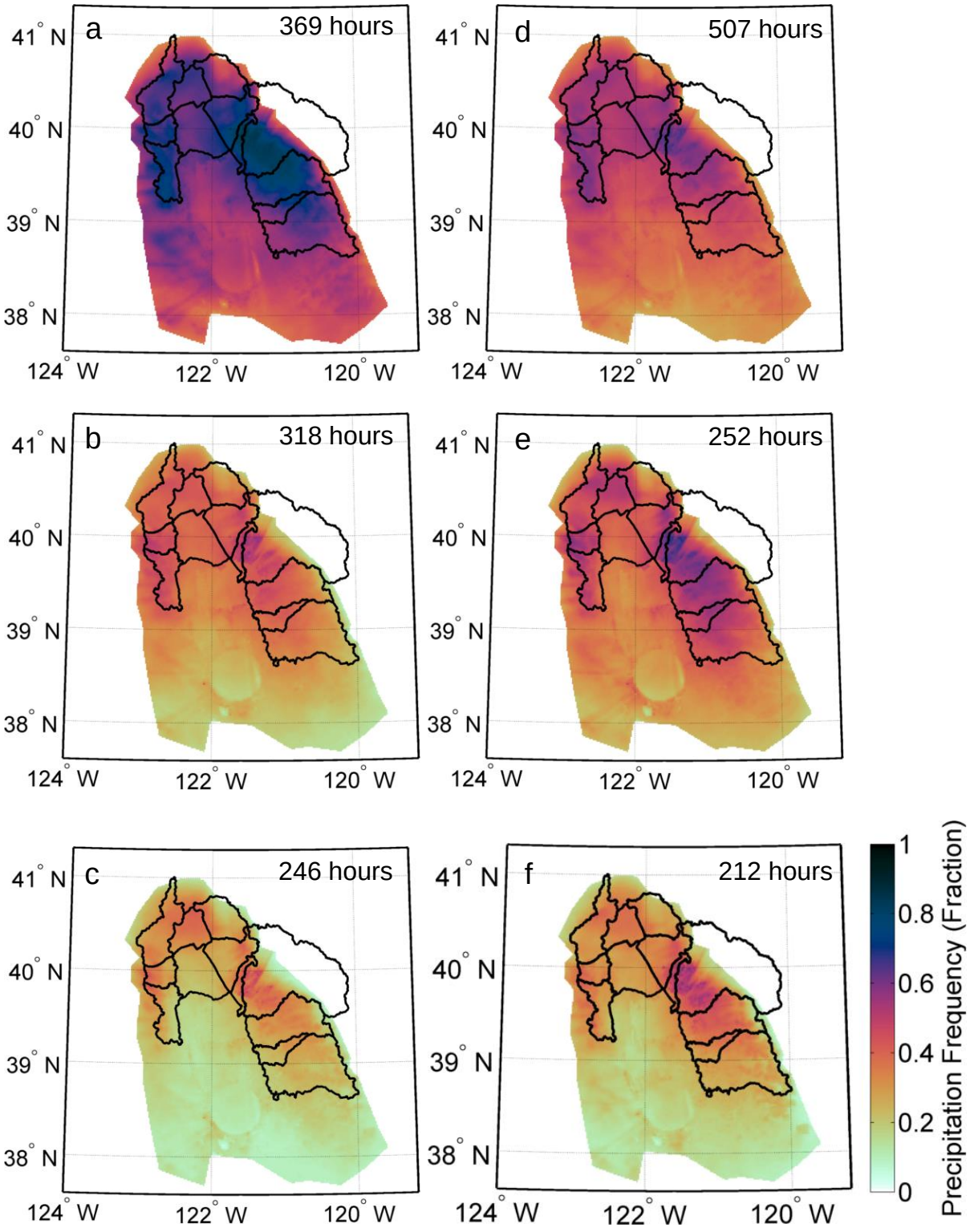
a
369 hours
d
507 hours
b
318 hours
e
252 hours
c
246 hours
f
212 hours
41° N
40° N
39° N
38° N
124° W
122° W
120° W
1
0.8
0.6
0.4
0.2
0
Precipitation Frequency (Fraction)

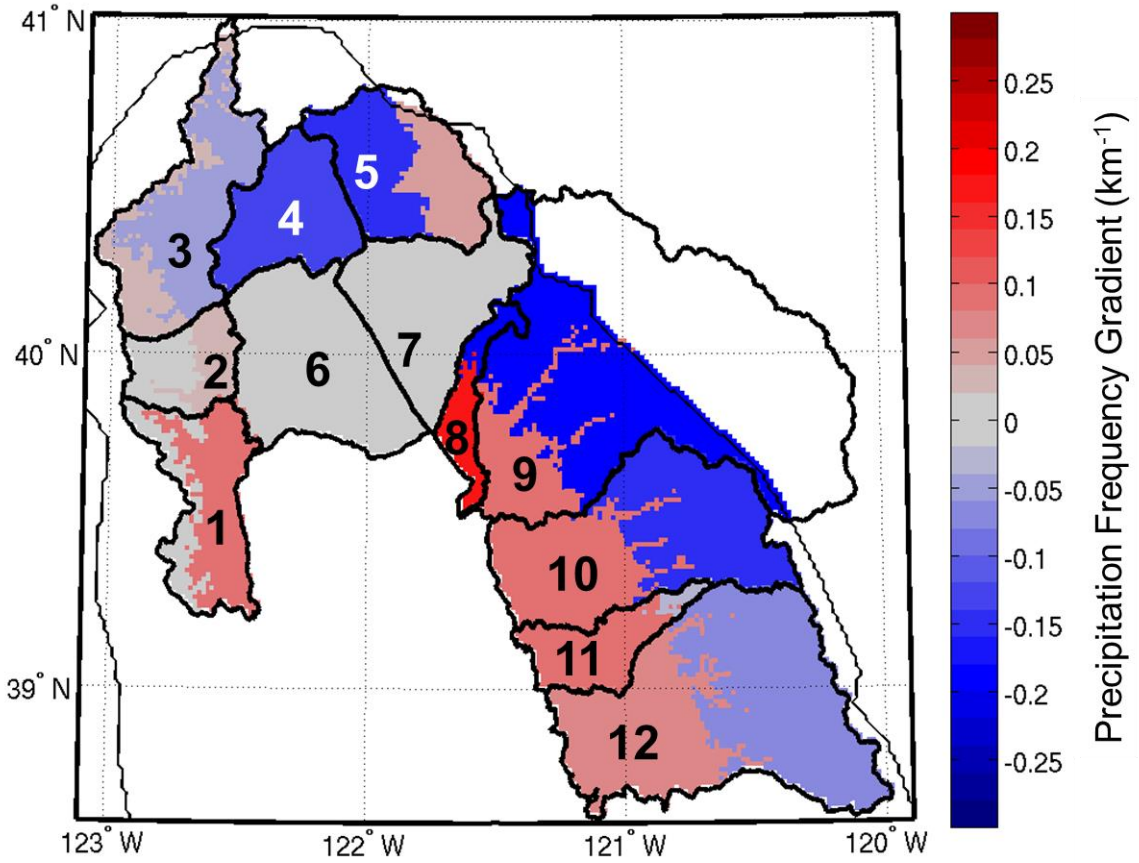

Figure 3.13 Precipitation frequency gradient in units of km^{-1} using the 64 storm precipitation frequency composite (Fig. 2.6) is shaded with red colors denoting positive precipitation frequency gradients, blue colors denoting negative precipitation frequency gradients, and gray colors denoting near zero precipitation frequency gradients. Basins have been divided into elevations above and below 1 km MSL where applicable and are shaded according to their precipitation frequency gradients over their appropriate elevation ranges. Portions of basins where numbers are overlaid indicate elevations below 1 km MSL, and numbers on each basin correspond to the basin numbers provided in Fig. 2.1. The thin, black line indicates the radar data quality mask, where data are not used in the calculation of the precipitation frequency gradient. Thick, black lines indicate the 12 watershed boundaries.

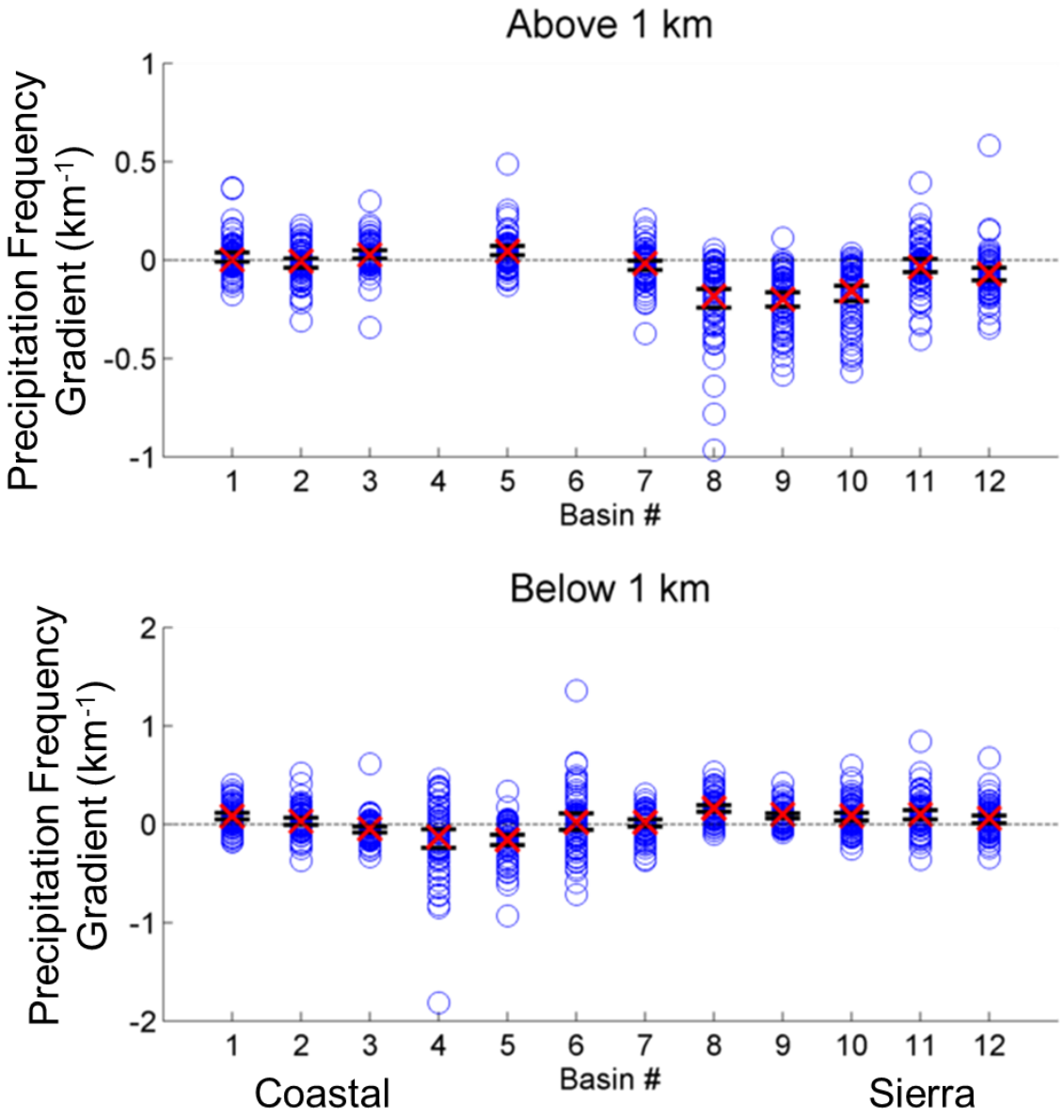

Figure 3.14 Precipitation frequency gradient in units of km-1 for each of 64 single-storm precipitation frequency composites (hollow, blue circles) above (top panel) and below (bottom panel) 1 km MSL. The 95% confidence interval in the mean assuming a normal distribution is indicated by the black, horizontal dashes. Red Xs indicate the 64 atmospheric river event composite precipitation frequency gradient as in Fig. 3.13. Basin numbers correspond to the basin numbers in Fig. 2.1.

Figure 3.15 Precipitation frequency as a function of elevation MSL from Sierra barrier jet altitude (top) and wind direction at Bodega Bay at the onset of atmospheric river conditions (bottom) environmental variable composites versus elevation within portions of the Feather, Bear, Yuba, and American watersheds and portions of low elevations of the Central Valley used in Lundquist et al. (2010). Hollow circles indicate the 50th percentile of the distribution of precipitation frequency in each elevation bin. Small circles and connecting dashed horizontal lines indicate the 25th and 75th percentiles of the distribution of precipitation frequency in each elevation bin. Thick, solid lines indicate the linear best fit through the 50th percentiles of the distribution for the below and above 1 km MSL separately. Gold colors indicate the westerly wind direction and low altitude Sierra barrier jet precipitation frequency composites. Magenta colors indicate the southwesterly wind direction and middle altitude Sierra barrier jet precipitation frequency composites. Navy blue colors indicate the southerly wind direction and high altitude Sierra barrier jet precipitation frequency composites. Black colors indicate the no Sierra barrier jet composites.

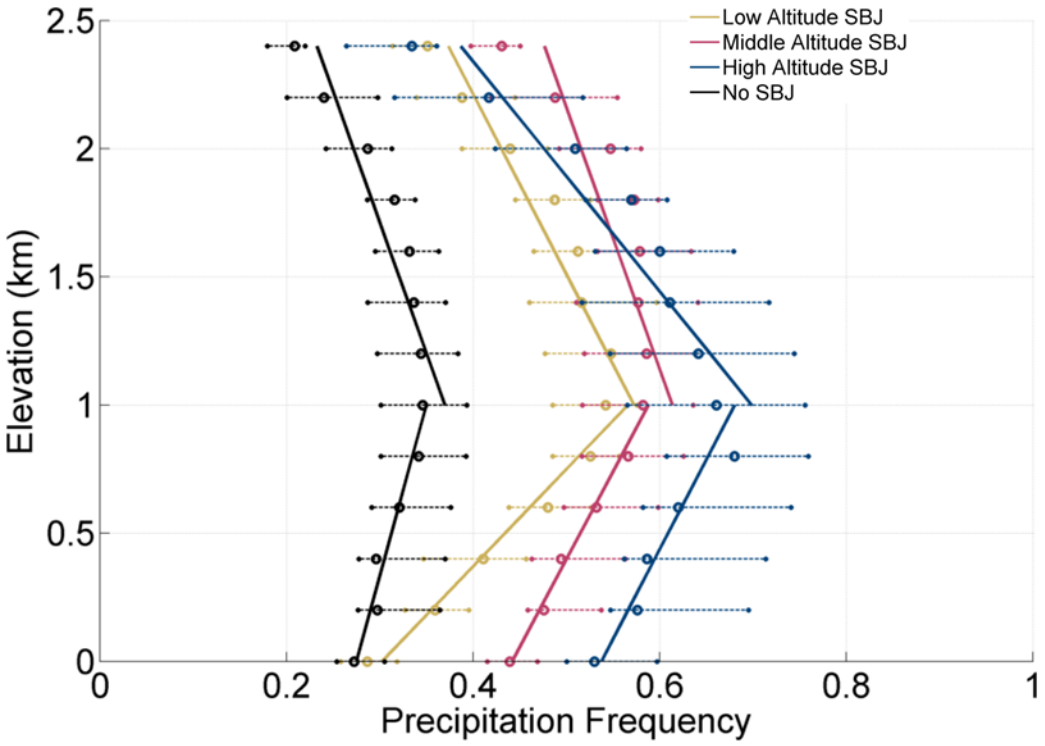
Low Altitude SBJ
Middle Altitude SBJ
High Altitude SBJ
No SBJ
Elevation (km)
Precipitation Frequency
0
0.5
1
1.5
2
2.5
0.2
0.4
0.6
0.8

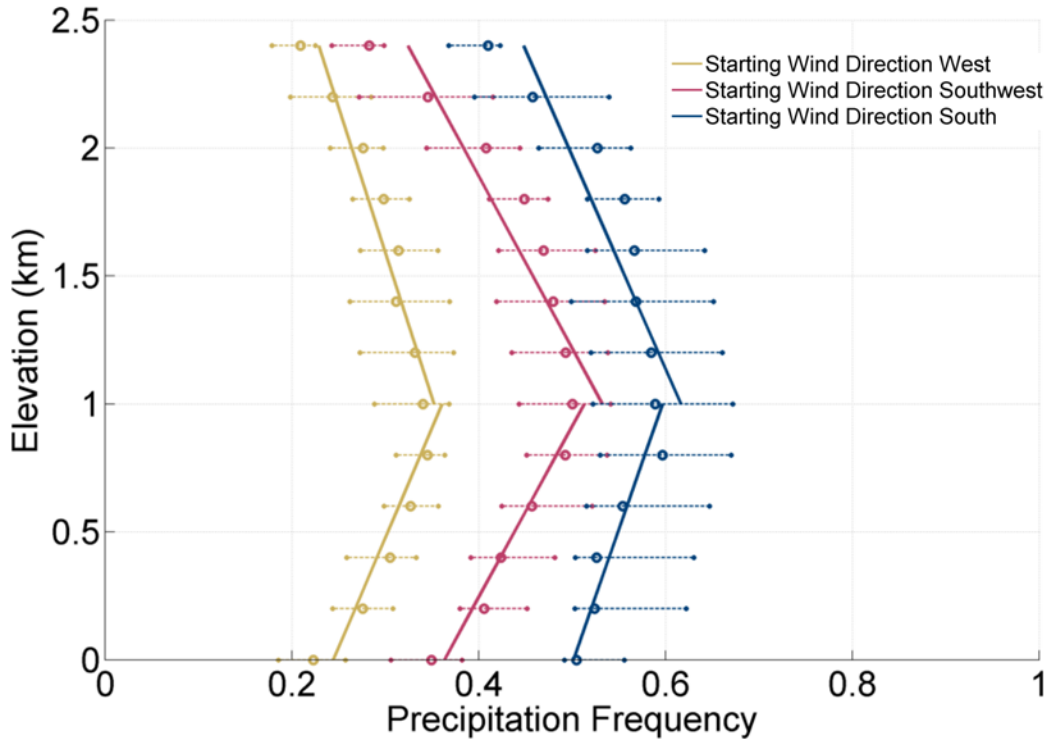
Starting Wind Direction West
Starting Wind Direction Southwest
Starting Wind Direction South
Elevation (km)
Precipitation Frequency
0
0.5
1
1.5
2
2.5
0.2
0.4
0.6
0.8

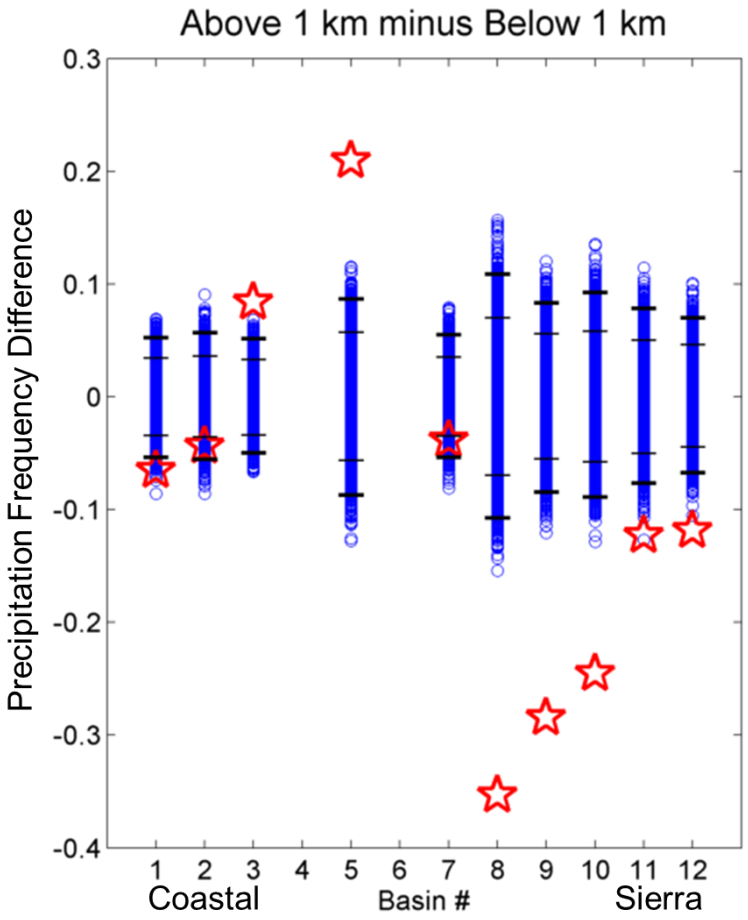

Figure 3.16 Results of the Monte Carlo test of the significance of the 1 km inflection point in precipitation frequency gradient along mountain slopes. The true value of the mean difference in precipitation frequency gradient above and below 1 km of 64 precipitation frequency composites in each watershed are indicated by hollow, red stars. The mean precipitation frequency gradient above 1 km minus the precipitation frequency gradient below 1 km in each basin using random groupings of precipitation frequency gradients of the individual 64 atmospheric river precipitation frequency maps are indicated by hollow, blue circles. The inner 90% (thin) and 99% (thick) of the random grouping distributions are indicated by black dashes. Basin numbers correspond to the basin numbers in Fig. 2.1. Basins 4 and 6 are the Redding and Tehama basins that do not extend above 1 km MSL, so the difference in precipitation frequency gradient above and below 1 km MSL cannot be calculated.

Table 3.1 Summary of relationships among the wind direction at the start of the atmospheric river conditions at Bodega Bay and environmental variable and cyclone characteristics.

Wind direction at onset of atmospheric river conditions	**Southerly**	**Westerly**
Duration of atmospheric river event	longer	shorter
Height of Sierra barrier jet	higher	lower
Magnitude of mean upslope winds	higher	lower
Storm total upslope IWV flux	higher	lower
Precipitation frequency in the Central Valley	higher	lower
Precipitation frequency gradient on the Sierra Nevada slopes (Change in precipitation frequency from valley to Sierra slopes)	smaller	larger

CHAPTER IV - Conclusions

In this study, NWS radar-derived precipitation frequency is used to characterize the spatial distribution and variability of precipitation from 64 atmospheric river events in the northern Central Valley of California and the interior mountain slopes. Three locations in the radar domain frequently experience locally higher precipitation frequencies, regardless of varying environmental factors: the lee slopes of the Coastal Mountains, the northern end of the Central Valley, and the windward slopes of the northern Sierra Nevada Mountains, especially near the Plumas National Forest (centered at 40.0 ºN, 120.7 ºW, Reeves et al. 2008). Precipitation frequencies along the lee Coastal Mountain slopes and at high altitudes of the Sierra Nevada slopes tend to have higher storm-to-storm variability than other regions in the radar domain. Figure 3.9 illustrates the drastic differences in precipitation frequency from event to event. These three events caution against expecting similar precipitation patterns from all atmospheric river events.

We observed a number of covariations among environmental variables and wind direction at the onset of atmospheric river conditions on the coast. Southerly winds at the onset of atmospheric river conditions are associated with longer durations of atmospheric river conditions, higher magnitudes of upslope (from 230 degrees) winds, storm total IWV flux, and higher altitude Sierra barrier jets compared to atmospheric river conditions with westerly winds. We stress that the relationship among wind direction and Sierra barrier jet altitude is ambiguous given the weaknesses in the commonly used definition of the Sierra barrier jet (Neiman et al. 2010, 2013, Lundquist et al. 2010) in that there are no thermodynamic constraints on the wind profile. This means that a jet in the central valley oriented parallel to the Sierra Nevadas (such as the pre-frontal low-level jet in an atmospheric river) may be flagged as a Sierra barrier jet even if it is not located within a stable barrier.

Sixty-three percent of the cyclones associated with the atmospheric rivers in this study are in the mature stages of the Norwegian cyclone model (stages 3 and 4) and 49% of the cyclones have a northeastward component to the 24-hour cyclone track. Relationships among cyclone latitude, longitude, and wind direction at the coast at the onset of atmospheric

river conditions are weak. There appears to be a relationship between the orientation of the cold front associated with the atmospheric river and the wind direction at the coast at the onset of atmospheric river conditions. A north-south oriented cold front is more likely to be associated with southerly winds at the coast and a more nearly west-east oriented cold front is more likely to be associated with westerly winds at the coast.

The atmospheric river events are placed into three categories based on wind direction at a coastal wind profiler at the onset of atmospheric river conditions: southerly (154.5 - 186.0^{o}), southwesterly (186.0 - 230.5^{o}), and westerly (230.5 - 287.5^{o}). Southerly and southwesterly events are the only events that last longer than 20 hours, and their winds tend to turn westerly with time (Fig. 2.2). In a given hour, southerly storms are more likely to be raining everywhere in the domain. This implies that in southerly storms, the precipitation area is more widespread throughout the duration of atmospheric river conditions as opposed to the westerly cases (Fig. 3.11). Precipitation frequency in the westerly events is maximized at the three previously mentioned hotspots, with a distinct minimum over the low elevations of the Central Valley. We emphasize that southerly events produce greater values of precipitation frequency as a baseline, and the difference in orographic enhancement on middle slopes of the Sierra Nevada Mountains are weak.

A Sierra barrier jet was not observed in 38% of the periods where Sierra barrier jet data were available. Low altitude Sierra barrier jet periods are more likely to produce weaker precipitation frequencies than high altitude Sierra barrier jet periods, especially at the low elevations of the Central Valley. The slight co-variation between wind direction and the height of the Sierra barrier jet makes the attribution of precipitation frequency patterns to solely the Sierra barrier jet altitude or wind direction more difficult.

Consistent with previous studies (Colle 2004, Smith and Barstad 2004, James and Houze 2005, Yuter et al. 2011), greater mean upslope wind speeds are associated with higher frequencies of precipitation (Fig. 3.12a-c). Events in this study with the highest total wind speeds, regardless of the speed of the upslope component, are more likely to have southerly wind directions at the onset of atmospheric river conditions. Thus, high upslope speed events tend to produce precipitation patterns similar to southerly wind events.

The gradient of precipitation frequency with elevation was calculated above and below 1 km altitude MSL in an effort to evaluate the results of a 27-year average of PRISM and linear model output for this region where precipitation accumulation was shown to have an inflection point at 1 km MSL (Lundquist et al. 2010). Our radar-derived results generally concur with the Smith and Barstad (2004) linear model as analyzed by Lundquist et al. (2010). Atmospheric river events tend to produce increasing precipitation frequency from sea level to 1 km altitude, and decreasing precipitation frequency above 1 km along the Sierra Mountains (Fig. 3.13). PRISM indicates nearly constant precipitation with height above 1 km altitude, which does not agree with our radar observations. Because of our greater spatial observational coverage and PRISM's limited rain gauge inputs, we are confident that the radar observations in this study are more representative of the ground truth. Thus, PRISM will over-predict precipitation at elevations above 1 km the Sierra Nevadas. This has direct implications for water resource management in reservoirs located above 1 km MSL on the Sierra Nevada slopes.

The 1 km MSL inflection point was determined to be significant (99% not due to chance) for the Stony Creek and Shasta Bally basins on the lee of the Coastal Range, and the Whitmore, Butte Creek, Feather River, Yuba River, Bear River, and American River basins along the windward Sierra Nevada slopes (Fig. 3.16). As wind direction shifts, there is a more pronounced change in precipitation frequency in the valley as compared to middle elevations. Thus, the gradient in precipitation frequency and by implication, orographic enhancement by terrain, is primarily governed by the change in precipitation frequency at low elevations in the northern portion of California's central valley.

Future work should attempt to quantify the relationship between the orientation of the cold front and atmospheric river characteristics. While trends in this study hint that a north-south oriented cold front is more likely to produce southerly winds at the onset of atmospheric river conditions at Bodega Bay, CA, this relationship should be quantified. Additionally, future work should include thermodynamic constraints on the definition of a Sierra barrier jet, such that a jet flagged by a wind profiler must also be within a stable barrier.

REFERENCES

Bao, J-W, S. A. Michelson, P. J. Neiman, F. M. Ralph, and J. M. Wilczak, 2006: Interpretation of Enhanced Integrated Water Vapor Bands Associated with Extratropical Cyclones: Their Formation and Connection to Tropical Moisture. Mon. Wea. Rev., 134, 1063–1080. doi: http://dx.doi.org/10.1175/MWR3123.1

Bevis M., Businger S., Herring T. A., Rocken C., Anthes R. A.and Ware R. H., 1992: GPS meteorology: remote sensing of the atmospheric water vapor using the global positioning system. *Journal of Geophysical Research*, **97**, 75–94.

Biasutti, M., S. E. Yuter, C. D. Burleyson, and A. H. Sobel, 2011: Very high resolution rainfall patterns measured by TRMM precipitation radar: seasonal and diurnal cycles. Clim. Dyn., 39, 239–258, doi:10.1007/s00382-011-1146-6.

Bjerknes, J., and H. Solberg, 1922: Life cycle of cyclones and the polar front theory of atmospheric circulation. Geofys. Publ.,3 (1), 3–18.

Colle, Brian A., 2004: Sensitivity of Orographic Precipitation to Changing Ambient Conditions and Terrain Geometries: An Idealized Modeling Perspective. J. Atmos. Sci., 61, 588–606.

Cunningham, J., and S. Yuter, 2014: Instability Characteristics of Radar-Derived Mesoscale Organization Modes within Cool-Season Precipitation near Portland, Oregon*. *Monthly Weather Review*, **142**, 1738–1757, doi:10.1175/MWR-D-13-00133.1.

Daly, C., P. Neilson, andD. L. Phillips, 1994:Astatistical-topographic model for mapping climatological precipitation over mountainous terrain. J. Appl. Meteor., 33, 140–158.

Dettinger, M., F. Ralph, T. Das, P. Neiman, and D. Cayan, 2011: Atmospheric Rivers, Floods and the Water Resources of California. Water, 3, doi:10.3390/w3020445

Doneaud, AndréA., Amos Makarau, and L. Ronald Johnson, 1988: A Modified ATI Technique for Nowcasting Convective Rain Volumes over Areas. J. Appl. Meteor., 27, 491–502.

Duan, J., and Coauthors, 1996: GPS meteorology: direct estimation of the absolute value of precipitable water. *Journal of Applied Meteorology*, **35**, 830–838.

Galewsky, J., and Adam Sobel, 2005: Moist Dynamics and Orographic Precipitation in Northern and Central California during the New Year's Flood of 1997. Mon. Wea. Rev., 133, 1594–1612. doi: http://dx.doi.org/10.1175/MWR2943.1

Hagen, M., and S. E. Yuter, 2003: Relation between radar reflectivity and rainfall rate during the MAP-SOP. Quart. J. Roy. Meteor. Soc., **129**, 477–493.

James, C., and R. Houze, 2005: Modification of Precipitation by Coastal Orography in Storms Crossing Northern California. Monthly Weather Review, 133, 3110–3131, doi:10.1175/MWR3019.1.

Jeton, A. E., M. D. Dettinger, and J. LaRue Smith, 1996: Potential effects of climate change on streamflow, eastern and western slopes of the Sierra Nevada, California and Nevada. USGS Water Resources Investigations Rep. 95-4260, 44 pp.

Kingsmill, D., P. Neiman, B. Moore, M. Hughes, S. Yuter, and F. Ralph, 2013: Kinematic and Thermodynamic Structures of Sierra Barrier Jets and Overrunning Atmospheric Rivers during a Landfalling Winter Storm in Northern California. Mon. Wea. Rev., 141, 20152036, doi:10.1175/MWR-D-12-00277.1.

Lackmann, G.M. and John R. Gyakum, 1999: Heavy Cold-Season Precipitation in the Northwestern United States: Synoptic Climatology and an Analysis of the Flood of 17–18 January 1986. Wea. Forecasting, 14, 687–700. doi: http://dx.doi.org/10.1175/1520-0434(1999)014<0687:HCSPIT>2.0.CO;2

Lund, J. R., 2007: Envisioning Futures for the Sacramento–San Joaquin Delta. Public Policy Institute of California, 285 pp.

Lundquist, Jessica D., Justin R. Minder, Paul J. Neiman, Ellen Sukovich, 2010: Relationships between Barrier Jet Heights, Orographic Precipitation Gradients, and Streamflow in the Northern Sierra Nevada. *J. Hydrometeor*, **11**, 1141–1156.

Marwitz, J.D., 1983: The Kinematics of Orographic Airflow During Sierra Storms. J. Atmos. Sci., 40, 1218–1227. doi: http://dx.doi.org/10.1175/1520-0469(1983)040<1218:TKOOAD>2.0.CO;2

Marwitz, J.D,. 1986: A Comparison of Winter Orographic Storms over the San Juan Mountains and the Sierra Nevada. Meteorological Monographs, 21, 109–114. doi: http://dx.doi.org/10.1175/0065-9401-21.43.109

Marwitz, J.D., 1987: Deep Orographic Storms over the Sierra Nevada. Part I: Thermodynamic and Kinematic Structure. J. Atmos. Sci., 44, 159–173. doi: http://dx.doi.org/10.1175/1520-0469(1987)044<0159:DOSOTS>2.0.CO;2

Mattioli, V., E. R. Westwater, C. Cimini, J. S. Liljegren, B. M. Lesht, S. I. Gutman, and F. J. Schmidlin, 2007: Analysis of radiosonde and ground-based remotely sensed PWV data from the 2004 North Slope of Alaska Arctic Winter Radiometric Experiment. J. Atmos. Oceanic Technol., 24, 415–431.

Medina, Ellen Sukovich, and Robert A. Houze Jr., 2007: Vertical Structures of Precipitation in Cyclones Crossing the Oregon Cascades. Mon. Wea. Rev., 135, 3565–3586. doi: http://dx.doi.org/10.1175/MWR3470.1

Mohr, C. G., L. Jay Miller, R. L. Vaughan, and H. W. Frank, 1986: The merger of mesoscale datasets into a common Cartesian format for efficient and systematic analyses. J. Atmos. Oceanic Technol., 3, 143–161

NOAA National Weather Service, Radar Operations Center (1991): NOAA Next Generation Radar (NEXRAD) Level II Base Data. NOAA National Centers for Environmental Information. doi:10.7289/V5W9574V [2016]

Neiman, P. J., F. M. Ralph, A. B. White, D. E. Kingsmill, and P. O. G.Persson, 2002: The statistical relationship between upslope flow and rainfall in California's coastal mountains: Observations during CALJET. Mon. Wea. Rev., 130, 1468–1492.

Neiman, P. J., F. M. Ralph, G. A. Wick, J. Lundquist, and M. D. Dettinger, 2008: Meteorological characteristics and overland precipitation impacts of atmospheric rivers affecting the west coast of North America based on eight years of SSM/I satellite observations. J. Hydrometeor., 9, 22–47.

Neiman, P., D. Gottas, A. White, S. Gutman, and F. Ralph, 2009: A water vapour flux tool for precipitation forecasting. Proceedings of the ICE - Water Management, 162, 8394, doi:10.1680/wama.2009.162.2.83.

Neiman, P., E. Sukovich, F. Ralph, and M. Hughes, 2010: A Seven-Year Wind Profiler–Based Climatology of the Windward Barrier Jet along California's Northern Sierra Nevada. *Mon. Wea. Rev.*, **138**, 12061233, doi:10.1175/2009MWR3170.1.

Neiman, Paul J., Mimi Hughes, Benjamin J. Moore, F. Martin Ralph, and Ellen M. Sukovich, 2013: Sierra Barrier Jets, Atmospheric Rivers, and Precipitation Characteristics in Northern California: A Composite Perspective Based on a Network of Wind Profilers. Mon. Wea. Rev., **141**, 4211–4233. doi: 10.1175/MWR-D-13-00112.1

Oye, D., and M. Case, 1995: REORDER: A program for gridding radar data—Installation and use manual for the UNIX version. Atmospheric Technology Division, National Center for Atmospheric Research, 20 pp. [Available from Atmospheric Technology Division, NCAR, P.O. Box 3000, Boulder, CO 80307].

Panziera, L., and U. Germann, 2010: The relation between airflow and orographic precipitation on the southern side of the Alps as revealed by weather radar. Quart. J. Roy. Meteor. Soc., 136, 222–238.

Parish, T.R. 1982: Surface Airflow Over East Antarctica. Mon. Wea. Rev., 110, 84–90. doi: http://dx.doi.org/10.1175/1520-0493(1982)110<0084:SAOEA>2.0.CO;2

Pierrehumbert, R. T., and B. Wyman, 1985: Upstream effects of mesoscale mountains. J. Atmos. Sci., 42, 977–1003.

Ralph, F. M., P. J. Neiman, and G. A. Wick, 2004: Satellite and CALJET aircraft observations of atmospheric rivers over the eastern North Pacific Ocean during the winter of 1997/98. Mon. Wea. Rev., 132, 1721–1745.

Ralph, F. M., and Coauthors, 2005: Improving short term (0–48 hour) cool season quantitative precipitation forecasting: Recommendations from a USWRP workshop. *Bull. Amer. Meteor. Soc.*, **86,** 1619–1632.

Ralph, F. M., P. J. Neiman, G. A. Wick, S. I. Gutman, M. D. Dettinger, D. R. Cayan, and A. B. White, 2006: Flooding on California's Russian River: The role of atmospheric rivers. Geophys. Res. Lett., 33, L13801, doi:10.1029/2006GL026689.

Ralph, F., T. Coleman, P. Neiman, R. Zamora, and M. Dettinger, 2013: Observed Impacts of Duration and Seasonality of Atmospheric-River Landfalls on Soil Moisture and

Runoff in Coastal Northern California. J. Hydrometeor, 14, 443-459, doi:10.1175/JHM-D-12-076.1.

Reeves, H.D., and Yuh-Lang Lin, 2007: The Effects of a Mountain on the Propagation of a Preexisting Convective System for Blocked and Unblocked Flow Regimes. J. Atmos. Sci., 64, 2401–2421. doi: http://dx.doi.org/10.1175/JAS3959.1

Reeves, Heather Dawn, Yuh-Lang Lin, Richard Rotunno, 2008: Dynamic Forcing and Mesoscale Variability of Heavy Precipitation Events over the Sierra Nevada Mountains. *Mon. Wea. Rev.*, **136**, 62–77, doi:10.1175/2007MWR2164.1

Reynolds, D. W., and A. S. Dennis, 1986: A review of the Sierra Cooperative Pilot Project. Bull. Amer. Meteor. Soc., 67, 513–523.

Saha, S., and Coauthors, 2010: The NCEP Climate Forecast System Reanalysis. Bull. Amer. Meteor. Soc., **91**, 1015–1097, doi:10.1175/ 2010BAMS3001.1

Schultz, David M., and Geraint Vaughan, 2011: Occluded Fronts and the Occlusion Process: A Fresh Look at Conventional Wisdom. Bull. Amer. Meteor. Soc., 92, 443–466.

Smith, B. L., S. E. Yuter, P. J. Neiman, and D. E. Kingsmill, 2010: Water vapor fluxes and orographic precipitation over northern California associated with a landfalling atmospheric river. Mon. Wea. Rev., 138, 74–100.

Smith, Ronald B. and Idar Barstad, 2004: A Linear Theory of Orographic Precipitation. J. Atmos. Sci., 61, 1377–1391.

Steiner, M., O. Bousquet, R. A. Houze, B. F. Smull, and M. Mancini. 2003. Airflow within major alpine river valleys under heavy rainfall. Quart. J. Roy. Meteor. Soc. 129:411–432.

Yuter, S.E., D. A. Stark, J. A. Crouch, M. J. Payne, and B. A. Colle, 2011: The impact of varying environmental conditions on the spatial and temporal patterns of orographic precipitation over the Pacific Northwest near Portland, Oregon. J. Hydrometeor., **12**, 329–351, doi:10.1175/2010JHM1239.1.

Zhu, Y., and R. E. Newell, 1998: A proposed algorithm for moisture fluxes from atmospheric rivers. Mon. Wea. Rev., 126, 725–735.

APPENDICES

Appendix A

Table of all start and end times from Ralph et al. (2013) used in the current study and the environmental variable values and categories used in environmental variable subsets.

Start Date (MM/DD/YYYY) & Time (UTC)	End Date (MM/DD/YYYY) & Time (UTC)	AR duration (hours)	Wind direction at AR onset at BBY (degrees)	Wind direction at AR onset at BBY Category	Mean upslope wind speed at BBY (m/s)	Mean upslope wind speed at BBY category	Time integrated upslope IWV flux (cm m/s)	Time-integrated upslope IWV flux category	SBJ period duration (hours)	CCO SBJ altitude (m MSL)	CCO SBJ altitude Category
03/19/2005 0400	03/19/2005 1600	12	154.89	south	13.656	high	411.4	middle	12	1328	high
03/22/2005 0100	03/22/2005 1000	9	158.18	south	16.895	high	390.8	middle	9	1171	middle
03/27/2005 1900	03/28/2005 2000	9	180.61	south	15.763	high	360.6	middle	1	NAN	no sbj
03/28/2005 2000	03/28/2005 0400								8	945	middle
05/15/2005 1100	05/15/2005 2100	10	283.86	west	4.282	low	156.2	low	10	NAN	no sbj
06/08/2005 0400	06/08/2005 1400	10							10	NAN	no sbj
06/17/2005 2000	06/18/2005 0400	8							8	NAN	no sbj
11/03/2005 1900	11/04/2005 0800	13	237.39	west	9.616	low	288.8	middle	13	708	middle
11/07/2005 0600	11/07/2005 0800	20	224.14	southwest	10.653	middle	593.8	high	2	NAN	no sbj
11/07/2005 0800	11/07/2005 2000								12	503	low
11/07/2005 2000	11/08/2005 0200								6	NAN	no sbj
11/25/2005 0500	11/25/2005 1700	12	239.29	west	9.726	low	391.8	middle	12	NAN	no sbj
11/28/2005 2000	11/29/2005 1300	17	188.27	southwest	10.710	middle	488.0	high	17	NAN	no sbj
12/18/2005 0500	12/20/2005 0000	43	169.39	south	16.335	high	1820.6	high	43	1180	middle
12/20/2005 1000	12/21/2005 0000	14	169.30	south	12.388	middle	496.7	high	14	NAN	no sbj
12/25/2005 1700	12/25/2005 0100	16	197.00	southwest	10.260	middle	163.3	low	8	NAN	no sbj
12/26/2005 0100	12/26/2005 0900								8	1059	middle
12/27/2005 0700	12/28/2005 1700	34	185.65	south	14.988	high	1610.8	high	34	968	middle
12/30/2005 0400	12/30/2005 0600	36	192.69	southwest	17.121	high	1894.1	high	2	NAN	no sbj
12/30/2005 0600	12/31/2005 1600								34	639	low
01/01/2006 1500	01/02/2006 0200	11	172.13	south	18.155	high	449.4	high	11	1056	middle
01/03/2006 2100	01/04/2006 0600	9	193.26	southwest	15.098	high			9	924	middle
01/10/2006 2300	01/11/2006 0300	10	254.10	west	7.525	low	210.1	low	4	NAN	no sbj
01/11/2006 0300	01/11/2006 0900								6	639	low
01/28/2006 1400	01/29/2006 0200	14	228.57	southwest	10.180	middle			12	537	low
01/29/2006 0200	01/29/2006 0400								2	NAN	no sbj
02/01/2006 0900	02/01/2006 2100	12	240.92	west	7.301	low	218.4	low	12	474	low
02/26/2006 1700	02/26/2006 1900	38	166.94	south	17.577	high	1768.9	high	2	NAN	no sbj
02/26/2006 1900	02/27/2006 2200								27	1340	high
02/27/2006 2200	02/28/2006 0700								9	NAN	no sbj
03/05/2006 0800	03/05/2006 1200	21	175.07	south	16.385	high	807.1	high	4	NAN	no sbj
03/05/2006 1200	03/06/2006 0500								17	1350	high
05/19/2006 1400	05/20/2006 0900	19	232.87	southwest	9.328	low	443.1	high	19	NAN	no sbj
05/23/2006 0600	05/23/2006 1400	8	178.77	south	8.814	low	159.1	low	8	NAN	no sbj
11/02/2006 0700	11/02/2006 1200	14	193.67	southwest	11.999	middle	473.9	high	5	NAN	no sbj
11/02/2006 1200	11/02/2006 2100								9	1039	middle

Start Date (MM/DD/YYYY) & Time (UTC)	End Date (MM/DD/YYYY) & Time (UTC)	AR duration (hours)	Wind direction at AR onset at BBY (degrees)	Wind direction at AR onset at BBY Category	Mean upslope wind speed at BBY (m/s)	Mean upslope wind speed at BBY category	Time-integrated upslope IWV flux (cm m/s)	Time-integrated upslope IWV flux category	SBJ period duration (hours)	CCO SBJ altitude (m MSL)	CCO SBJ altitude Category
11/08/2006 0400	11/08/2006 1300	9	287.21	west	4.826	low	137.7	low	9	NAN	no sbj
11/13/2006 0500	11/14/2006 0900	28	230.33	southwest	8.991	low	709.5	high	28	982	middle
11/16/2006 0700	11/16/2006 1000	8	271.47	west	7.437	low	163.9	low	3	664	low
11/16/2006 1000	11/16/2006 1500								5	NAN	no sbj
12/08/2006 2200	12/09/2006 0300	11	160.35	south	11.958	middle	335.0	middle	5	NAN	no sbj
12/09/2006 0300	12/09/2006 0900								6	1111	middle
12/11/2006 1500	12/11/2006 2000	16	203.52	southwest	10.852	middle	338.0	middle	5	NAN	no sbj
12/11/2006 2000	12/12/2006 0700								11	677	low
12/13/2006 0500	12/13/2006 0800	21	247.31	west	6.266	low	375.7	middle	3	NAN	no sbj
12/13/2006 0800	12/13/2006 2000								12	663	low
12/13/2006 2000	12/14/2006 0200								6	NAN	no sbj
12/21/2006 0700	12/22/2006 0000	17	205.58	southwest	11.381	middle	468.1	high	17	NAN	no sbj
12/26/2006 1300	12/26/2006 1400	13	202.68	southwest	17.923	high	653.6	high	1	NAN	no sbj
12/26/2006 1400	12/27/2006 0200								12	1384	high
01/03/2007 2100	01/04/2007 1000	13	265.98	west	7.350	low	242.0	middle	13	609	low
02/21/2007 2300	02/22/2007 0400	10	197.30	southwest	14.872	high	319.9	middle	5	862	middle
02/22/2007 0400	02/22/2007 0900								5	NAN	no sbj
05/01/2007 2200	05/02/2007 1100	13	287.50	west	6.578	low	232.2	middle	13	NAN	no sbj
07/18/2007 0000	07/18/2007 0800	8							8	NAN	no sbj
09/22/2007 0700	09/22/2007 1900	12							12	NAN	no sbj
10/09/2007 1900	10/10/2007 1000	15	194.49	southwest	10.589	middle	437.5	high	15	NAN	no sbj
10/12/2007 1000	10/12/2007 1800	8	175.07	south	9.666	low	211.0	low	8	NAN	no sbj
10/18/2007 1400	10/19/2007 0800	18	252.11	west	6.435	low	357.1	middle	18	NAN	no sbj
12/02/2007 1900	12/03/2007 0600	42	186.92	southwest	12.711	middle	1430.4	high	11	NAN	no sbj
12/03/2007 0600	12/03/2007 1600								10	768	middle
12/03/2007 1600	12/03/2007 2000								4	NAN	no sbj
12/03/2007 2000	12/04/2007 1100								15	1043	middle
12/04/2007 1100	12/04/2007 1300								2	NAN	no sbj
12/19/2007 2200	12/20/2007 1000	12	212.72	southwest	12.627	middle	410.0	middle	12	844	middle
01/10/2008 0900	01/10/2008 1800	9	237.31	southwest	9.122	low	222.7	low	9	NAN	no sbj
01/26/2008 0200	01/26/2008 1400	12	162.01	south	15.572	high	427.5	high	12	1643	high
02/02/2008 1900	02/03/2008 0700	12	232.39	southwest	12.783	high	341.9	middle	12	685	low
03/28/2008 1800	03/29/2008 0200	8	250.69	west	10.237	middle	178.7	low	8	NAN	no sbj
10/02/2008 0900	10/02/2008 1900	10	246.38	west	7.013	low			10	NAN	no sbj
10/03/2008 1400	10/04/2008 0800	18	250.35	west	10.320	middle			18	NAN	no sbj
10/31/2008 0500	10/31/2008 1600	11	159.63	south	13.181	high	367.6	middle	11	NAN	no sbj
12/21/2008 1400	12/21/2008 1700	12	236.88	southwest	12.076	middle	360.8	middle	3	NAN	no sbj
12/21/2008 1700	12/22/2008 0200								9	1004	middle
12/24/2008 1300	12/25/2008 0600	20	161.17	south	15.165	high	694.1	high	17	1575	high
12/25/2008 0600	12/25/2008 0900								3	NAN	no sbj
01/02/2009 0800	01/02/2009 1600	8	263.21	west	8.217	low	149.7	low	8	NAN	no sbj

Start Date (MM/DD/YYYY) & Time (UTC)	End Date (MM/DD/YYYY) & Time (UTC)	AR duration (hours)	Wind direction at AR onset at BBY (degrees)	Wind direction at AR onset at BBY Category	Mean upslope wind speed at BBY (m/s)	Mean upslope wind speed at BBY category	Time-integrated upslope IWV flux (cm m/s)	Time-integrated upslope IWV flux category	SBJ period duration (hours)	CCO SBJ altitude (m MSL)	CCO SBJ altitude Category
02/22/2009 0200	02/22/2009 1200	26	165.06	south	14.649	high	935.6	high	10	NAN	no sbj
02/22/2009 1200	02/23/2009 0200								14	982	middle
02/23/2009 0200	02/23/2009 0400								2	NAN	no sbj
03/01/2009 0900	03/01/2009 1600	10	164.38	south	11.513	middle	270.6	middle	7	NAN	no sbj
03/01/2009 1600	03/01/2009 1900								3	1342	high
03/15/2009 2000	03/16/2009 0500	9	211.42	southwest	7.841	low	172.6	low	9	NAN	no sbj
05/01/2009 1800	05/02/2009 0400	10	168.14	south	14.124	high	389.4	middle	10	NAN	no sbj
05/02/2009 1300	05/02/2009 2100	8	201.51	southwest	8.613	low	201.4	low	8	NAN	no sbj
05/03/2009 0500	05/03/2009 1500	10	191.45	southwest	10.372	middle	276.6	middle	10	NAN	no sbj
10/13/2009 0200	10/13/2009 0700	24	168.59	south	15.468	high	1132.1	high	5	NAN	no sbj
10/13/2009 0700	10/14/2009 0200								19	897	middle
12/15/2009 1900	12/16/2009 0300								8	NAN	no sbj
12/16/2009 0300	12/16/2009 1400								11	1550	high
01/17/2010 2000 01/17/2010 2100	01/17/2010 2100 01/18/2010 0500	9	198.79	southwest	17.408	high	329.1	middle	1 8	NAN 1295	no sbj high
03/29/2010 0200	03/29/2010 0700	18	243.64	west	10.171	middle	449.3	high	5	NAN	no sbj
03/29/2010 0700	03/29/2010 2000								13	1315	high
04/02/2010 1300	04/02/2010 2200	9	223.70	southwest	12.680	middle	269.0	middle	9	NAN	no sbj

Appendix B

Clutter map algorithm

1. Gathered low-level stability from all KOAK soundings available between 2001-2010
2. Downloaded 25 clear air periods (from NCEI). A clear air period is defined as the hour following a sounding with low-level stability in the 50th percentile or greater of all low-level stabilities
3. Composited all 25 hours together in polar space yielding a precipitation frequency > 13 dBZ map in units of % (fraction)
4. Grid cells where precipitation frequency was greater than 25% were flagged as clutter
5. A radius of 25 km (KBBX) and 30 km (KDAX) was also flagged as clutter due to high concentration of non-meteorological precipitation frequency near the antenna
6. 25 additional clear air periods were downloaded from NCEI for testing the cluttermap
7. Cluttermap is applied to only the lowest tilt of the volume. The radius 25 km around KBBX and 30 km around KDAX was removed from all tilts
8. Testing clear air periods were interpolated to a 3D Cartesian grid and composited yielding a precipitation frequency > 13 dBZ map in units of % (fraction)
9. The final composite yielded no grid cells with a precipitation frequency greater than 25%; cluttermap removes all clutter; cluttermap testing passes

Appendix C

Reflectivity calibration algorithm

Two volumes from both radars are shown as an example of the application of the reflectivity calibration algorithm.

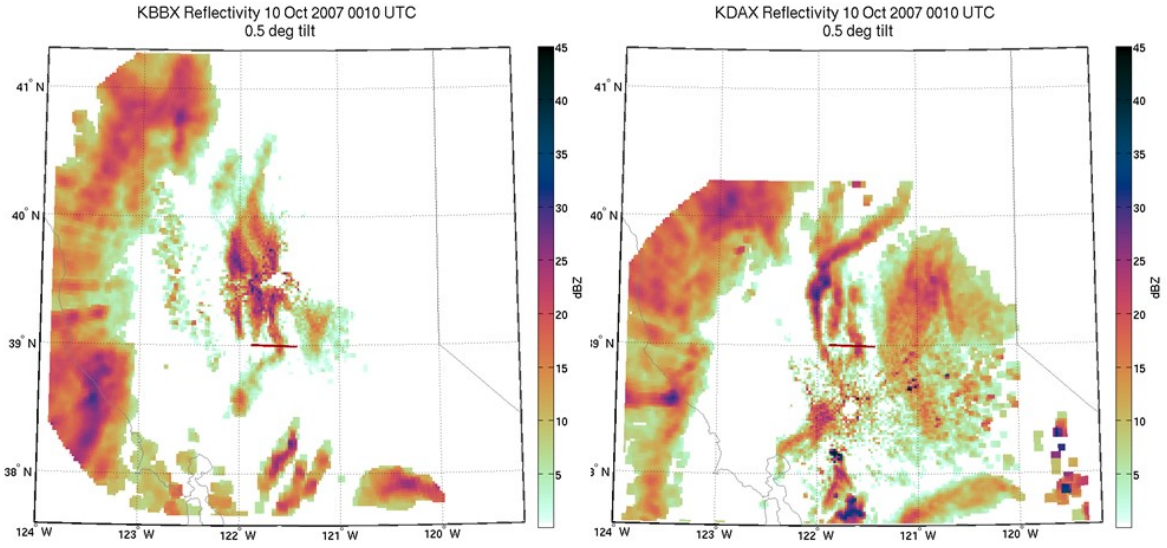

Figure C.1 shows the lowest tilt (0.5°) in the volume at 0010 UTC on the 10th of October, 2007, roughly the middle of the atmospheric river event from both KBBX (Fig C.1, left panel) and KDAX (Fig C.1, right panel). The horizontal red denotes the curtain 39 km in length, equidistant from both radars and perpendicular to the line that connects the radars where the reflectivities from both radars are compared.

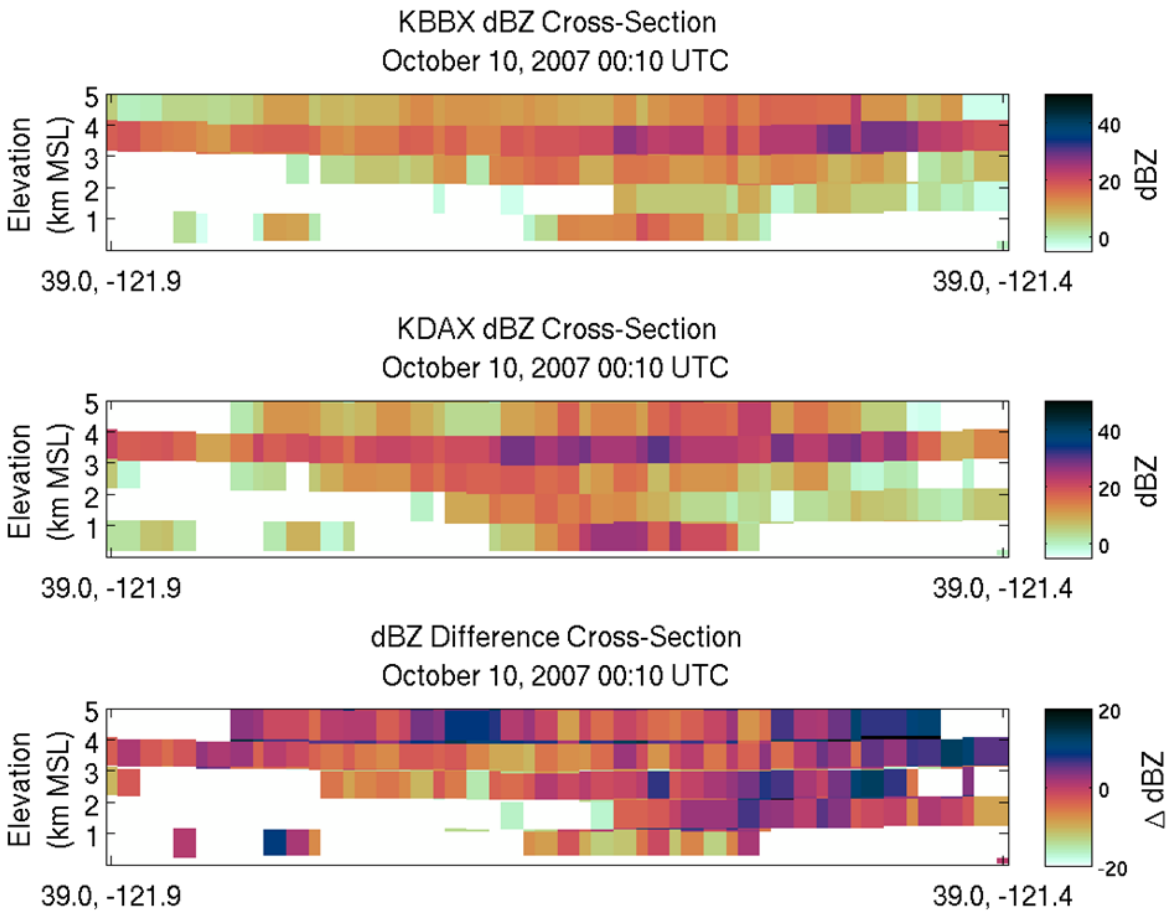

Figure C.2 The curtain through the entire volume along the red line. Neither volume has been quality controlled. The top panel shows reflectivity values from the KBBX radar, the middle panel shows reflectivity values from the KDAX radar, and the bottom panel shows the difference in reflectivity values between the reflectivity values between KDAX and KBBX (KBBX minus KDAX). The difference between a grid location with no data and a grid location that contains data returns a value of no data.

The process of calculating the differences in reflectivity from KBBX and KDAX along this curtain is repeated for every half hour of data throughout the duration of the atmospheric river event.

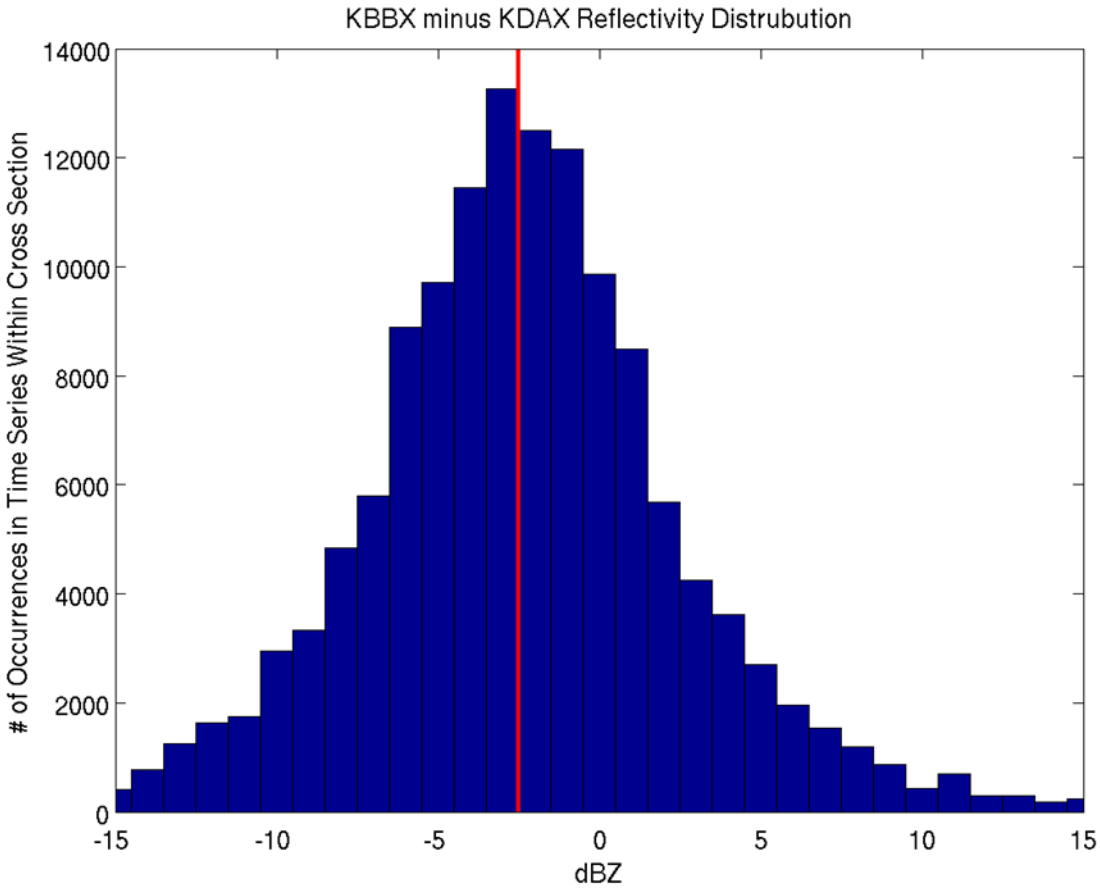

Figure C.3 Histogram of the dBZ differences along the curtain for all half-hourly data in the event. The red line indicates the median difference value (-2.5 dBZ).

The median difference value (-2.5 dBZ) is used as the offset value for KBBX. This means that KBBX consistently reports a dBZ value lower than KDAX, so a 13 dBZ target seen by KDAX is equivalent to 10.5 dBZ from KBBX for this event.

This process is repeated for all events in the 64 atmospheric river dataset. Unique offsets using this algorithm are applied to each of the precipitation frequency composite maps.

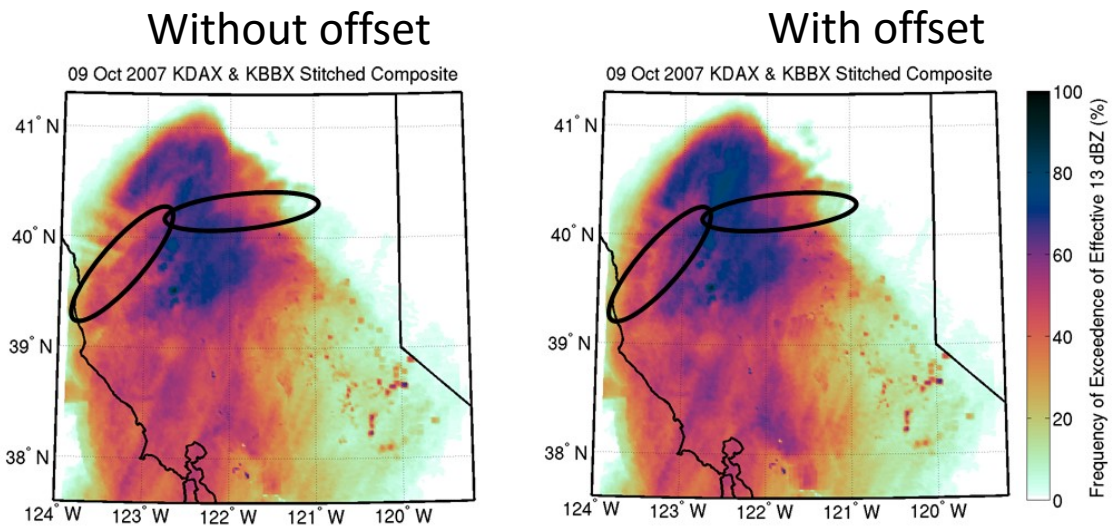

Figure C.4 Results of the reflectivity offset correction. The left panel shows what the precipitation frequency composite looks like with no offset correction applied. The right panel shows what the precipitation frequency composite looks like with the offset correction of -2.5 dBZ applied to the KBBX radar. The black ovals denote locations where the edges of the boundary from the extent of the KDAX radar domain have been smoothed by the reflectivity calibration.

Appendix D

Chronological overview of 64 atmospheric river events: Precipitation frequency maps and environmental variables

Events are arranged in chronological order. Data have been quality controlled. The abbreviation BBY refers to the Bodega Bay wind profiler and the abbreviation CCO refers to the Chico wind profiler. Thick black lines show basin boundaries, and thin gray line shows 1 km MSL.

19 Mar 2005

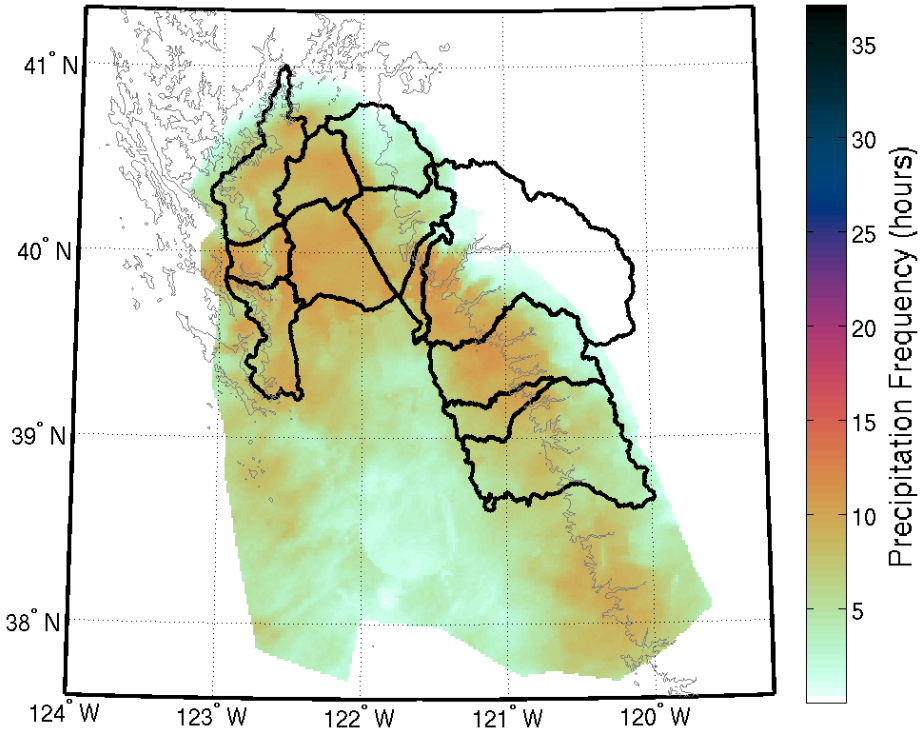

Variables	Value	Category
Storm Duration (hours)	12	-
KBBX Radar Offset (dBZ)	-1	-
BBY – Wind Direction at AR onset (°)	154.89	South
BBY – Mean Upslope Wind (m s^{-1})	13.656	High
BBY – Total Upslope IWV Flux (cm m s^{-1})	411.4	Middle

CCO Barrier Jet Timeline	Altitude (m)		Magnitude (ms^{-1})	
20050319:0400 – 20050319:1600	1328	High	19.19	Middle

22 Mar 2005

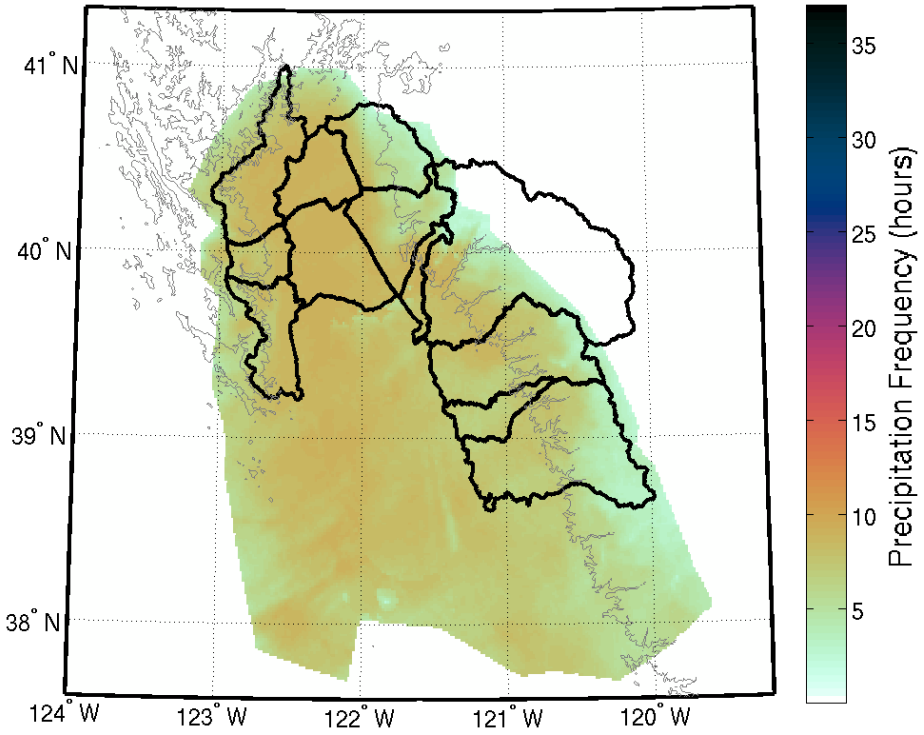

Variables	Value	Category
Storm Duration (hours)	9	-
KBBX Radar Offset (dBZ)	-1	-
BBY – Wind Direction at AR onset (°)	158.18	South
BBY – Mean Upslope Wind (m s^{-1})	16.895	High
BBY – Total Upslope IWV Flux (cm m s^{-1})	390.8	Middle

CCO Barrier Jet Timeline	Altitude (m)		Magnitude (ms^{-1})	
20050322:0100 – 20050322:1000	1171	Middle	22.6	Middle

27 Mar 2005

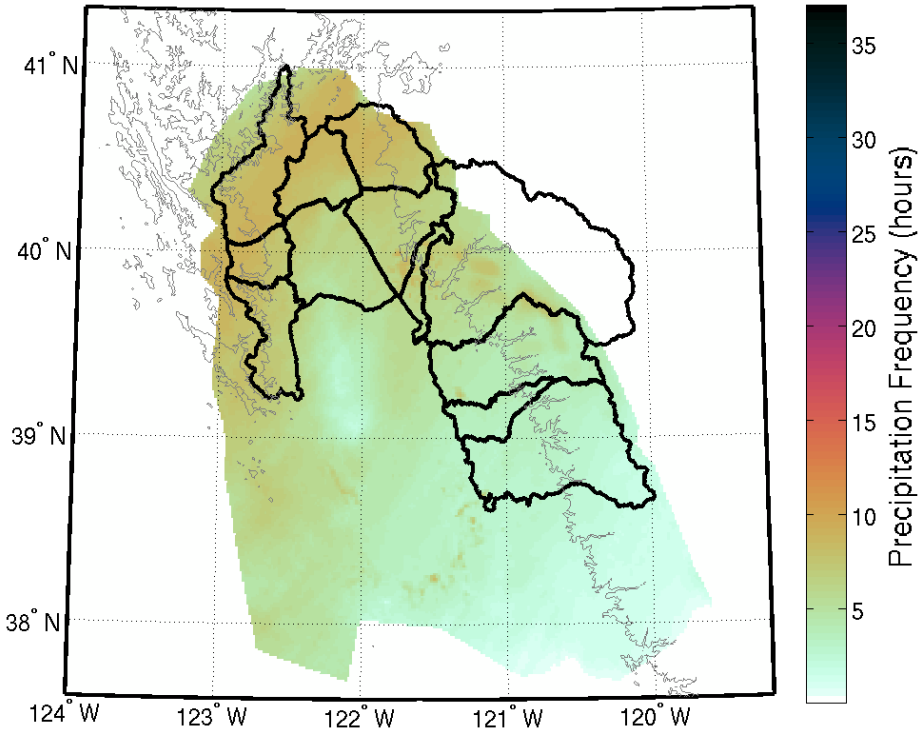

Variables	Value	Category
Storm Duration (hours)	9	-
KBBX Radar Offset (dBZ)	-2	-
BBY – Wind Direction at AR onset (°)	180.61	South
BBY – Mean Upslope Wind (m s^{-1})	15.763	High
BBY – Total Upslope IWV Flux (cm m s^{-1})	360.6	Middle

CCO Barrier Jet Timeline	Altitude (m)		Magnitude (ms^{-1})	
20050327:1900 – 20050327:2000	-	-	-	-
20050327:2000 – 20050328:0400	945	Middle	23.33	High

15 May 2005

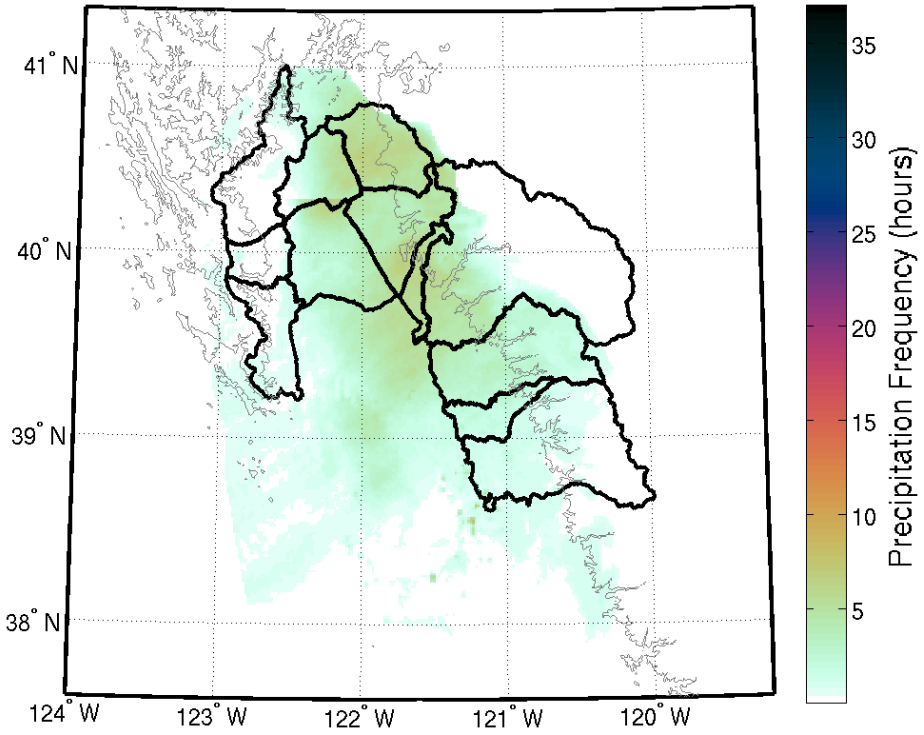

Variables	Value	Category
Storm Duration (hours)	10	-
KBBX Radar Offset (dBZ)	0	-
BBY – Wind Direction at AR onset (°)	283.86	West
BBY – Mean Upslope Wind (m s^{-1})	4.282	Low
BBY – Total Upslope IWV Flux (cm m s^{-1})	156.2	Low

CCO Barrier Jet Timeline	Altitude (m)		Magnitude (ms^{-1})	
20050515:1100 – 20050515:2100	-	-	-	-

08 Jun 2005

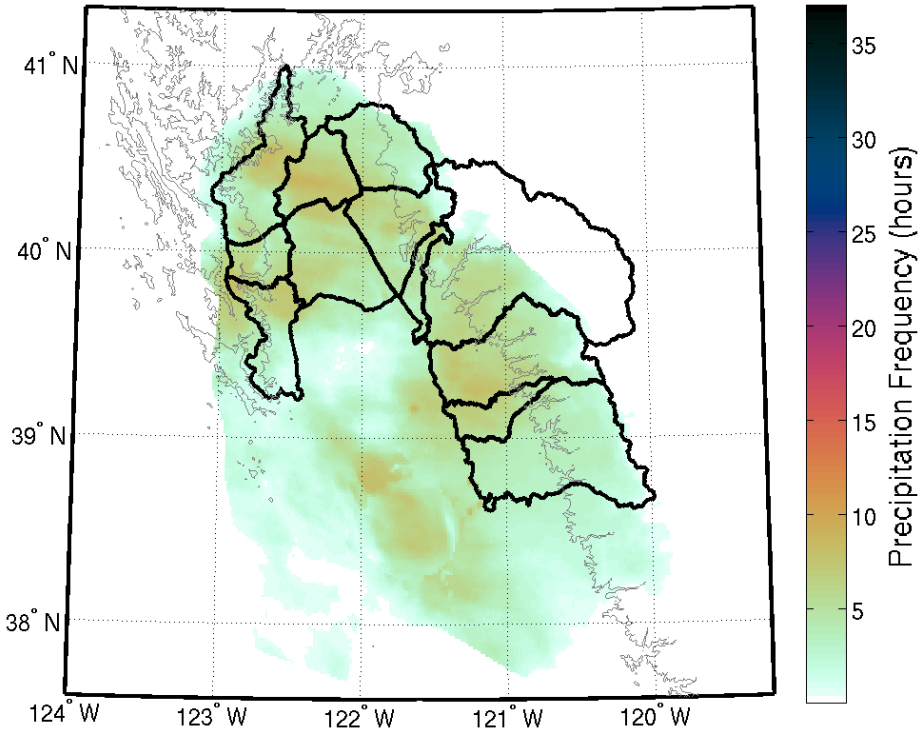

Variables	Value	Category
Storm Duration (hours)	10	-
KBBX Radar Offset (dBZ)	-1	-
BBY – Wind Direction at AR onset (°)	-	-
BBY – Mean Upslope Wind (m s^{-1})	-	-
BBY – Total Upslope IWV Flux (cm m s^{-1})	-	-

CCO Barrier Jet Timeline	Altitude (m)		Magnitude (ms^{-1})	
20050608:0400 – 20050608:1400	-	-	-	-

17 Jun 2005

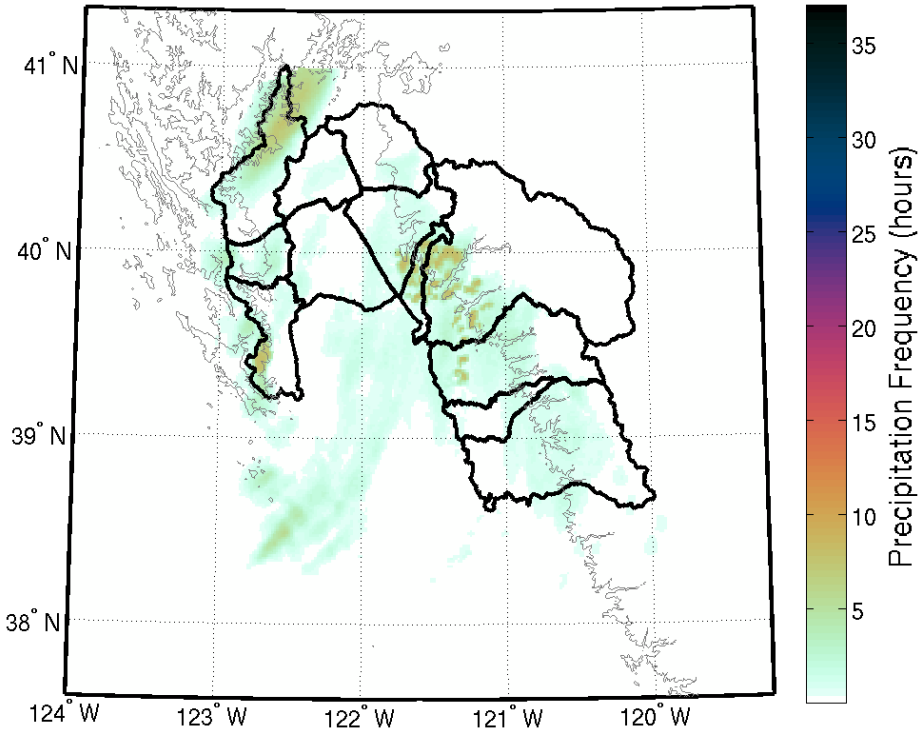

Variables	Value	Category
Storm Duration (hours)	8	-
KBBX Radar Offset (dBZ)	0	-
BBY – Wind Direction at AR onset (°)	-	-
BBY – Mean Upslope Wind (m s^{-1})	-	-
BBY – Total Upslope IWV Flux (cm m s^{-1})	-	-

CCO Barrier Jet Timeline	Altitude (m)		Magnitude (ms^{-1})	
20050617:2000 – 20050618:0400	-	-	-	-

03 Nov 2005

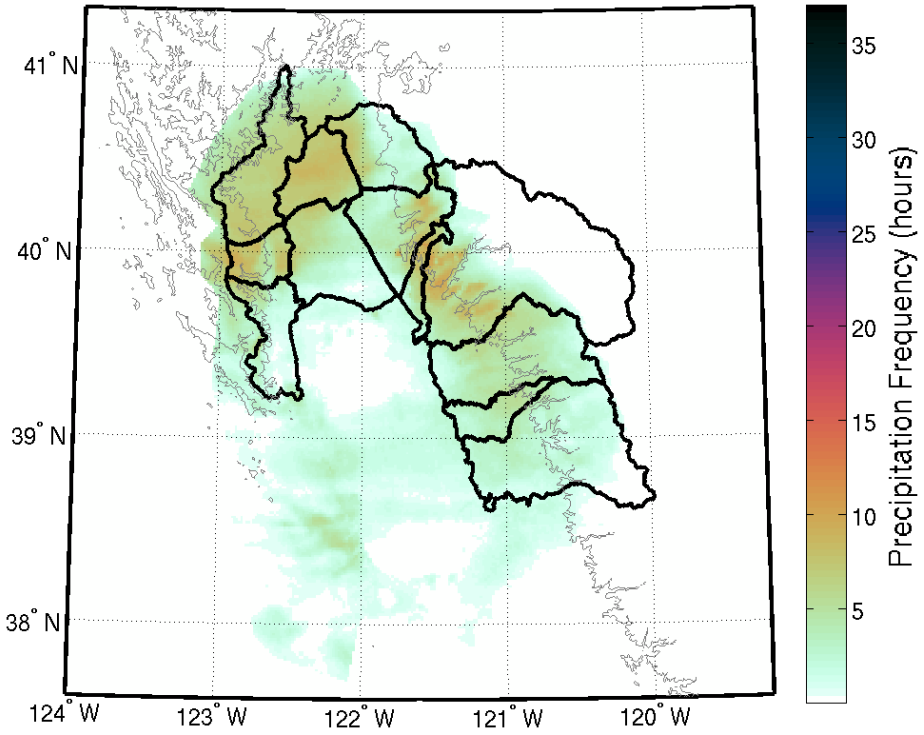

Variables	Value	Category
Storm Duration (hours)	13	-
KBBX Radar Offset (dBZ)	-3	-
BBY – Wind Direction at AR onset (°)	237.39	West
BBY – Mean Upslope Wind (m s^{-1})	9.616	Low
BBY – Total Upslope IWV Flux (cm m s^{-1})	288.8	Middle

CCO Barrier Jet Timeline	Altitude (m)		Magnitude (ms^{-1})	
20051103:1900 – 20051104:0800	708	Middle	16.72	Low

07 Nov 2005

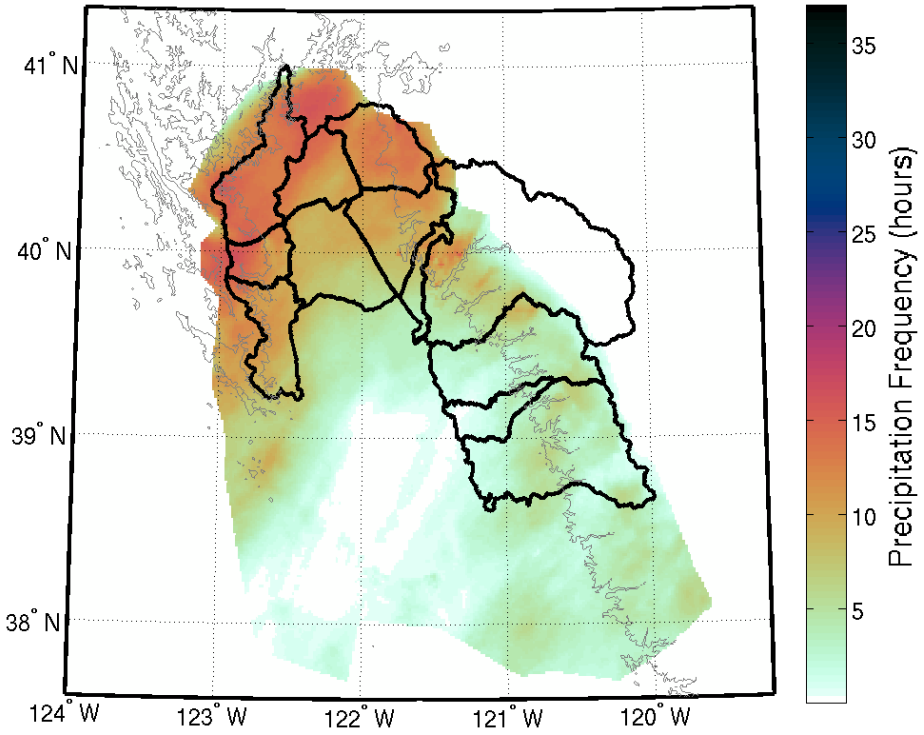

Variables	Value	Category
Storm Duration (hours)	20	-
KBBX Radar Offset (dBZ)	-2	-
BBY – Wind Direction at AR onset (°)	224.14	Southwest
BBY – Mean Upslope Wind (m s^{-1})	10.653	Middle
BBY – Total Upslope IWV Flux (cm m s^{-1})	593.8	High

CCO Barrier Jet Timeline	Altitude (m)		Magnitude (ms^{-1})	
20051107:0600 – 20051107:0800	-	-	-	-
20051107:0800 – 20051107:2000	503	Low	17.85	Middle
20051107:2000 – 20051108:0200	-	-	-	-

25 Nov 2005

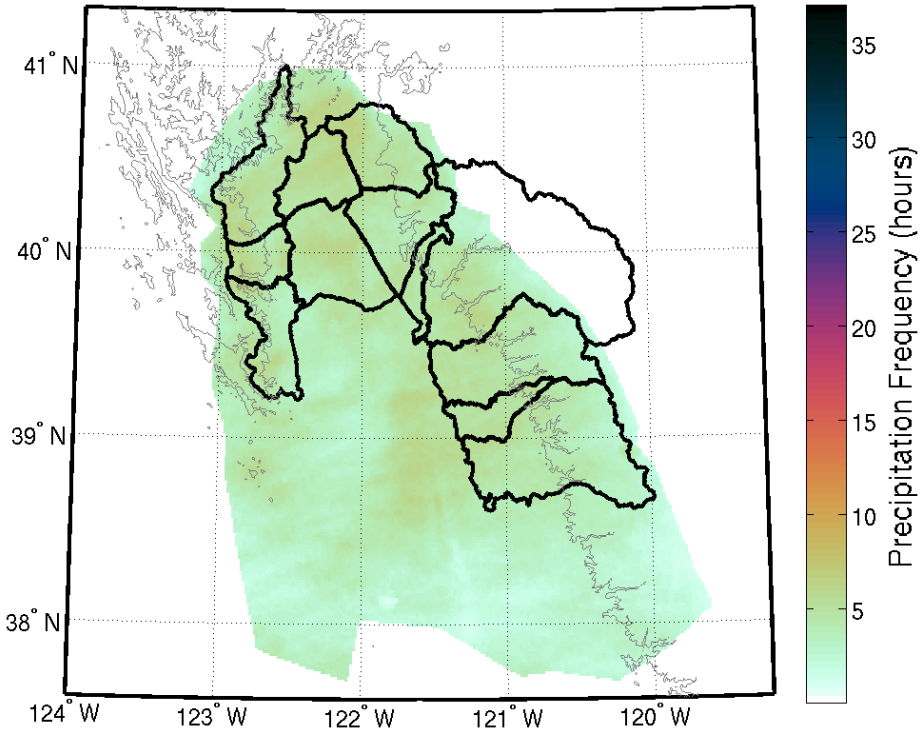

Variables	Value	Category
Storm Duration (hours)	12	-
KBBX Radar Offset (dBZ)	-1	-
BBY – Wind Direction at AR onset (°)	239.29	West
BBY – Mean Upslope Wind (m s^{-1})	9.726	Low
BBY – Total Upslope IWV Flux (cm m s^{-1})	391.8	Middle

CCO Barrier Jet Timeline	Altitude (m)		Magnitude (ms^{-1})	
20051125:0500 – 20051125:1700	-	-	-	-

28 Nov 2005

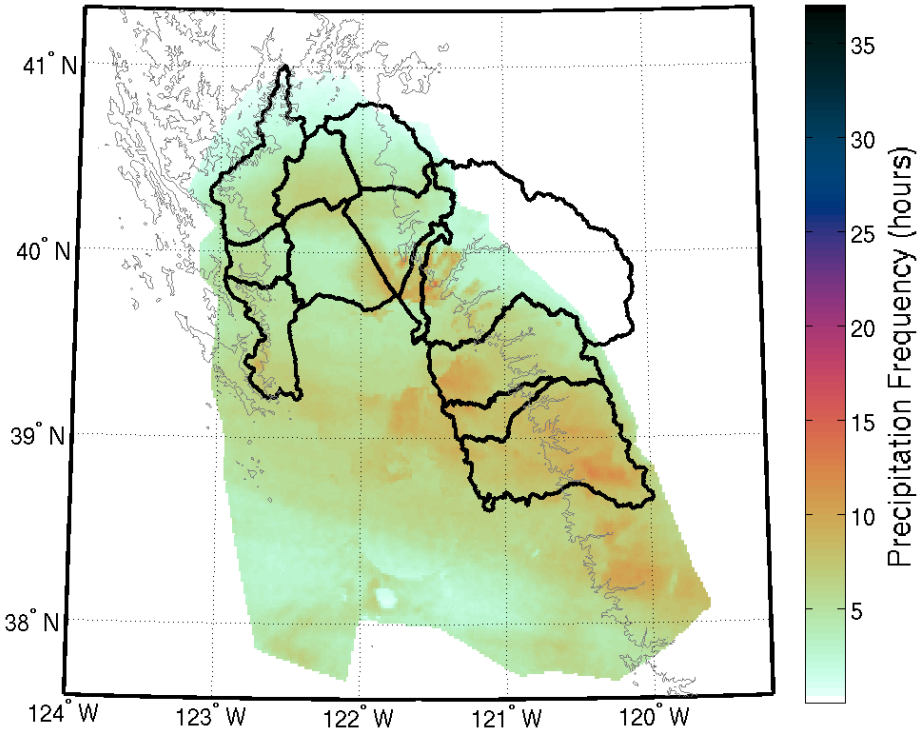

Variables	Value	Category
Storm Duration (hours)	17	-
KBBX Radar Offset (dBZ)	-4	-
BBY – Wind Direction at AR onset (°)	188.27	Southwest
BBY – Mean Upslope Wind (m s^{-1})	10.710	Middle
BBY – Total Upslope IWV Flux (cm m s^{-1})	488.0	High

CCO Barrier Jet Timeline	Altitude (m)		Magnitude (ms^{-1})	
20051128:2000 – 20051129:1300	-	-	-	-

18 Dec 2005

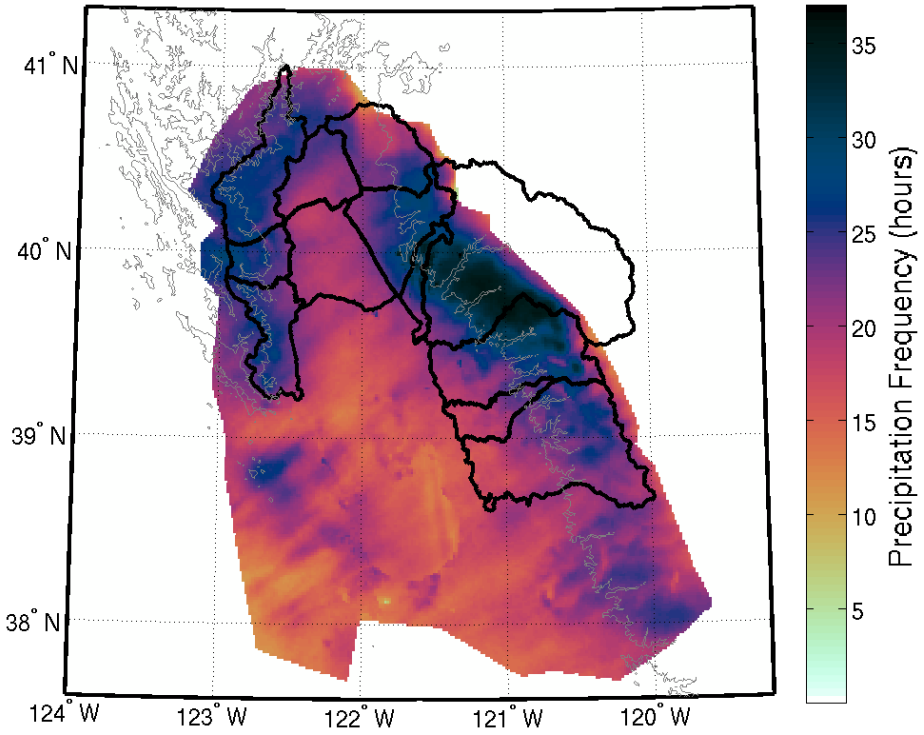

Variables	**Value**	**Category**
Storm Duration (hours)	43	-
KBBX Radar Offset (dBZ)	-3	-
BBY – Wind Direction at AR onset (°)	169.39	South
BBY – Mean Upslope Wind (m s^{-1})	16.335	High
BBY – Total Upslope IWV Flux (cm m s^{-1})	1820.6	High

CCO Barrier Jet Timeline	**Altitude (m)**		**Magnitude (ms^{-1})**	
20051218:0500 – 20051220:0000	1180	Middle	19.62	Middle

20 Dec 2005

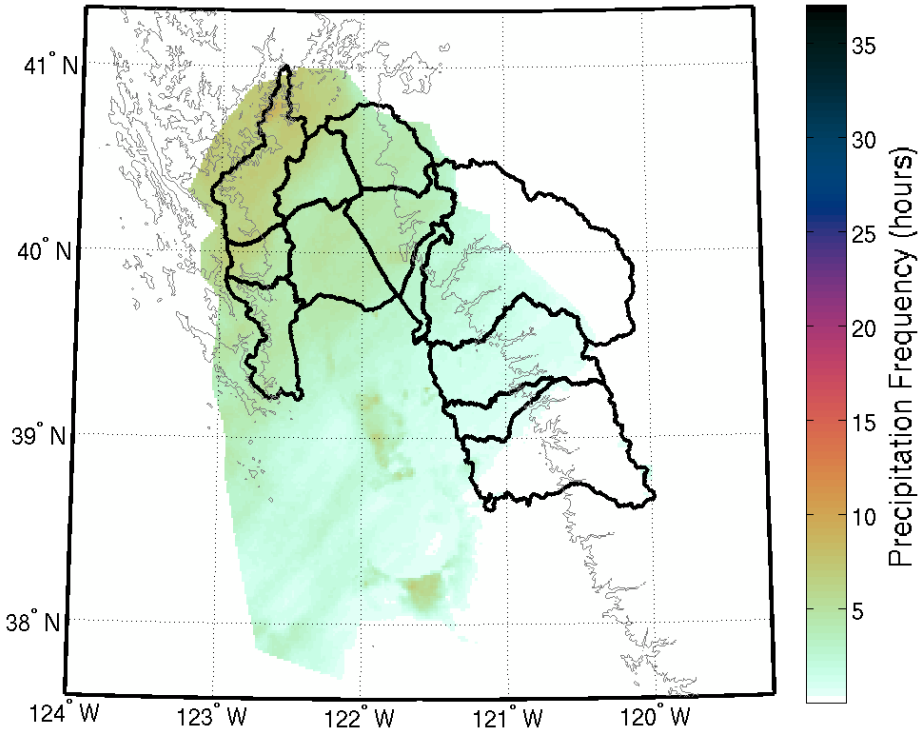

Variables	Value	Category
Storm Duration (hours)	14	-
KBBX Radar Offset (dBZ)	-2.5	-
BBY – Wind Direction at AR onset (°)	169.30	South
BBY – Mean Upslope Wind (m s^{-1})	12.388	Middle
BBY – Total Upslope IWV Flux (cm m s^{-1})	496.7	High

CCO Barrier Jet Timeline	Altitude (m)		Magnitude (ms^{-1})	
20051220:1000 – 20051221:0000	-	-	-	-

25 Dec 2005

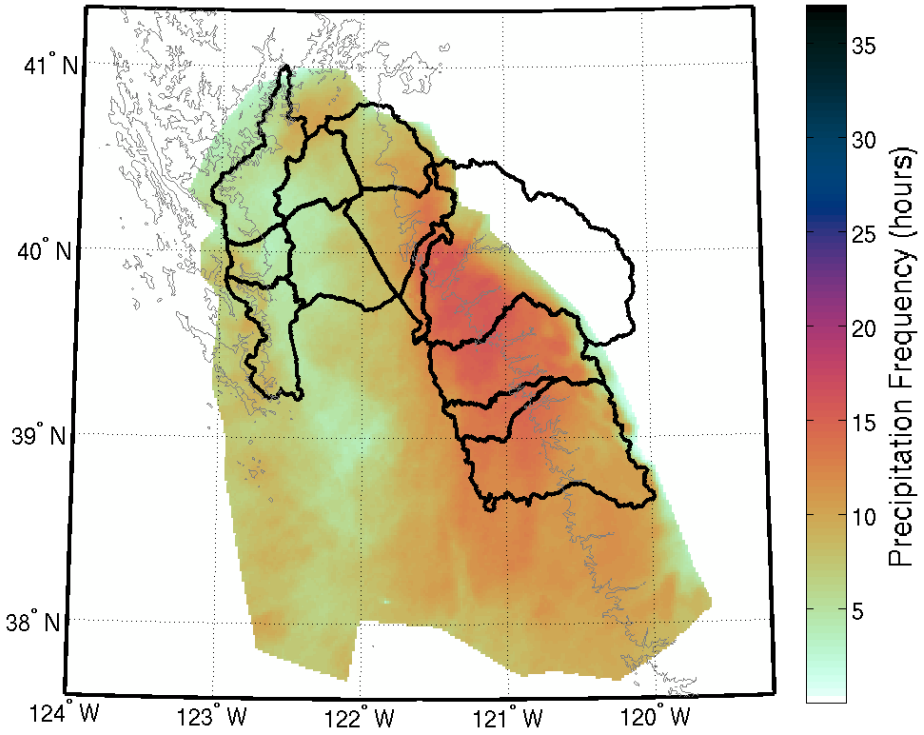

Variables	Value	Category
Storm Duration (hours)	16	-
KBBX Radar Offset (dBZ)	-3.5	-
BBY – Wind Direction at AR onset (°)	197.00	Southwest
BBY – Mean Upslope Wind (m s^{-1})	10.260	Middle
BBY – Total Upslope IWV Flux (cm m s^{-1})	163.3	Low

CCO Barrier Jet Timeline	Altitude (m)		Magnitude (ms^{-1})	
20051225:1700 – 20051226:0100	-	-	-	-
20051226:0100 – 20051226:0900	1059	Middle	17.57	Middle

27 Dec 2005

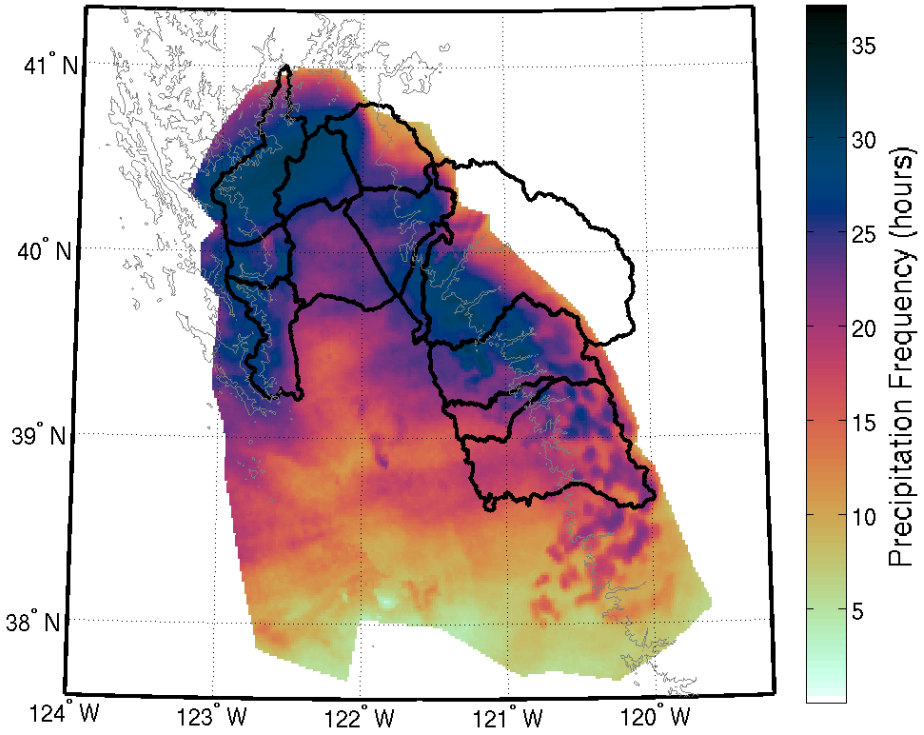

Variables	Value	Category
Storm Duration (hours)	34	-
KBBX Radar Offset (dBZ)	-3.5	-
BBY – Wind Direction at AR onset (°)	185.65	South
BBY – Mean Upslope Wind (m s^{-1})	14.988	High
BBY – Total Upslope IWV Flux (cm m s^{-1})	1610.8	High

CCO Barrier Jet Timeline	Altitude (m)		Magnitude (ms^{-1})	
20051227:0700 – 20051228:1700	968	Middle	19.43	Middle

30 Dec 2005

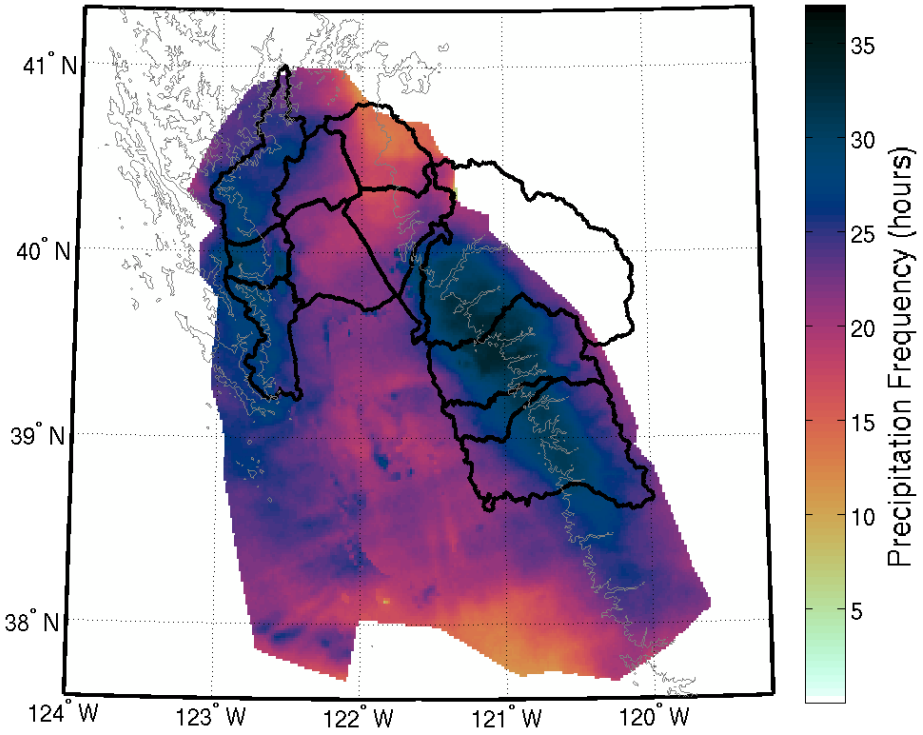

Variables	Value	Category
Storm Duration (hours)	36	-
KBBX Radar Offset (dBZ)	-3.5	-
BBY – Wind Direction at AR onset (°)	192.69	Southwest
BBY – Mean Upslope Wind (m s^{-1})	17.121	High
BBY – Total Upslope IWV Flux (cm m s^{-1})	1894.1	High

CCO Barrier Jet Timeline	Altitude (m)		Magnitude (ms^{-1})	
20051230:0400 – 20051230:0500	-	-	-	-
20051230:0500 – 20051231:1600	639	Low	20.42	High

01 Jan 2006

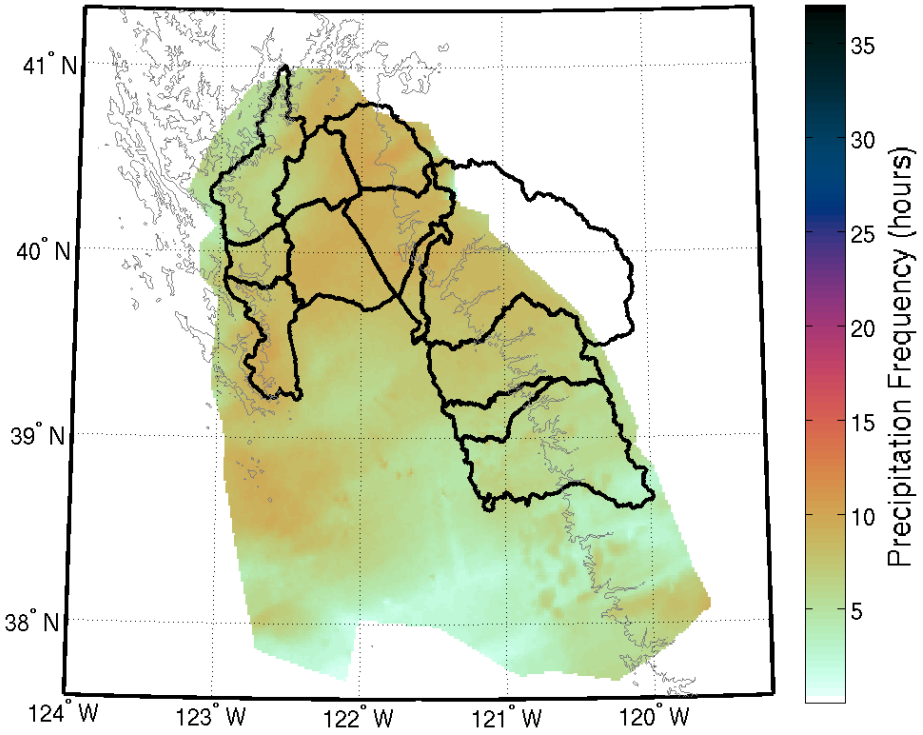

Variables	Value	Category
Storm Duration (hours)	11	-
KBBX Radar Offset (dBZ)	-3.5	-
BBY – Wind Direction at AR onset (°)	172.13	South
BBY – Mean Upslope Wind (m s^{-1})	18.155	High
BBY – Total Upslope IWV Flux (cm m s^{-1})	449.4	High

CCO Barrier Jet Timeline	Altitude (m)		Magnitude (ms^{-1})	
20060101:1500 – 20060102:0200	1056	Middle	22.99	High

03 Jan 2006

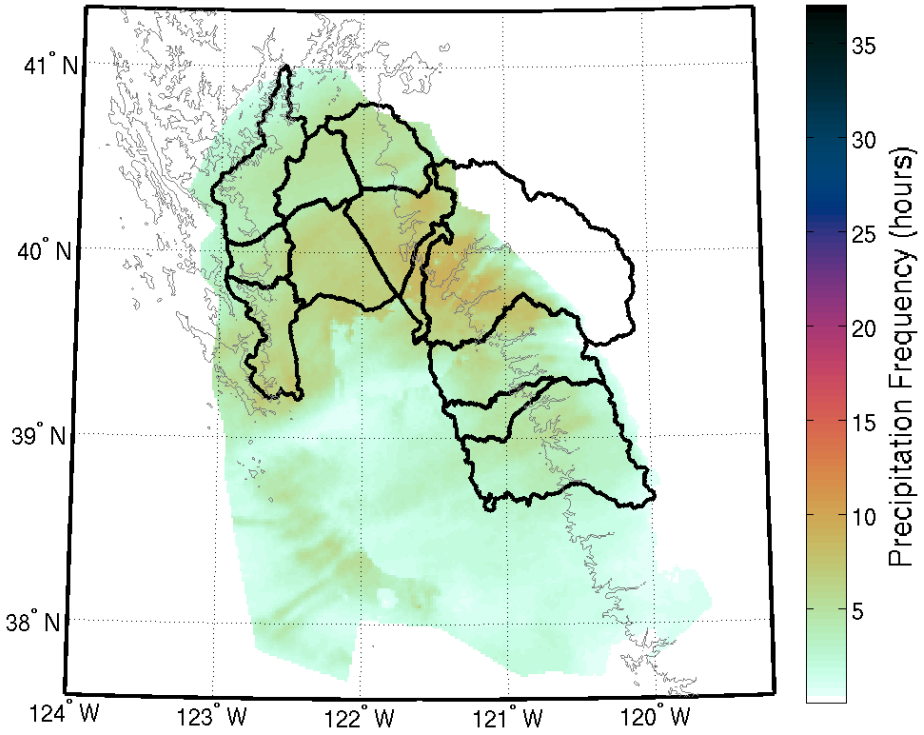

Variables	Value	Category
Storm Duration (hours)	9	-
KBBX Radar Offset (dBZ)	-12	-
BBY – Wind Direction at AR onset (°)	193.26	Southwest
BBY – Mean Upslope Wind (m s^{-1})	15.098	High
BBY – Total Upslope IWV Flux (cm m s^{-1})	-	-

CCO Barrier Jet Timeline	Altitude (m)		Magnitude (ms^{-1})	
20060103:2100 – 20060104:0600	924	Middle	17.3	Middle

10 Jan 2006

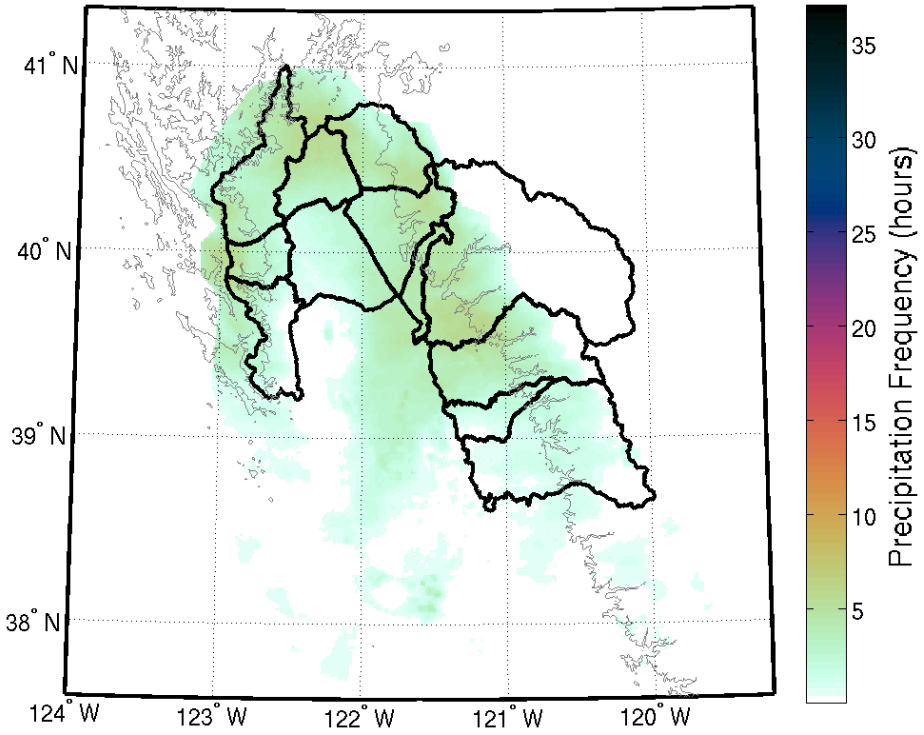

Variables	Value	Category
Storm Duration (hours)	10	-
KBBX Radar Offset (dBZ)	-3	-
BBY – Wind Direction at AR onset (°)	254.10	West
BBY – Mean Upslope Wind (m s^{-1})	7.525	Low
BBY – Total Upslope IWV Flux (cm m s^{-1})	210.1	Low

CCO Barrier Jet Timeline	Altitude (m)		Magnitude (ms^{-1})	
20060110:2300 - 20060111:0300	-	-	-	-
20060111:0300 – 20060111:0900	639	Low	15.89	Low

28 Jan 2006

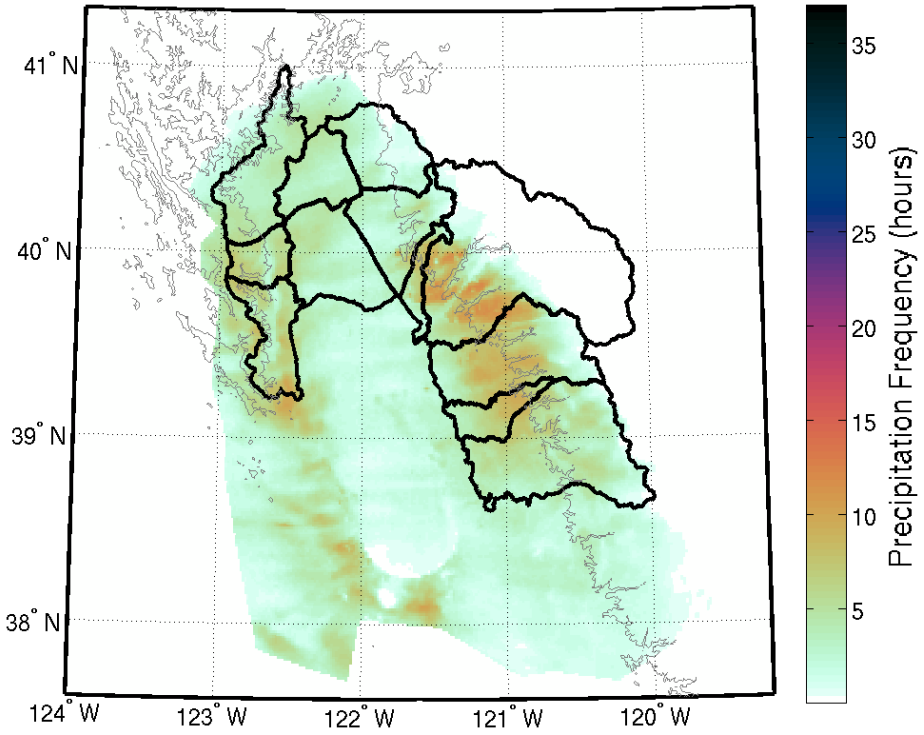

Variables	Value	Category
Storm Duration (hours)	14	-
KBBX Radar Offset (dBZ)	-4	-
BBY – Wind Direction at AR onset (°)	228.57	Southwest
BBY – Mean Upslope Wind (m s^{-1})	10.180	Middle
BBY – Total Upslope IWV Flux (cm m s^{-1})	-	-

CCO Barrier Jet Timeline	Altitude (m)		Magnitude (ms^{-1})	
20060128:1400 – 20060129:0200	537	Low	18.09	Middle
20060129:0200 – 20060129:0400	-	-	-	-

01 Feb 2006

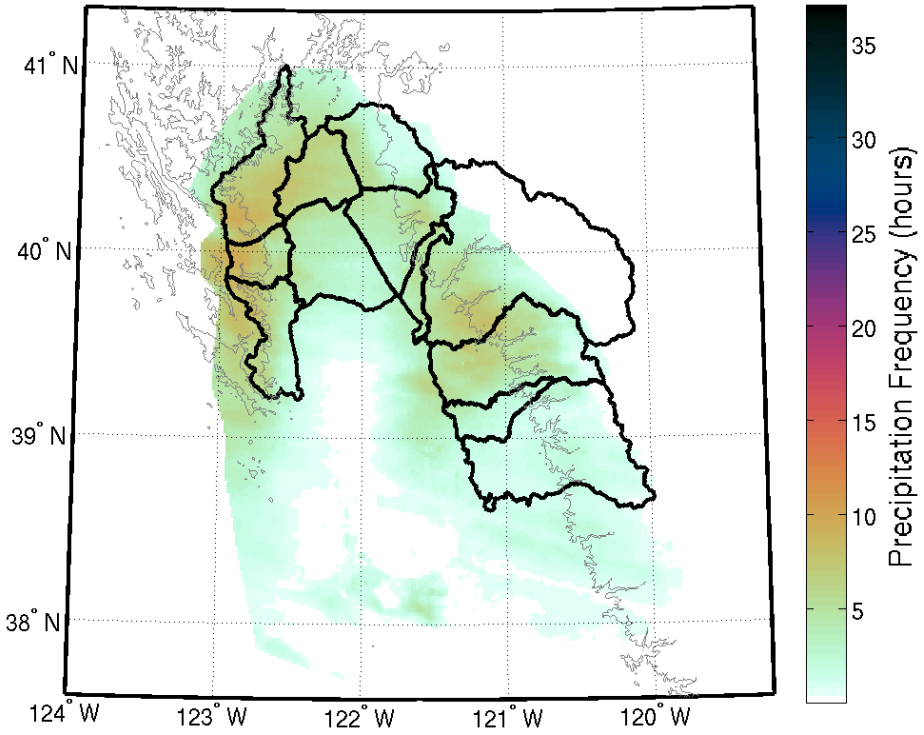

Variables	Value	Category
Storm Duration (hours)	12	-
KBBX Radar Offset (dBZ)	-3	-
BBY – Wind Direction at AR onset (°)	240.92	West
BBY – Mean Upslope Wind (m s^{-1})	7.301	Low
BBY – Total Upslope IWV Flux (cm m s^{-1})	218.4	Low

CCO Barrier Jet Timeline	Altitude (m)		Magnitude (ms^{-1})	
20060201:0900 – 20060201:2100	474	Low	14.58	Low

26 Feb 2006

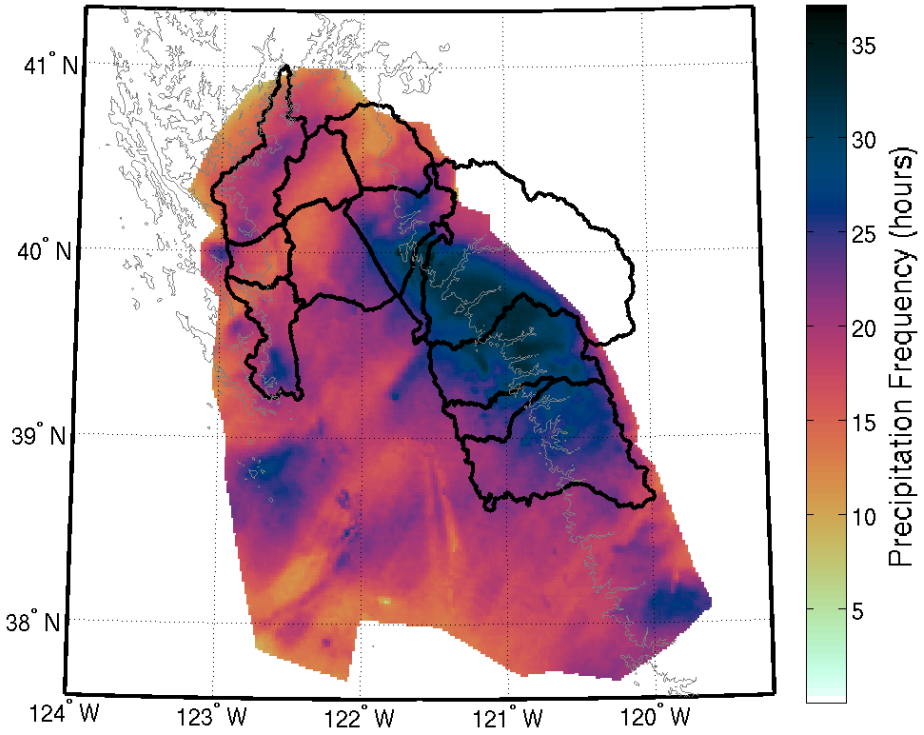

Variables	Value	Category
Storm Duration (hours)	38	-
KBBX Radar Offset (dBZ)	-3	-
BBY – Wind Direction at AR onset (°)	166.94	South
BBY – Mean Upslope Wind (m s^{-1})	17.577	High
BBY – Total Upslope IWV Flux (cm m s^{-1})	1768.9	High

CCO Barrier Jet Timeline	Altitude (m)		Magnitude (ms^{-1})	
20060226:1700 – 20060226:1900	-	-	-	-
20060226:1900 – 20060227:2200	1340	High	28.35	High
20060227:2200 – 20060228:0700	-	-	-	-

05 Mar 2006

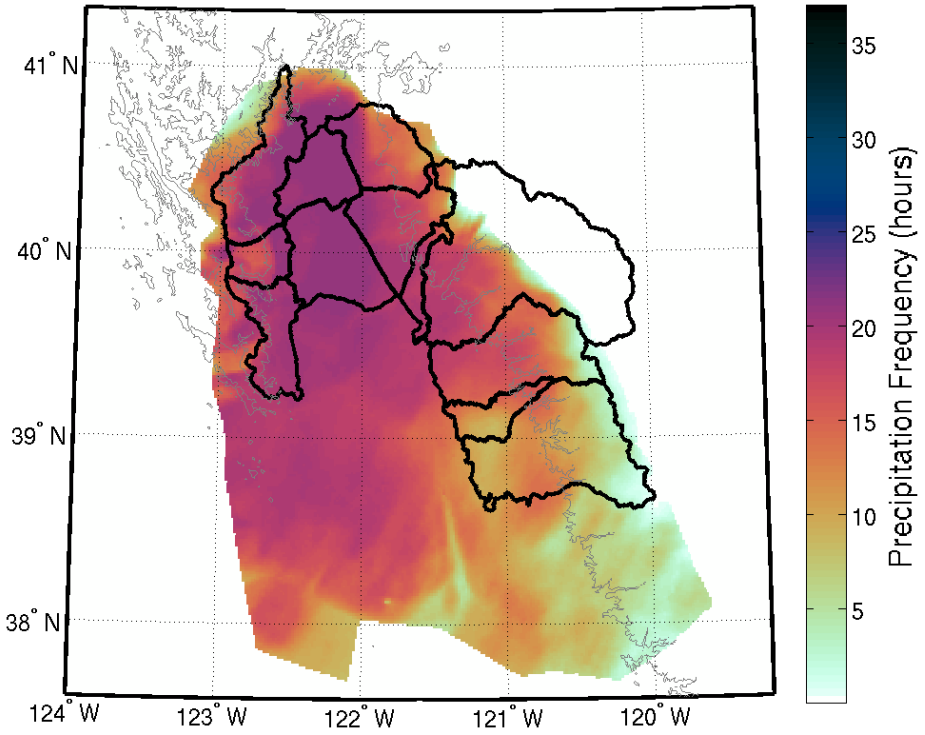

Variables	Value	Category
Storm Duration (hours)	21	-
KBBX Radar Offset (dBZ)	-3.5	-
BBY – Wind Direction at AR onset (°)	175.07	South
BBY – Mean Upslope Wind (m s^{-1})	16.385	High
BBY – Total Upslope IWV Flux (cm m s^{-1})	807.1	High

CCO Barrier Jet Timeline	Altitude (m)		Magnitude (ms^{-1})	
20060305:0800 – 20060305:1200	-	-	-	-
20060305:1200 – 20060306:0500	1350	High	25.68	High

19 Mar 2006

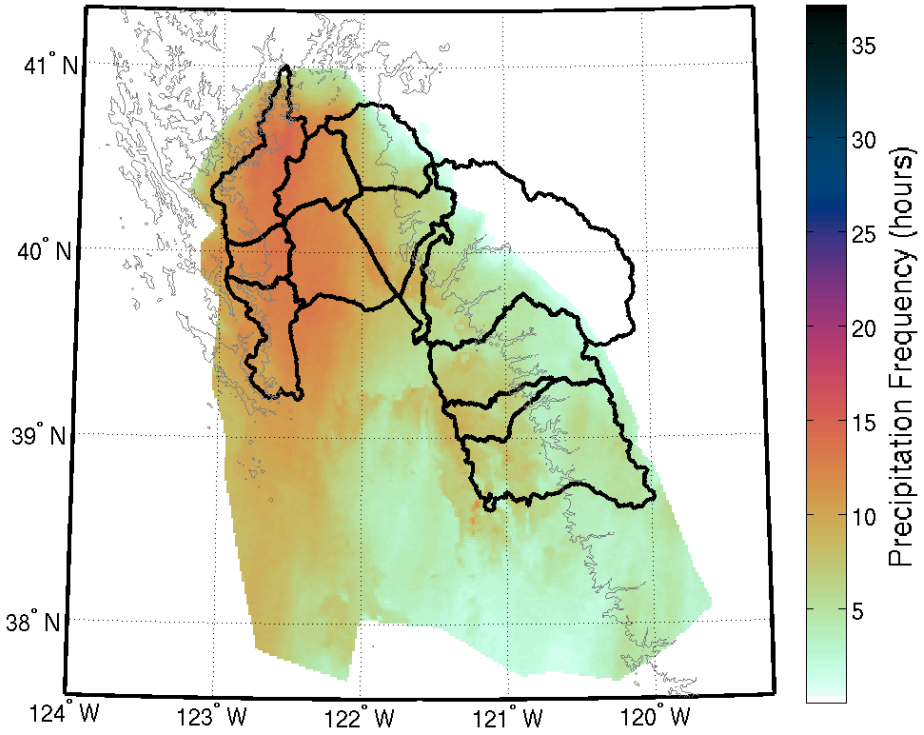

Variables	Value	Category
Storm Duration (hours)	19	-
KBBX Radar Offset (dBZ)	-2	-
BBY – Wind Direction at AR onset (°)	232.87	Southwest
BBY – Mean Upslope Wind (m s^{-1})	9.328	Low
BBY – Total Upslope IWV Flux (cm m s^{-1})	443.1	High

CCO Barrier Jet Timeline	Altitude (m)		Magnitude (ms^{-1})	
20060519:1400 – 20060520:0900	-	-	-	-

23 Mar 2006

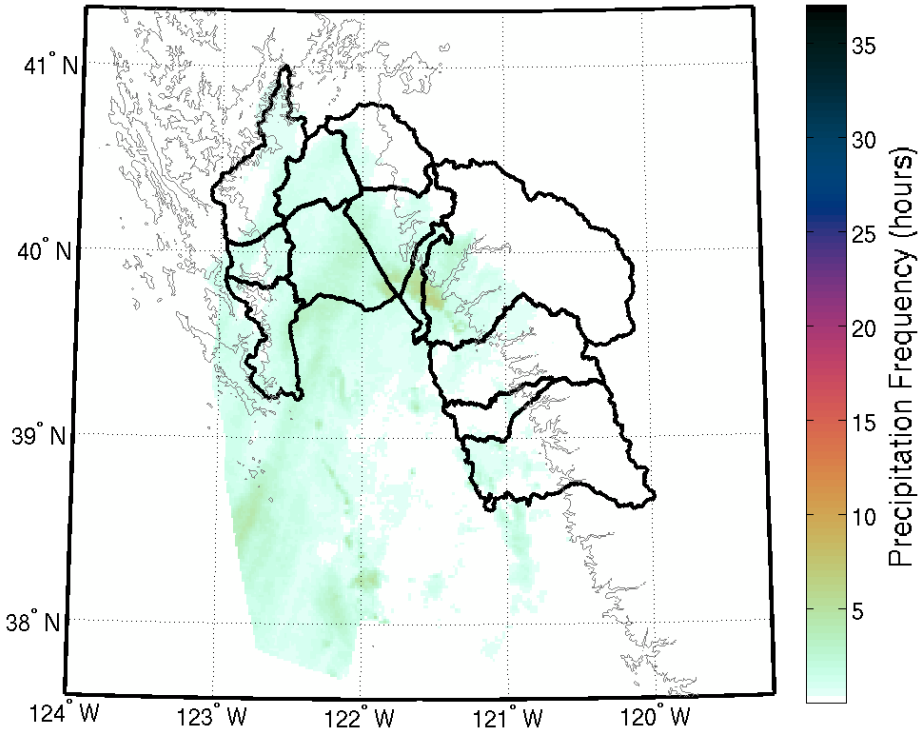

Variables	Value	Category
Storm Duration (hours)	19	-
KBBX Radar Offset (dBZ)	-2	-
BBY – Wind Direction at AR onset (°)	232.87	Southwest
BBY – Mean Upslope Wind (m s^{-1})	9.328	Low
BBY – Total Upslope IWV Flux (cm m s^{-1})	443.1	High

CCO Barrier Jet Timeline	Altitude (m)		Magnitude (ms^{-1})	
20060519:1400 – 20060520:0900	-	-	-	-

02 Nov 2006

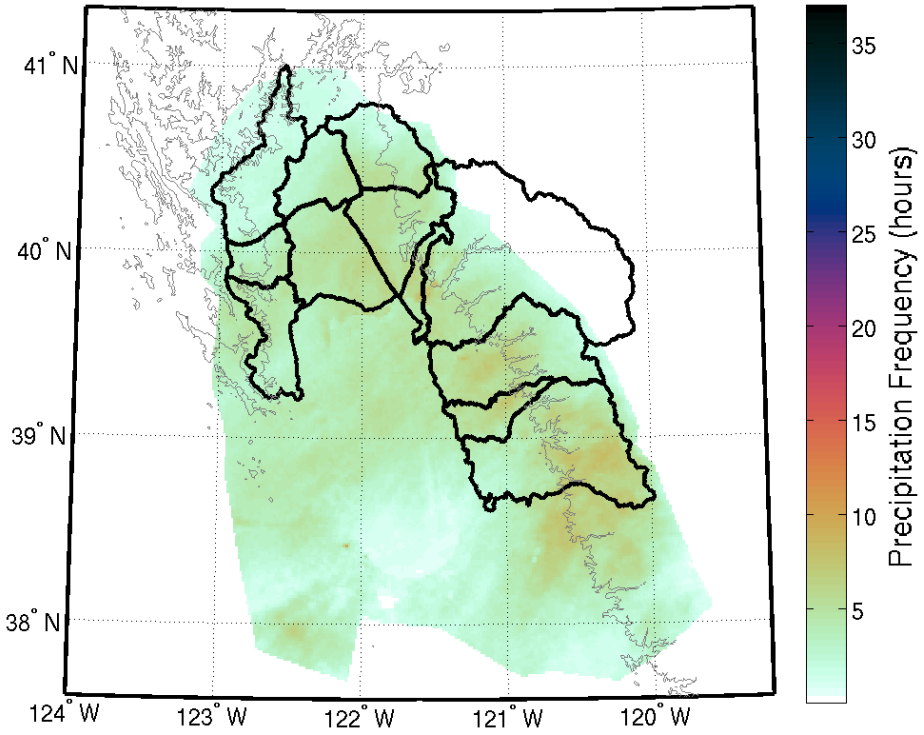

Variables	Value	Category
Storm Duration (hours)	14	-
KBBX Radar Offset (dBZ)	-3.5	-
BBY – Wind Direction at AR onset (°)	193.67	Southwest
BBY – Mean Upslope Wind (m s^{-1})	11.999	Middle
BBY – Total Upslope IWV Flux (cm m s^{-1})	473.9	High

CCO Barrier Jet Timeline	Altitude (m)		Magnitude (ms^{-1})	
20061102:0700 – 20061102:1200	-	-	-	-
20061102:1200 – 20061102:2100	1039	Middle	14.86	Low

08 Nov 2006

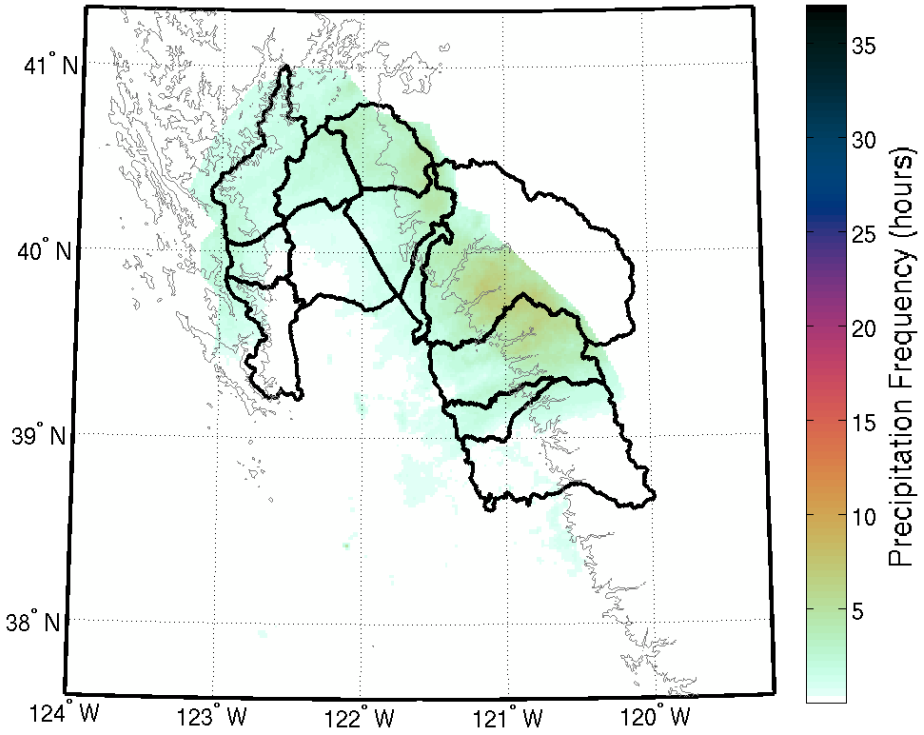

Variables	Value	Category
Storm Duration (hours)	14	-
KBBX Radar Offset (dBZ)	-4	-
BBY – Wind Direction at AR onset (°)	287.21	West
BBY – Mean Upslope Wind (m s^{-1})	4.826	Low
BBY – Total Upslope IWV Flux (cm m s^{-1})	137.7	Low

CCO Barrier Jet Timeline	Altitude (m)		Magnitude (ms^{-1})	
20061108:0400 – 20061108:1300	-	-	-	-

13 Nov 2006

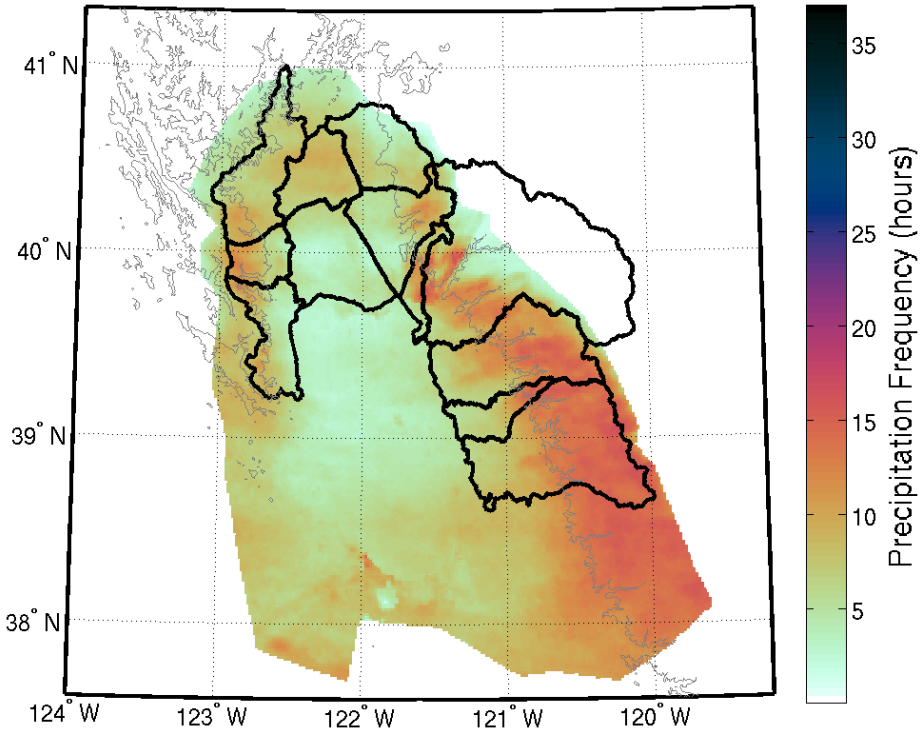

Variables	Value	Category
Storm Duration (hours)	14	-
KBBX Radar Offset (dBZ)	-3.5	-
BBY – Wind Direction at AR onset (°)	230.33	Southwest
BBY – Mean Upslope Wind (m s^{-1})	8.991	Low
BBY – Total Upslope IWV Flux (cm m s^{-1})	709.5	High

CCO Barrier Jet Timeline	Altitude (m)		Magnitude (ms^{-1})	
20061113:0500 – 20061114:0800	982	Middle	17.06	Middle

16 Nov 2006

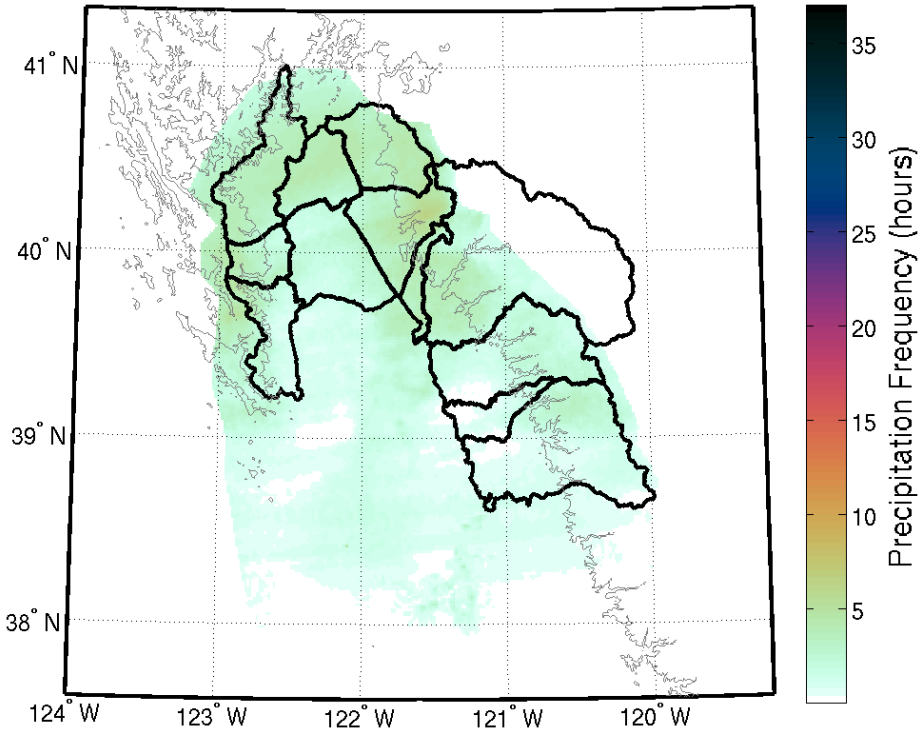

Variables	Value	Category
Storm Duration (hours)	14	-
KBBX Radar Offset (dBZ)	-3.5	-
BBY – Wind Direction at AR onset (°)	271.47	West
BBY – Mean Upslope Wind (m s^{-1})	7.437	Low
BBY – Total Upslope IWV Flux (cm m s^{-1})	163.9	Low

CCO Barrier Jet Timeline	Altitude (m)		Magnitude (ms^{-1})	
20061116:0700 – 20061116:1000	664	Low	13.31	Low
20061116:1000 – 20061116:1500	-	-	-	-

08 Dec 2006

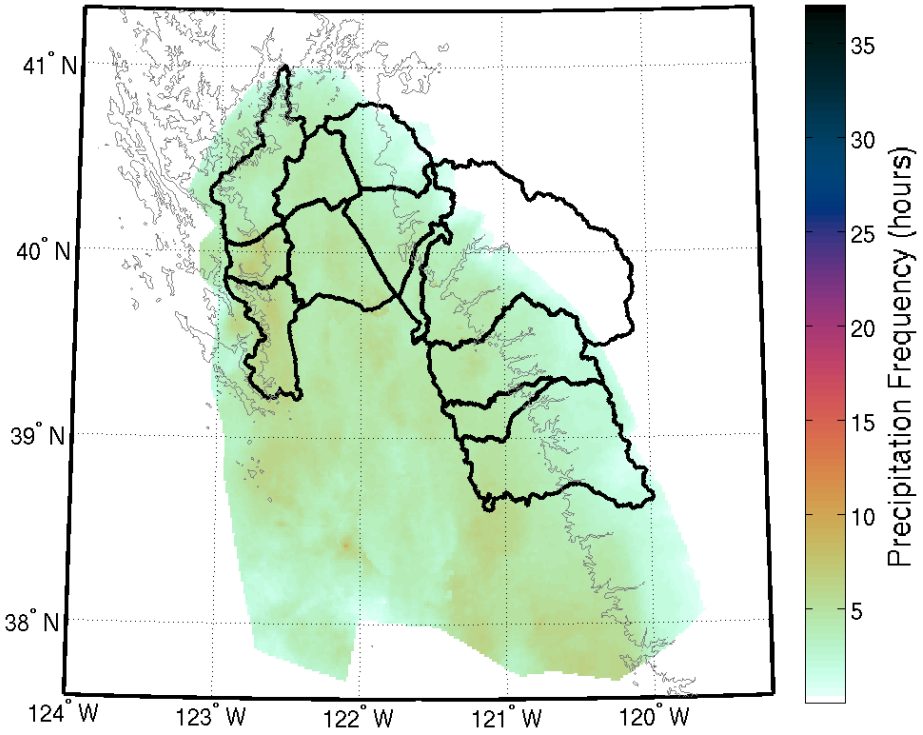

Variables	Value	Category
Storm Duration (hours)	11	-
KBBX Radar Offset (dBZ)	-3.5	-
BBY – Wind Direction at AR onset (°)	160.35	South
BBY – Mean Upslope Wind (m s^{-1})	11.958	Middle
BBY – Total Upslope IWV Flux (cm m s^{-1})	335.0	Middle

CCO Barrier Jet Timeline	Altitude (m)		Magnitude (ms^{-1})	
20061208:2200 – 20061209:0300	-	-	-	-
20061209:0300 – 20061209:0600	1111	Middle	24.26	High

11 Dec 2006

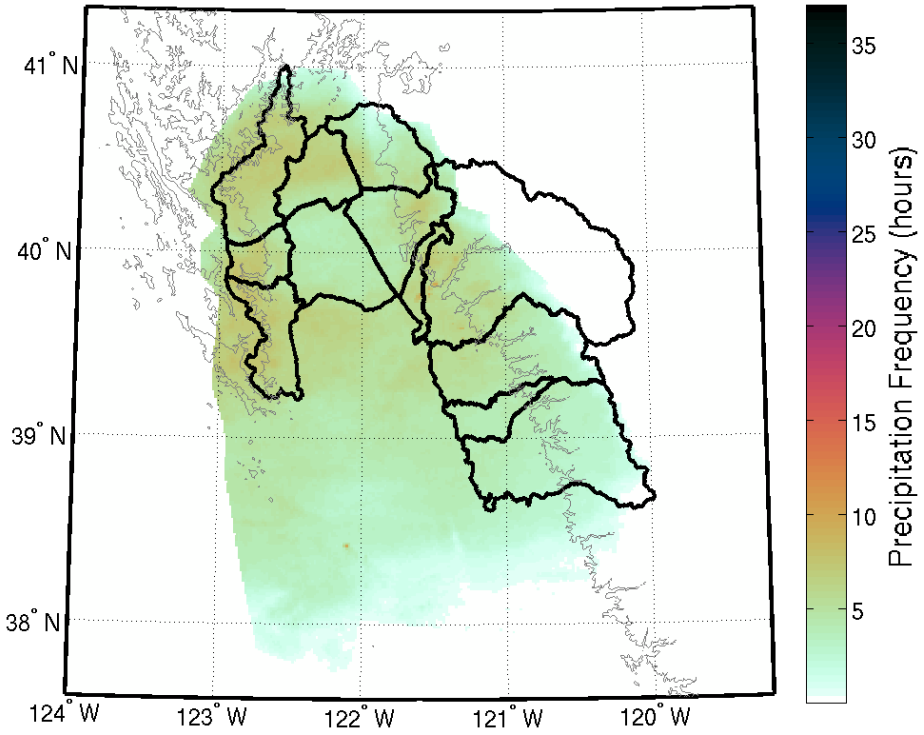

Variables	**Value**	**Category**
Storm Duration (hours)	16	-
KBBX Radar Offset (dBZ)	-3.5	-
BBY – Wind Direction at AR onset (°)	203.52	Southwest
BBY – Mean Upslope Wind (m s^{-1})	10.852	Middle
BBY – Total Upslope IWV Flux (cm m s^{-1})	338.0	Middle

CCO Barrier Jet Timeline	**Altitude (m)**		**Magnitude (ms^{-1})**	
20061211:1500 – 20061211:2000	-	-	-	-
20061211:2000 – 20061212:0700	677	Low	16.01	Low

13 Dec 2006

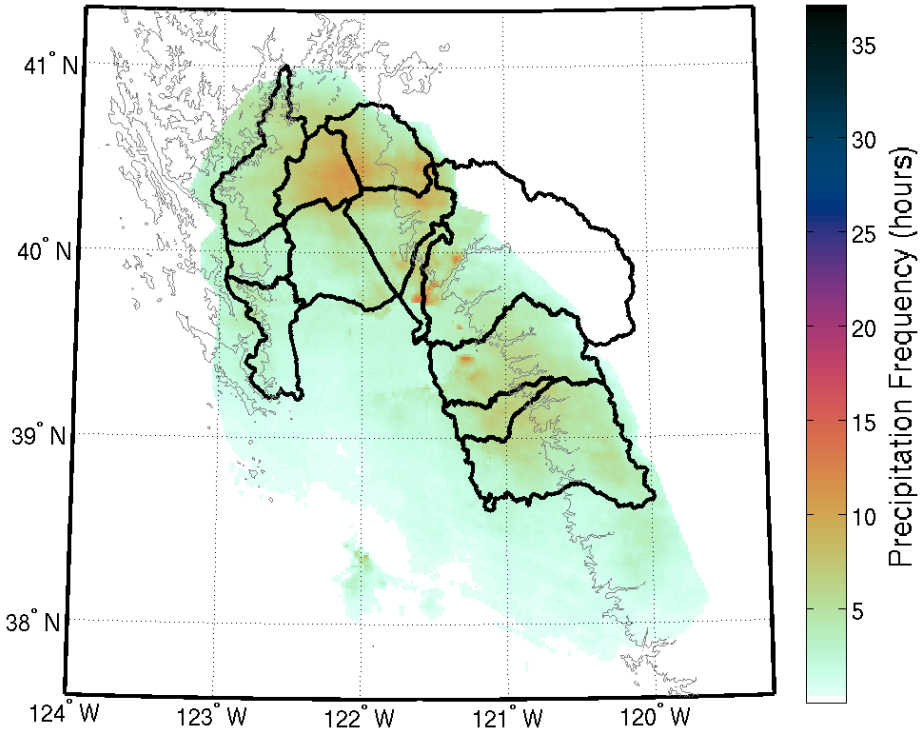

Variables	Value	Category
Storm Duration (hours)	21	-
KBBX Radar Offset (dBZ)	-4.5	-
BBY – Wind Direction at AR onset (°)	247.31	West
BBY – Mean Upslope Wind (m s^{-1})	6.266	Low
BBY – Total Upslope IWV Flux (cm m s^{-1})	375.7	Middle

CCO Barrier Jet Timeline	Altitude (m)		Magnitude (ms^{-1})	
20061213:0500 – 20061213:0800	-	-	-	-
20061213:0800 – 20061213:2000	663	Low	14.5	Low
20061213:2000 – 20061214:0200	-	-	-	-

21 Dec 2006

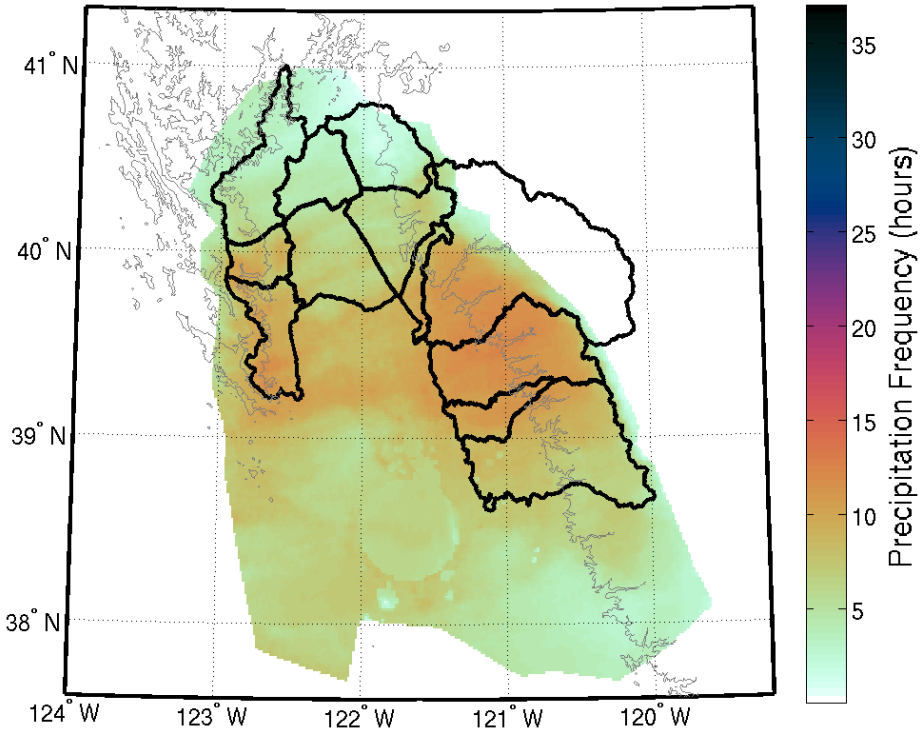

Variables	Value	Category
Storm Duration (hours)	17	-
KBBX Radar Offset (dBZ)	-3.5	-
BBY – Wind Direction at AR onset (°)	205.58	Southwest
BBY – Mean Upslope Wind (m s^{-1})	11.381	Middle
BBY – Total Upslope IWV Flux (cm m s^{-1})	468.1	High

CCO Barrier Jet Timeline	Altitude (m)		Magnitude (ms^{-1})	
20061221:0700 – 20061222:0000	-	-	-	-

26 Dec 2006

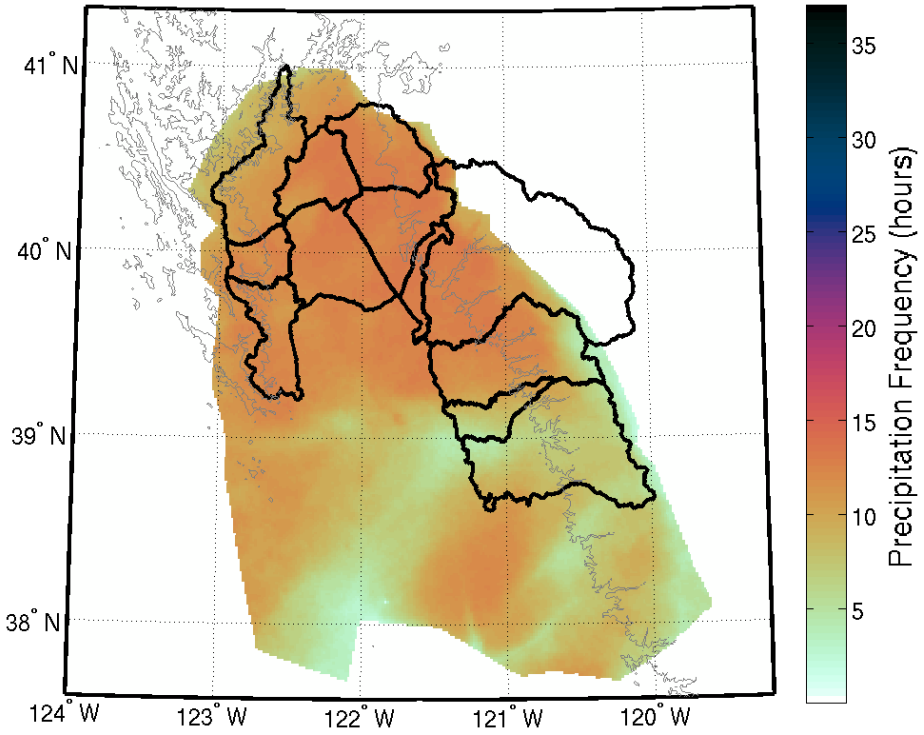

Variables	Value	Category
Storm Duration (hours)	13	-
KBBX Radar Offset (dBZ)	-3.5	-
BBY – Wind Direction at AR onset (°)	202.68	Southwest
BBY – Mean Upslope Wind (m s^{-1})	17.923	High
BBY – Total Upslope IWV Flux (cm m s^{-1})	653.6	High

CCO Barrier Jet Timeline	Altitude (m)		Magnitude (ms^{-1})	
20061226:1300 – 20061226:1400	-	-	-	-
20061226:1400 – 20061227:0200	1384	High	24.08	High

03 Jan 2007

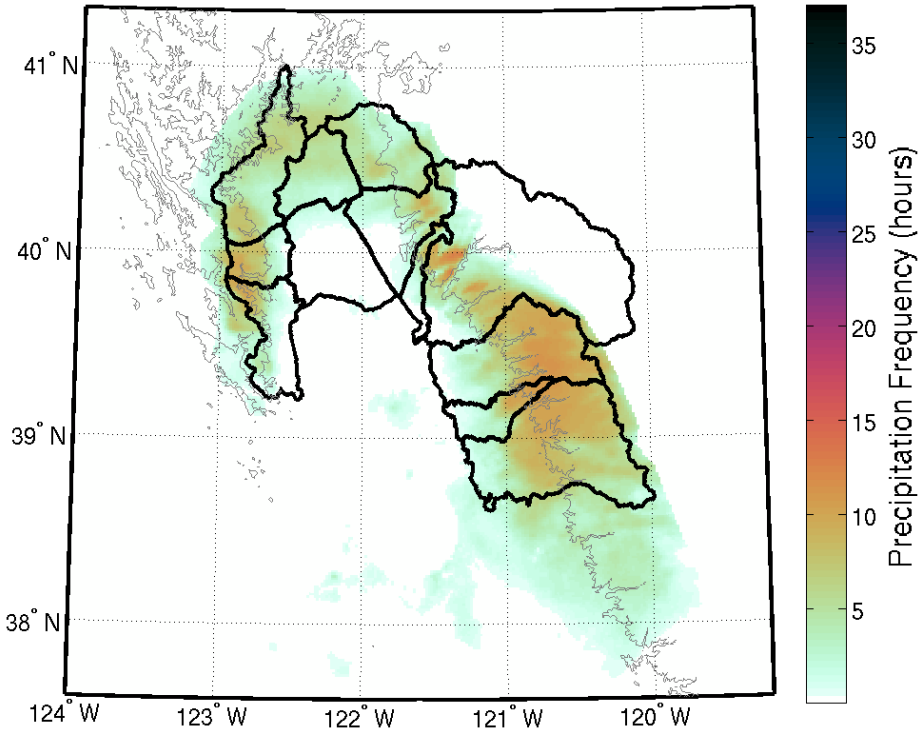

Variables	Value	Category
Storm Duration (hours)	13	-
KBBX Radar Offset (dBZ)	-3.5	-
BBY – Wind Direction at AR onset (°)	265.98	West
BBY – Mean Upslope Wind (m s^{-1})	7.350	Low
BBY – Total Upslope IWV Flux (cm m s^{-1})	242.0	Middle

CCO Barrier Jet Timeline	Altitude (m)		Magnitude (ms^{-1})	
20070103:2100 – 20070104:0900	609	Low	16.31	Low

21 Feb 2007

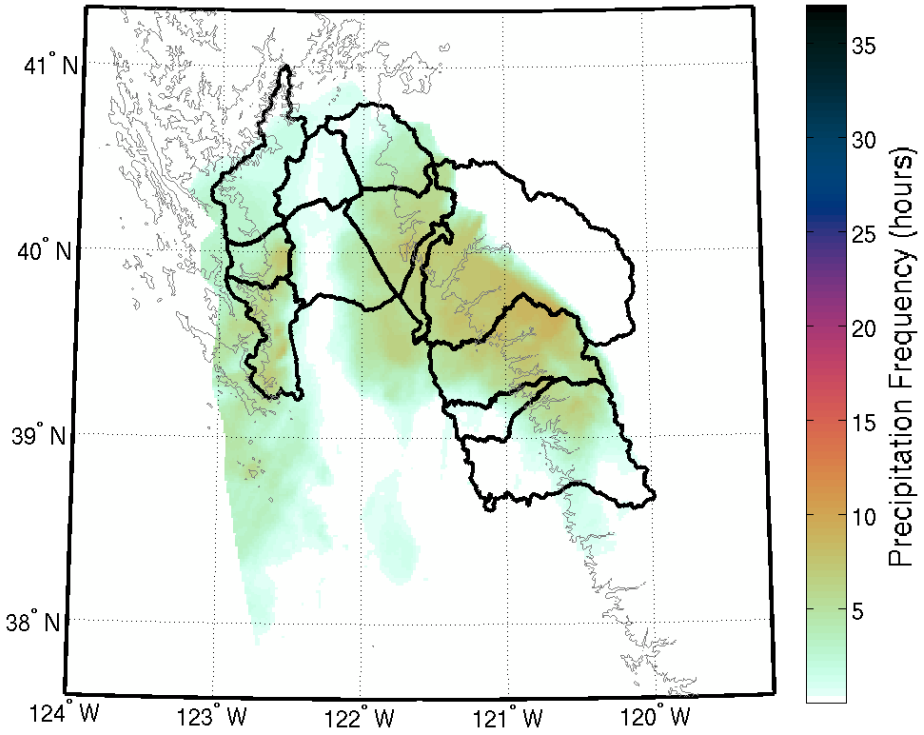

Variables	Value	Category
Storm Duration (hours)	10	-
KBBX Radar Offset (dBZ)	-3	-
BBY – Wind Direction at AR onset (°)	197.30	Southwest
BBY – Mean Upslope Wind (m s^{-1})	14.872	High
BBY – Total Upslope IWV Flux (cm m s^{-1})	319.9	Middle

CCO Barrier Jet Timeline	Altitude (m)		Magnitude (ms^{-1})	
20070221:2300 – 20070222:0400	862	Middle	15.42	Low

01 May 2007

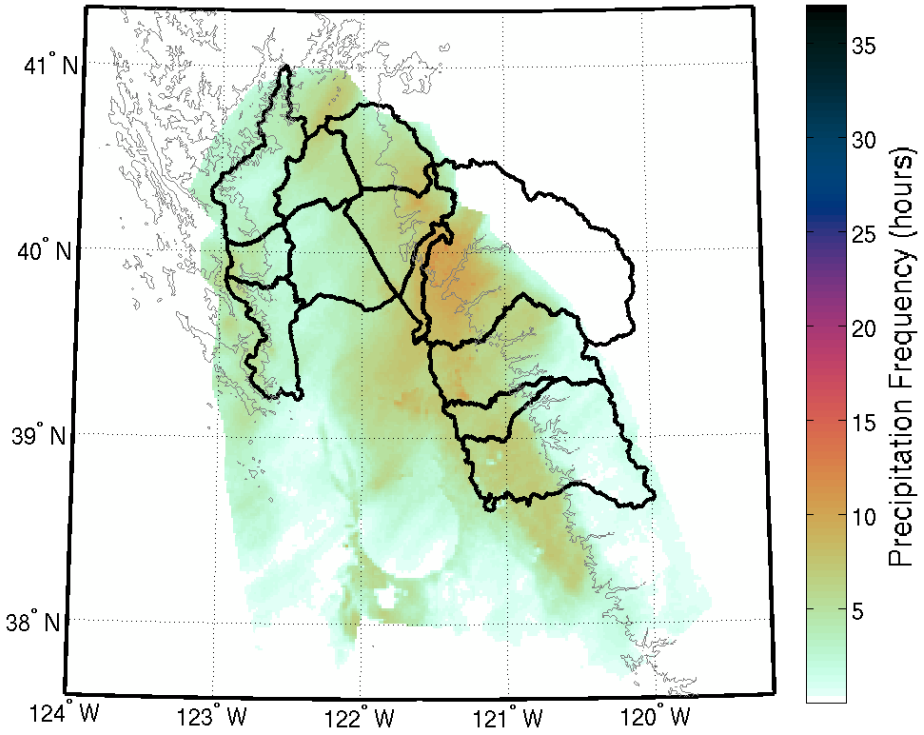

Variables	Value	Category
Storm Duration (hours)	13	-
KBBX Radar Offset (dBZ)	-2.5	-
BBY – Wind Direction at AR onset (°)	287.50	West
BBY – Mean Upslope Wind (m s^{-1})	6.578	Low
BBY – Total Upslope IWV Flux (cm m s^{-1})	232.2	Middle

CCO Barrier Jet Timeline	Altitude (m)		Magnitude (ms^{-1})	
20070501:2200 – 20070502:1100	-	-	-	-

18 Jul 2007

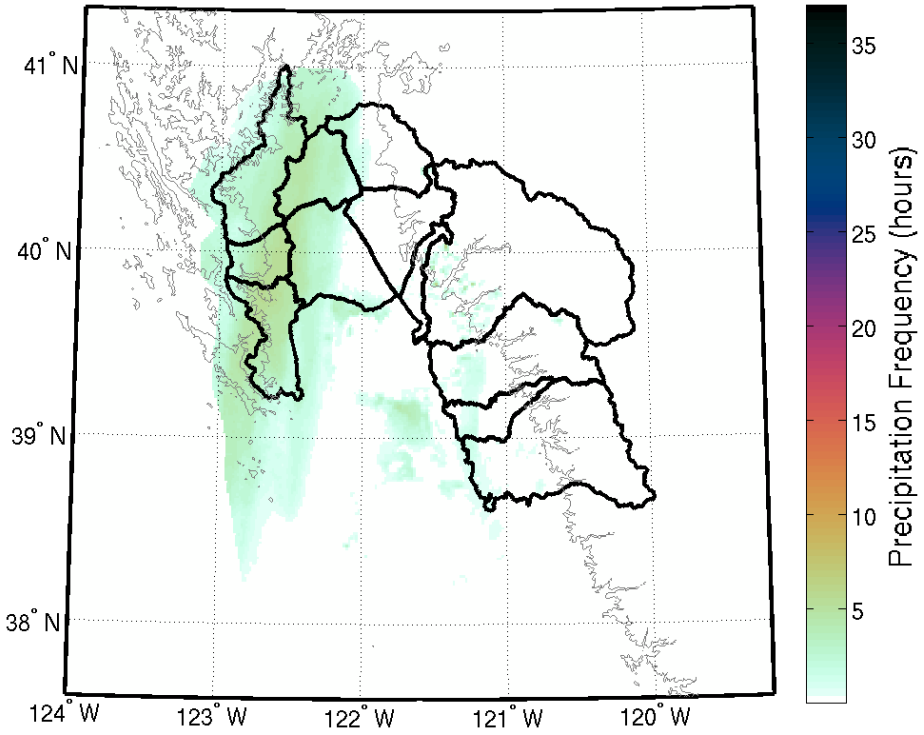

Variables	Value	Category
Storm Duration (hours)	8	-
KBBX Radar Offset (dBZ)	-1.5	-
BBY – Wind Direction at AR onset (°)	-	-
BBY – Mean Upslope Wind (m s^{-1})	-	-
BBY – Total Upslope IWV Flux (cm m s^{-1})	-	-

CCO Barrier Jet Timeline	Altitude (m)		Magnitude (ms^{-1})	
20070718:0000 – 20070718:0800	-	-	-	-

22 Sep 2007

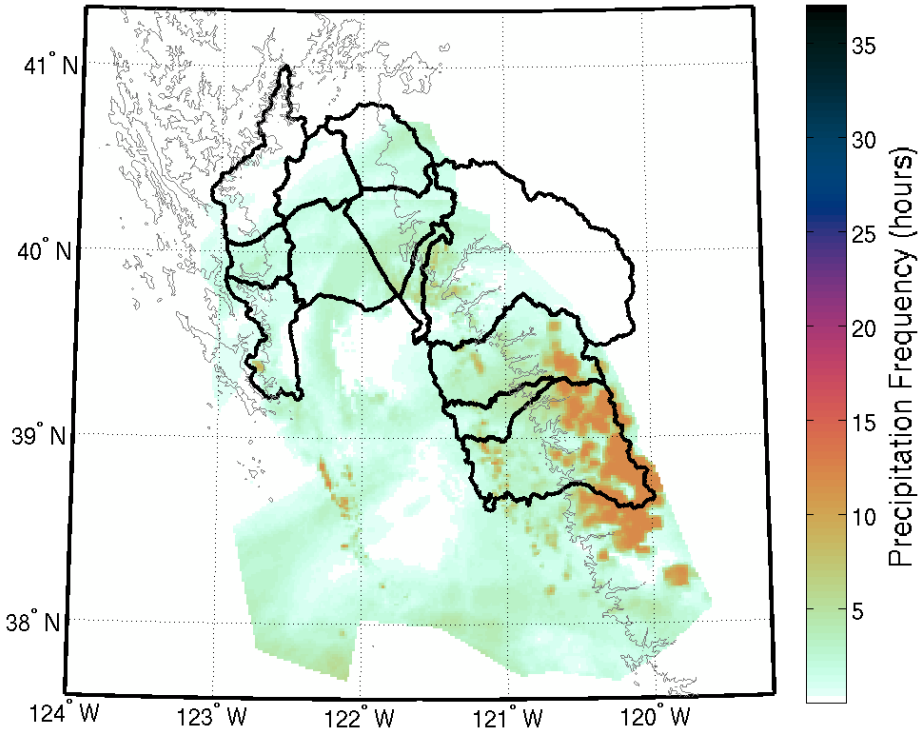

Variables	Value	Category
Storm Duration (hours)	12	-
KBBX Radar Offset (dBZ)	-2	-
BBY – Wind Direction at AR onset (°)	-	-
BBY – Mean Upslope Wind (m s^{-1})	-	-
BBY – Total Upslope IWV Flux (cm m s^{-1})	-	-

CCO Barrier Jet Timeline	Altitude (m)		Magnitude (ms^{-1})	
20070922:0700 – 20070922:1900	-	-	-	-

09 Oct 2007

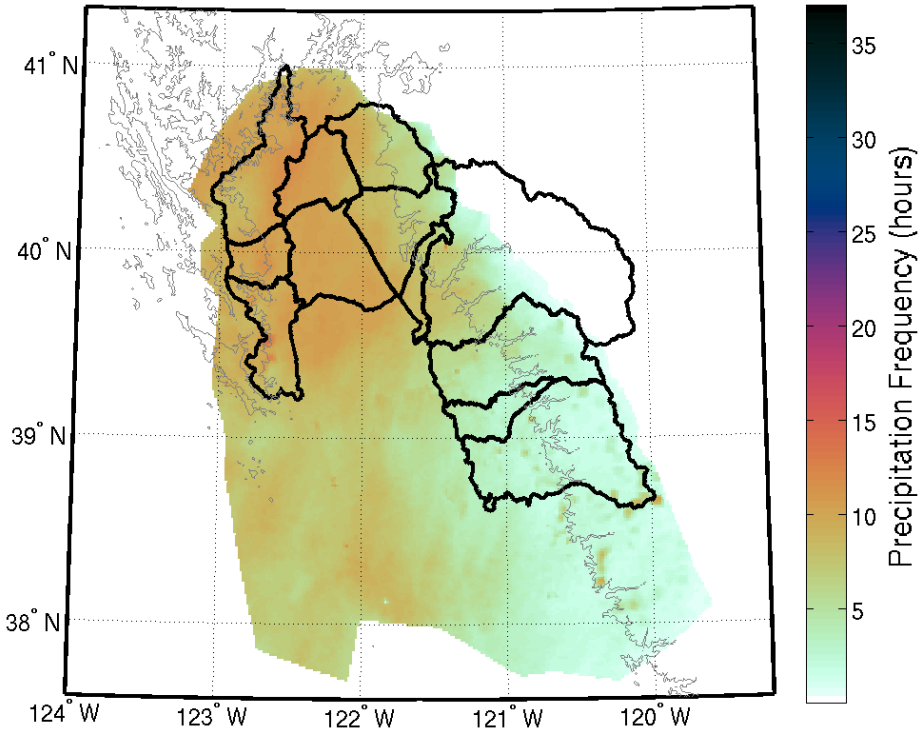

Variables	Value	Category
Storm Duration (hours)	15	-
KBBX Radar Offset (dBZ)	-2.5	-
BBY – Wind Direction at AR onset (°)	194.49	Southwest
BBY – Mean Upslope Wind (m s^{-1})	10.589	Middle
BBY – Total Upslope IWV Flux (cm m s^{-1})	437.5	High

CCO Barrier Jet Timeline	Altitude (m)		Magnitude (ms^{-1})	
20071009:1900 – 20071010:1000	-	-	-	-

12 Oct 2007

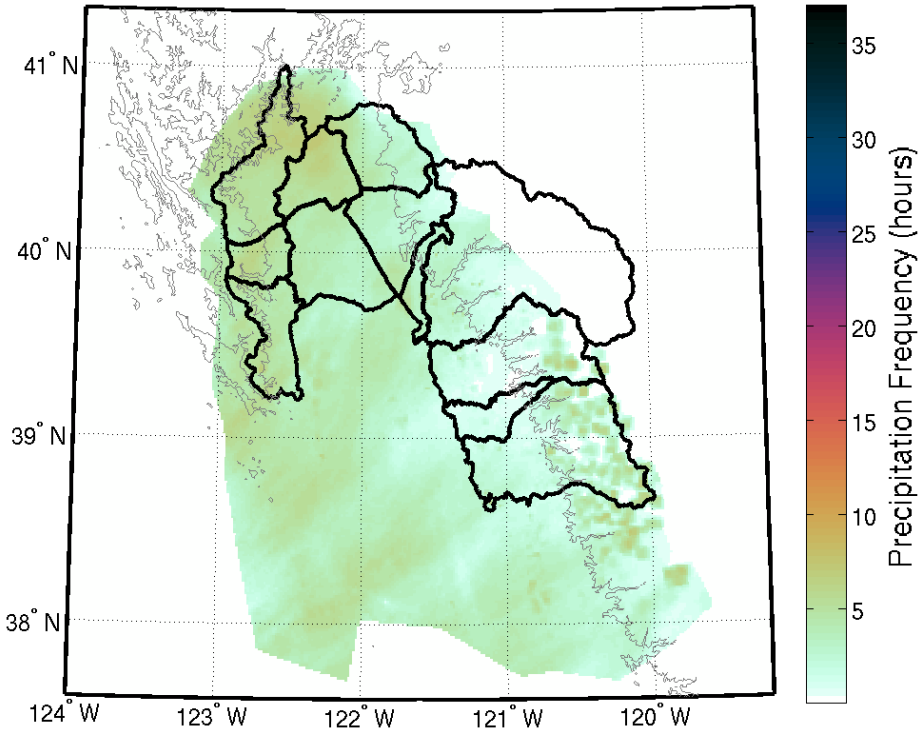

Variables	Value	Category
Storm Duration (hours)	8	-
KBBX Radar Offset (dBZ)	-2	-
BBY – Wind Direction at AR onset (°)	175.07	South
BBY – Mean Upslope Wind (m s^{-1})	9.666	Low
BBY – Total Upslope IWV Flux (cm m s^{-1})	211.0	Low

CCO Barrier Jet Timeline	Altitude (m)		Magnitude (ms^{-1})	
20071012:1000 – 20071012:1800	-	-	-	-

18 Oct 2007

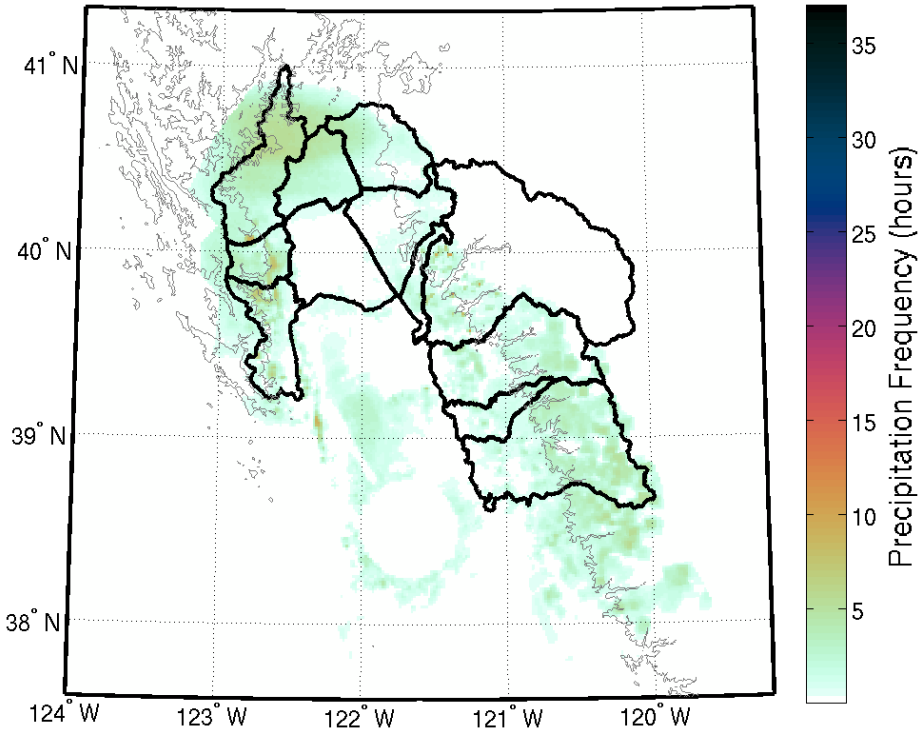

Variables	Value	Category
Storm Duration (hours)	18	-
KBBX Radar Offset (dBZ)	-2.5	-
BBY – Wind Direction at AR onset (°)	252.11	West
BBY – Mean Upslope Wind (m s^{-1})	6.435	Low
BBY – Total Upslope IWV Flux (cm m s^{-1})	357.1	Middle

CCO Barrier Jet Timeline	Altitude (m)		Magnitude (ms^{-1})	
20071018:1400 – 20071019:0800	-	-	-	-

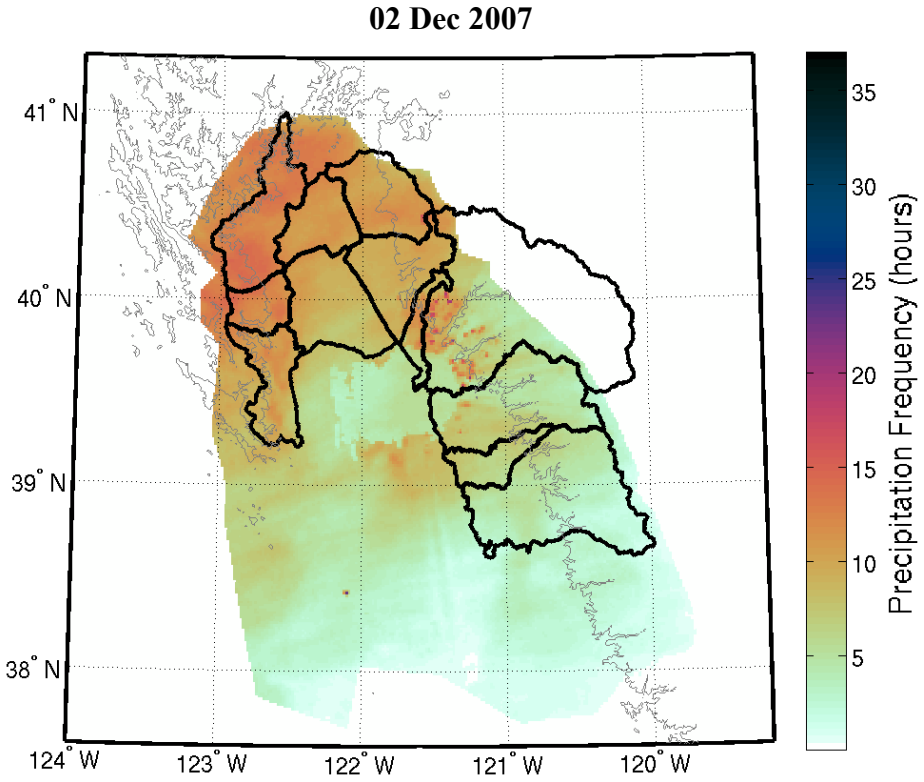
02 Dec 2007
41° N
40° N
39° N
38° N
124° W
123° W
122° W
121° W
120° W
35
30
25
20
15
10
5
Precipitation Frequency (hours)

02 Dec 2007

Variables	Value	Category
Storm Duration (hours)	42	-
KBBX Radar Offset (dBZ)	-2	-
BBY – Wind Direction at AR onset (°)	186.92	Southwest
BBY – Mean Upslope Wind (m s^{-1})	12.711	Middle
BBY – Total Upslope IWV Flux (cm m s^{-1})	1430.4	High

CCO Barrier Jet Timeline	Altitude (m)		Magnitude (ms^{-1})	
20071202:1900 – 20071203:0600	-	-	-	-
20071203:0600 – 20071203:1600	768	Middle	19.52	Middle
20071203:1600 – 20071203:2000	-	-	-	-
20071203:2000 – 20071204:1100	1043	Middle	15.38	Low
20071204:1100 – 20071204:1300	-	-	-	-

19 Dec 2007

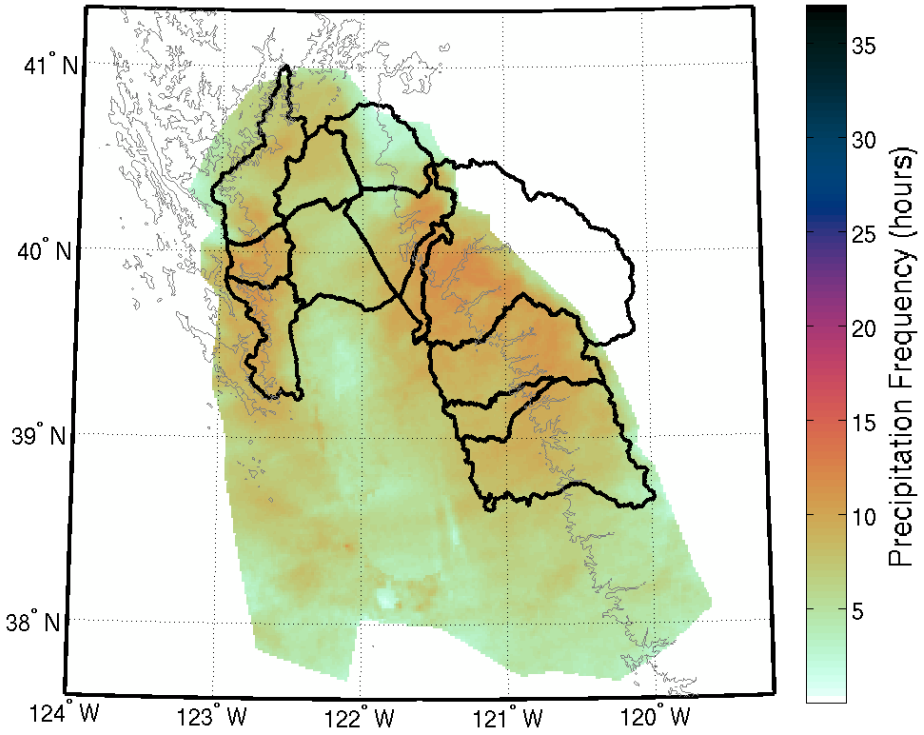

Variables	Value	Category
Storm Duration (hours)	12	-
KBBX Radar Offset (dBZ)	-1.5	-
BBY – Wind Direction at AR onset (°)	212.72	Southwest
BBY – Mean Upslope Wind (m s^{-1})	12.627	Middle
BBY – Total Upslope IWV Flux (cm m s^{-1})	410.0	Middle

CCO Barrier Jet Timeline	Altitude (m)		Magnitude (ms^{-1})	
20071219:2200 – 20071220:1000	844	Middle	18.63	Middle

10 Jan 2008

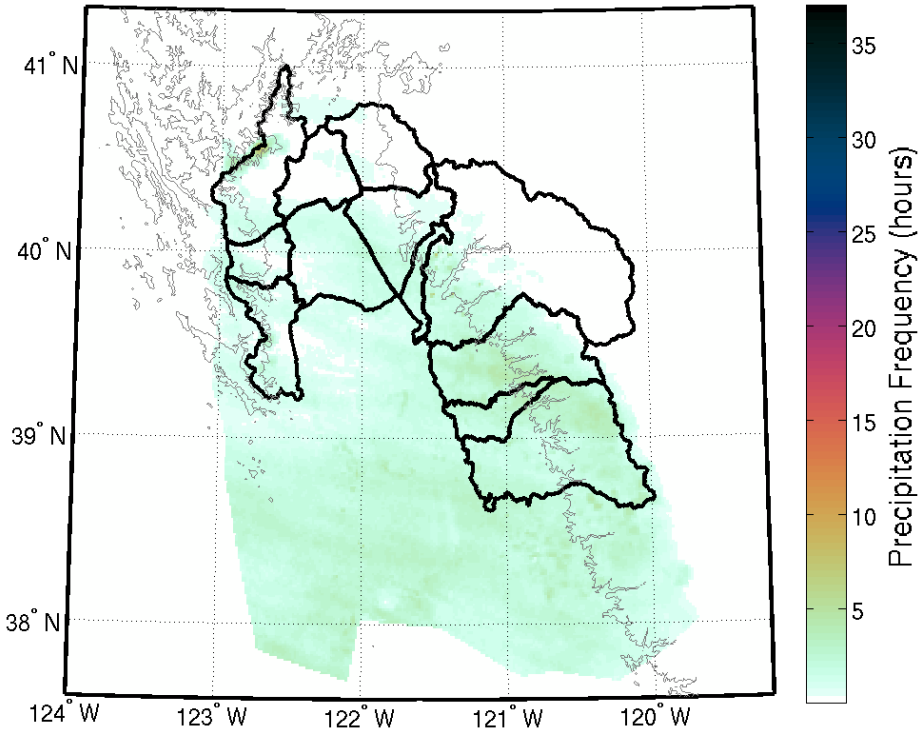

Variables	Value	Category
Storm Duration (hours)	9	-
KBBX Radar Offset (dBZ)	-2.5	-
BBY – Wind Direction at AR onset (°)	237.31	Southwest
BBY – Mean Upslope Wind (m s^{-1})	9.122	Low
BBY – Total Upslope IWV Flux (cm m s^{-1})	222.7	Low

CCO Barrier Jet Timeline	Altitude (m)		Magnitude (ms^{-1})	
20080110:0900 – 20080110:1800	-	-	-	-

26 Jan 2008

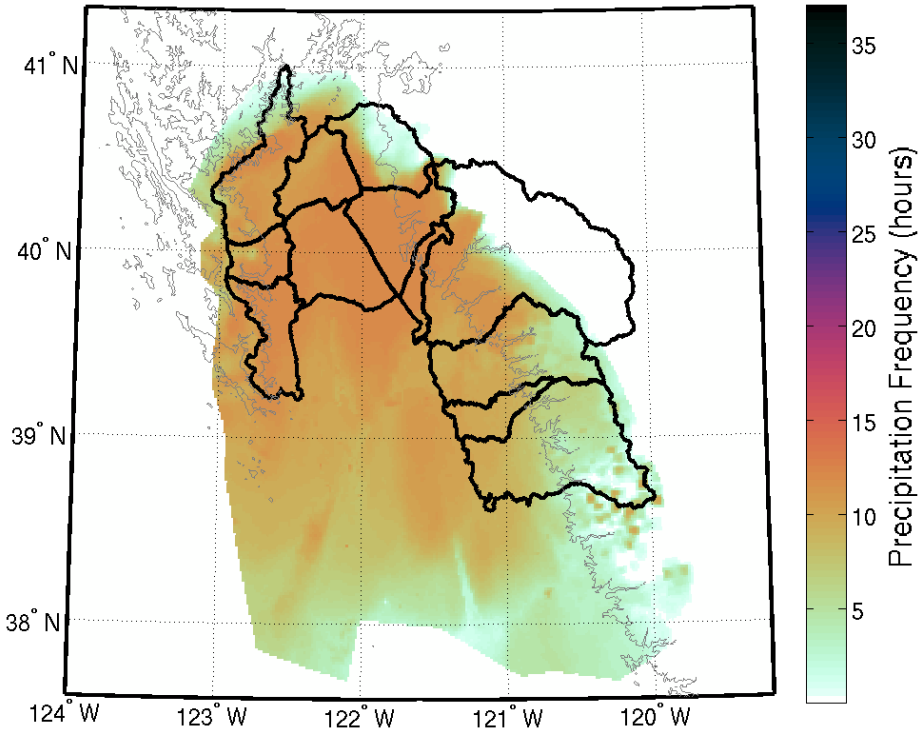

Variables	Value	Category
Storm Duration (hours)	12	-
KBBX Radar Offset (dBZ)	-2.5	-
BBY – Wind Direction at AR onset (°)	162.01	South
BBY – Mean Upslope Wind (m s^{-1})	15.572	High
BBY – Total Upslope IWV Flux (cm m s^{-1})	427.5	High

CCO Barrier Jet Timeline	Altitude (m)		Magnitude (ms^{-1})	
20080126:0200 – 20080126:1400	1642	High	23.00	High

02 Feb 2008

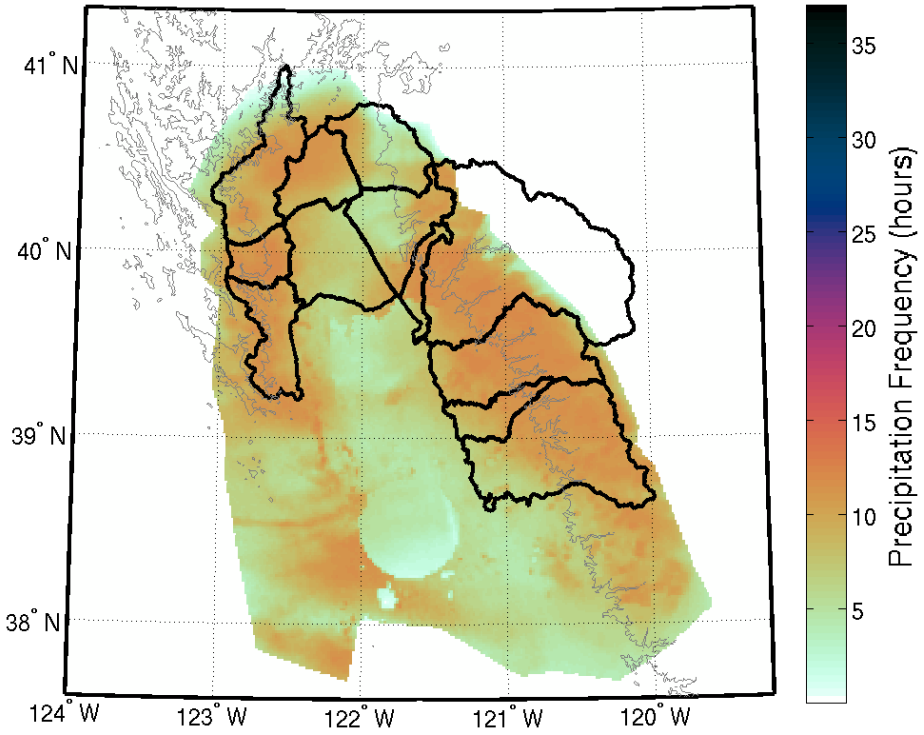

Variables	Value	Category
Storm Duration (hours)	12	-
KBBX Radar Offset (dBZ)	-3	-
BBY – Wind Direction at AR onset (°)	232.39	Southwest
BBY – Mean Upslope Wind (m s^{-1})	12.783	High
BBY – Total Upslope IWV Flux (cm m s^{-1})	341.9	Middle

CCO Barrier Jet Timeline	Altitude (m)		Magnitude (ms^{-1})	
20080202:1900 – 20080203:0700	685	Low	24.12	High

28 Mar 2008

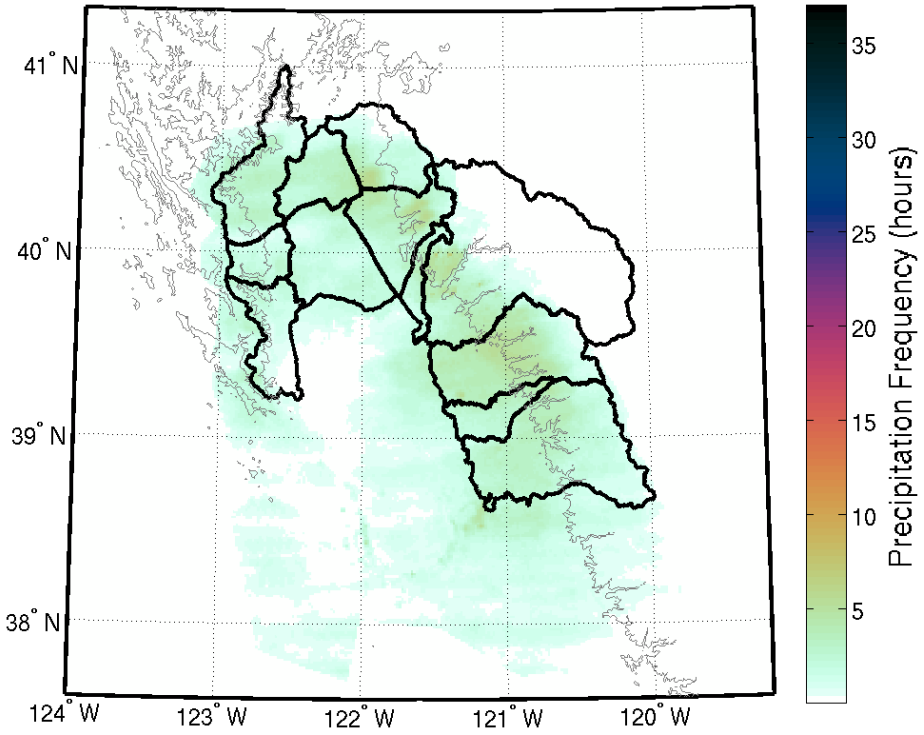

Variables	Value	Category
Storm Duration (hours)	8	-
KBBX Radar Offset (dBZ)	-2	-
BBY – Wind Direction at AR onset (°)	250.69	West
BBY – Mean Upslope Wind (m s^{-1})	10.237	Middle
BBY – Total Upslope IWV Flux (cm m s^{-1})	178.7	Low

CCO Barrier Jet Timeline	Altitude (m)		Magnitude (ms^{-1})	
20080328:1800 – 20080329:0200	-	-	-	-

02 Oct 2008

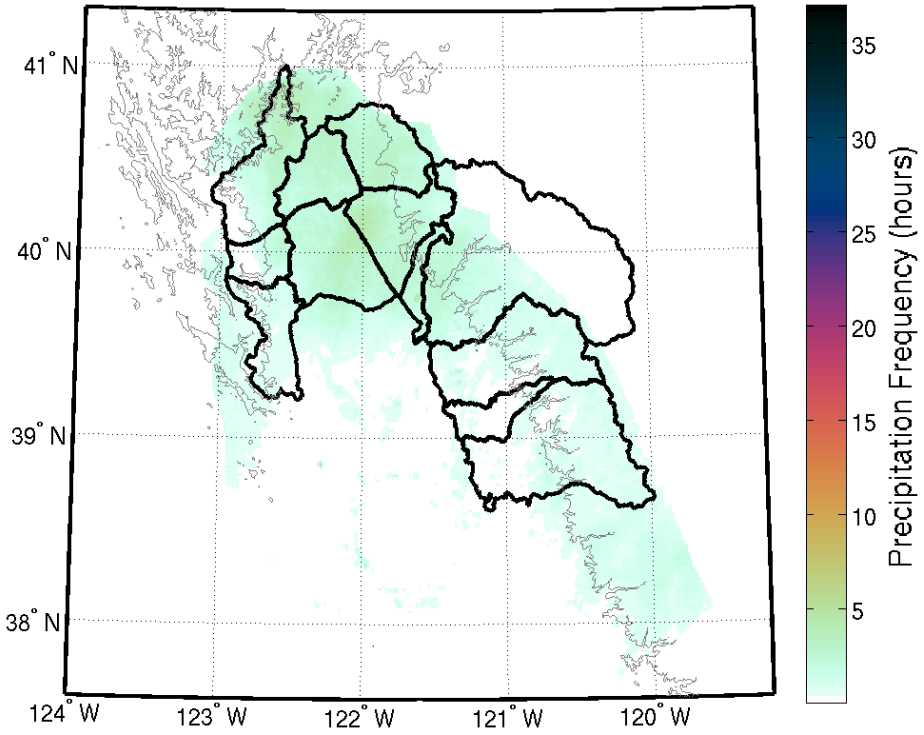

Variables	Value	Category
Storm Duration (hours)	10	-
KBBX Radar Offset (dBZ)	-4	-
BBY – Wind Direction at AR onset (°)	246.38	West
BBY – Mean Upslope Wind (m s^{-1})	7.013	Low
BBY – Total Upslope IWV Flux (cm m s^{-1})	-	-

CCO Barrier Jet Timeline	Altitude (m)		Magnitude (ms^{-1})	
20081002:0900 – 20081002:1900	-	-	-	-

03 Oct 2008

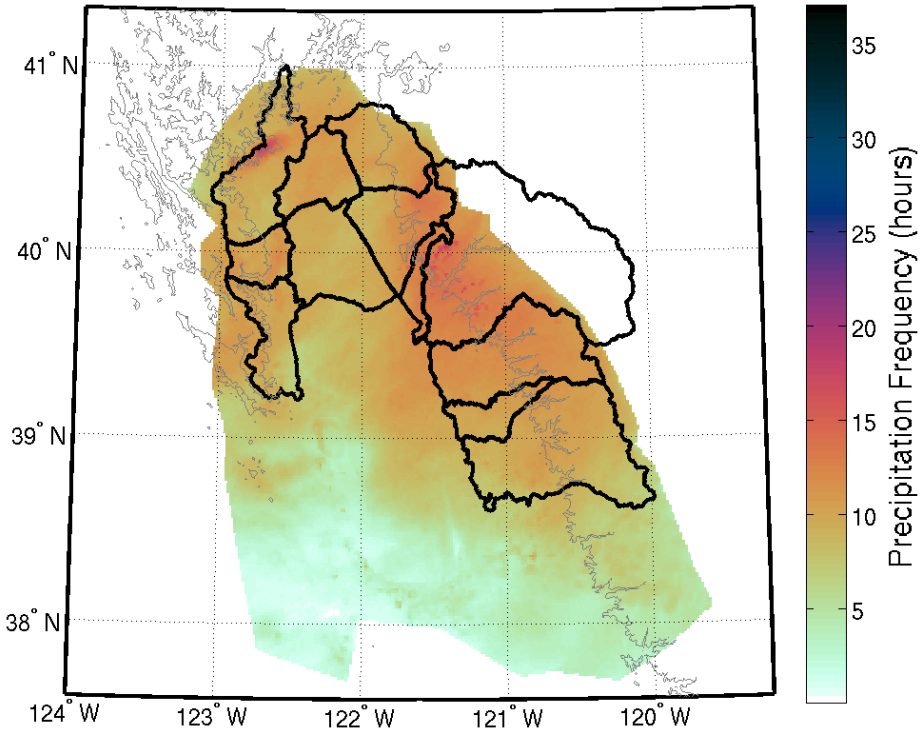

Variables	Value	Category
Storm Duration (hours)	18	-
KBBX Radar Offset (dBZ)	-3	-
BBY – Wind Direction at AR onset (°)	250.35	West
BBY – Mean Upslope Wind (m s^{-1})	10.320	Middle
BBY – Total Upslope IWV Flux (cm m s^{-1})	-	-

CCO Barrier Jet Timeline	Altitude (m)		Magnitude (ms^{-1})	
20081003:1400 – 20081004:0800	-	-	-	-

31 Oct 2008

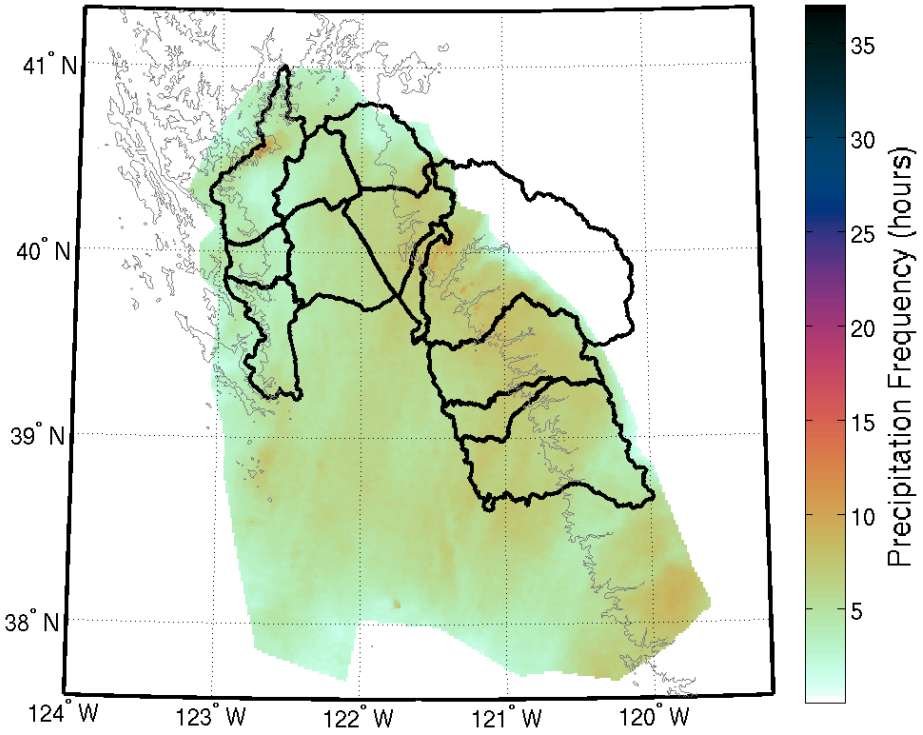

Variables	Value	Category
Storm Duration (hours)	11	-
KBBX Radar Offset (dBZ)	-3.5	-
BBY – Wind Direction at AR onset (°)	159.63	South
BBY – Mean Upslope Wind (m s^{-1})	13.181	High
BBY – Total Upslope IWV Flux (cm m s^{-1})	367.6	Middle

CCO Barrier Jet Timeline	Altitude (m)		Magnitude (ms^{-1})	
20081031:0500 – 20081031:1600	-	-	-	-

21 Dec 2008

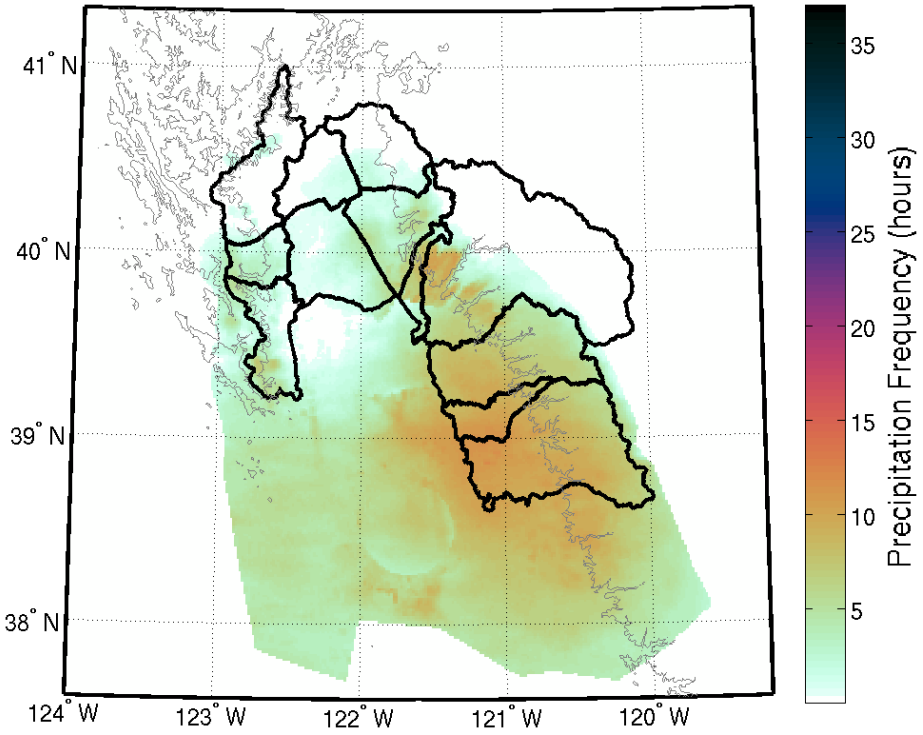

Variables	**Value**	**Category**
Storm Duration (hours)	12	-
KBBX Radar Offset (dBZ)	-4.5	-
BBY – Wind Direction at AR onset (°)	236.88	Southwest
BBY – Mean Upslope Wind (m s^{-1})	12.076	Middle
BBY – Total Upslope IWV Flux (cm m s^{-1})	360.8	Middle

CCO Barrier Jet Timeline	**Altitude (m)**		**Magnitude (ms^{-1})**	
20081221:1400 – 20081221:1700	-	-	-	-
20081221:1700 – 20081222:0200	1004	Middle	13.52	Low

24 Dec 2008

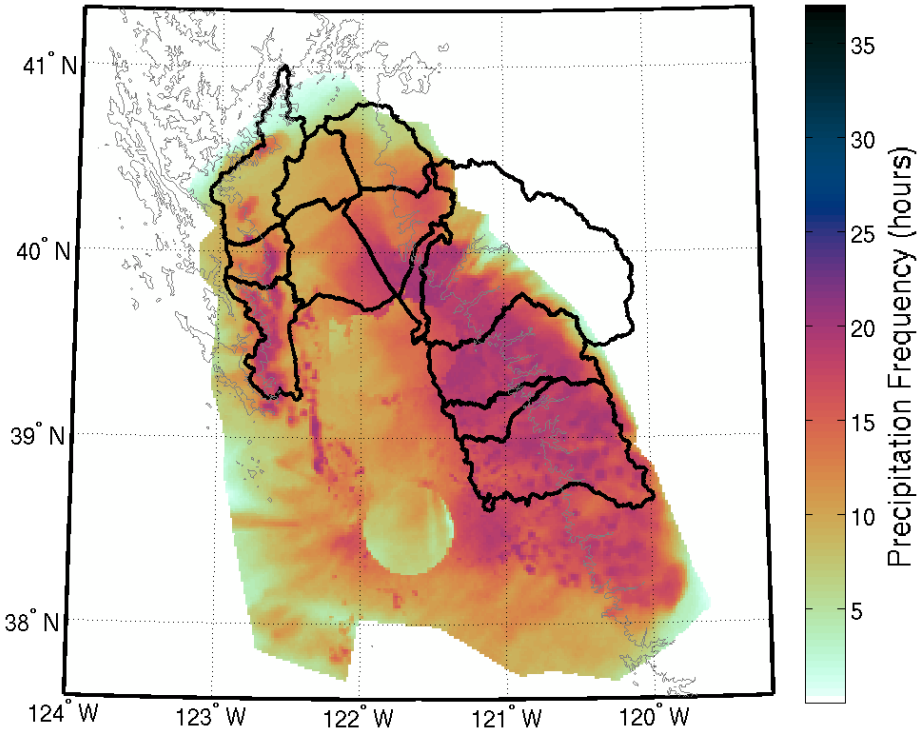

Variables	Value	Category
Storm Duration (hours)	20	-
KBBX Radar Offset (dBZ)	-4	-
BBY – Wind Direction at AR onset (°)	161.17	South
BBY – Mean Upslope Wind (m s^{-1})	15.165	High
BBY – Total Upslope IWV Flux (cm m s^{-1})	694.1	High

CCO Barrier Jet Timeline	Altitude (m)		Magnitude (ms^{-1})	
20081224:1300 – 20081225:0600	1575	High	13.52	Low
20081225:0600 – 20081225:0900	-	-	-	-

02 Jan 2009

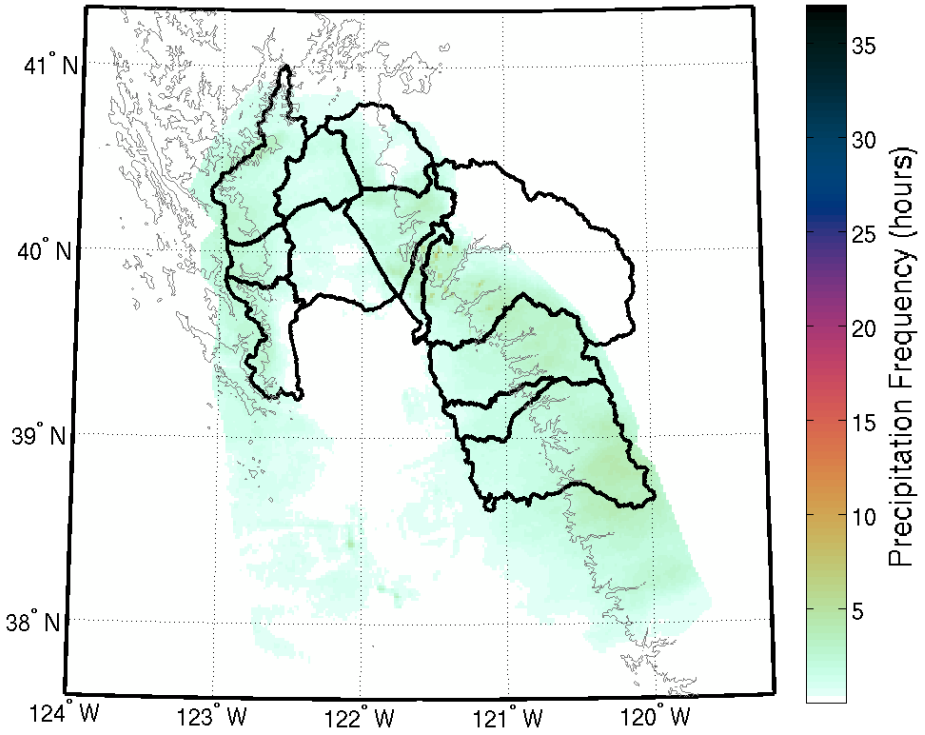

Variables	Value	Category
Storm Duration (hours)	8	-
KBBX Radar Offset (dBZ)	-2.5	-
BBY – Wind Direction at AR onset (°)	263.21	West
BBY – Mean Upslope Wind (m s^{-1})	8.217	Low
BBY – Total Upslope IWV Flux (cm m s^{-1})	149.7	Low

CCO Barrier Jet Timeline	Altitude (m)		Magnitude (ms^{-1})	
20090102:0800 – 20090102:1600	-	-	-	-

22 Feb 2009

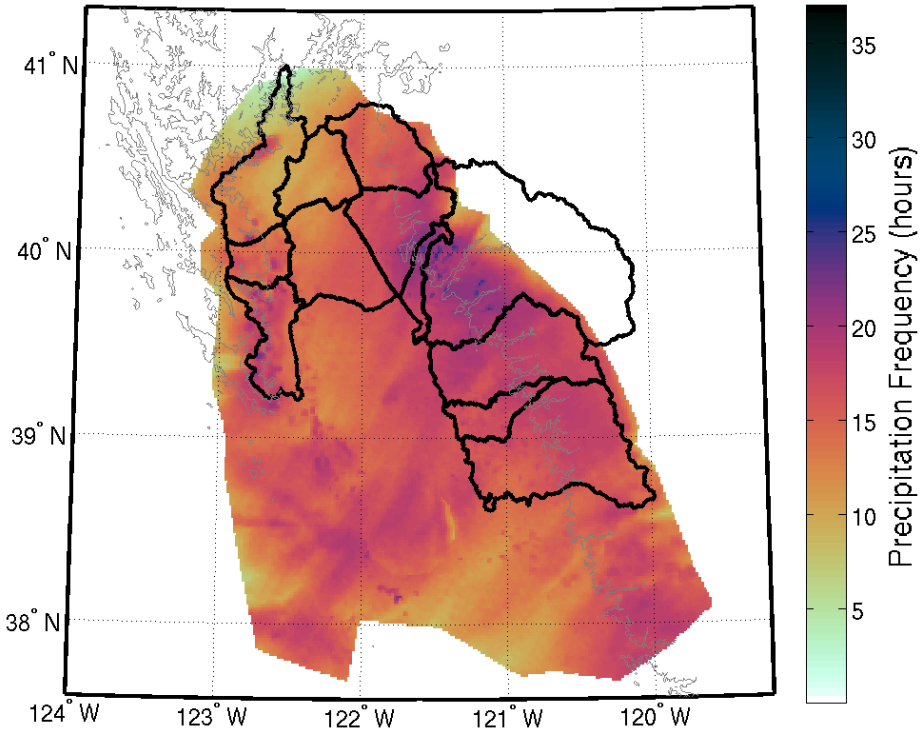

Variables	Value	Category
Storm Duration (hours)	26	-
KBBX Radar Offset (dBZ)	-4	-
BBY – Wind Direction at AR onset (°)	165.06	South
BBY – Mean Upslope Wind (m s^{-1})	14.649	High
BBY – Total Upslope IWV Flux (cm m s^{-1})	935.6	High

CCO Barrier Jet Timeline	Altitude (m)		Magnitude (ms^{-1})	
20090222:0200 – 20090222:1200	-	-	-	-
20090222:1200 – 20090223:0200	982	Middle	21.01	High
20090223:0200 – 20090223:0400	-	-	-	-

01 Mar 2009

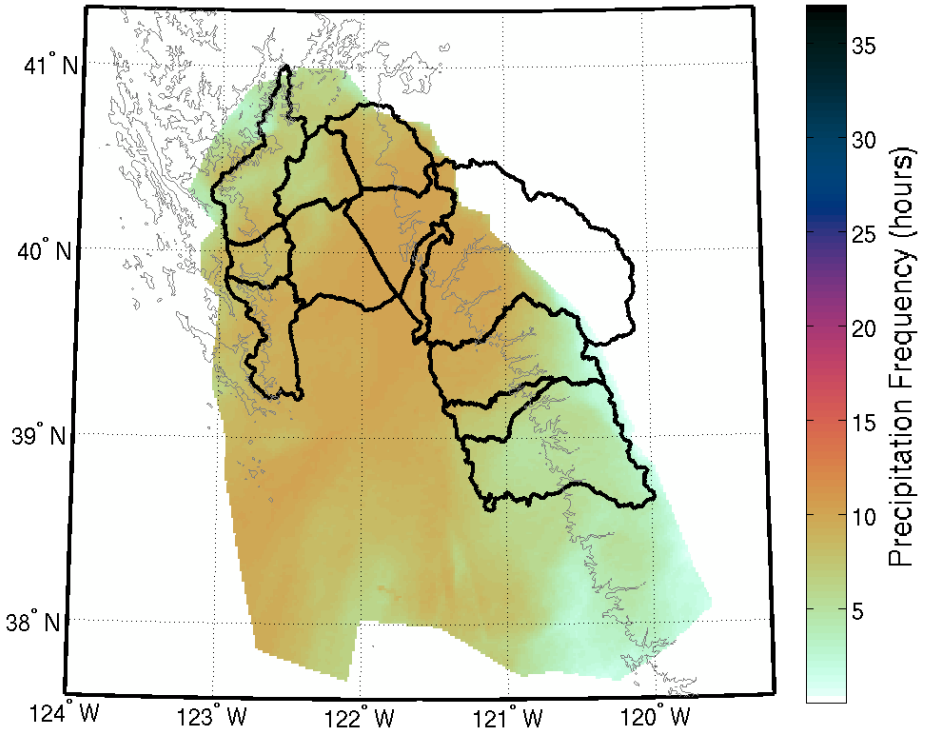

Variables	Value	Category
Storm Duration (hours)	10	-
KBBX Radar Offset (dBZ)	-2	-
BBY – Wind Direction at AR onset (°)	164.38	South
BBY – Mean Upslope Wind (m s^{-1})	11.513	Middle
BBY – Total Upslope IWV Flux (cm m s^{-1})	270.6	Middle

CCO Barrier Jet Timeline	Altitude (m)		Magnitude (ms^{-1})	
20090301:0900 – 20090301:1600	-	-	-	-
20090301:1600 – 20090301:1900	1342	High	19.68	Middle

15 Mar 2009

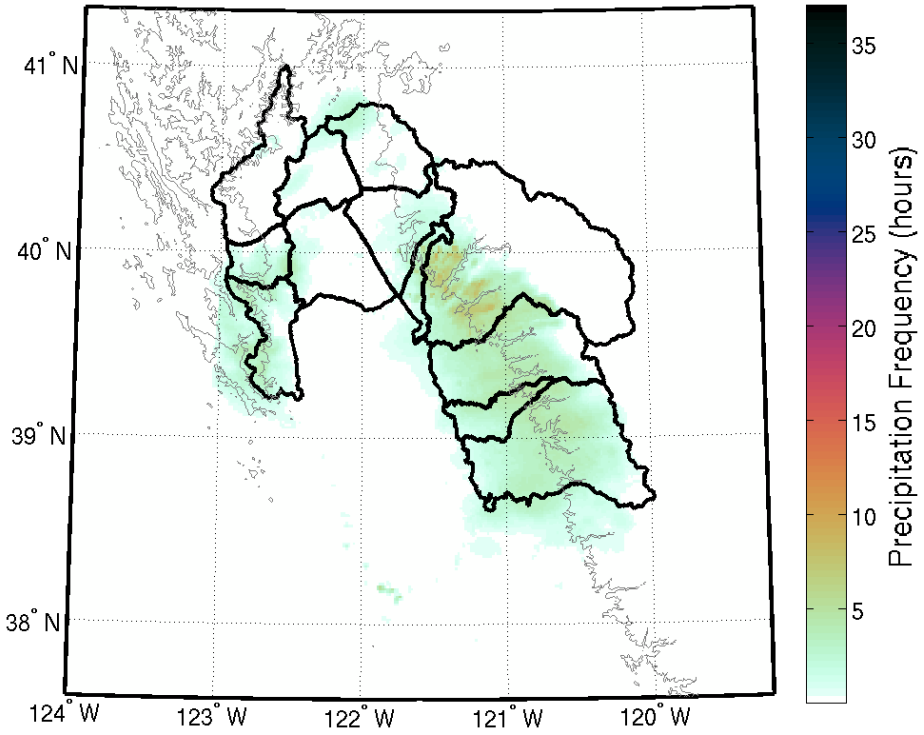

Variables	Value	Category
Storm Duration (hours)	9	-
KBBX Radar Offset (dBZ)	-4.5	-
BBY – Wind Direction at AR onset (°)	211.42	Southwest
BBY – Mean Upslope Wind (m s^{-1})	7.841	Low
BBY – Total Upslope IWV Flux (cm m s^{-1})	172.6	Low

CCO Barrier Jet Timeline	Altitude (m)		Magnitude (ms^{-1})	
20090315:2000 – 20090316:0500	-	-	-	-

01 May 2009

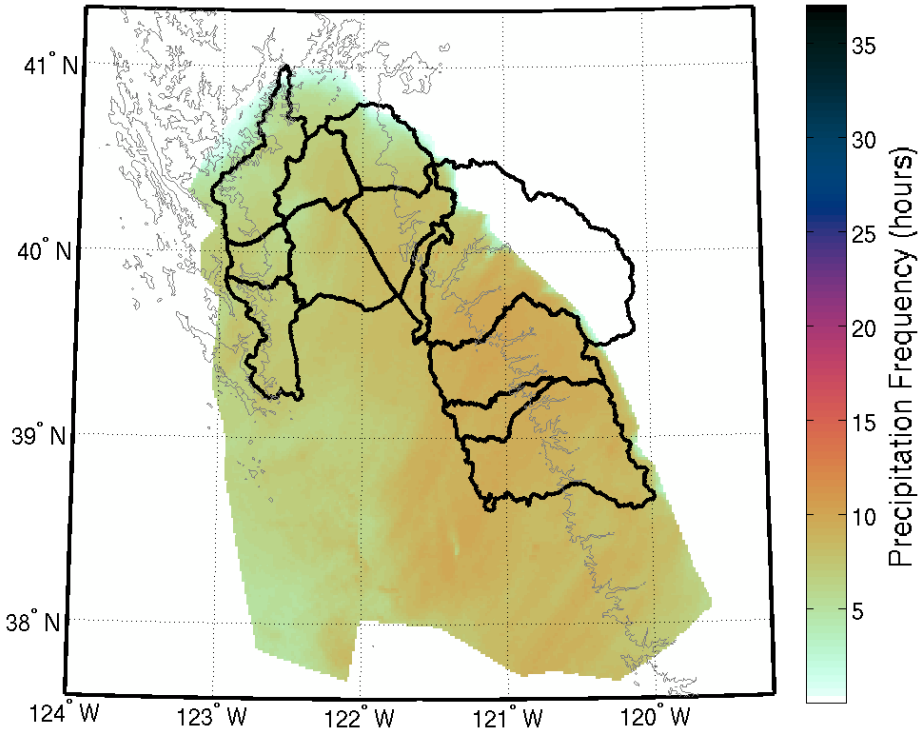

Variables	Value	Category
Storm Duration (hours)	10	-
KBBX Radar Offset (dBZ)	-4	-
BBY – Wind Direction at AR onset (°)	168.14	South
BBY – Mean Upslope Wind (m s^{-1})	14.124	High
BBY – Total Upslope IWV Flux (cm m s^{-1})	389.4	Middle

CCO Barrier Jet Timeline	Altitude (m)		Magnitude (ms^{-1})	
20090501:1800 – 20090502:0400	-	-	-	-

02 May 2009

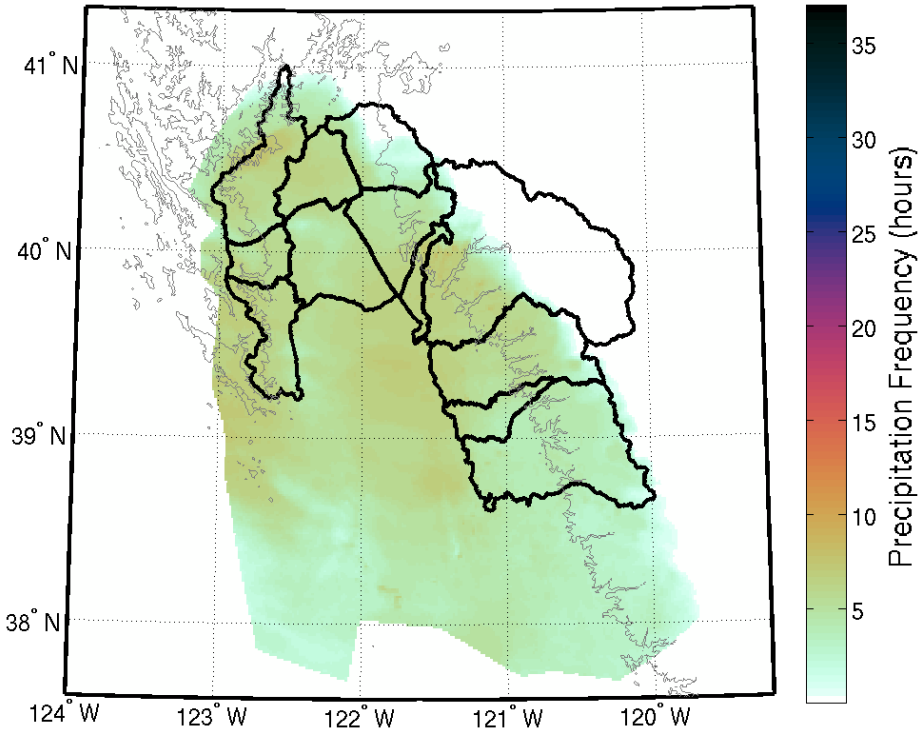

Variables	Value	Category
Storm Duration (hours)	8	-
KBBX Radar Offset (dBZ)	-3.5	-
BBY – Wind Direction at AR onset (°)	201.51	Southwest
BBY – Mean Upslope Wind (m s^{-1})	8.613	Low
BBY – Total Upslope IWV Flux (cm m s^{-1})	201.4	Low

CCO Barrier Jet Timeline	Altitude (m)		Magnitude (ms^{-1})	
20090502:1300 – 20090502:2100	-	-	-	-

03 May 2009

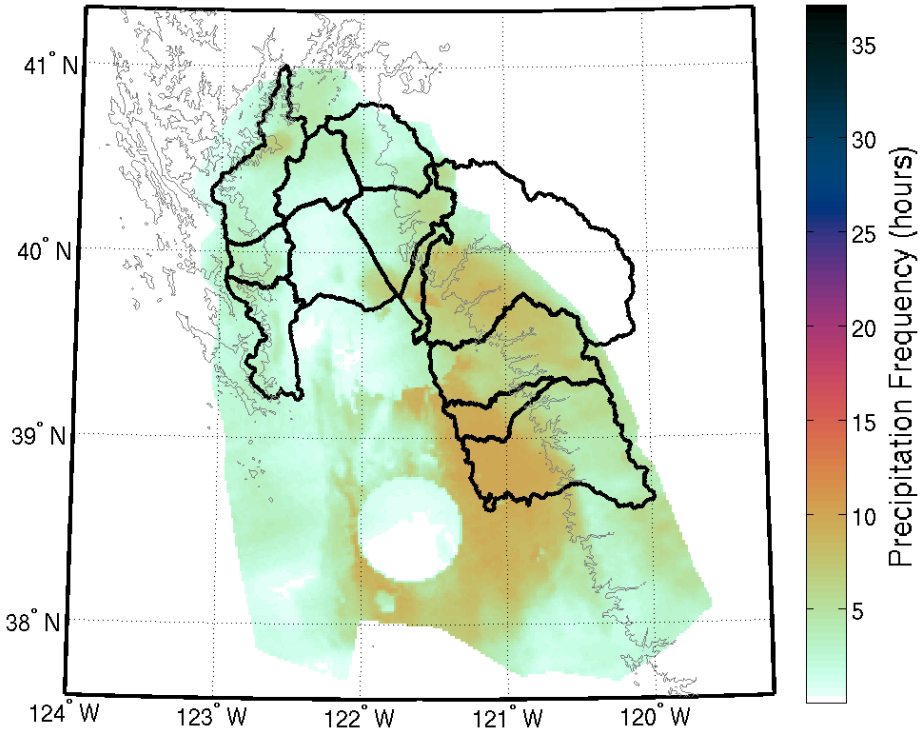

Variables	Value	Category
Storm Duration (hours)	10	-
KBBX Radar Offset (dBZ)	-0.5	-
BBY – Wind Direction at AR onset (°)	191.45	Southwest
BBY – Mean Upslope Wind (m s^{-1})	10.372	Middle
BBY – Total Upslope IWV Flux (cm m s^{-1})	276.6	Middle

CCO Barrier Jet Timeline	Altitude (m)		Magnitude (ms^{-1})	
20090503:0500 – 20090503:1500	-	-	-	-

13 Oct 2009

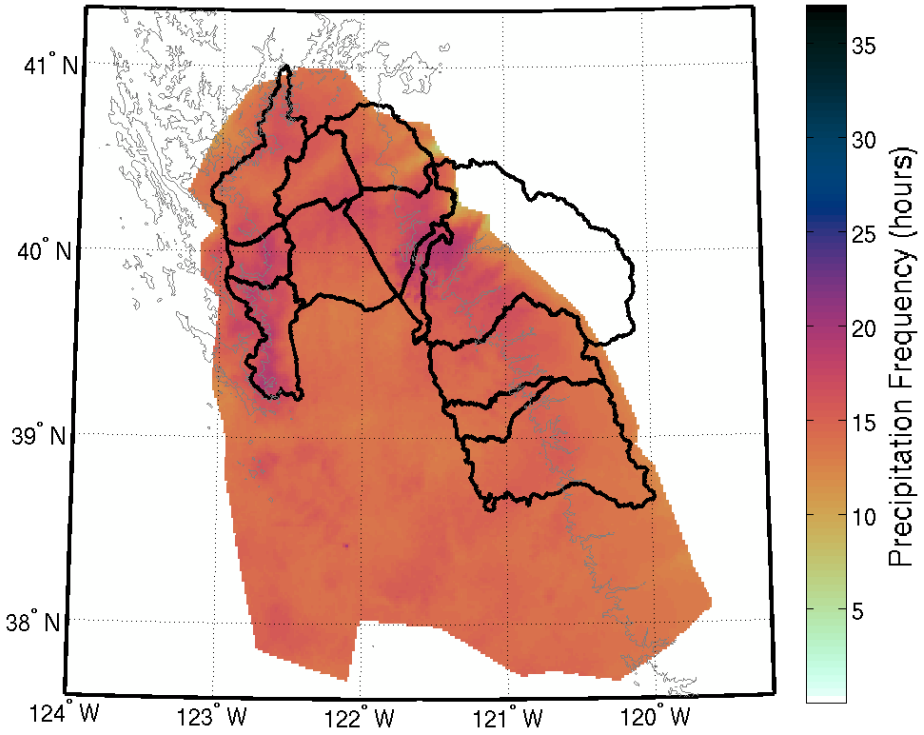

Variables	Value	Category
Storm Duration (hours)	24	-
KBBX Radar Offset (dBZ)	-3	-
BBY – Wind Direction at AR onset (°)	168.59	South
BBY – Mean Upslope Wind (m s^{-1})	15.468	High
BBY – Total Upslope IWV Flux (cm m s^{-1})	1132.1	High

CCO Barrier Jet Timeline	Altitude (m)		Magnitude (ms^{-1})	
20091013:0200 – 20091013:0700	-	-	-	-
20091013:0700 – 20091014:0200	897	Middle	29.16	High

15 Dec 2009

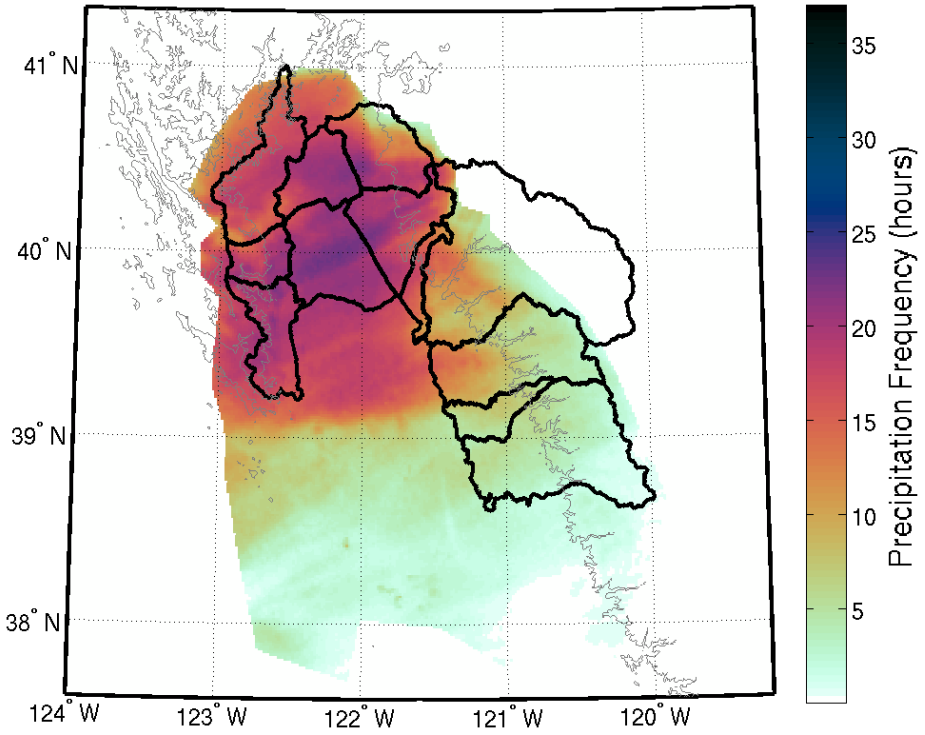

Variables	Value	Category
Storm Duration (hours)	25	-
KBBX Radar Offset (dBZ)	-3	-
BBY – Wind Direction at AR onset (°)	182.43	South
BBY – Mean Upslope Wind (m s^{-1})	11.049	Middle
BBY – Total Upslope IWV Flux (cm m s^{-1})	675.5	High

CCO Barrier Jet Timeline	Altitude (m)		Magnitude (ms^{-1})	
20091215:1300 – 20091215:1900	1331	High	15.04	Low
20091215:1900 – 20091216:0300	-	-	-	-
20091216:0300 – 20091216:1400	1550	High	16.48	Low

17 Jan 2010

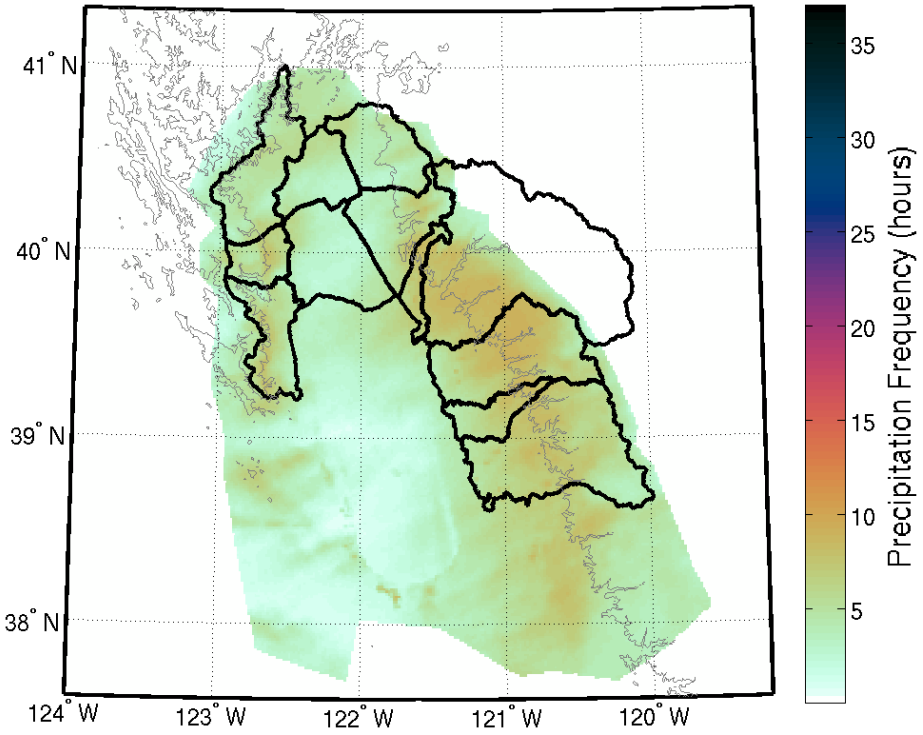

Variables	Value	Category
Storm Duration (hours)	9	-
KBBX Radar Offset (dBZ)	-4.5	-
BBY – Wind Direction at AR onset (°)	198.79	Southwest
BBY – Mean Upslope Wind (m s^{-1})	17.408	High
BBY – Total Upslope IWV Flux (cm m s^{-1})	329.1	Middle

CCO Barrier Jet Timeline	Altitude (m)		Magnitude (ms^{-1})	
20100117:2000 – 20100117:2100	-	-	-	-
20100117:2100 – 20100118:0500	1295	High	24.19	High

29 Mar 2010

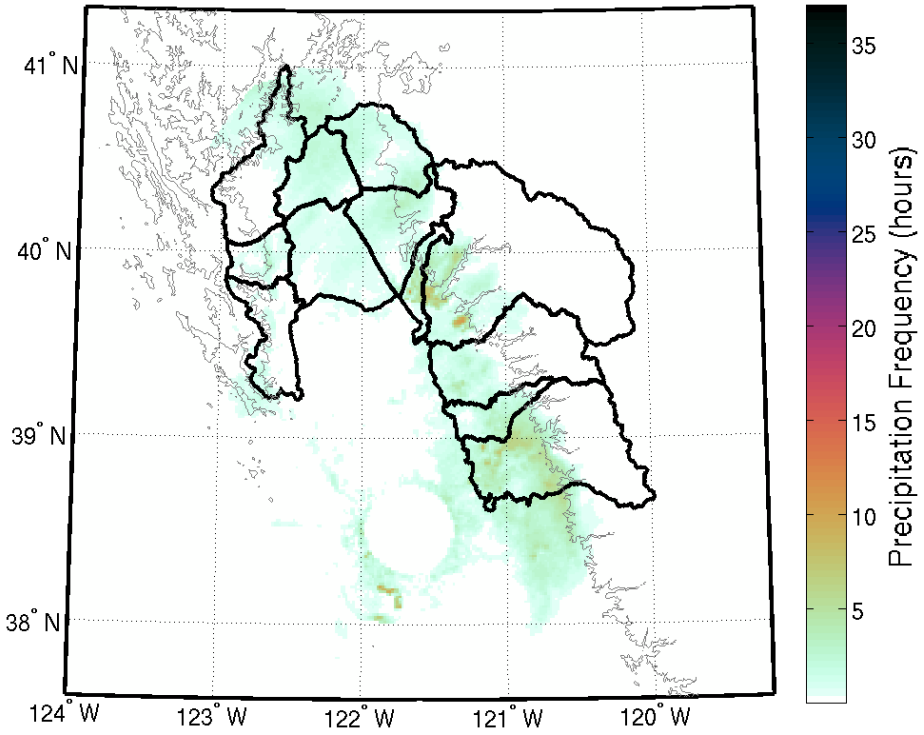

Variables	Value	Category
Storm Duration (hours)	18	-
KBBX Radar Offset (dBZ)	0	-
BBY – Wind Direction at AR onset (°)	243.64	West
BBY – Mean Upslope Wind (m s^{-1})	10.171	Middle
BBY – Total Upslope IWV Flux (cm m s^{-1})	449.3	High

CCO Barrier Jet Timeline	Altitude (m)		Magnitude (ms^{-1})	
20100329:0200 – 20100329:0700	-	-	-	-
20100329:0700 – 20100329:2000	1315	High	17.39	Middle

02 Apr 2010

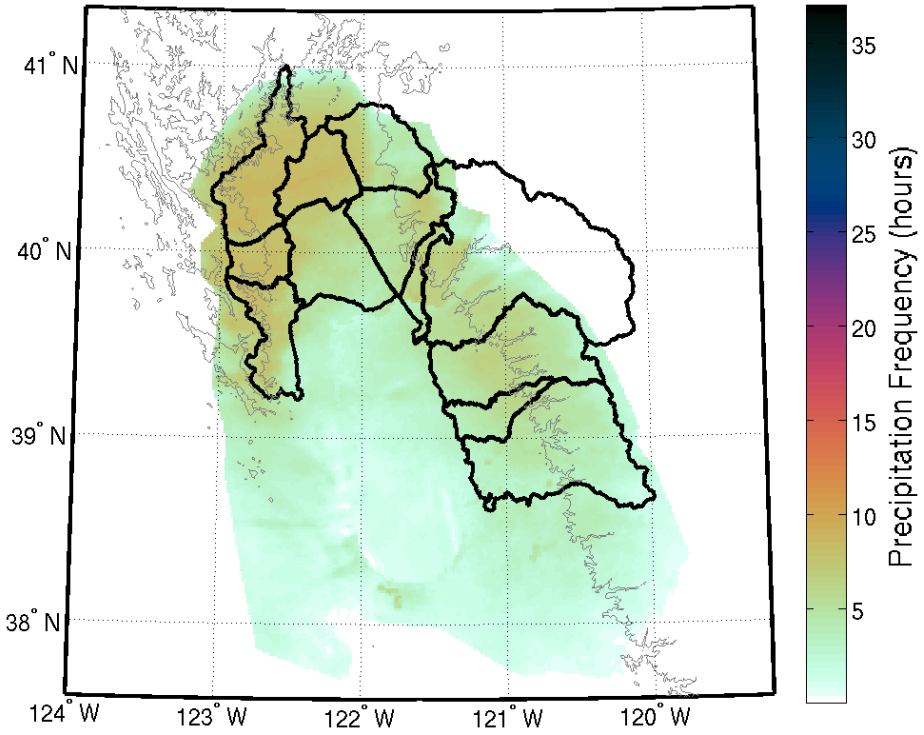

Variables	Value	Category
Storm Duration (hours)	9	-
KBBX Radar Offset (dBZ)	-3.5	-
BBY – Wind Direction at AR onset (°)	223.70	Southwest
BBY – Mean Upslope Wind (m s^{-1})	12.680	Middle
BBY – Total Upslope IWV Flux (cm m s^{-1})	269.0	Middle

CCO Barrier Jet Timeline	Altitude (m)		Magnitude (ms^{-1})	
20100402:1300 – 20100402:2200	-	-	-	-

Appendix E

Synoptic context for each of 64 atmospheric river events

Events are sorted from most southerly to most westerly winds at the onset of atmospheric river conditions at Bodega Bay. Synoptic analyses for atmospheric river events that do not have wind information at Bodega Bay are included at the end. The top panels show Climate Forecast System Reanalysis (CFSR) data. Contours show the 850 mb height (dam). Shading shows 1000 – 300 mb integrated vapor transport magnitude. The red x is the selected low for the CFSR dataset. The bottom panel shows the NWS/NCEP Ocean Prediction Center marine surface analyses. Contours of sea level pressure are displayed in green lines. Low and high pressure centers are indicated by red Ls and blue Hs, respectively. Fronts and available surface observations are denoted following standards. The red arrows extending from the centers of low pressure indicate the 24-hour cyclone forecast track. Red Xs indicate the 24-hour cyclone position forecast.

IVT & 850 mb Height
20050319-06

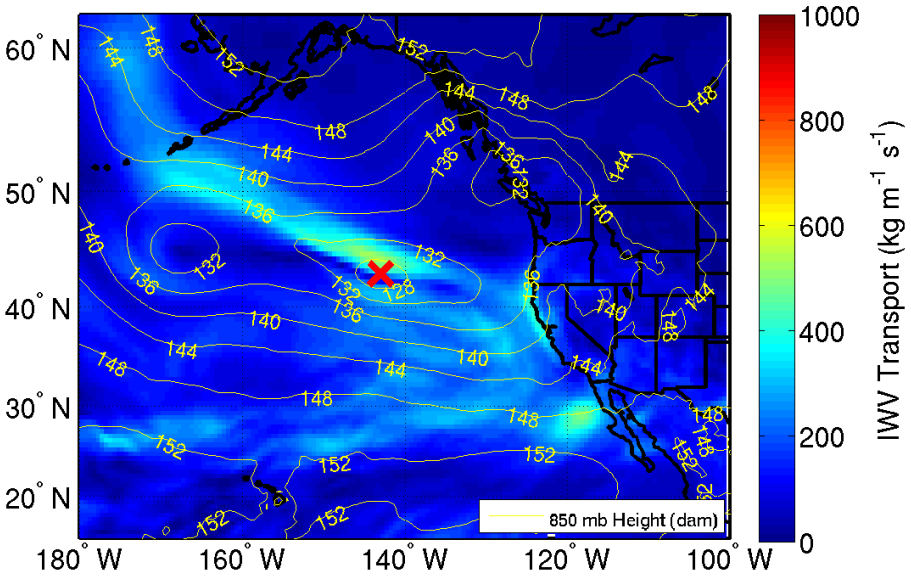

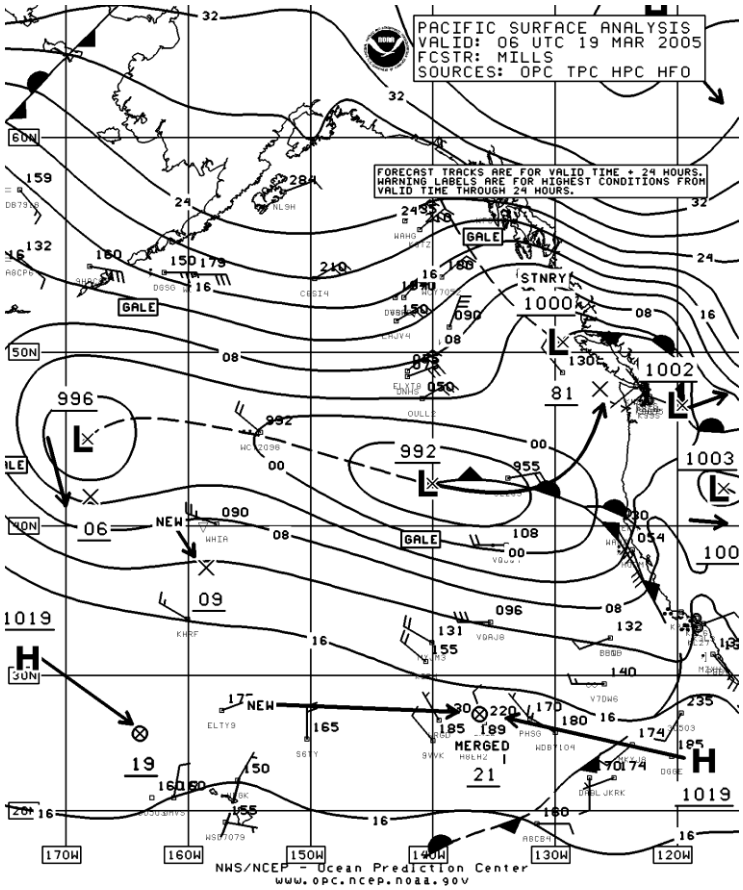

IVT & 850 mb Height
20050322-00

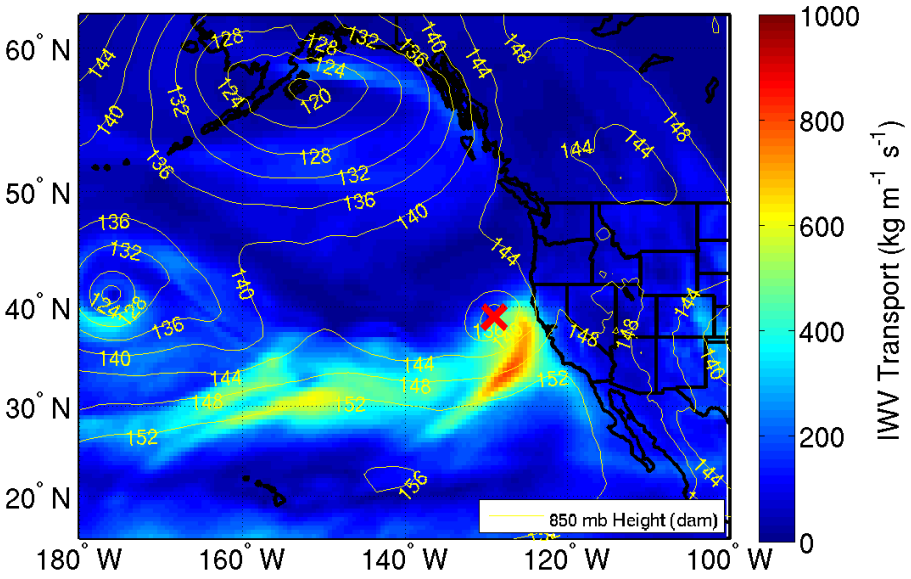

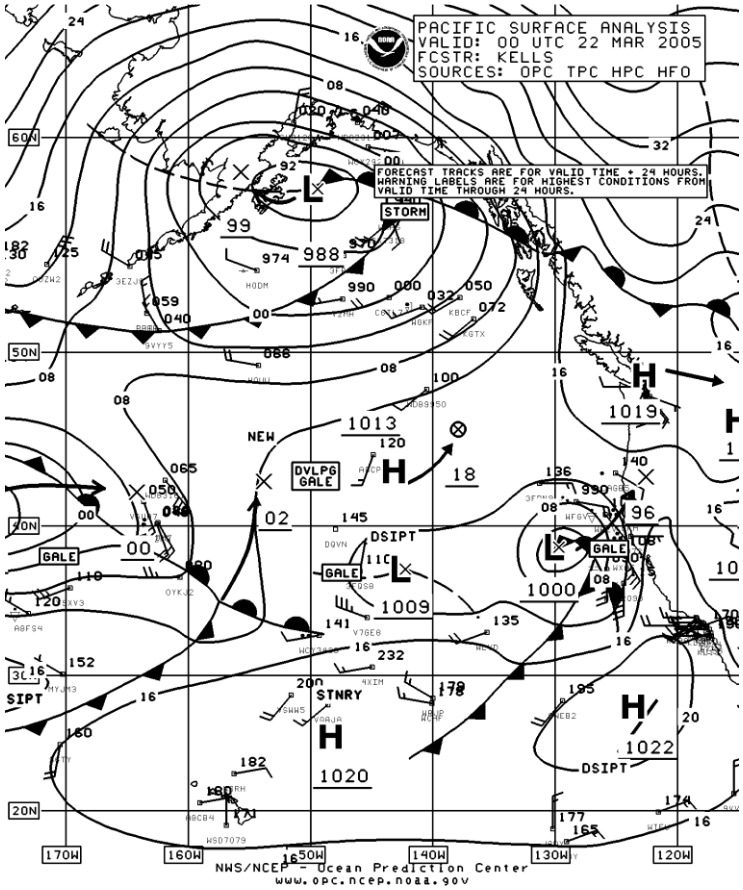

IVT & 850 mb Height
20081031-06

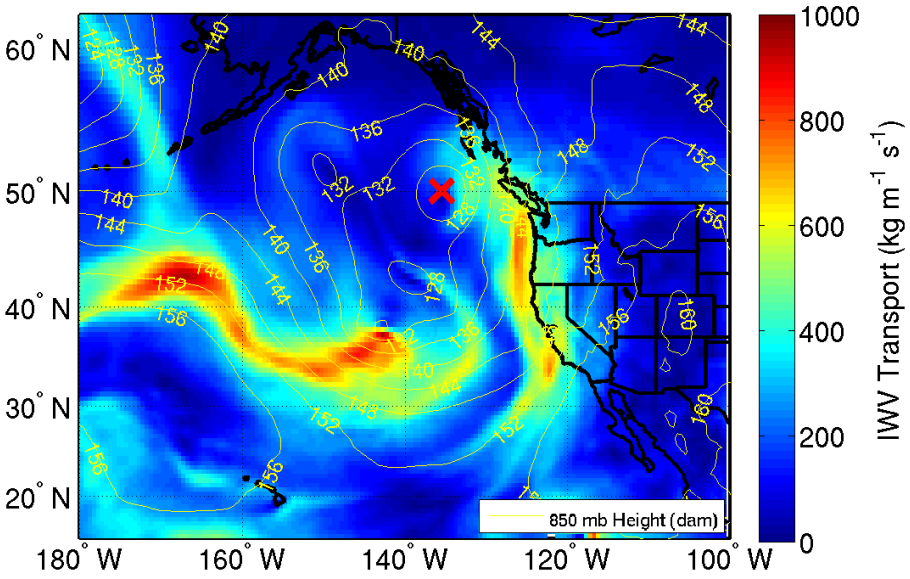

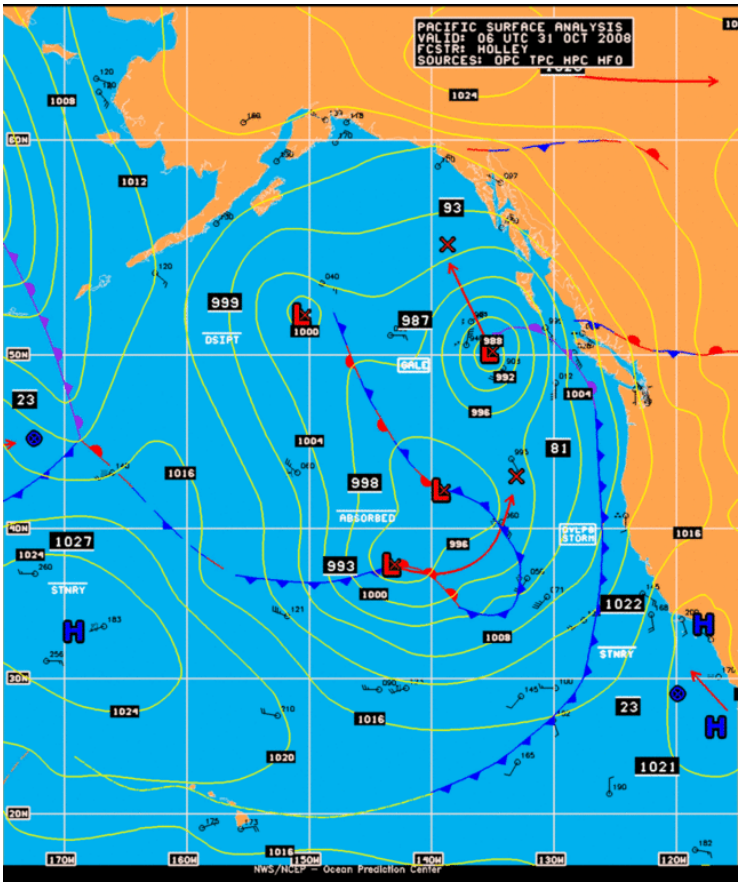

IVT & 850 mb Height
20061209-00

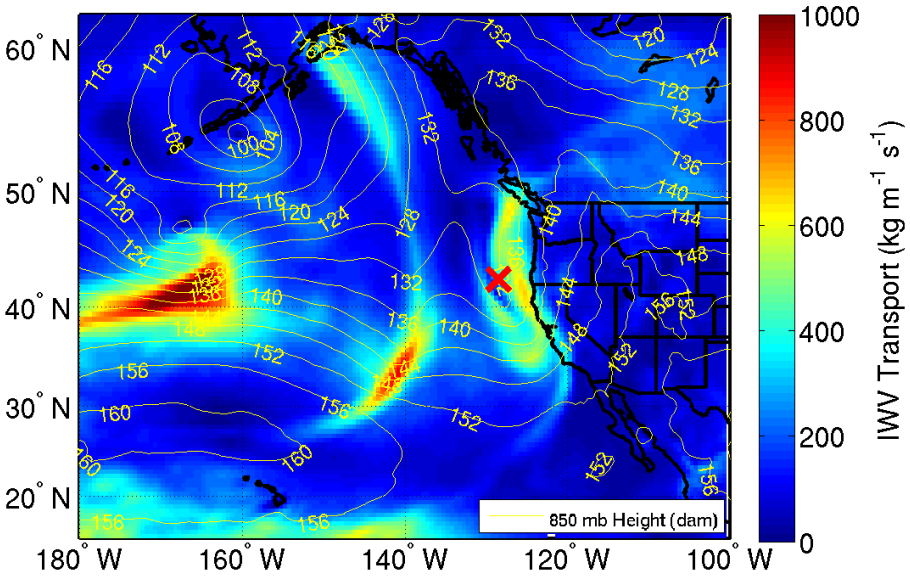

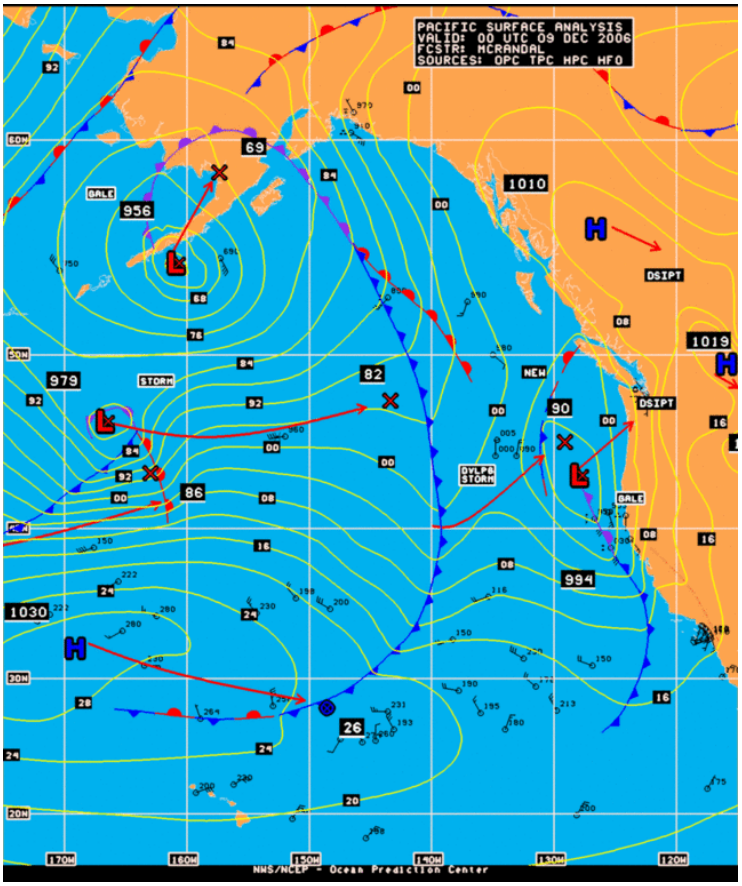

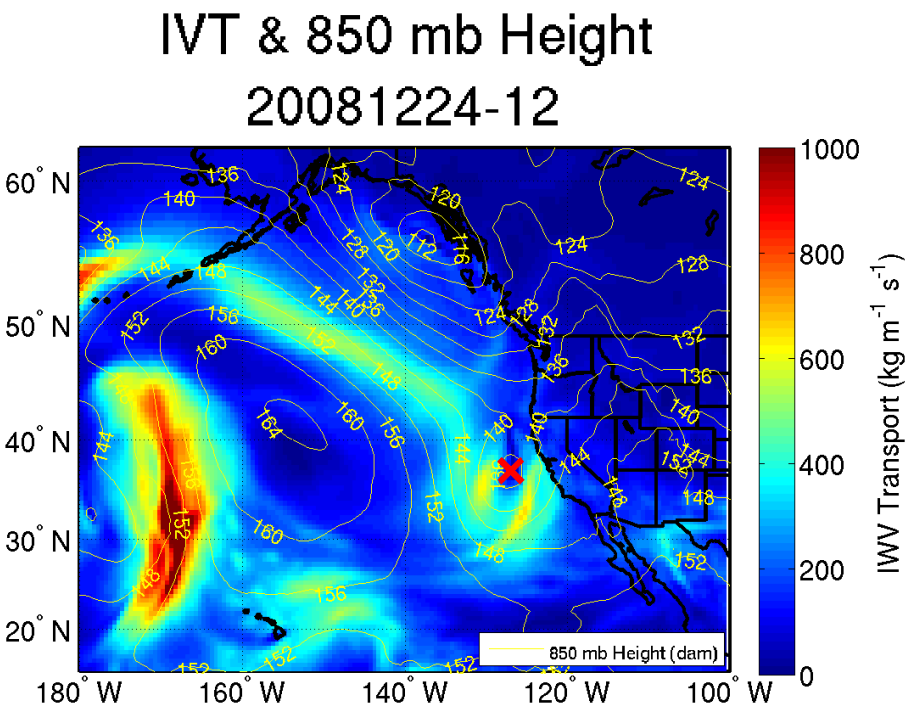
IVT & 850 mb Height
20081224-12
60° N
50° N
40° N
30° N
20° N
180° W
160° W
140° W
120° W
100° W
850 mb Height (dam)
1000
800
600
400
200
0
IWV Transport (kg m-1 s-1)

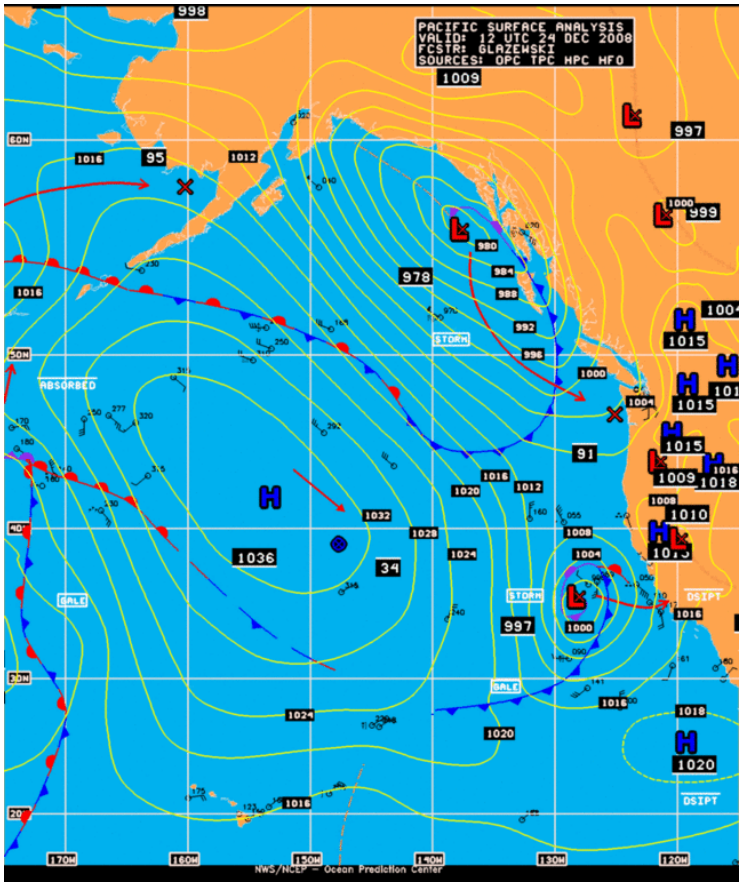
PACIFIC SURFACE ANALYSIS
VALID: 12 UTC 24 DEC 2008
FCSTR: GLAZEWSKI
SOURCES: OPC TPC HPC HFO
NWS/NCEP - Ocean Prediction Center

IVT & 850 mb Height
20080126-00

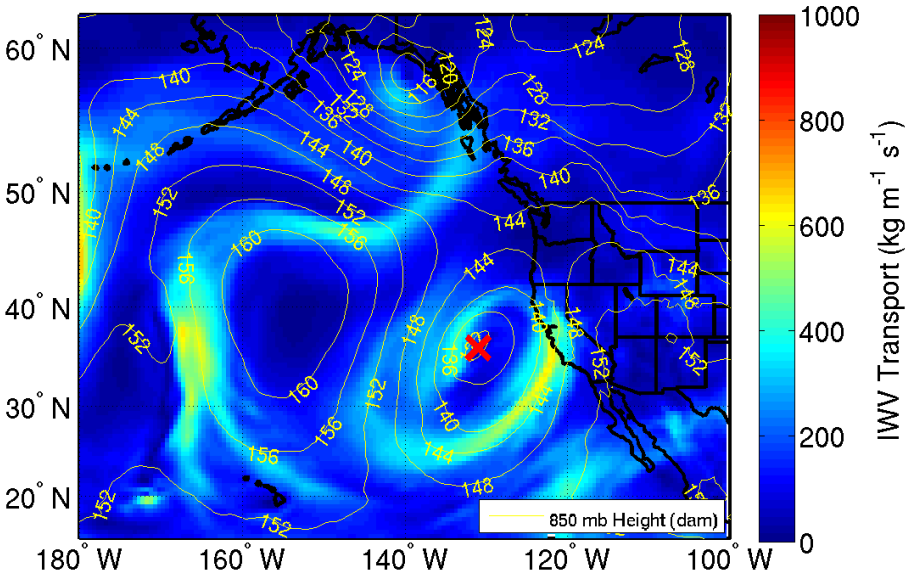

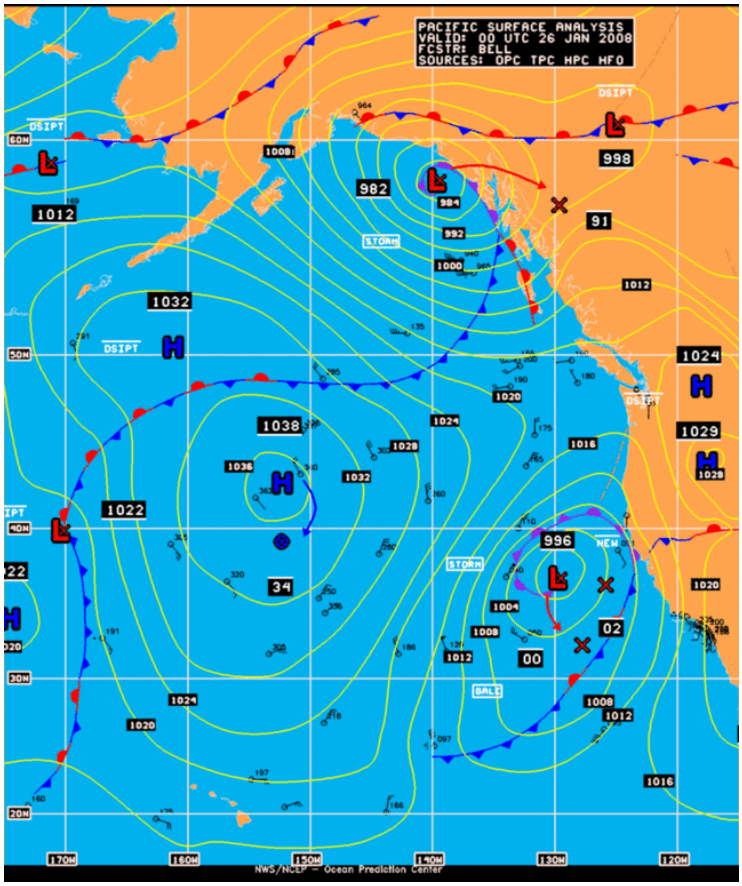

IVT & 850 mb Height
20090301-12

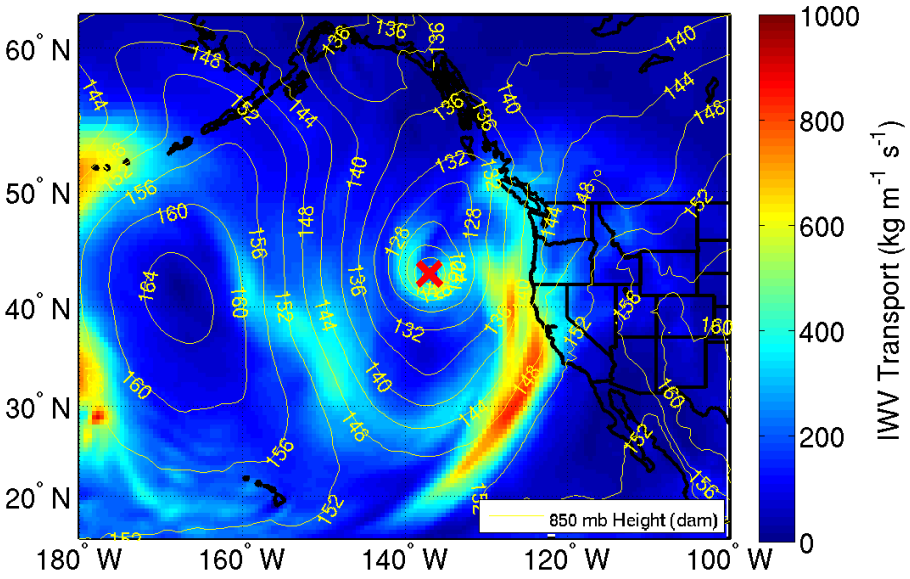

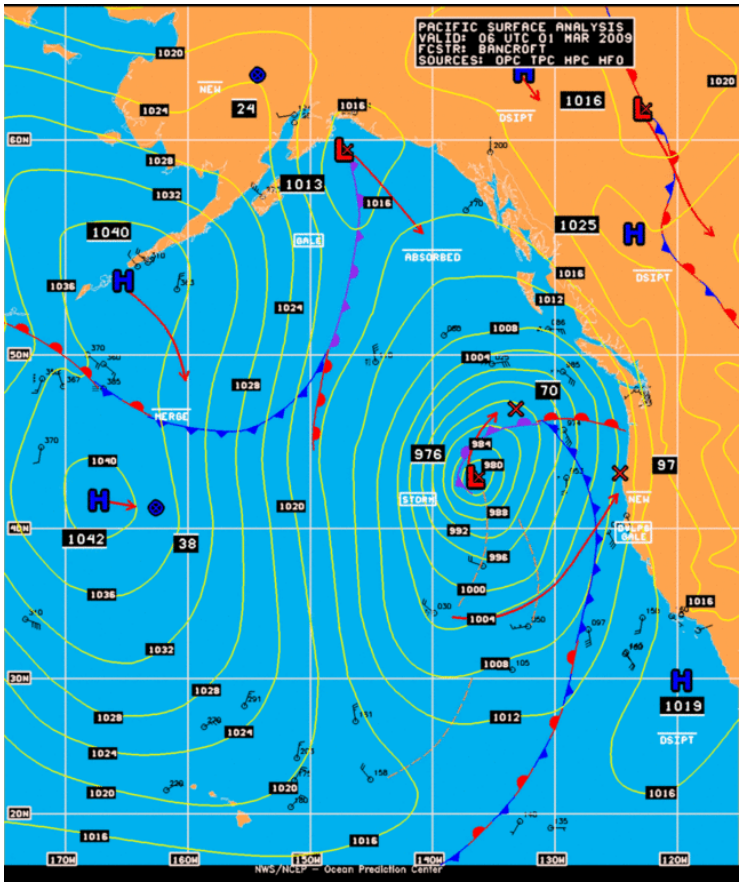

IVT & 850 mb Height
20090222-00

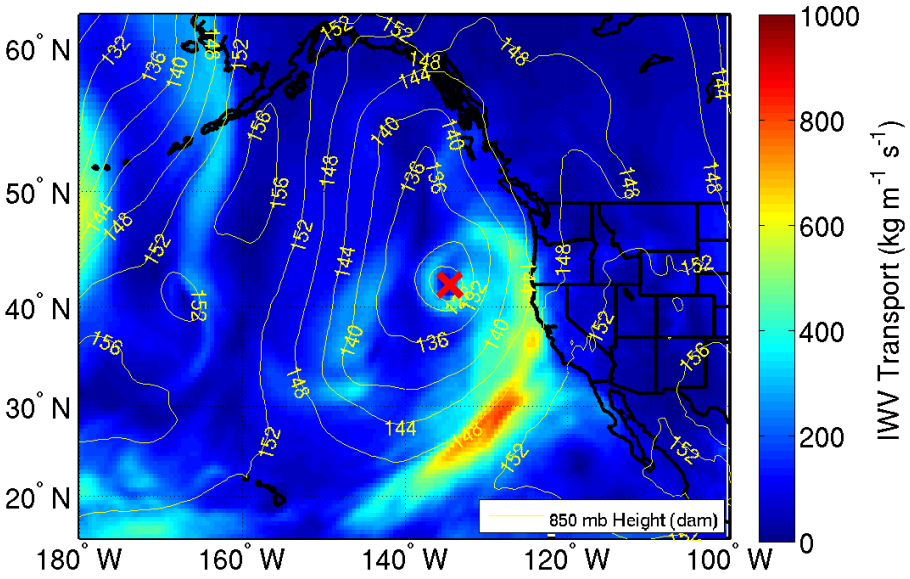

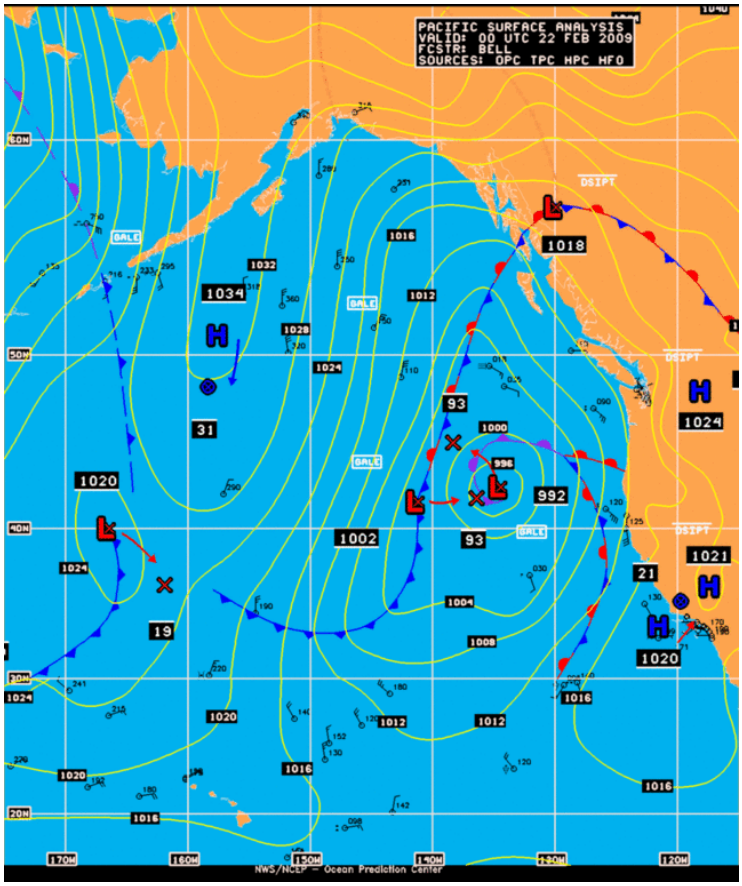

IVT & 850 mb Height
20060226-18

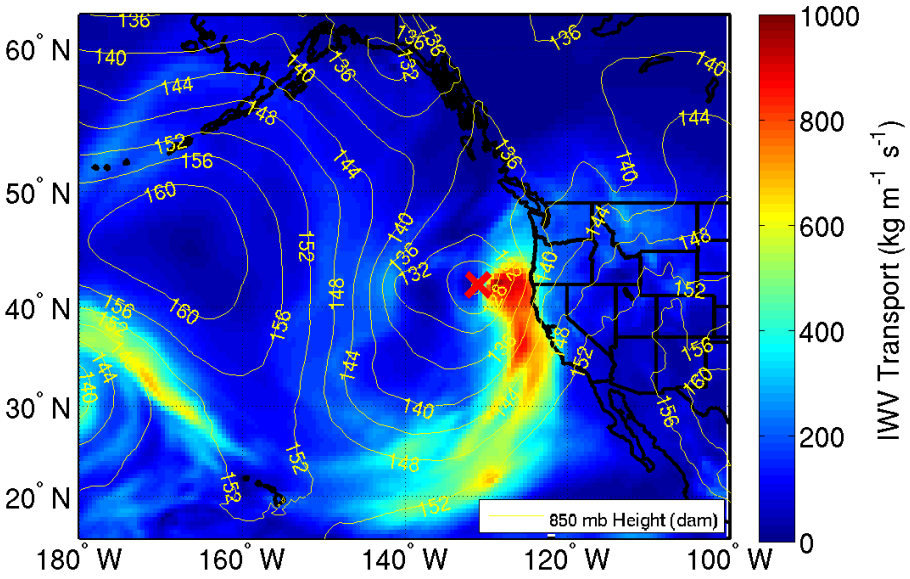

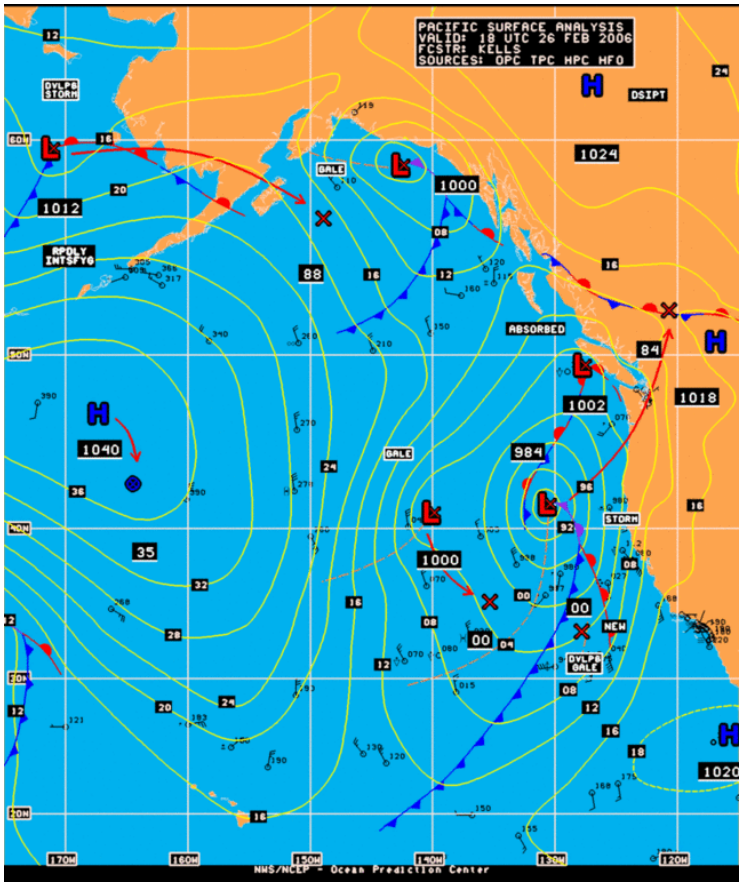

IVT & 850 mb Height
20090502-06

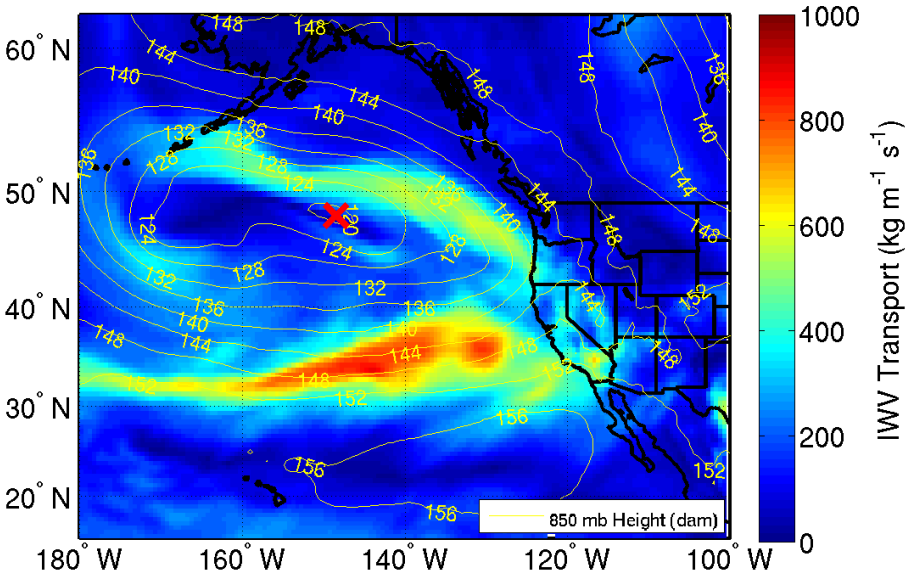

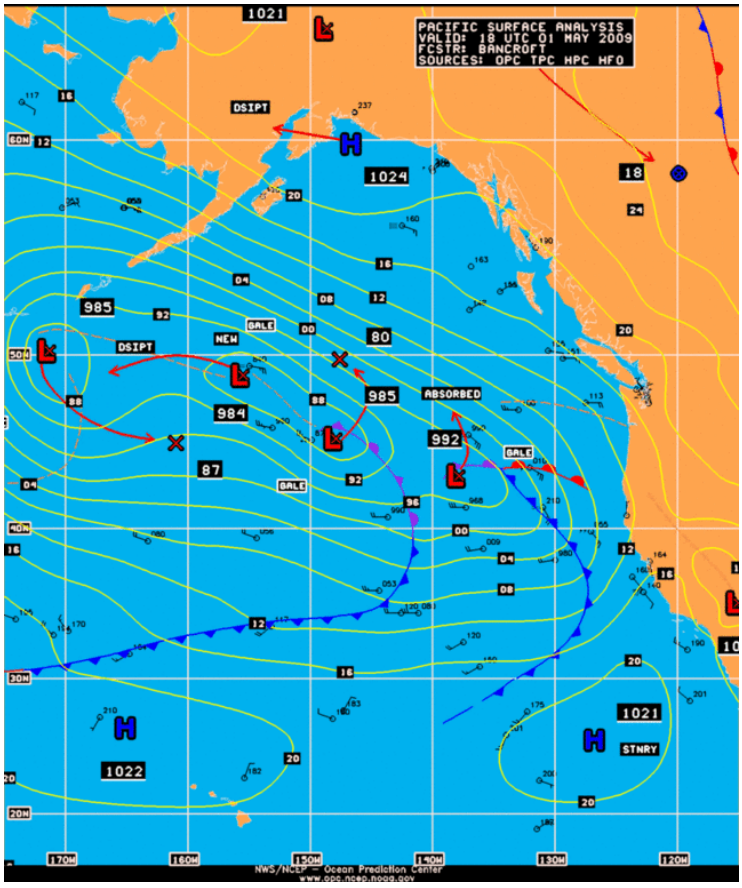

IVT & 850 mb Height
20091013-00

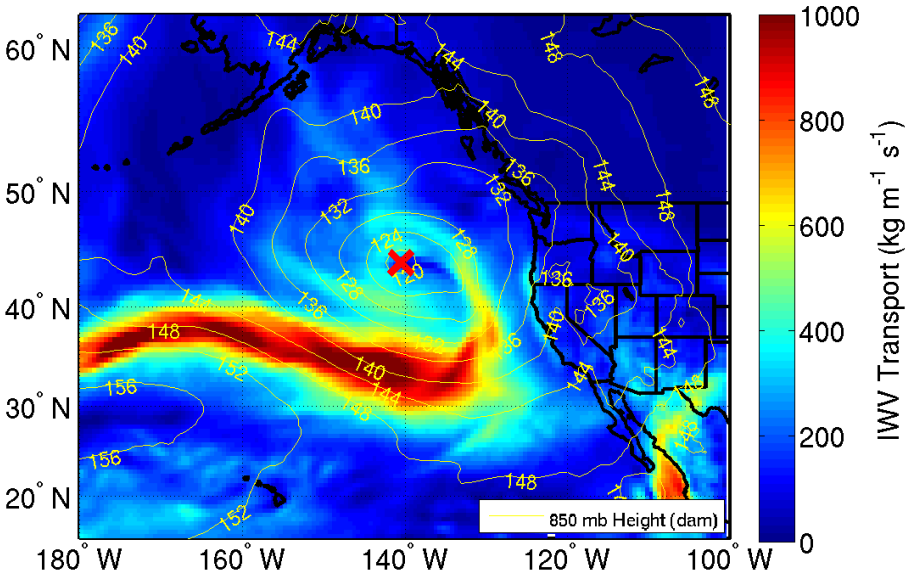

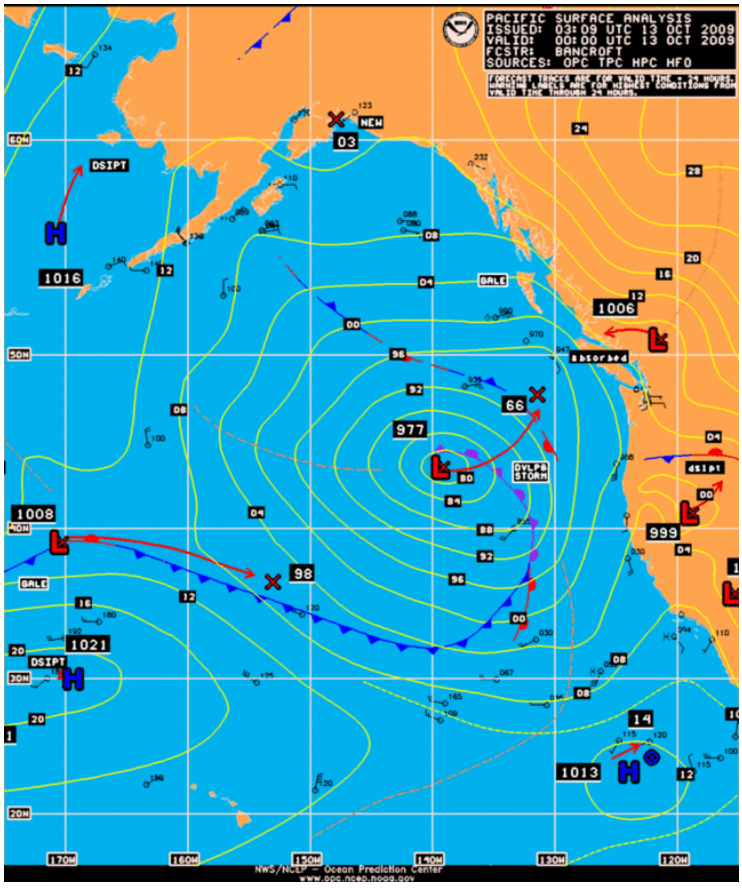

IVT & 850 mb Height
20051220-12

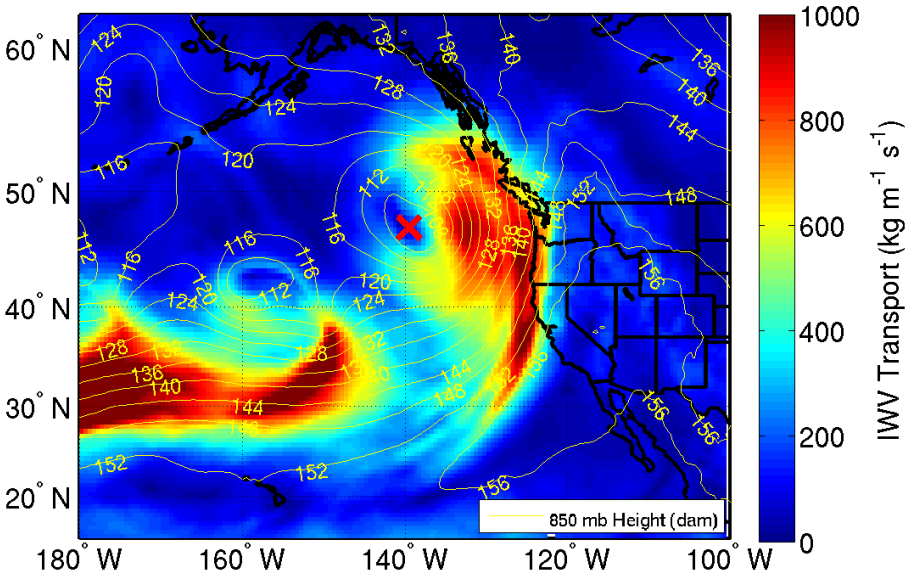

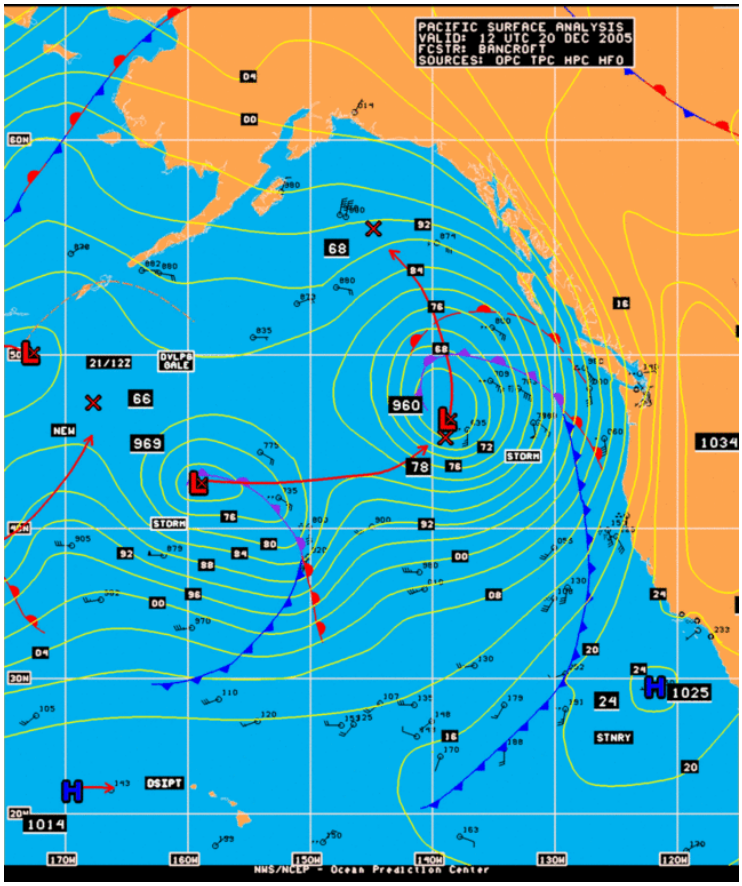

IVT & 850 mb Height
20051218-06

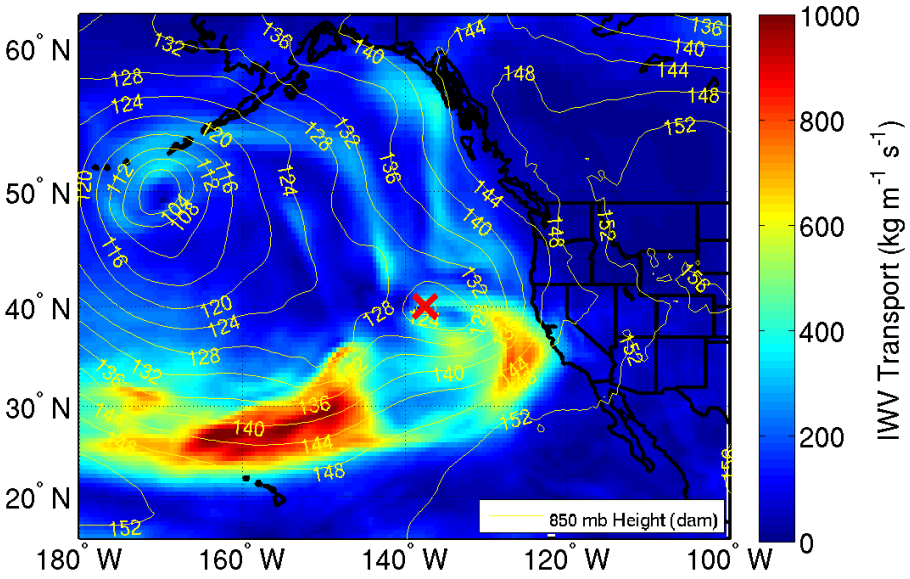

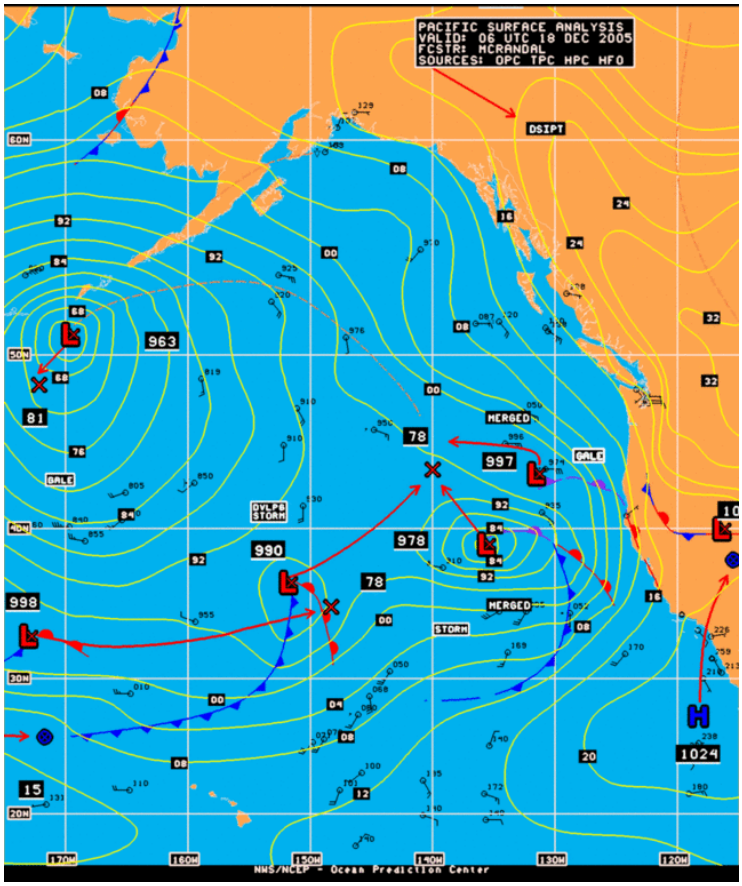

IVT & 850 mb Height
20060101-18

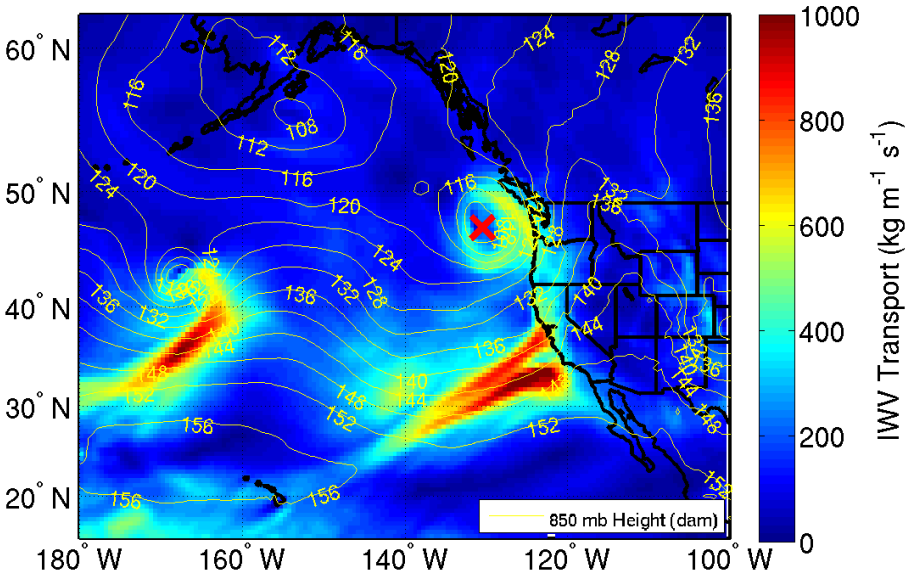

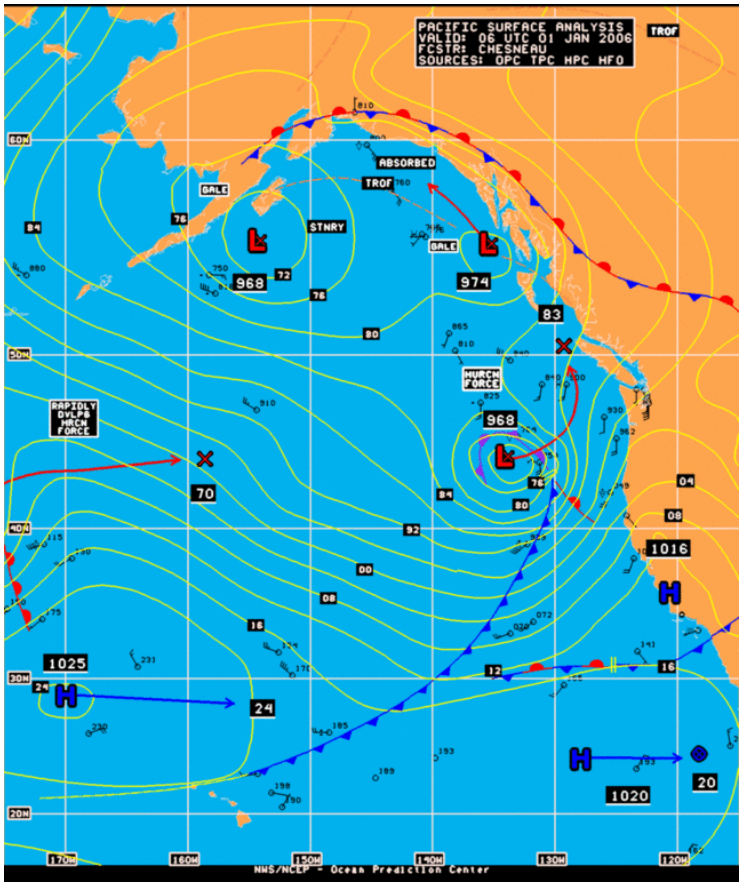

IVT & 850 mb Height
20071012-12

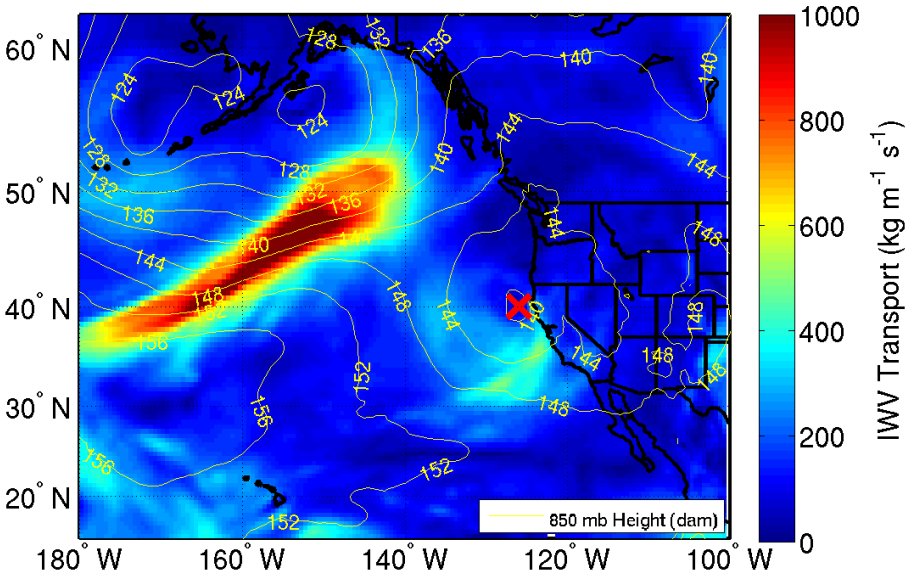

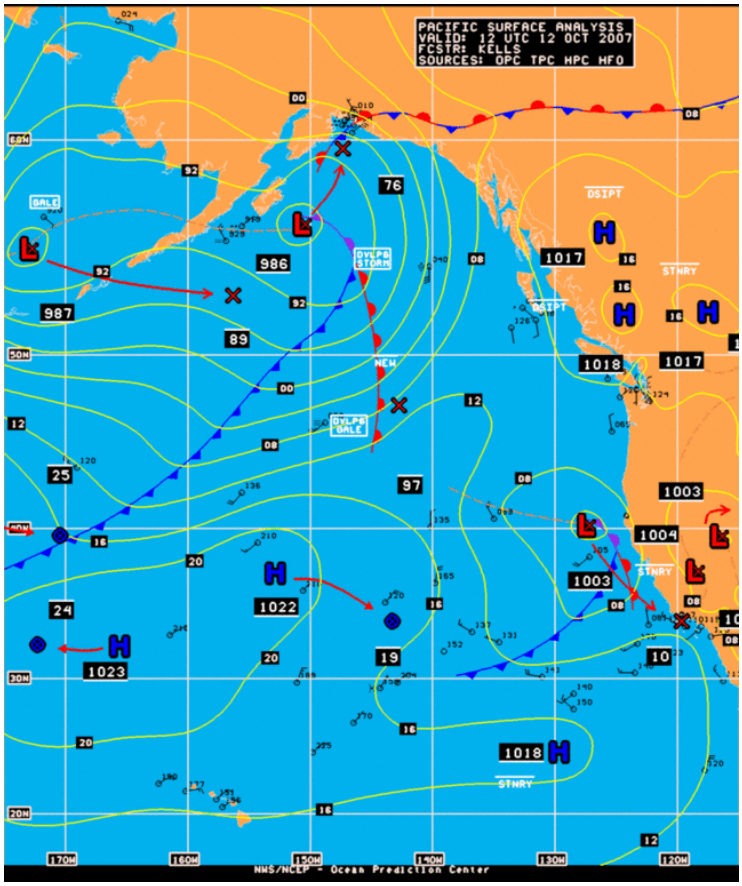

IVT & 850 mb Height
20060305-06

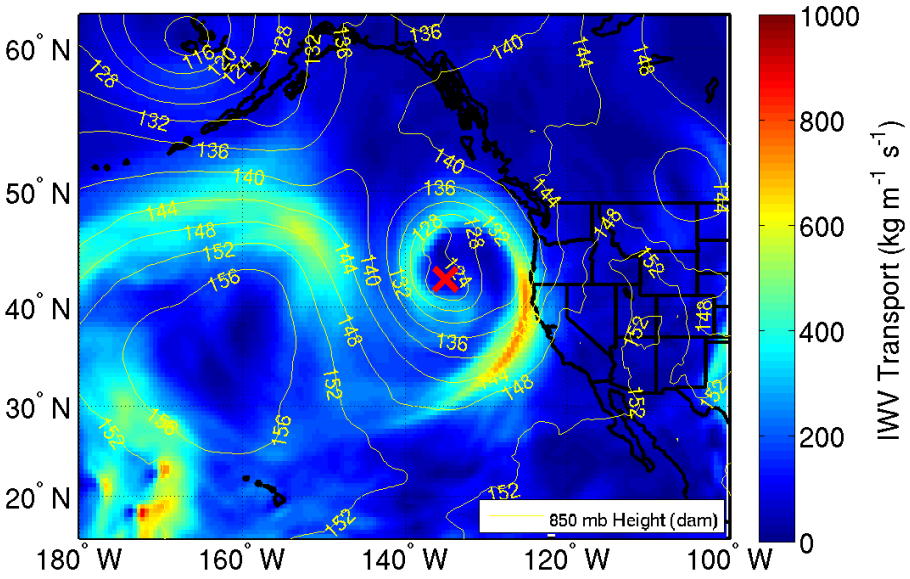

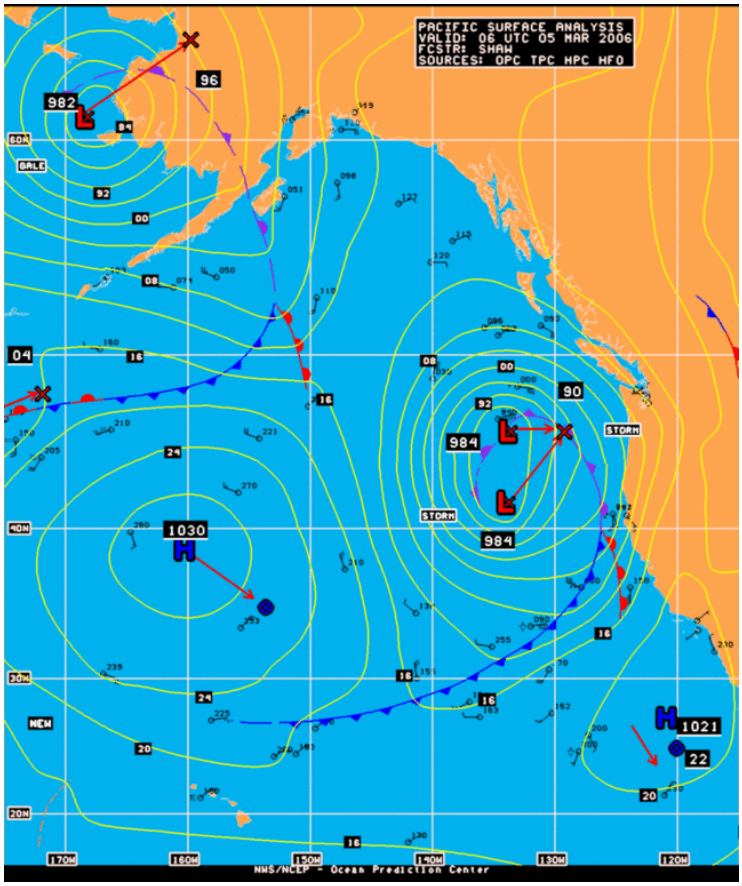

IVT & 850 mb Height
20060523-06

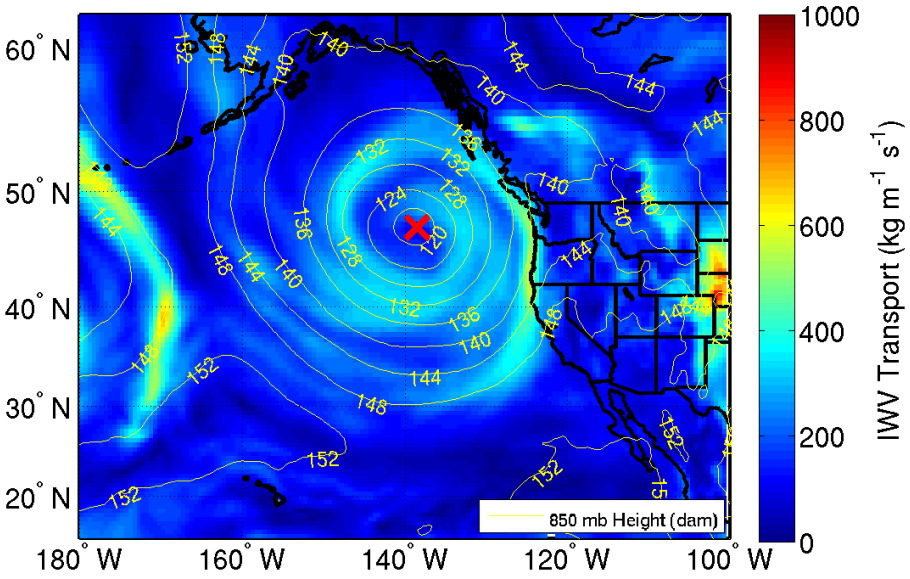

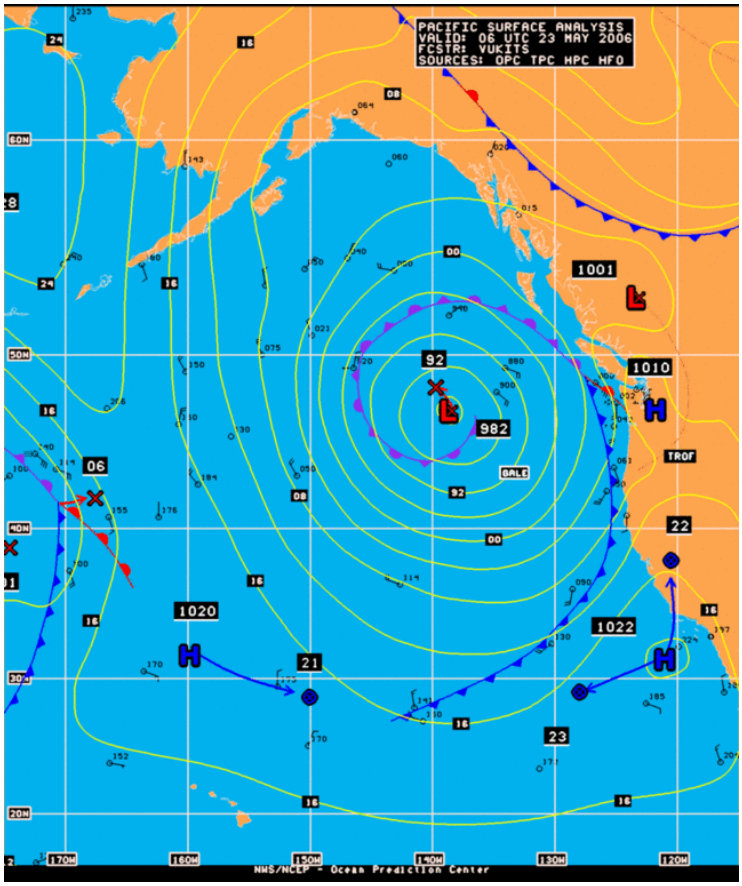

IVT & 850 mb Height
20050327-18

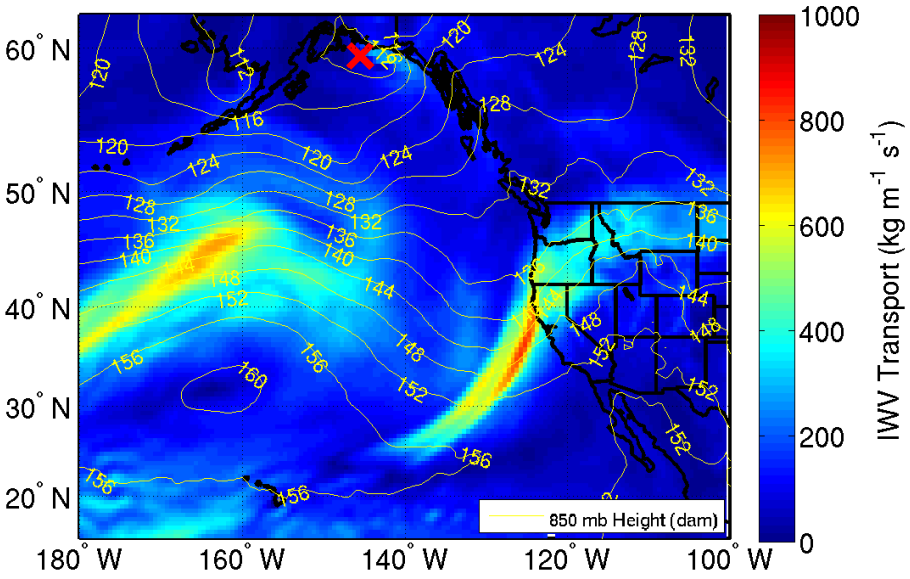

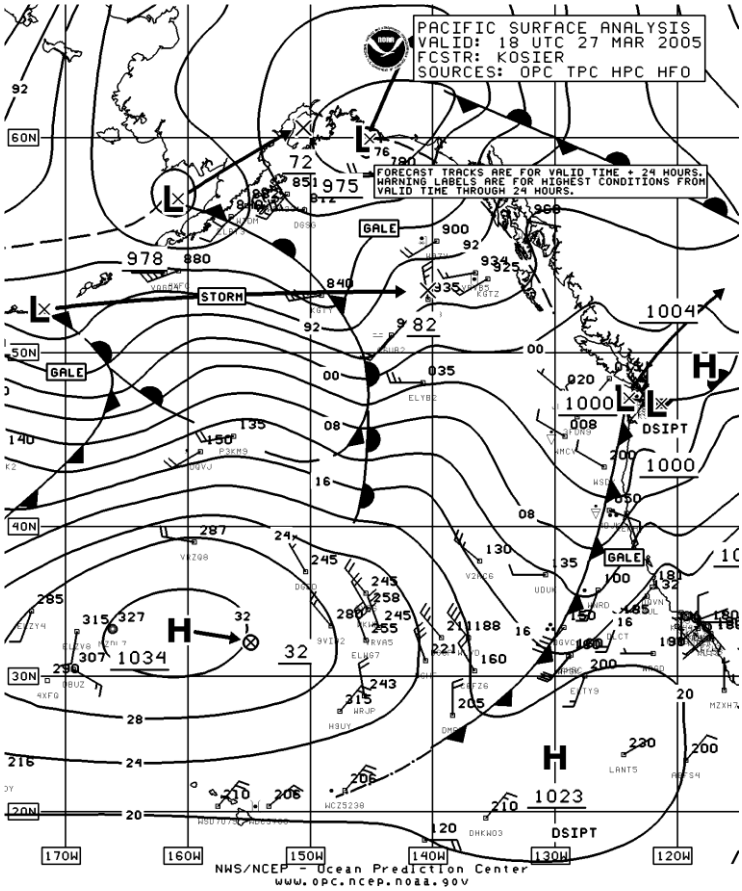

IVT & 850 mb Height
20091215-12

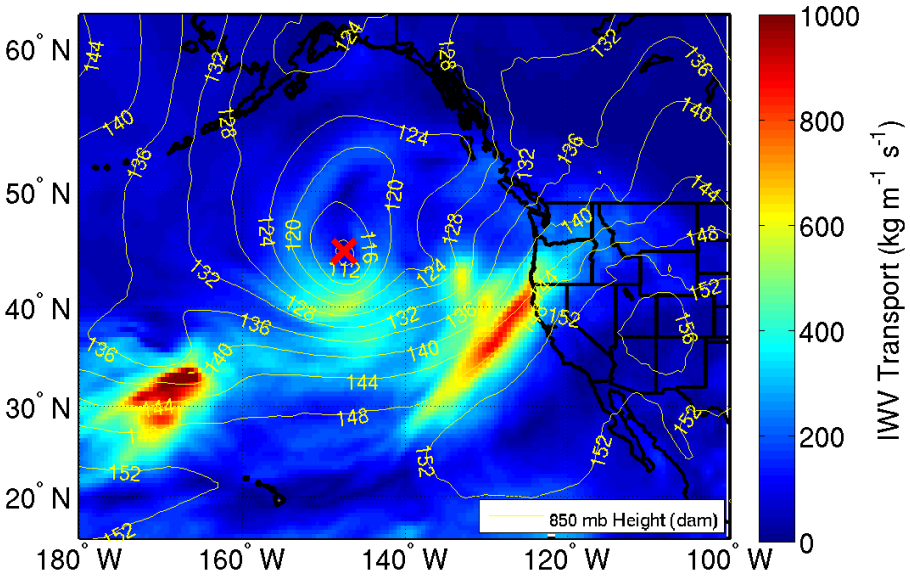

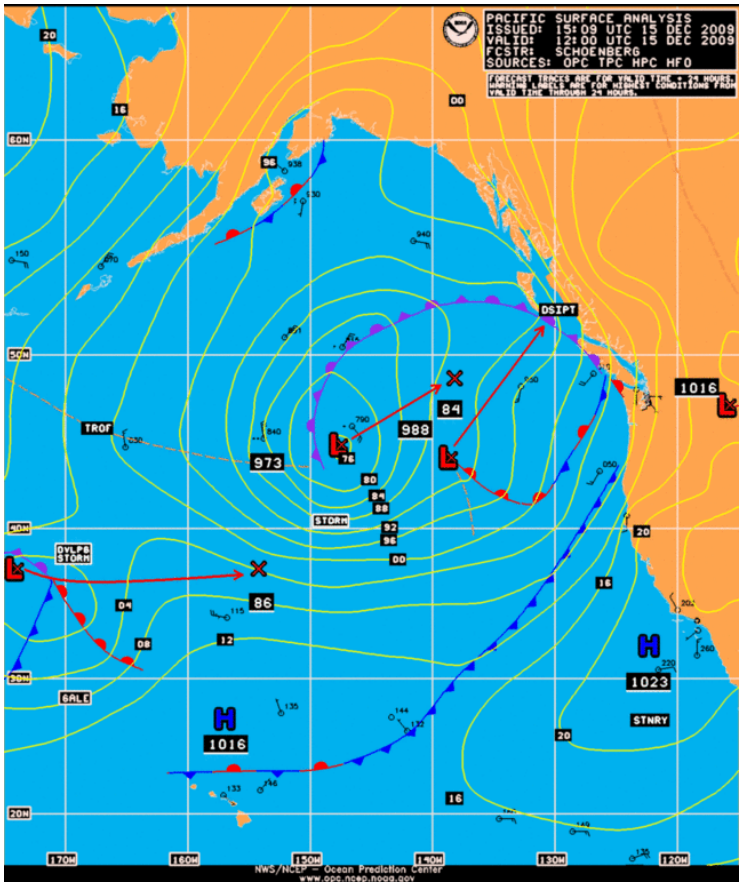

IVT & 850 mb Height
20051227-06

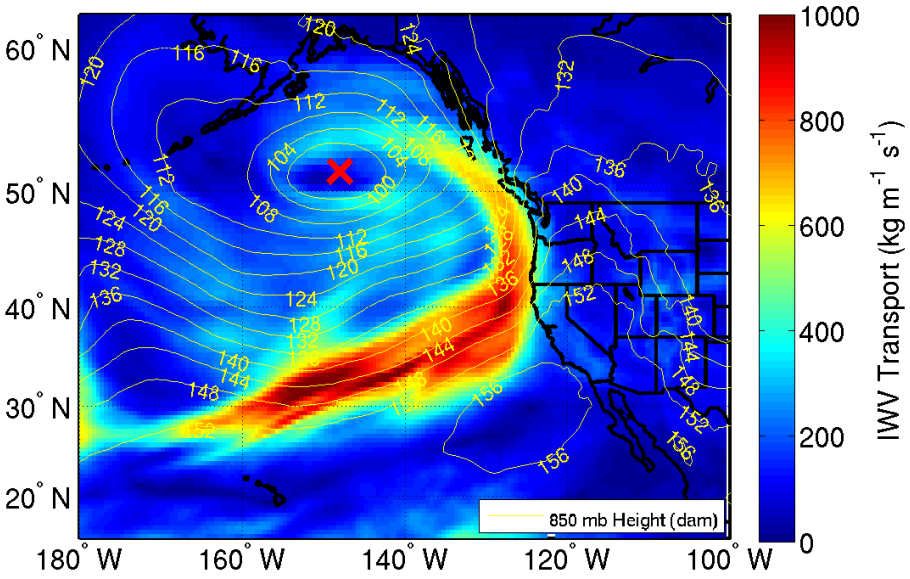

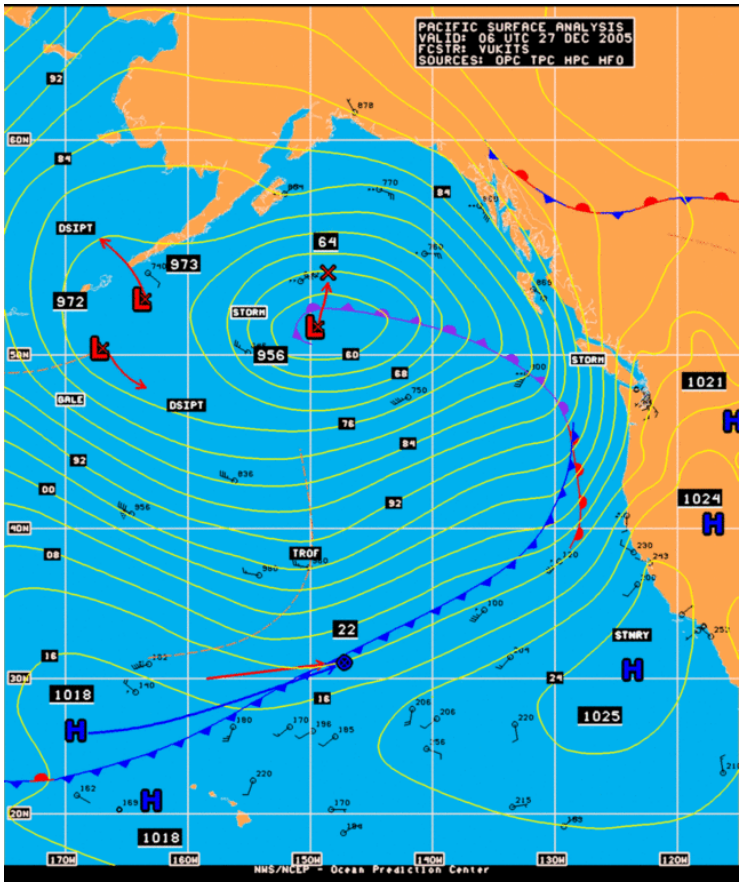

IVT & 850 mb Height
20071202-18

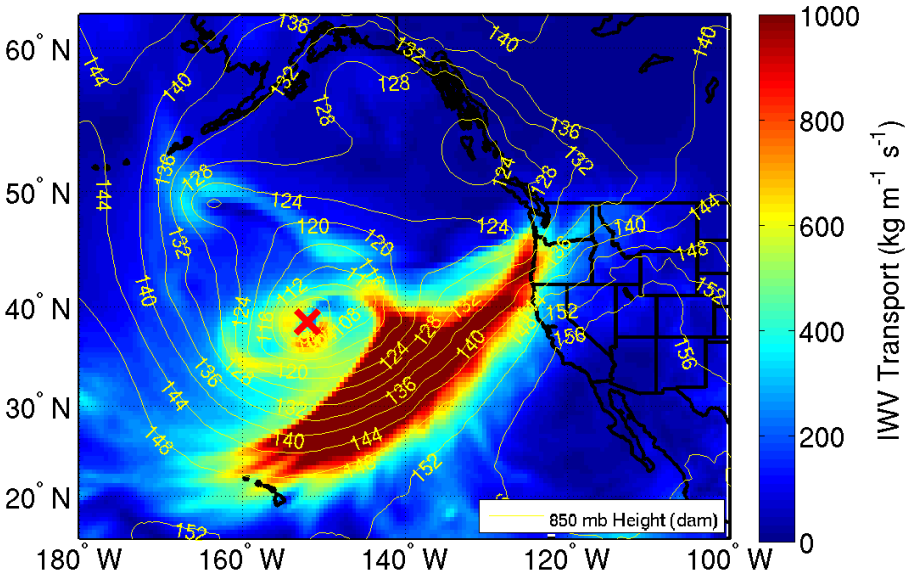

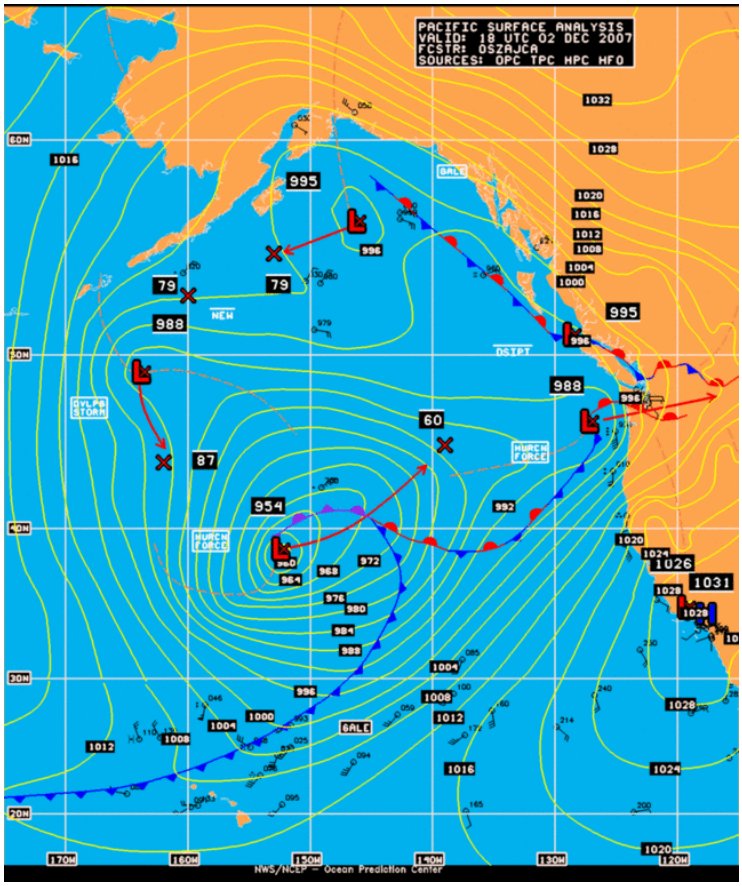

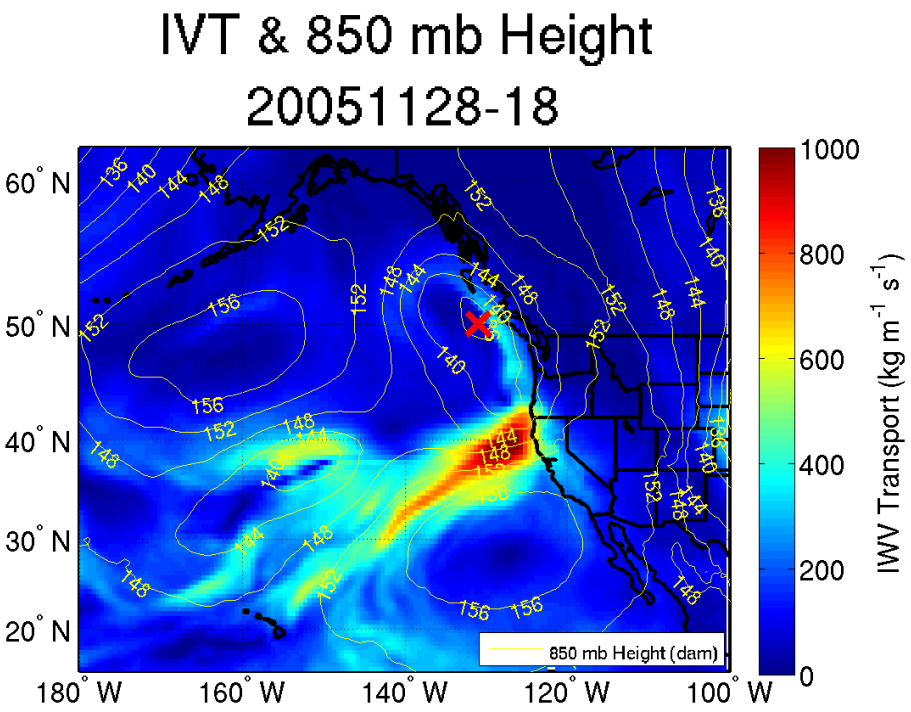
IVT & 850 mb Height
20051128-18
60˚ N
50˚ N
40˚ N
30˚ N
20˚ N
180˚ W
160˚ W
140˚ W
120˚ W
100˚ W
850 mb Height (dam)
1000
800
600
400
200
0
IWV Transport (kg m-1 s-1)

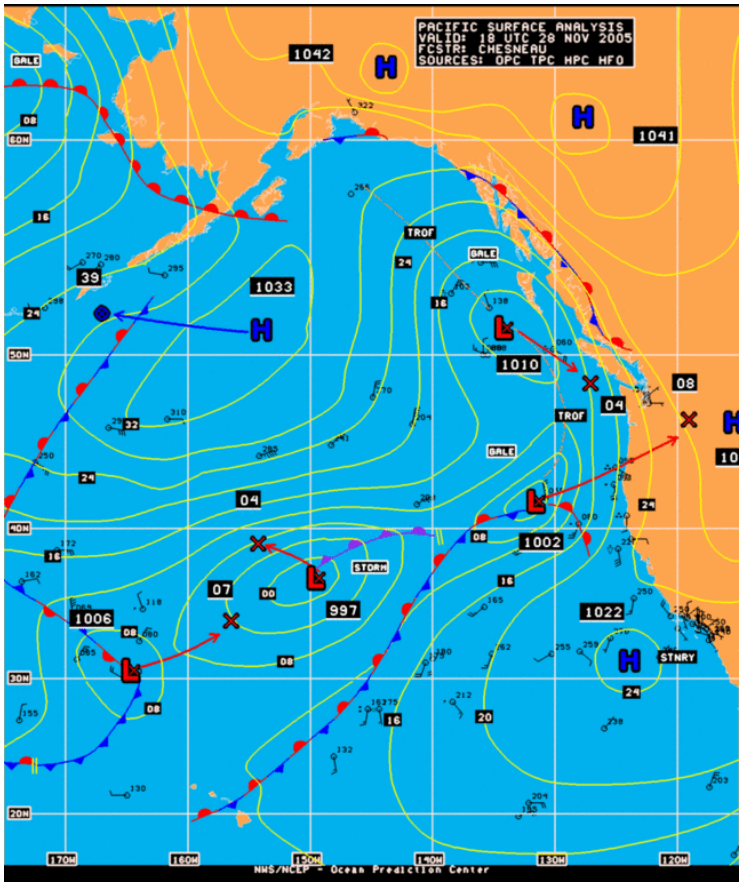
PACIFIC SURFACE ANALYSIS
VALID: 18 UTC 20 NOV 2005
FCSTR: CHESNEAU
SOURCES: OPC TPC HPC HFO
1042
1041
1033
1010
1002
1022
997
1006
TROF
STORM
STNRY
NWS/NCEP - Ocean Prediction Center

IVT & 850 mb Height
20090503-06

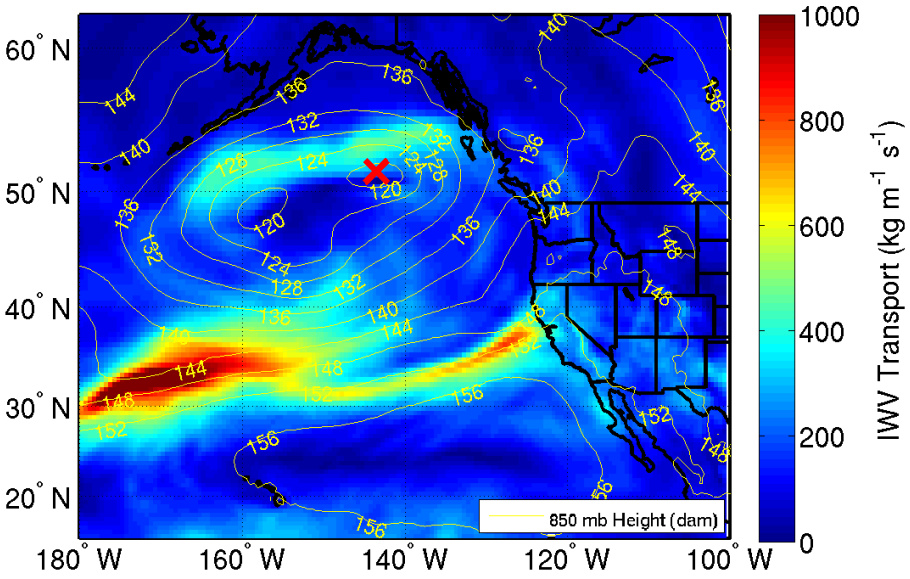

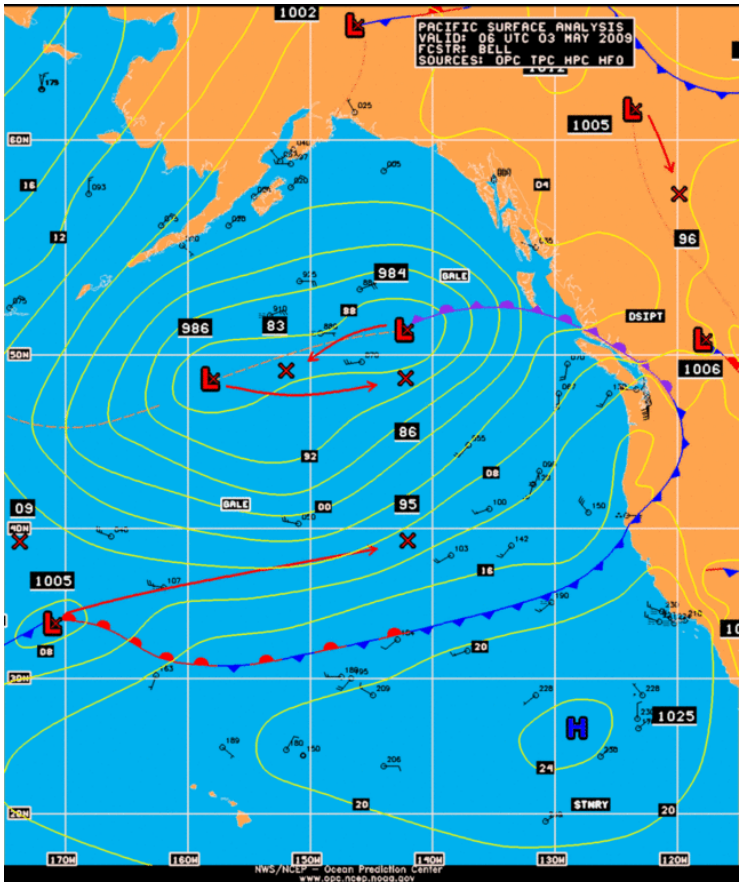

IVT & 850 mb Height
20051230-06

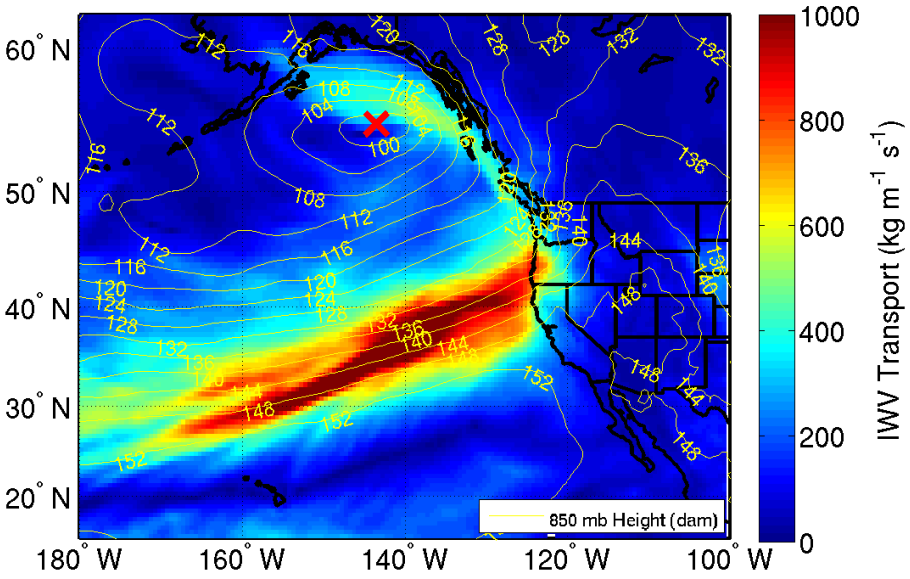

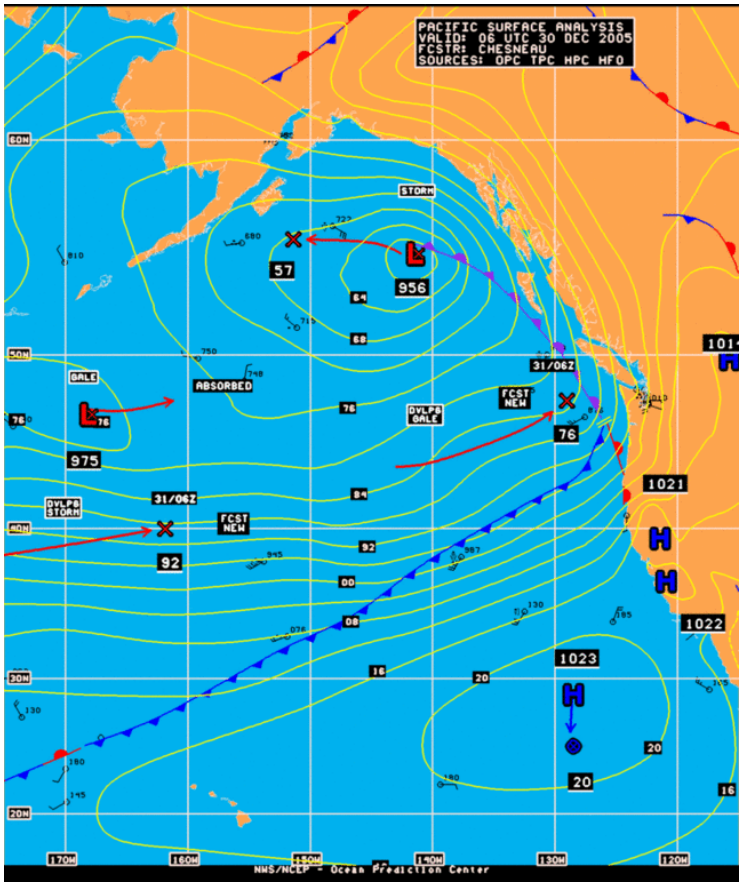

IVT & 850 mb Height
20060104-00

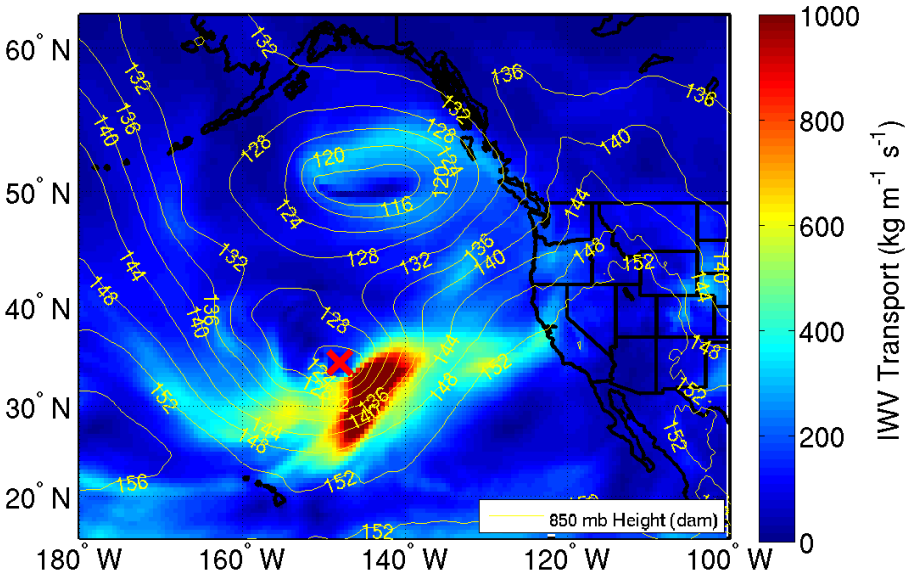

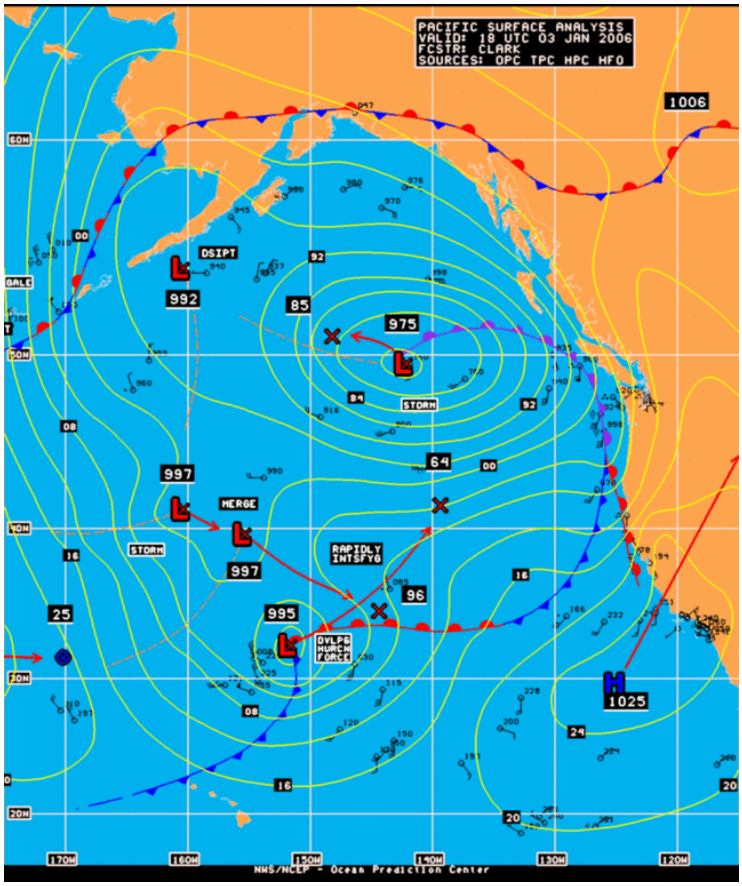

IVT & 850 mb Height
20061102-06

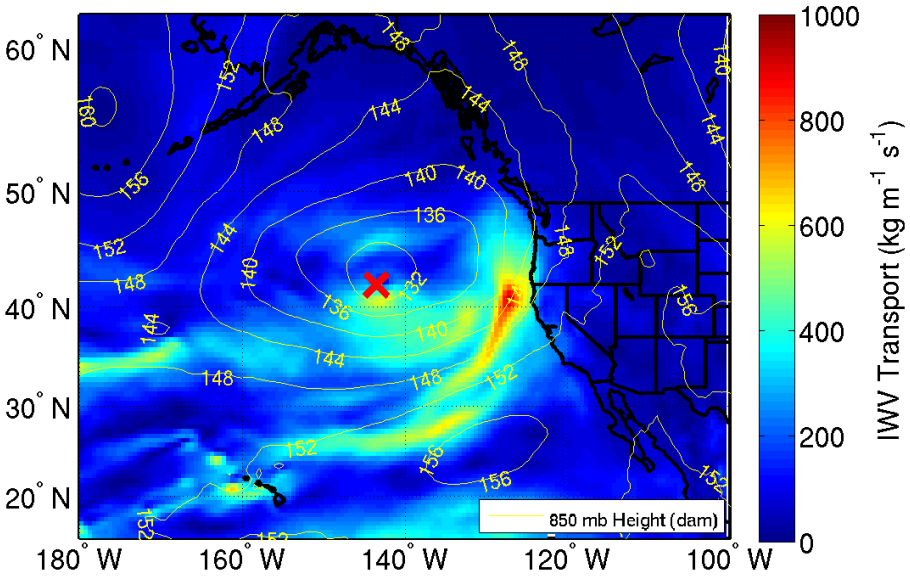

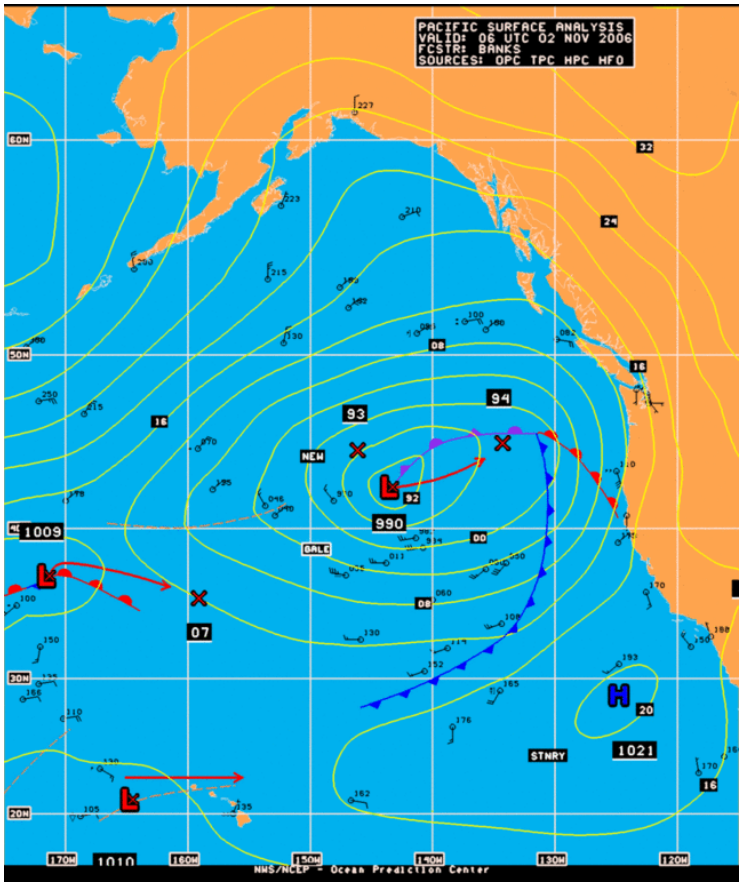

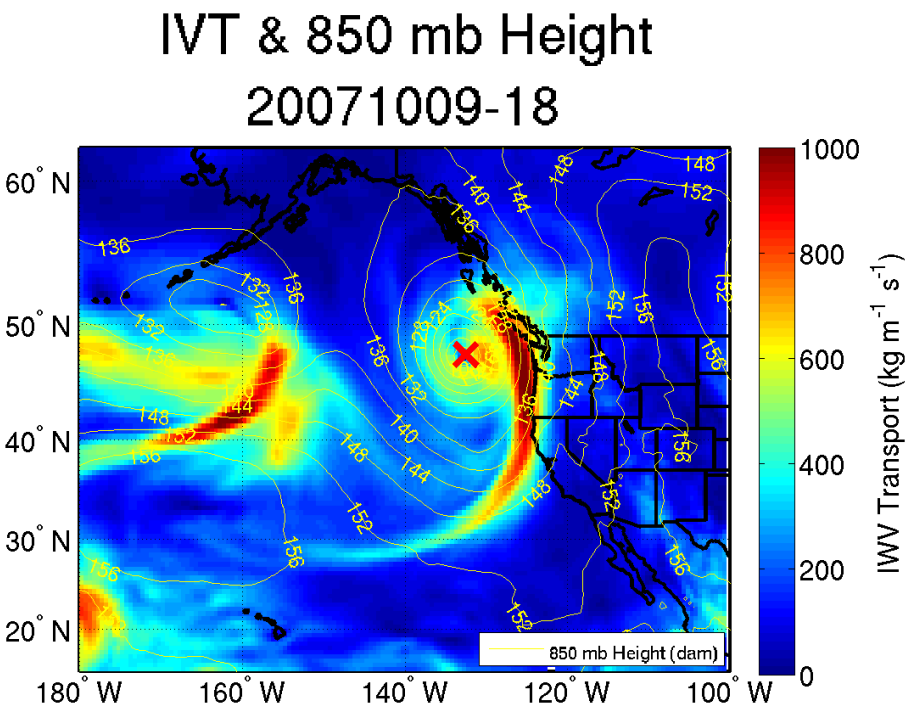
IVT & 850 mb Height
20071009-18
60˚ N
50˚ N
40˚ N
30˚ N
20˚ N
180˚ W
160˚ W
140˚ W
120˚ W
100˚ W
850 mb Height (dam)
1000
800
600
400
200
0
IWV Transport (kg m-1 s-1)

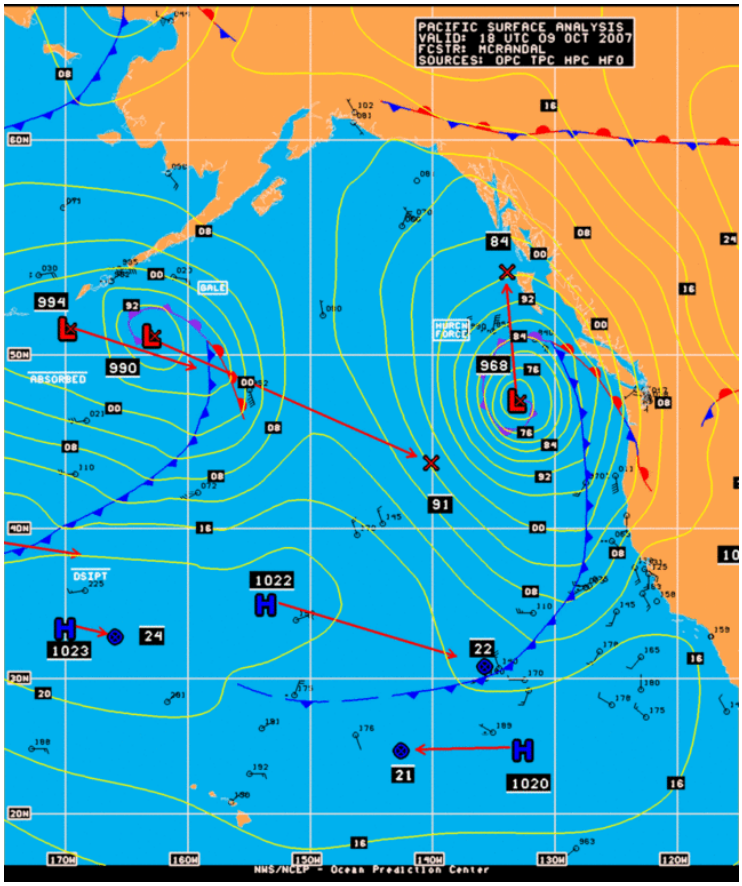
PACIFIC SURFACE ANALYSIS
VALID: 18 UTC 09 OCT 2007
FCSTR: MCRANDAL
SOURCES: OPC TPC HPC HFO
994
990
968
1022
1023
1020
91
84
24
22
21
ABSORBED
NWS/NCEP - Ocean Prediction Center

IVT & 850 mb Height
20051225-18

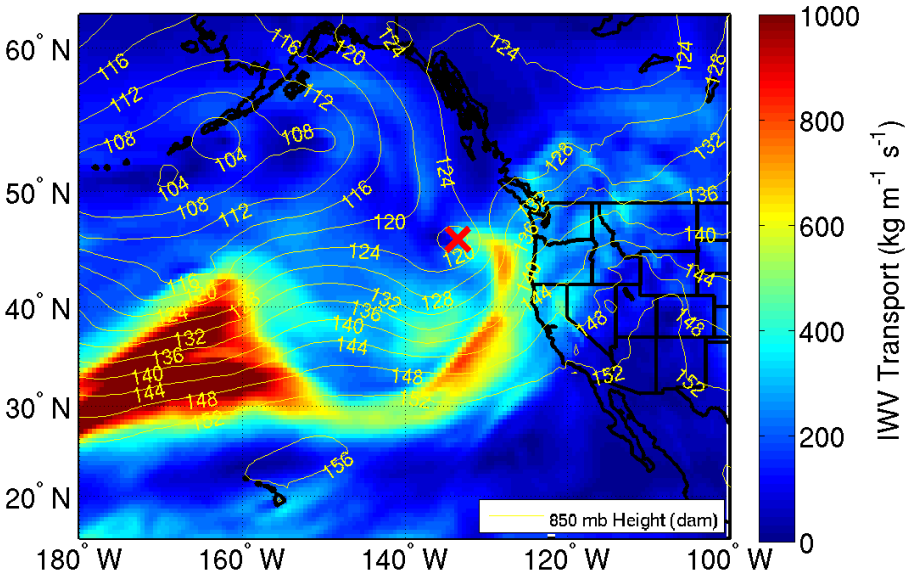

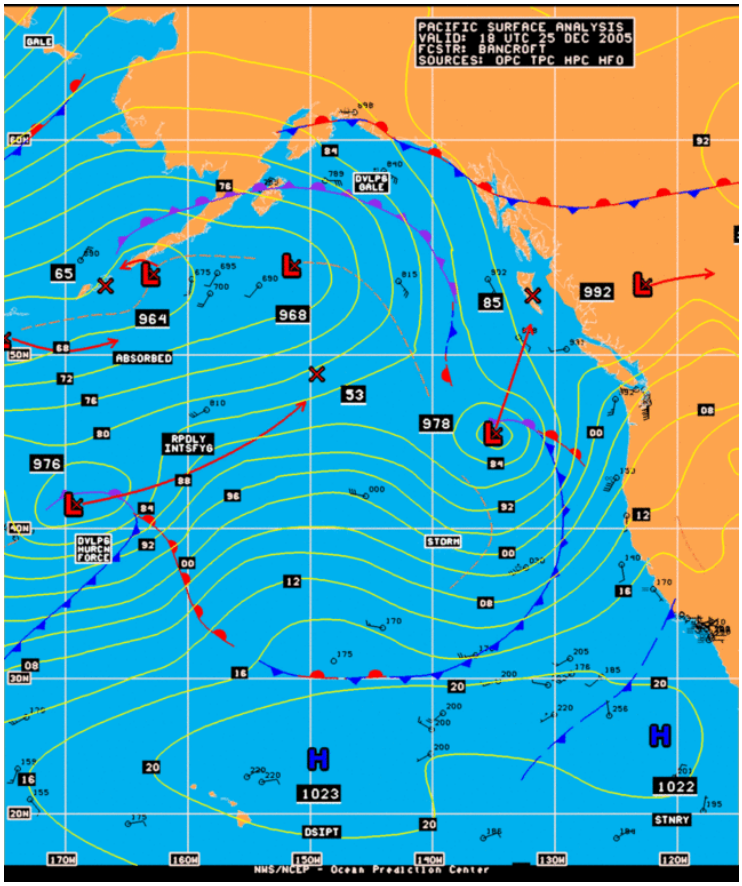

IVT & 850 mb Height
20070222-00

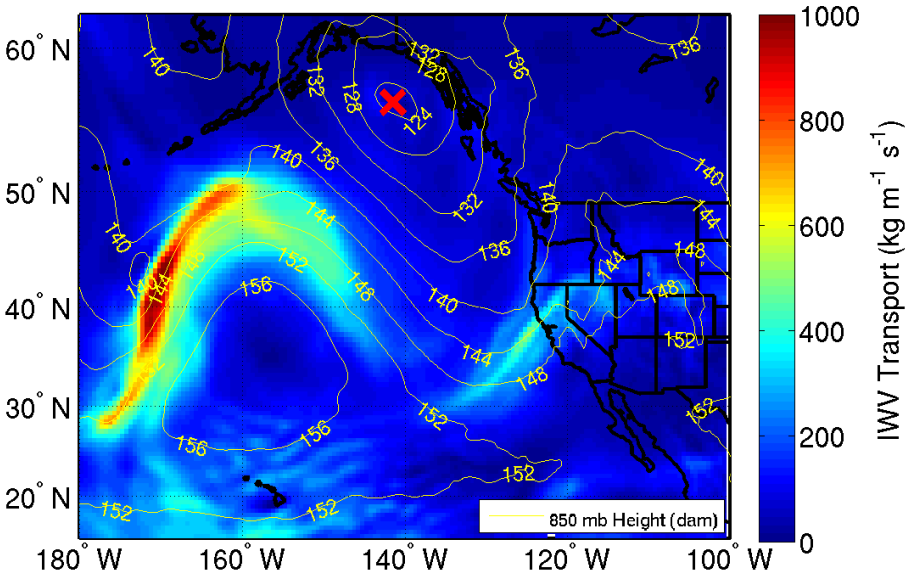

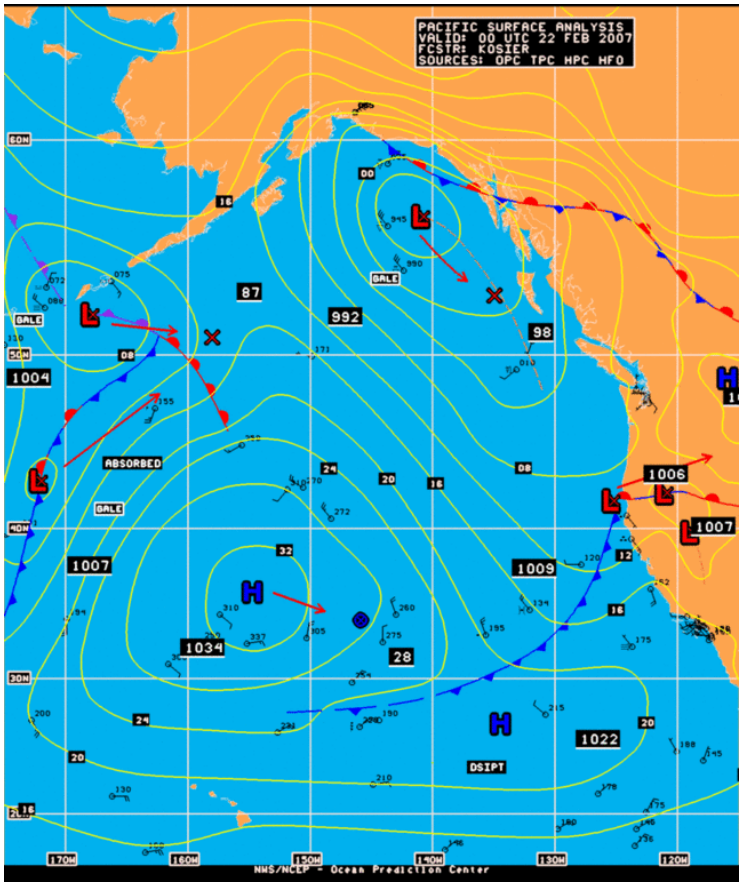

IVT & 850 mb Height
20100117-18

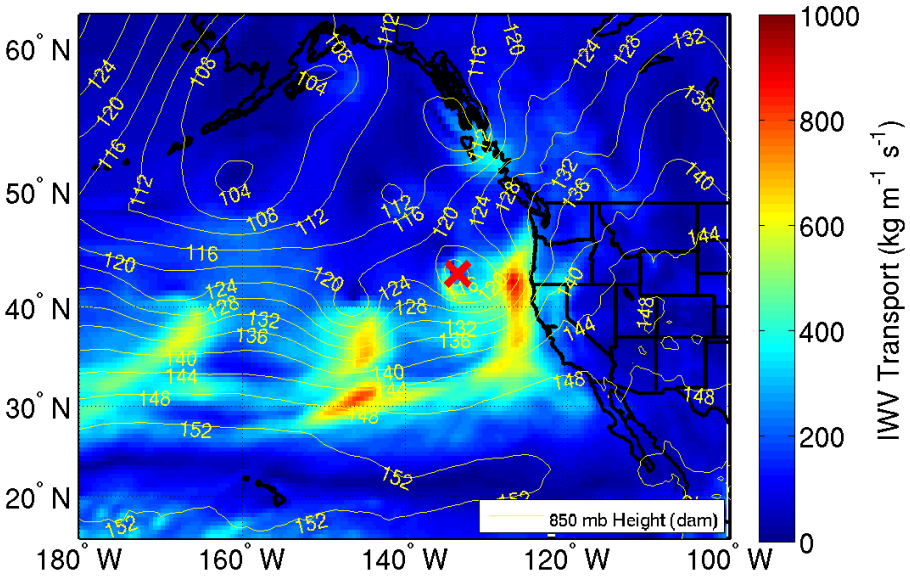

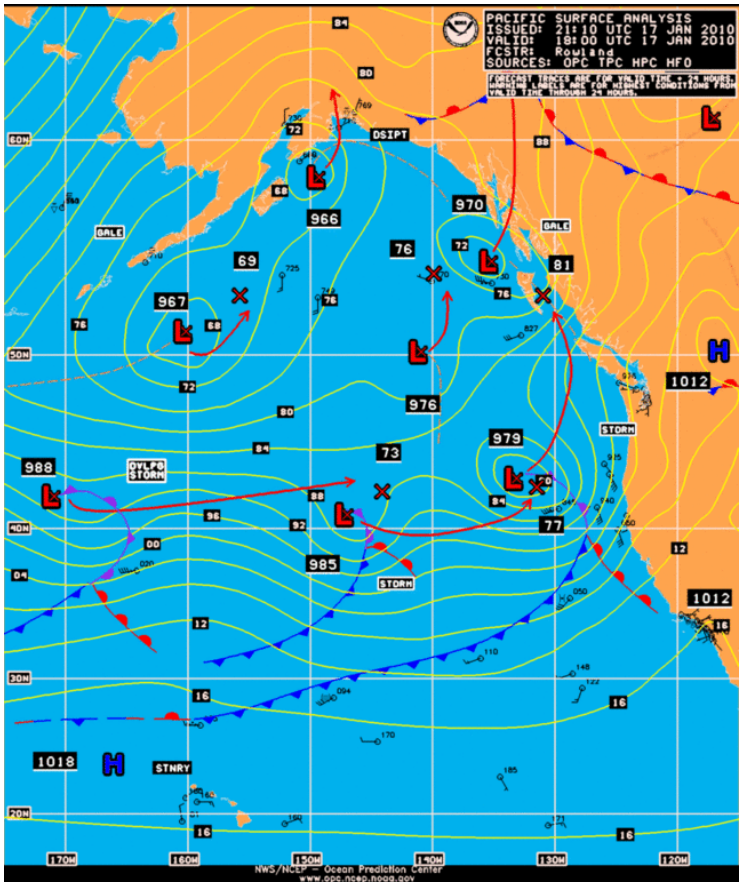

IVT & 850 mb Height
20090502-12

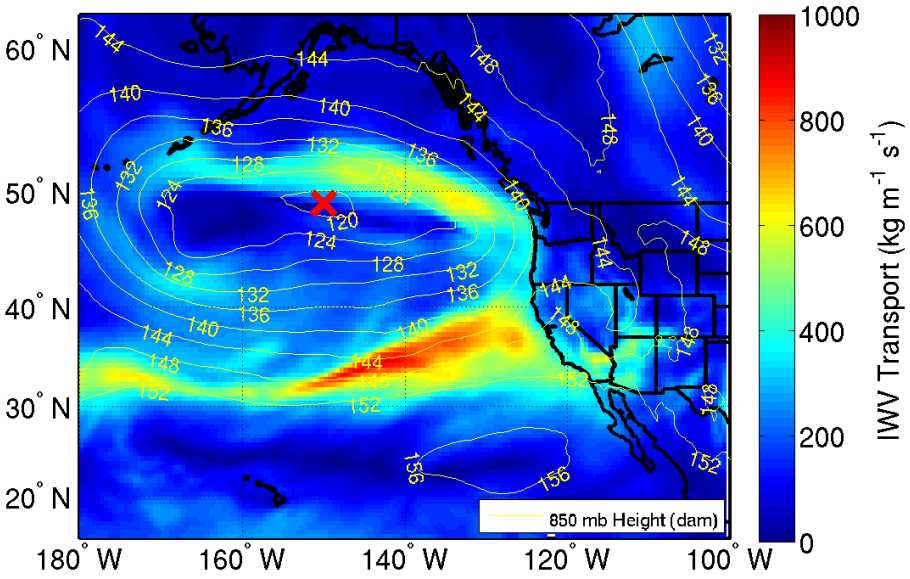

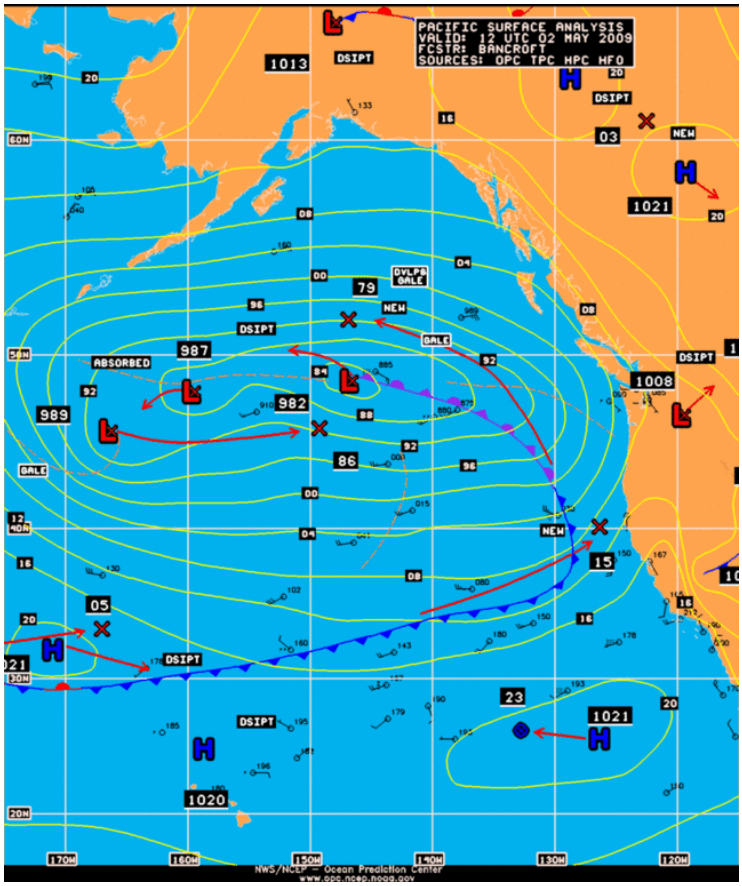

IVT & 850 mb Height
20061226-12

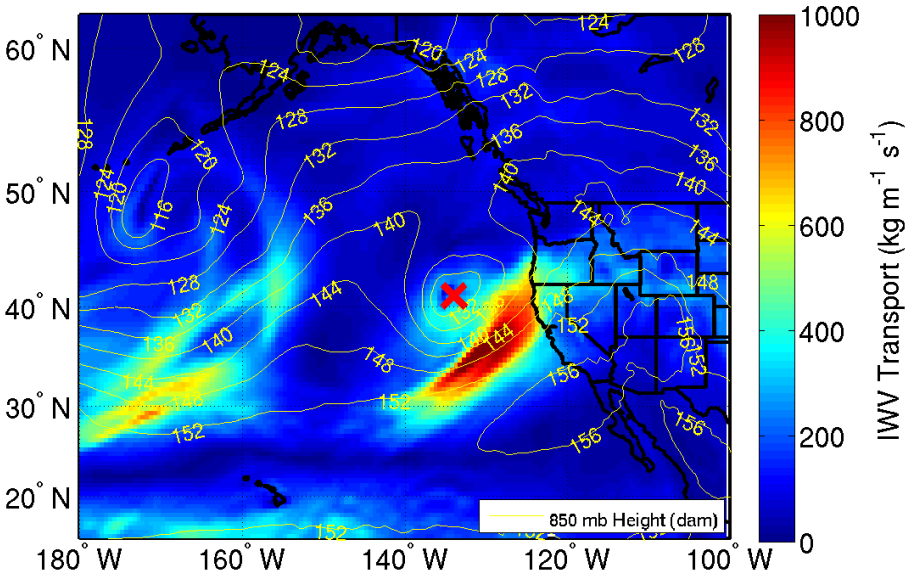

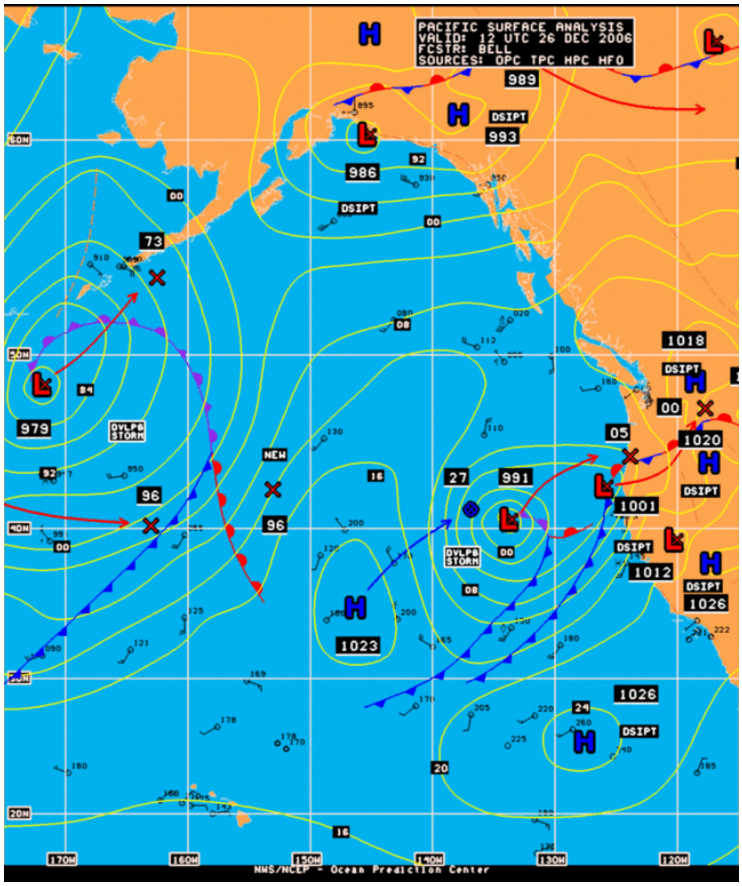

IVT & 850 mb Height
20061211-18

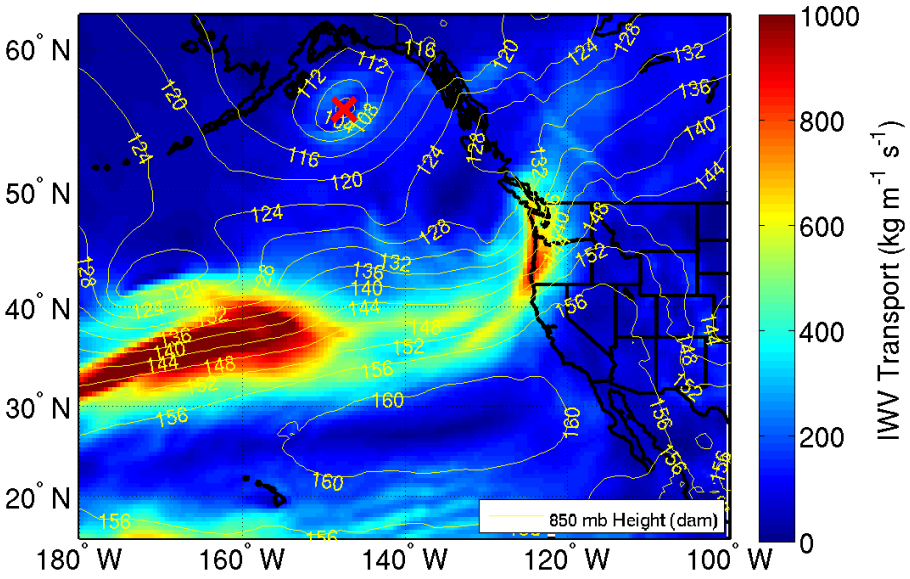

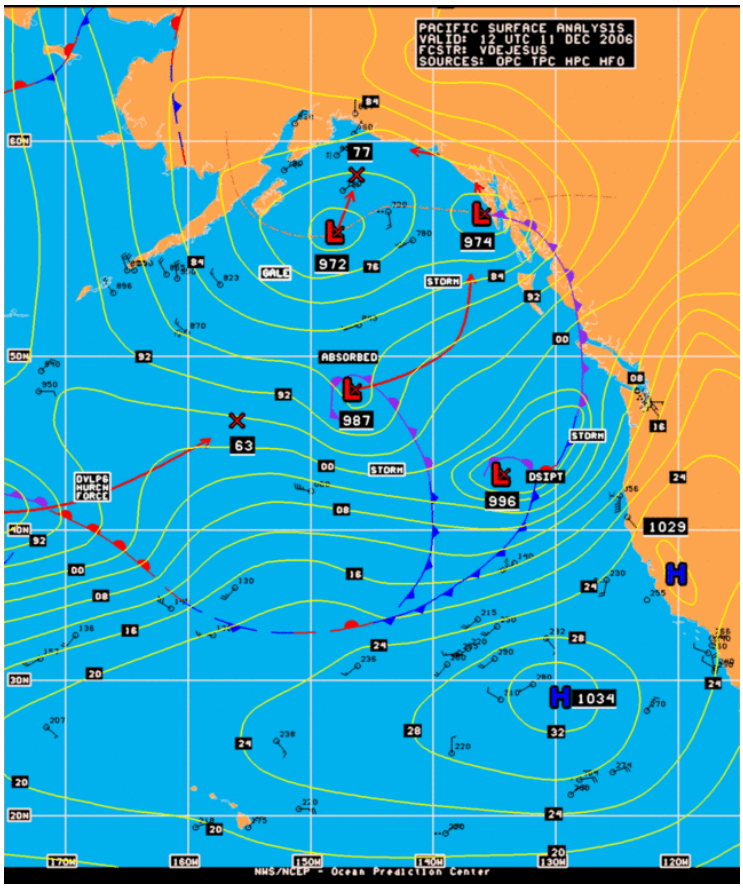

IVT & 850 mb Height
20061221-06

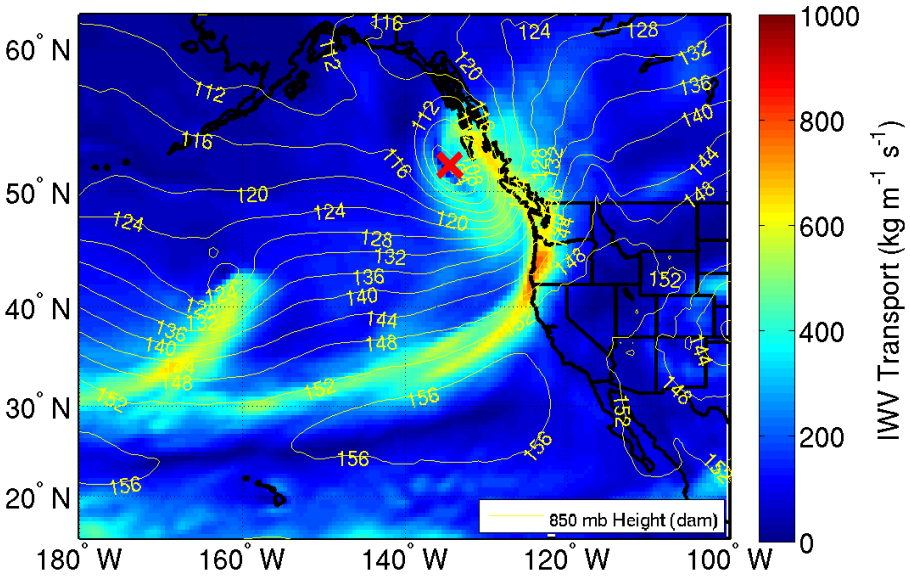

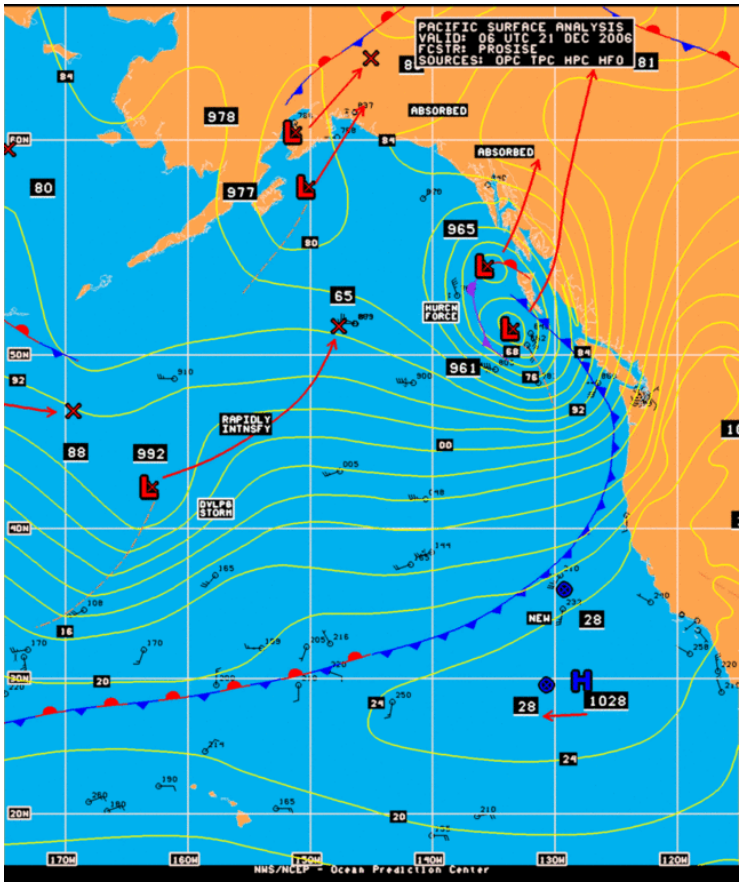

IVT & 850 mb Height
20090315-18

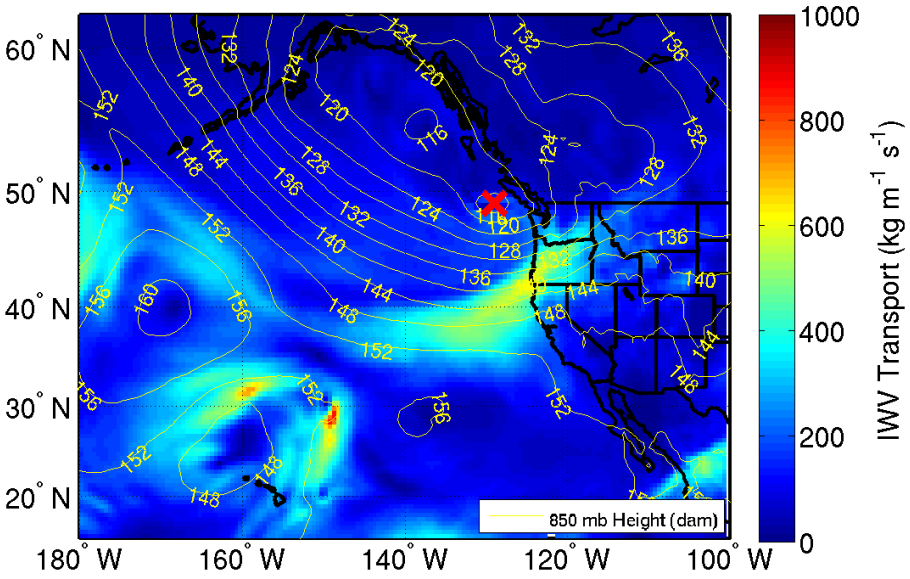

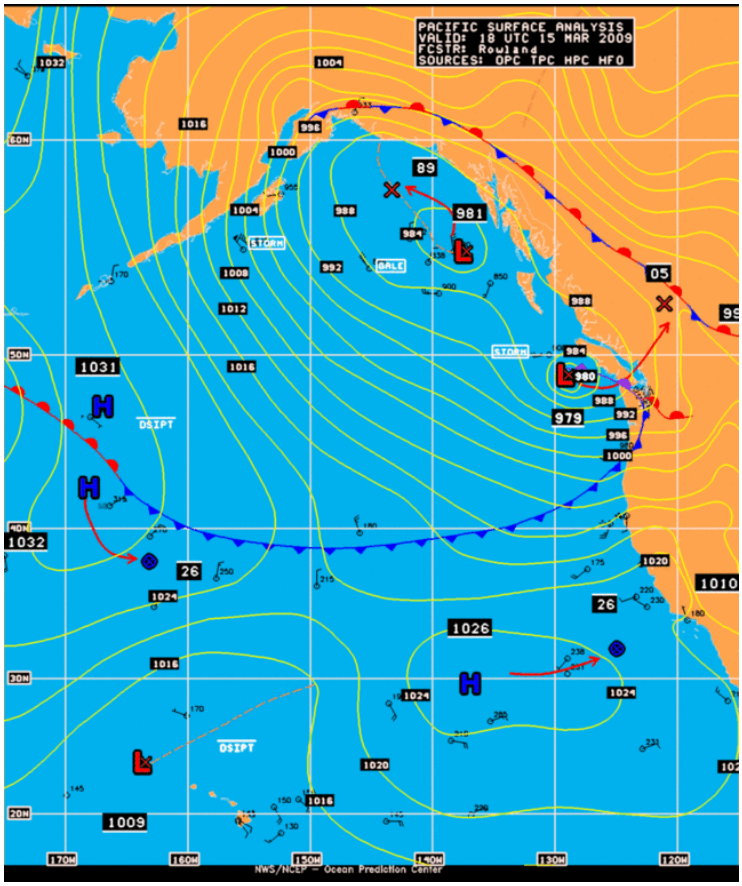

IVT & 850 mb Height
20071220-00

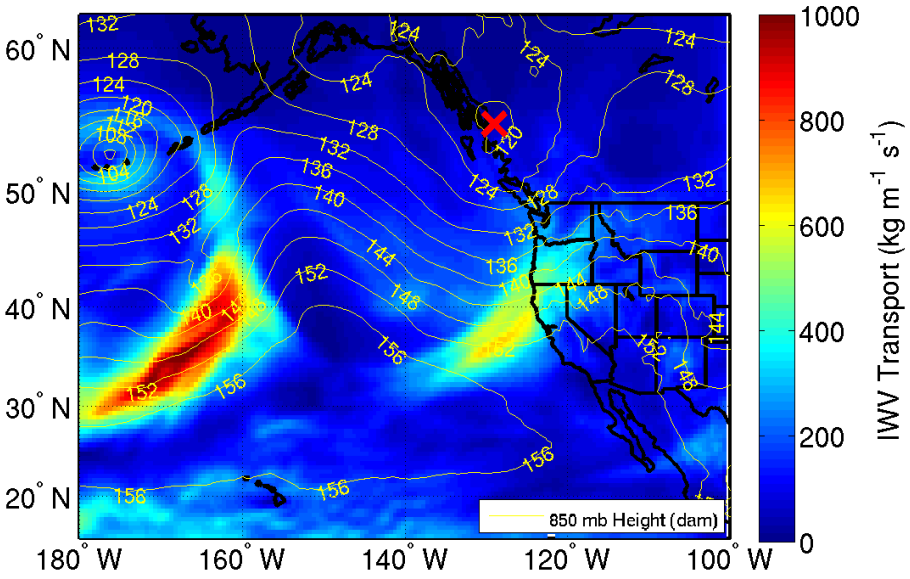

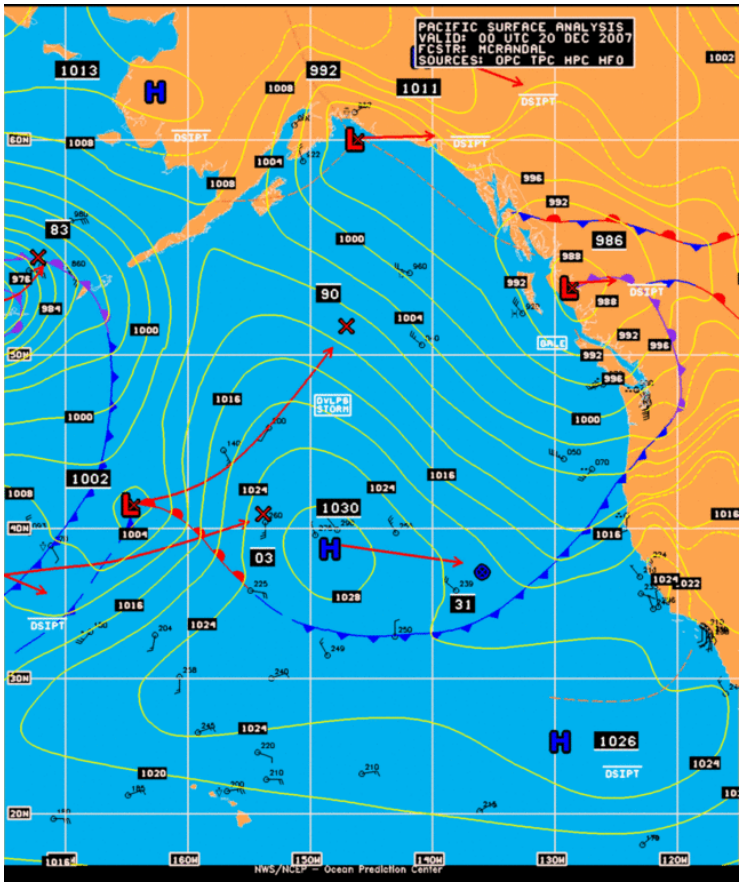

IVT & 850 mb Height
20100402-12

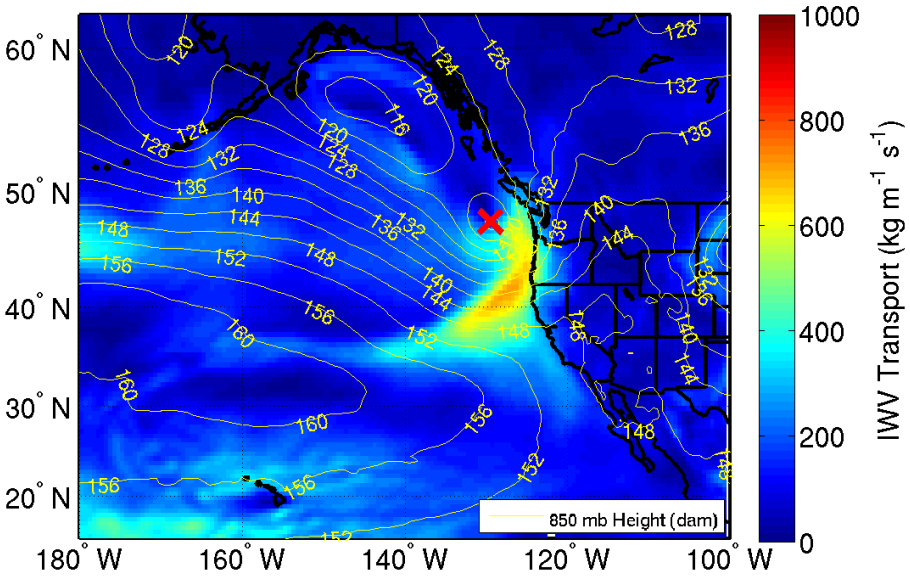

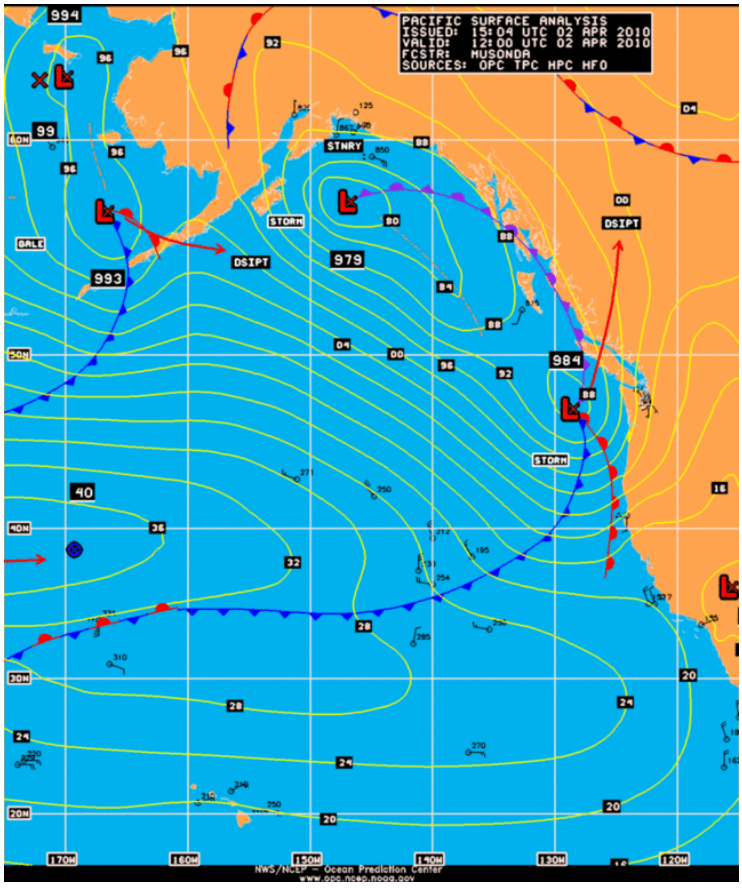

IVT & 850 mb Height
20051107-06

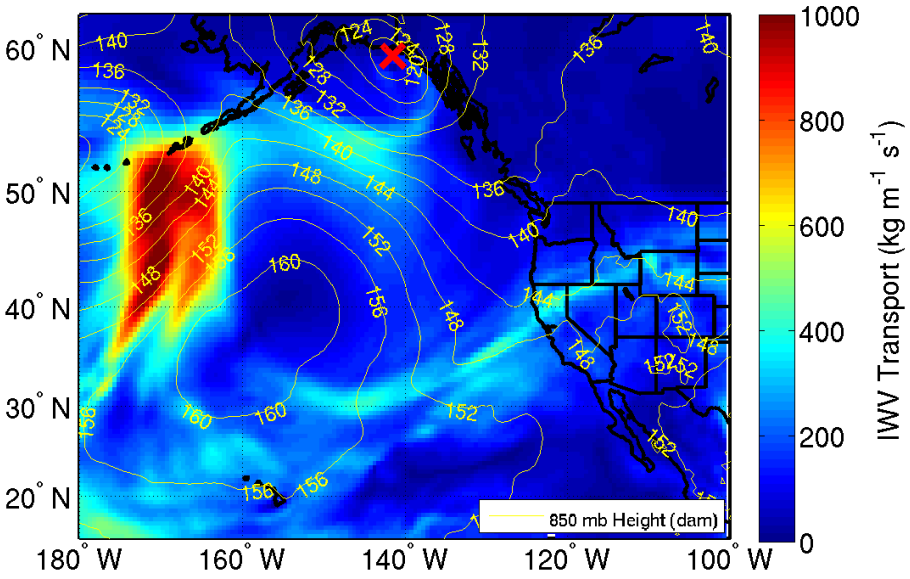

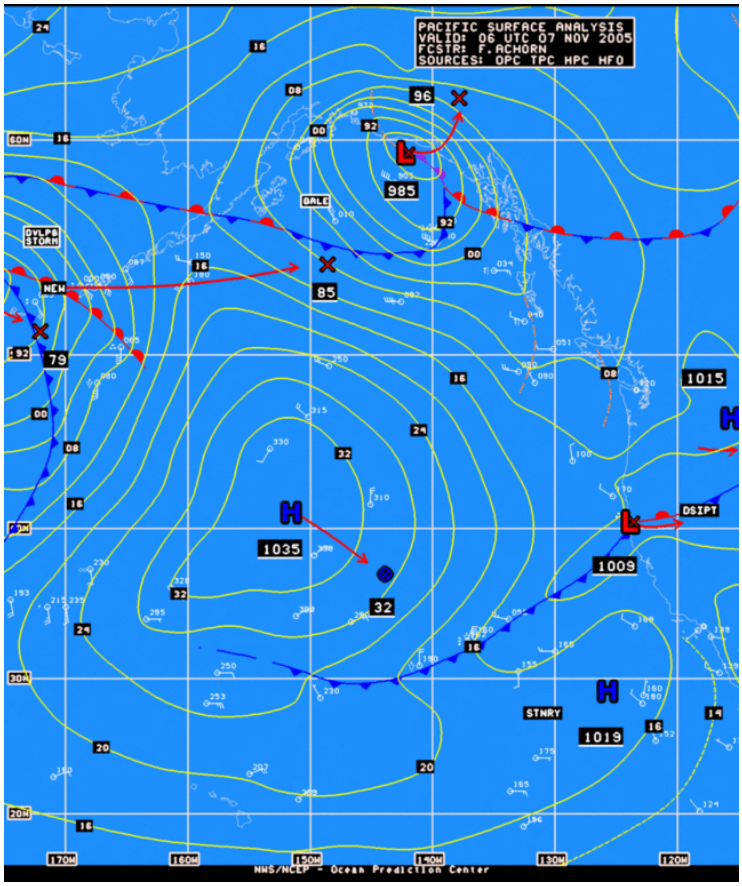

IVT & 850 mb Height
20060128-12

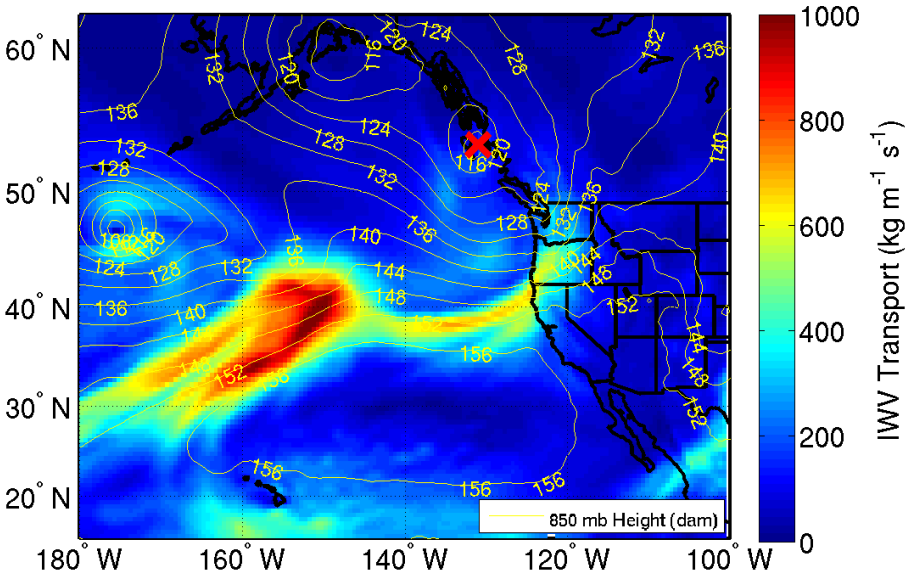

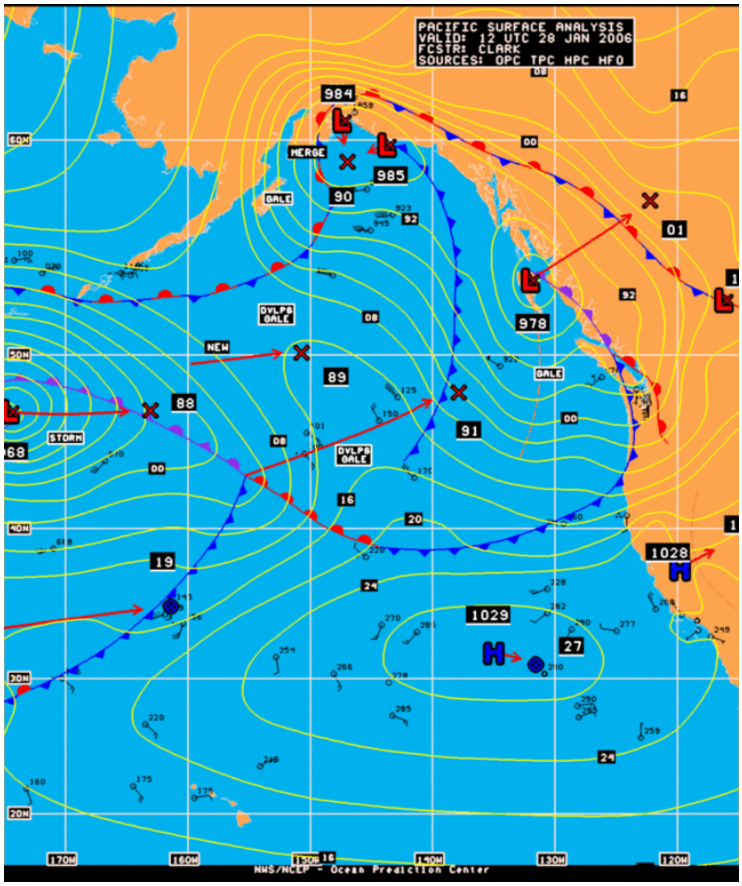

IVT & 850 mb Height
20061113-06

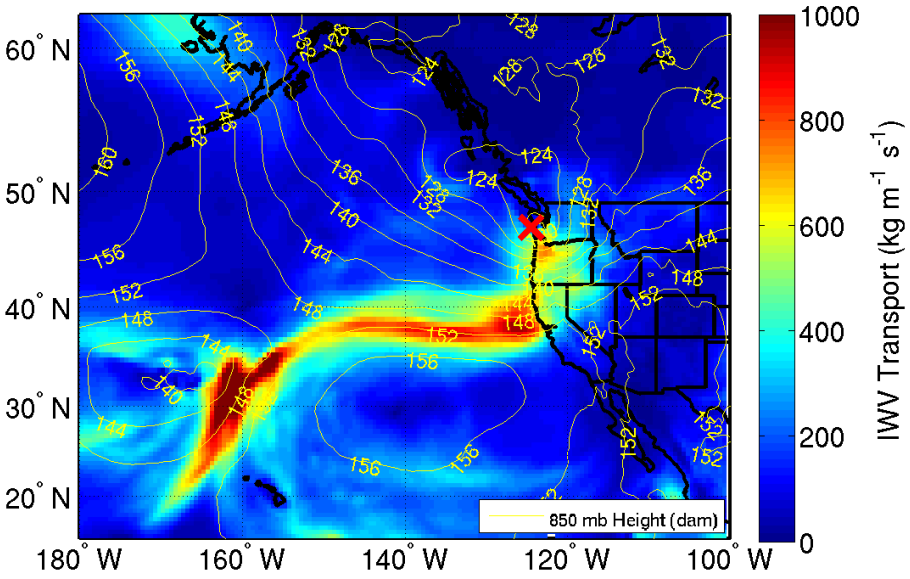

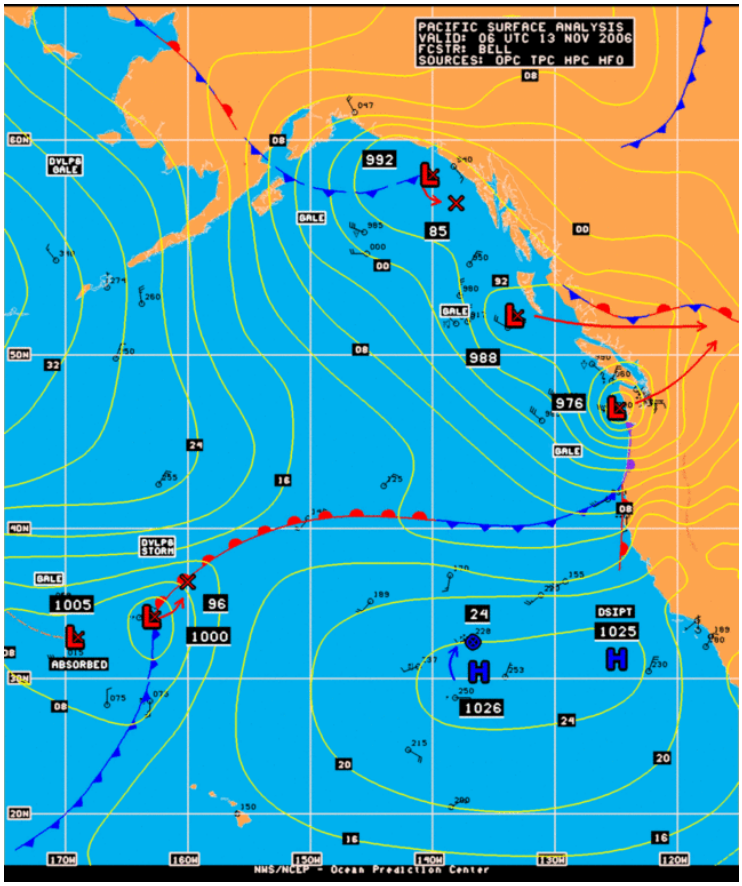

IVT & 850 mb Height
20080202-18

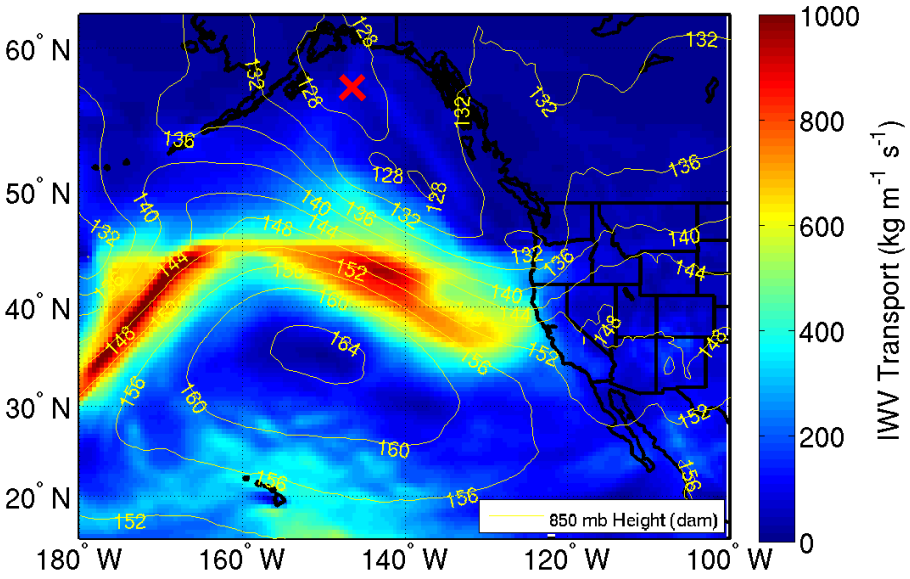

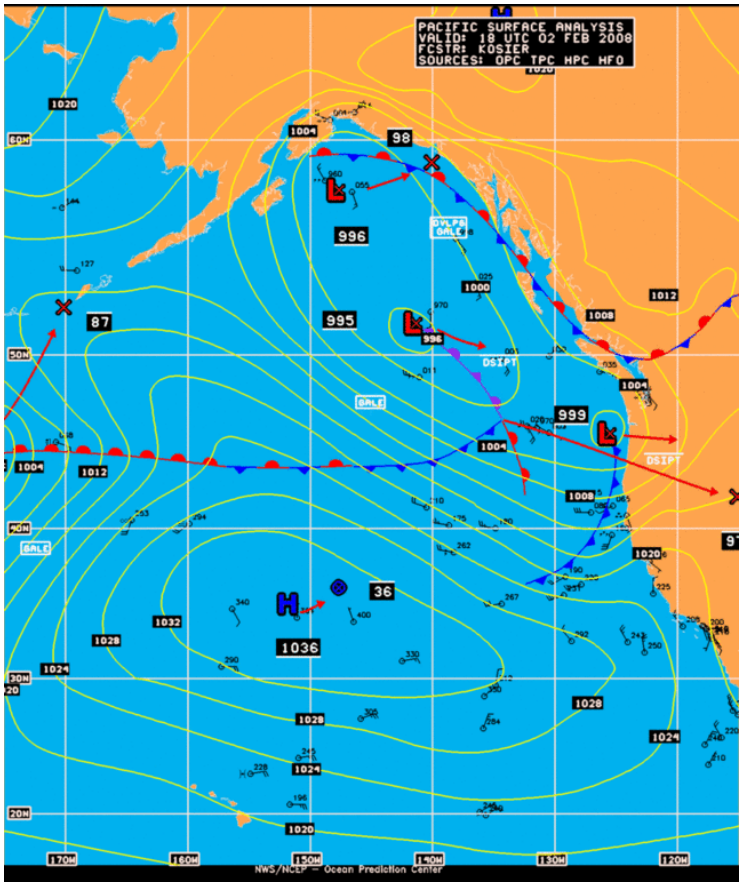

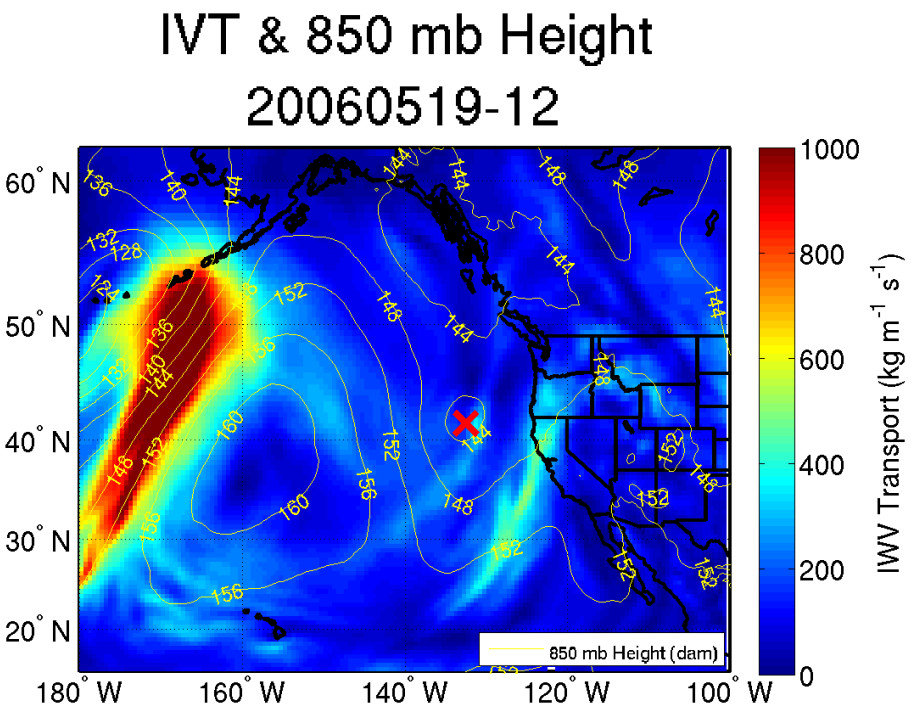
IVT & 850 mb Height
20060519-12
60˚ N
50˚ N
40˚ N
30˚ N
20˚ N
180˚ W
160˚ W
140˚ W
120˚ W
100˚ W
850 mb Height (dam)
1000
800
600
400
200
0
IWV Transport (kg m-1 s-1)

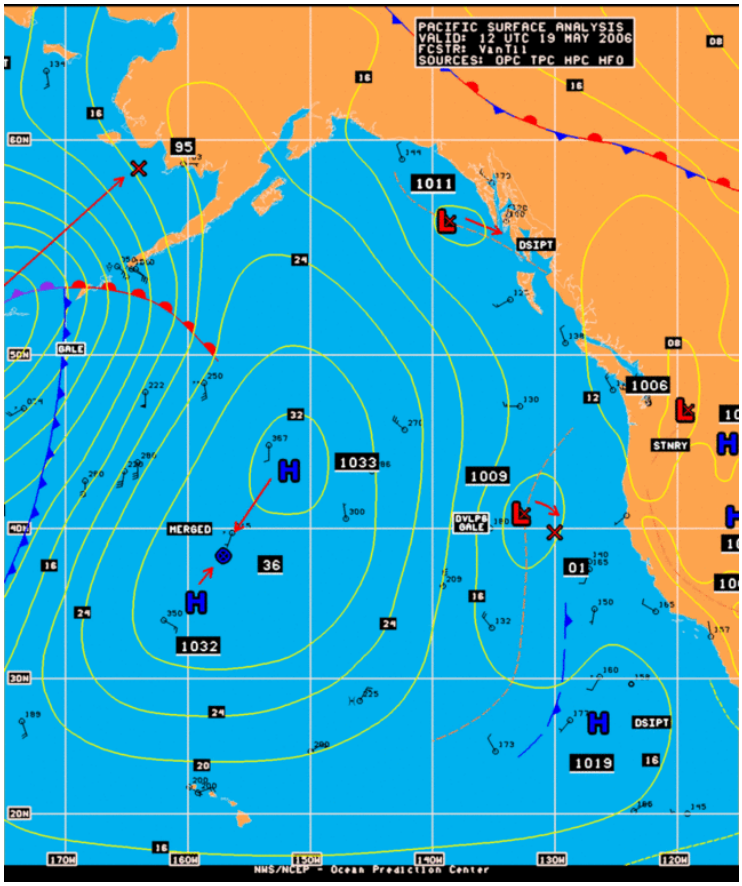
PACIFIC SURFACE ANALYSIS
VALID: 12 UTC 19 MAY 2006
FCSTR: VanTil
SOURCES: OPC TPC HPC HFO
1011
1033
1009
1006
1032
1019
DSIPT
STNRY
MERGED
GALE
NWS/NCEP - Ocean Prediction Center

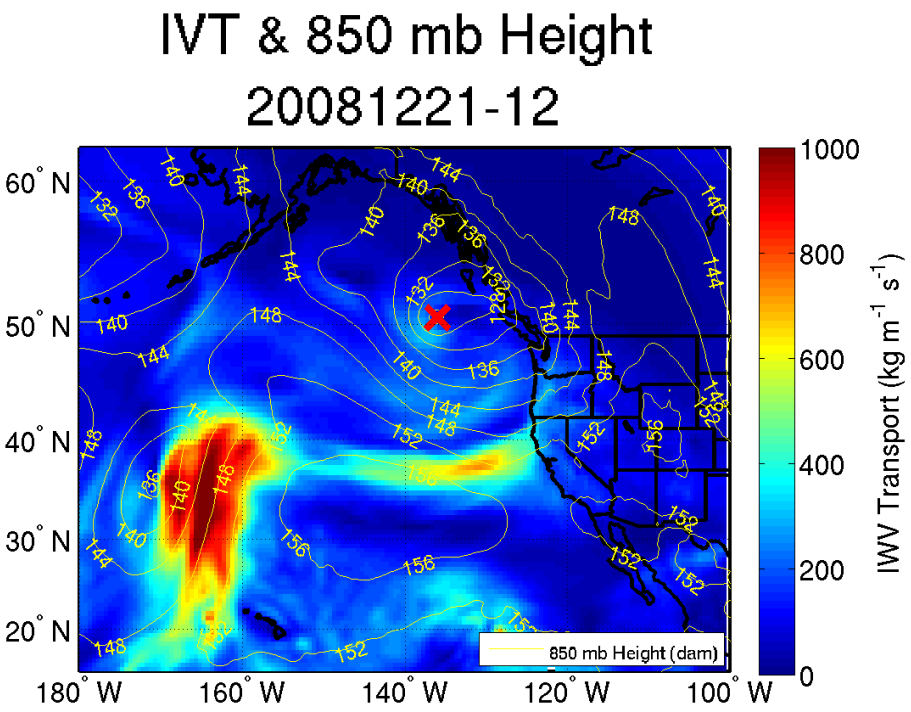
IVT & 850 mb Height
20081221-12
60˚ N
50˚ N
40˚ N
30˚ N
20˚ N
180˚ W
160˚ W
140˚ W
120˚ W
100˚ W
850 mb Height (dam)
1000
800
600
400
200
0
IWV Transport (kg m-1 s-1)

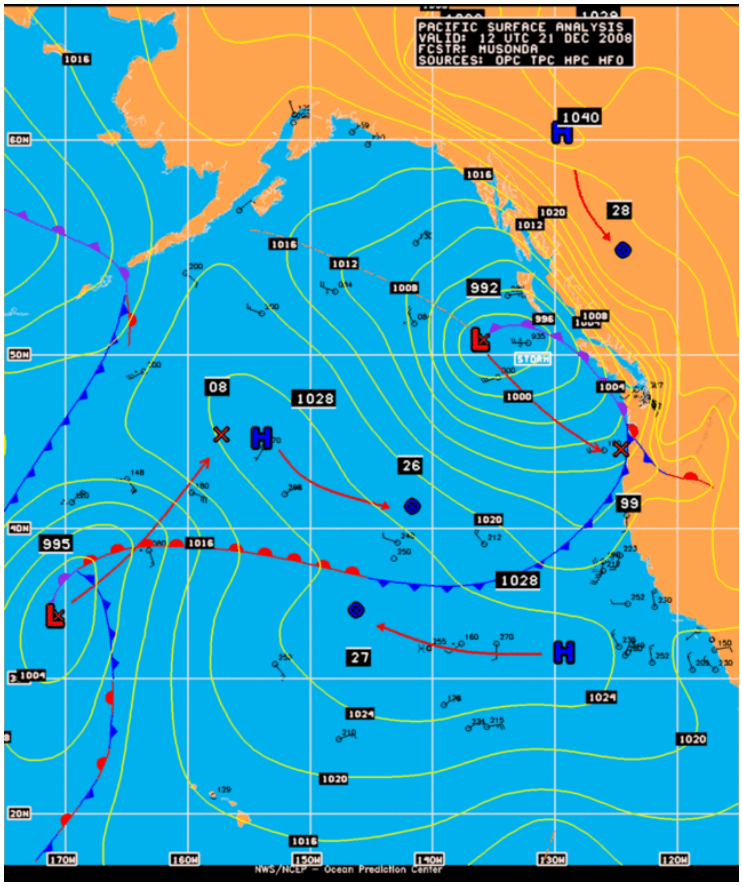
PACIFIC SURFACE ANALYSIS
VALID: 12 UTC 21 DEC 2008
FCSTR: MUSONDA
SOURCES: OPC TPC HPC HFO
1040
1028
992
995
1028
1024
1020
1016
NWS/NCEP - Ocean Prediction Center

IVT & 850 mb Height
20080110-12

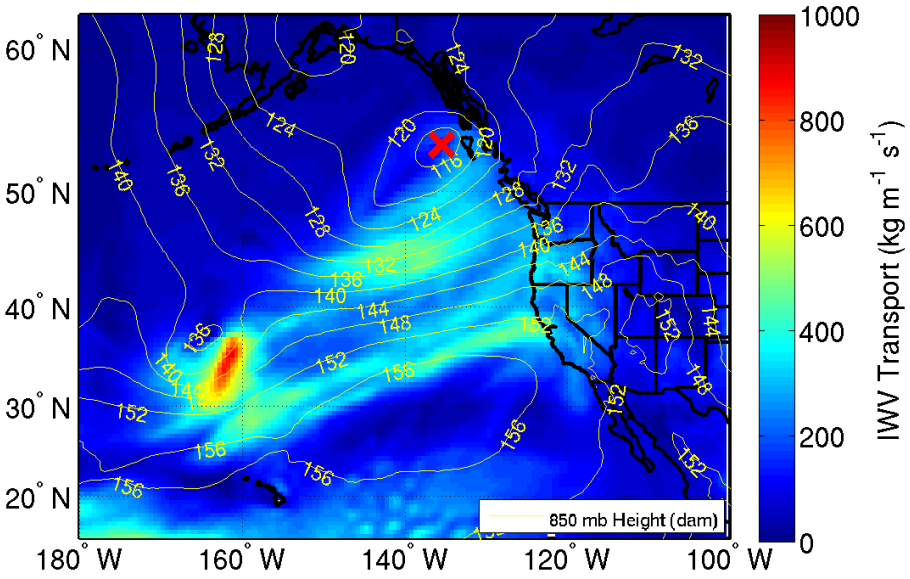

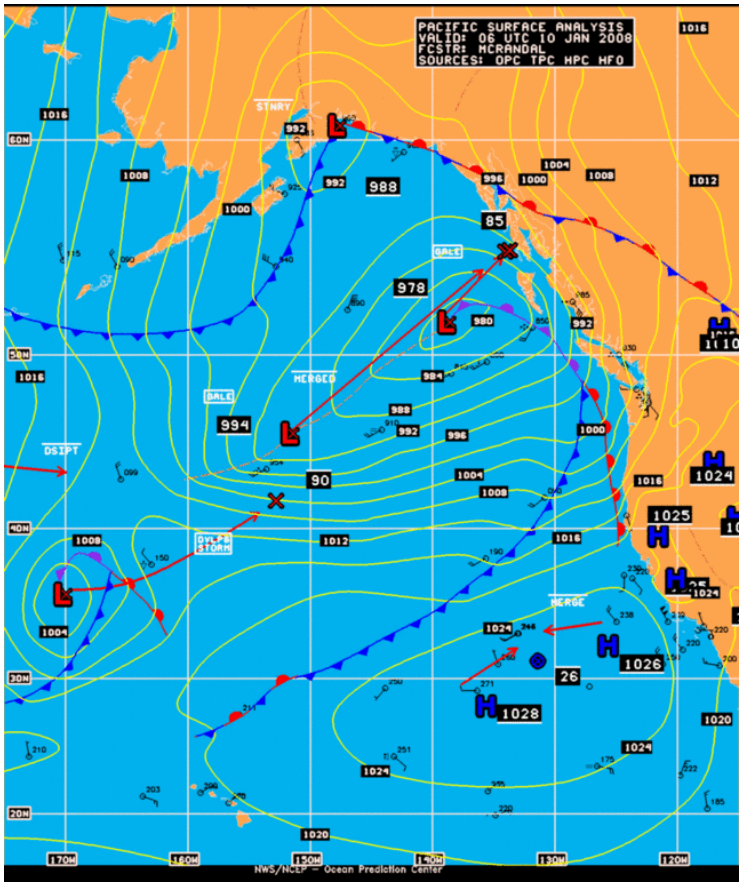

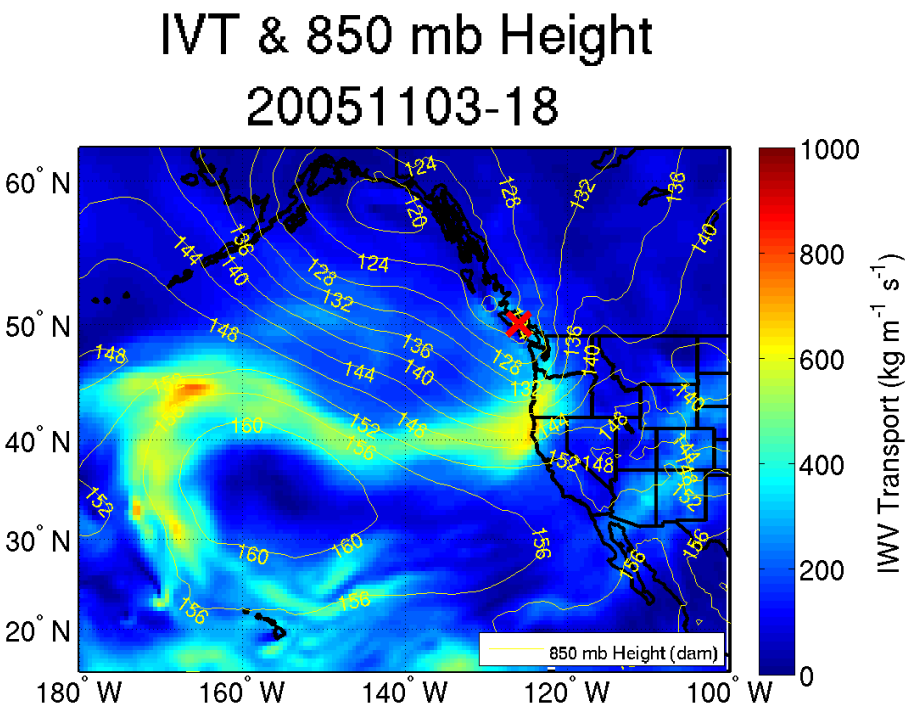
IVT & 850 mb Height
20051103-18
60˚ N
50˚ N
40˚ N
30˚ N
20˚ N
180˚ W
160˚ W
140˚ W
120˚ W
100˚ W
850 mb Height (dam)
1000
800
600
400
200
0
IWV Transport (kg m-1 s-1)

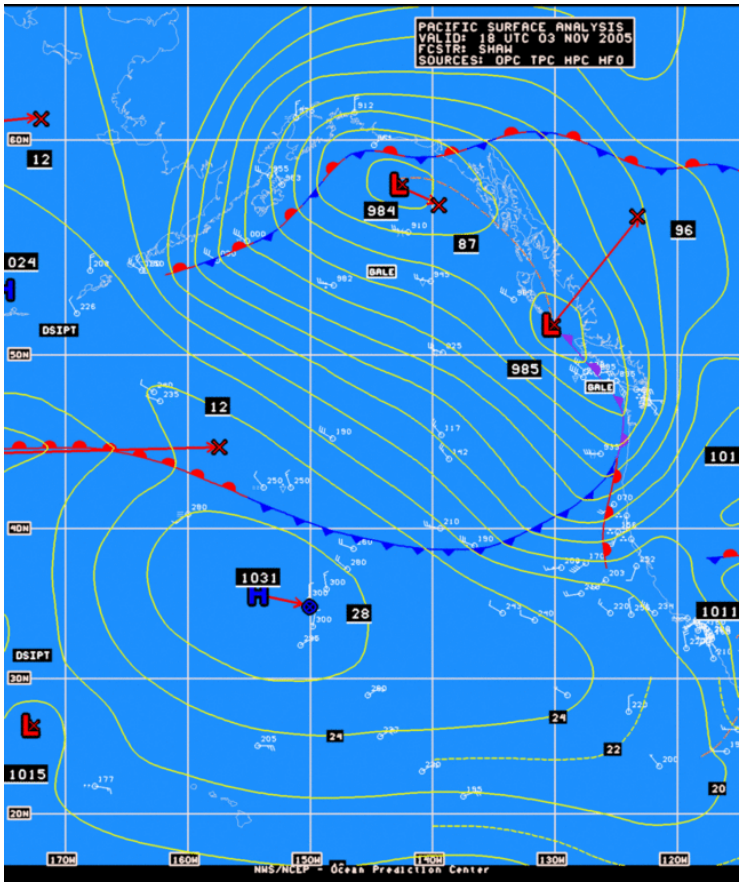
PACIFIC SURFACE ANALYSIS
VALID: 18 UTC 03 NOV 2005
FCSTR: SHAW
SOURCES: OPC TPC HPC HFO
984
87
985
1031
28
1015
1011
101
96
12
024
DSIPT
BALE
NWS/NCEP - Ocean Prediction Center

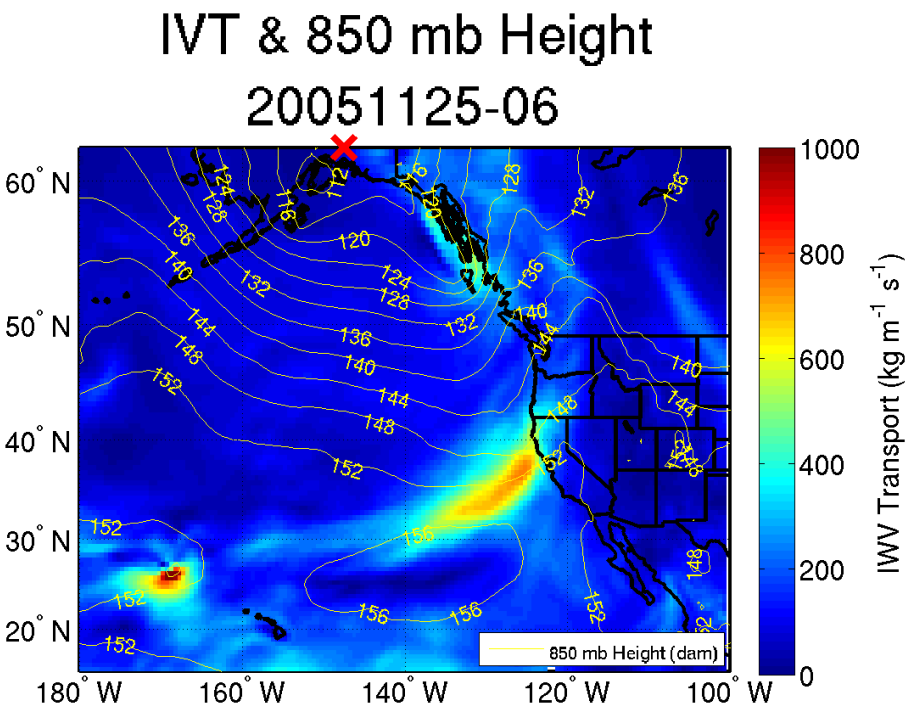
IVT & 850 mb Height
20051125-06
60˚ N
50˚ N
40˚ N
30˚ N
20˚ N
180˚ W
160˚ W
140˚ W
120˚ W
100˚ W
850 mb Height (dam)
1000
800
600
400
200
0
IWV Transport (kg m-1 s-1)

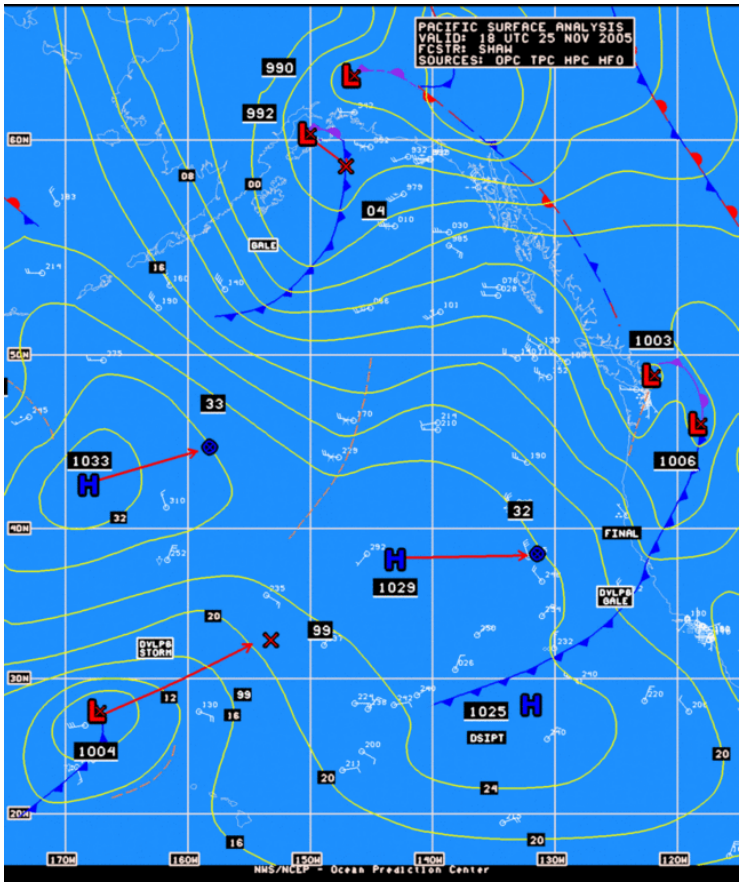
PACIFIC SURFACE ANALYSIS
VALID: 18 UTC 25 NOV 2005
FCSTR: SHAW
SOURCES: OPC TPC HPC HFO
990
992
1003
1033
1006
1029
1025
1004
FINAL
DSIPT
NWS/NCEP - Ocean Prediction Center

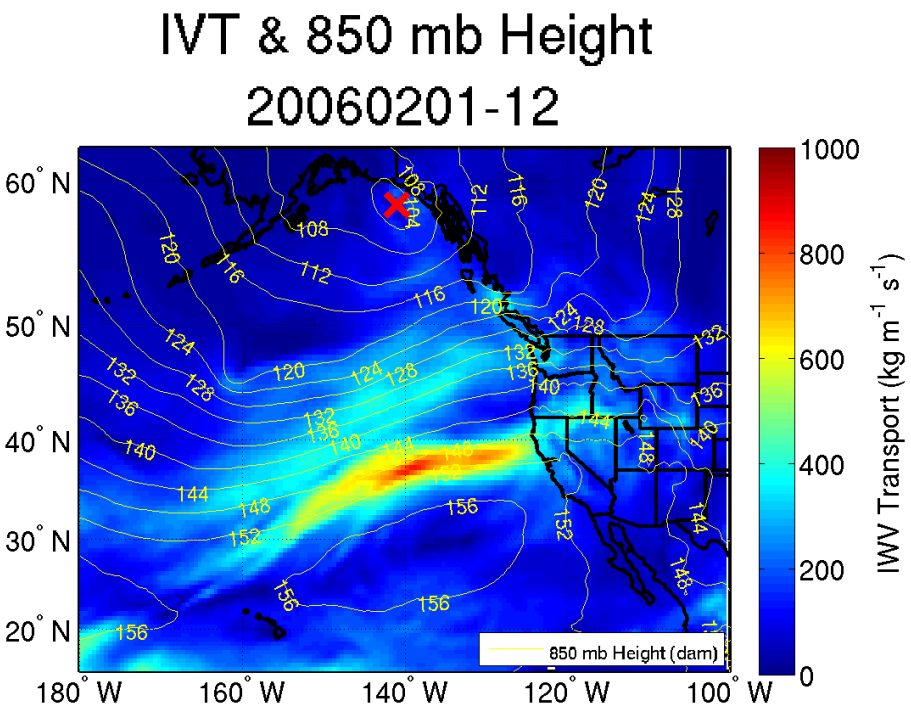
IVT & 850 mb Height
20060201-12
60° N
50° N
40° N
30° N
20° N
180° W
160° W
140° W
120° W
100° W
850 mb Height (dam)
IWV Transport (kg m-1 s-1)
1000
800
600
400
200
0

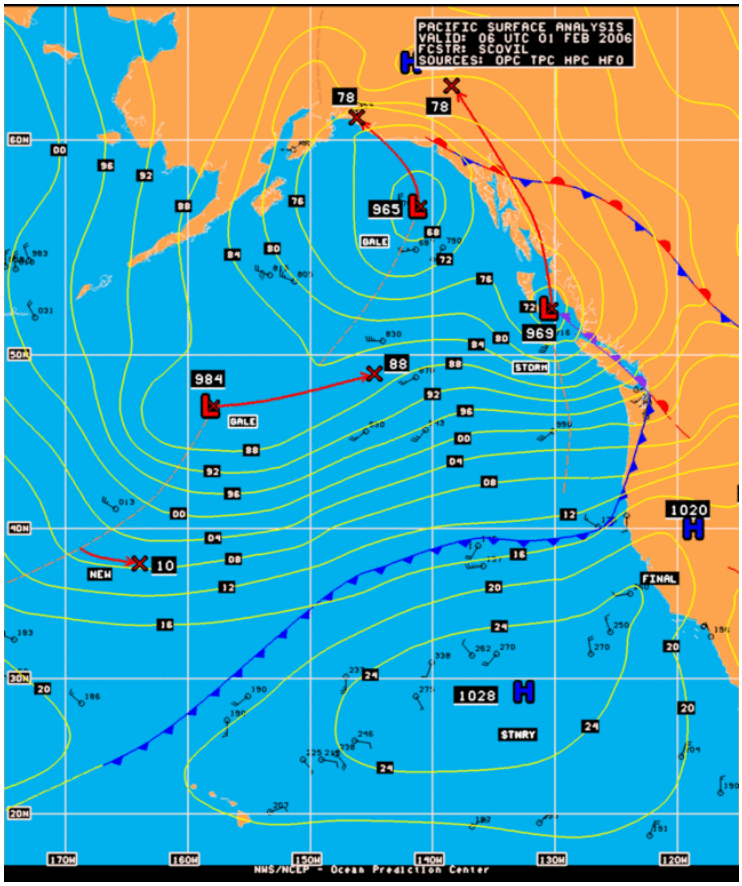
PACIFIC SURFACE ANALYSIS
VALID: 06 UTC 01 FEB 2006
FCSTR: SCOVIL
SOURCES: OPC TPC HPC HFO
965
969
984
1020
1028
GALE
STORM
FINAL
STNRY
NWS/NCEP - Ocean Prediction Center

IVT & 850 mb Height
20100329-00

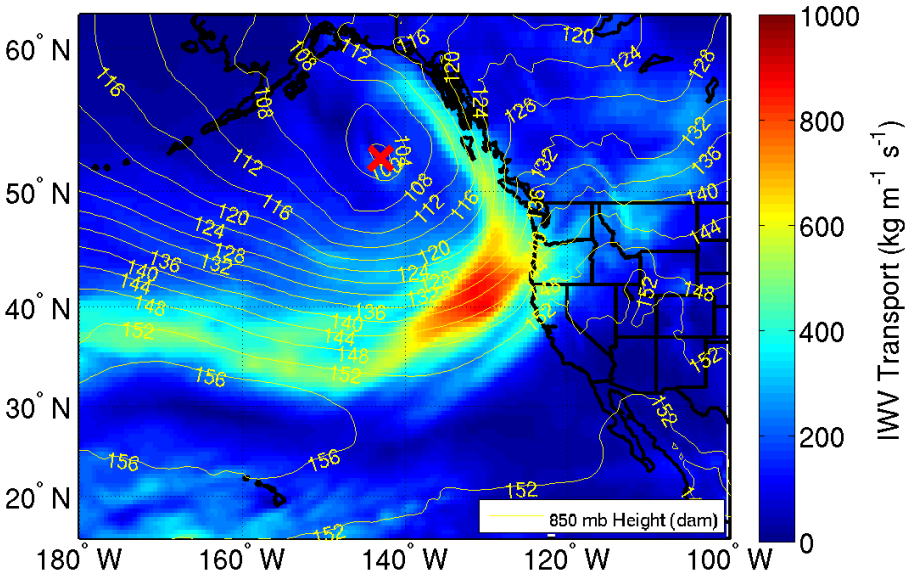

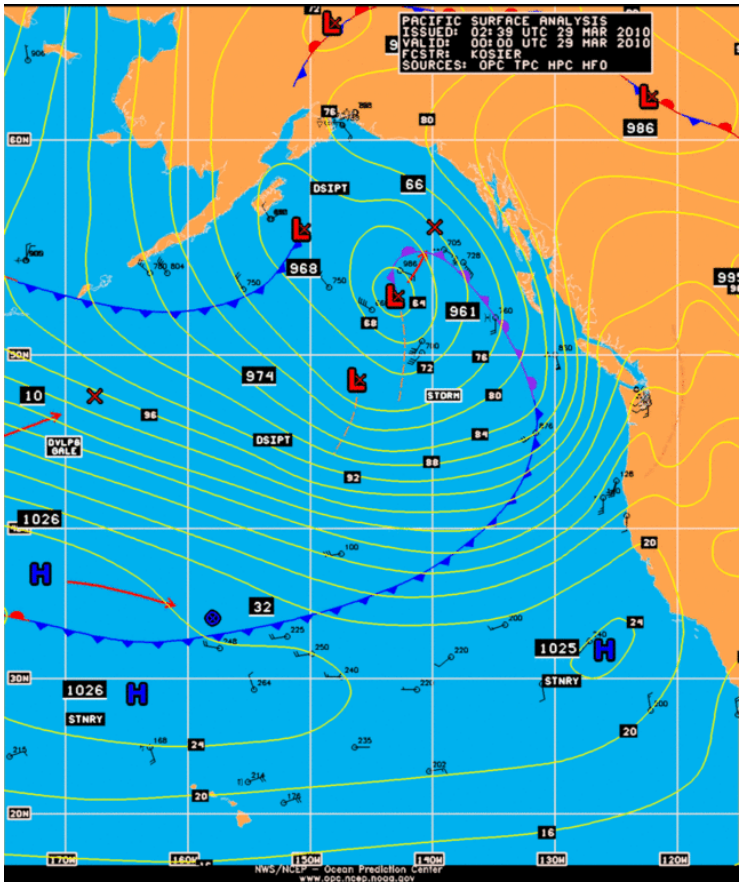

IVT & 850 mb Height
20081002-12

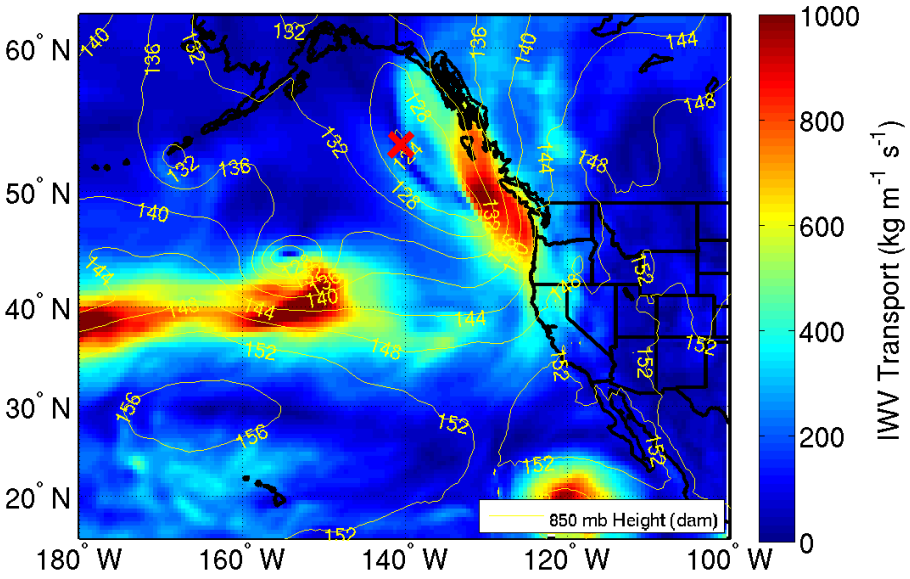

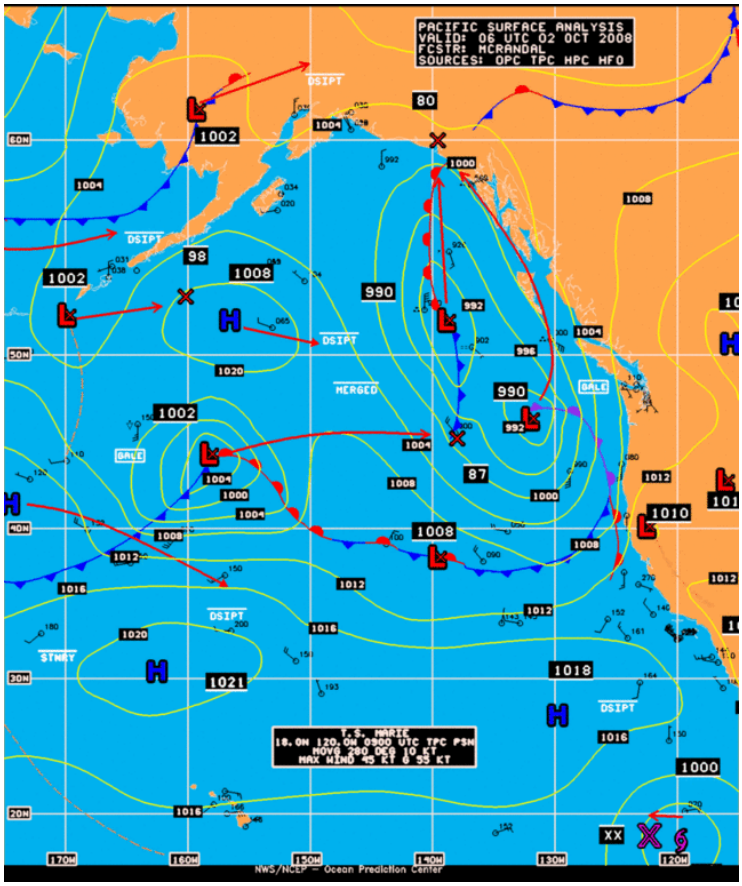

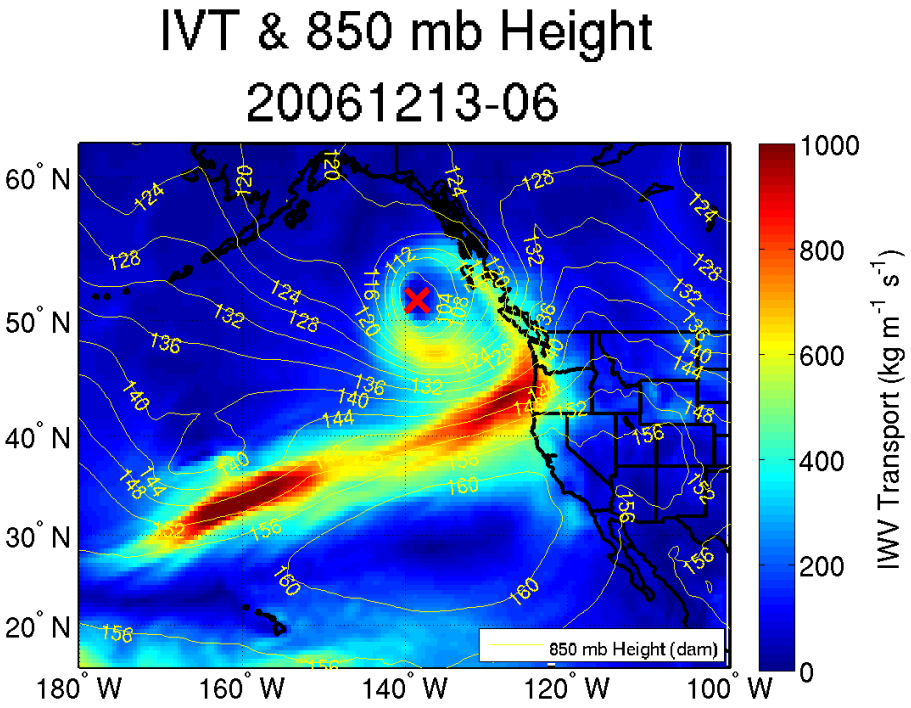
IVT & 850 mb Height
20061213-06
60˚ N
50˚ N
40˚ N
30˚ N
20˚ N
180˚ W
160˚ W
140˚ W
120˚ W
100˚ W
850 mb Height (dam)
1000
800
600
400
200
0
IWV Transport (kg m-1 s-1)

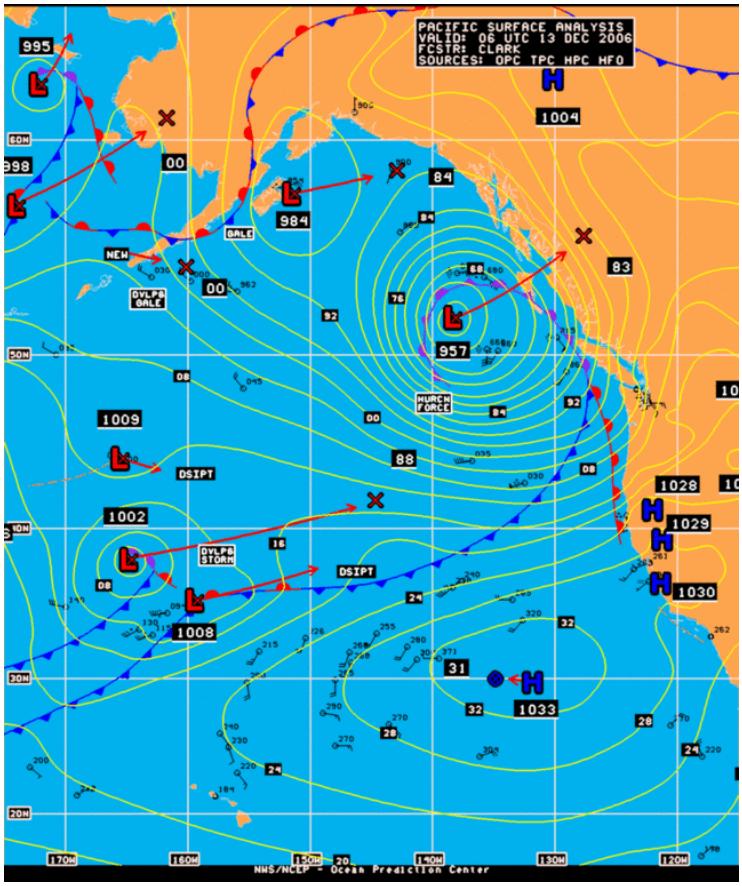
PACIFIC SURFACE ANALYSIS
VALID: 06 UTC 13 DEC 2006
FCSTR: CLARK
SOURCES: OPC TPC HPC HFO
995
1004
984
957
1009
1002
1008
1033
1028
1029
1030
DSIPT
DVLPG STORM
HURCN FORCE
NWS/NCEP - Ocean Prediction Center

IVT & 850 mb Height
20081003-12

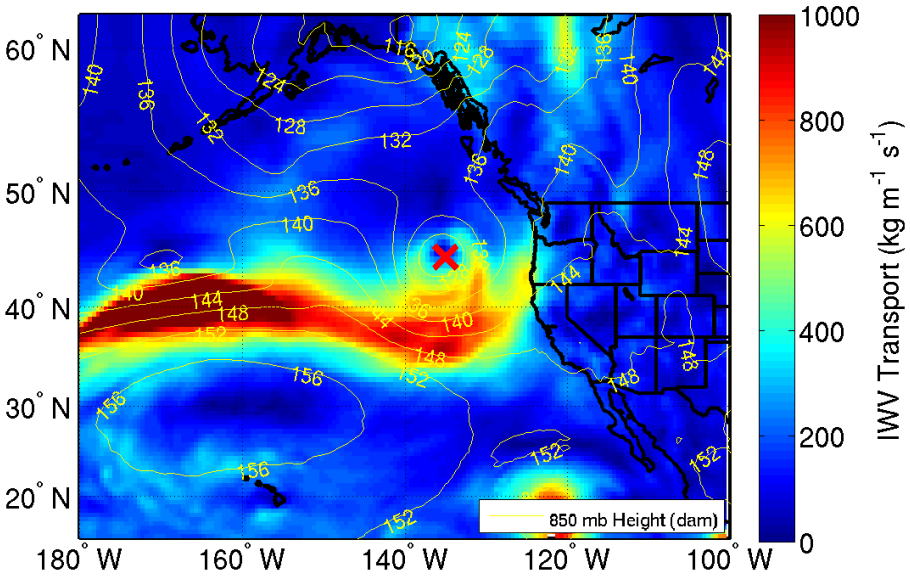

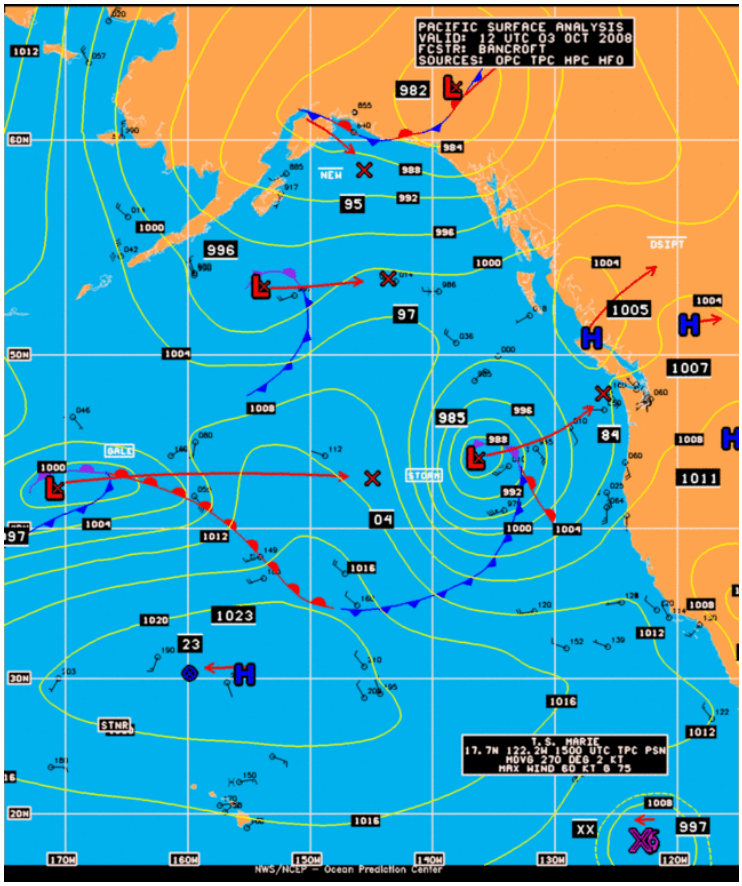

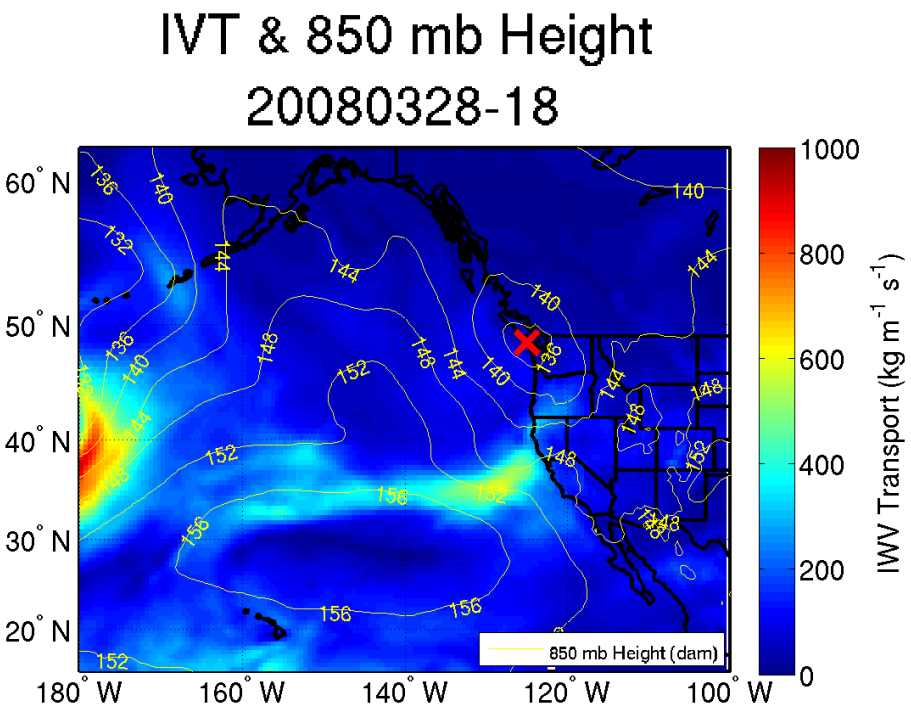

Surface analysis unavailable

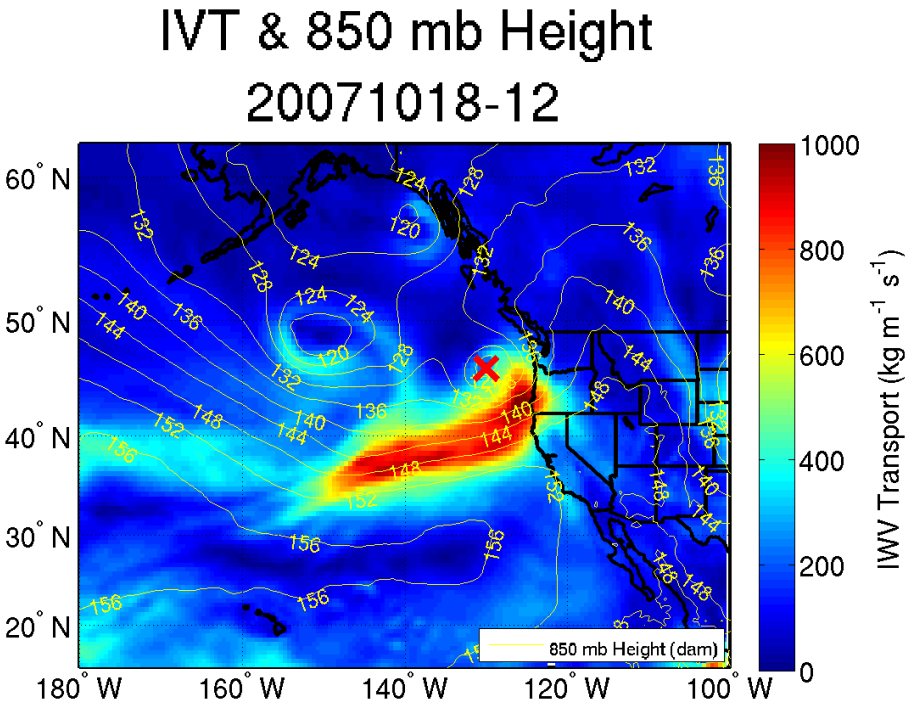
IVT & 850 mb Height
20071018-12
60˚ N
50˚ N
40˚ N
30˚ N
20˚ N
180˚ W
160˚ W
140˚ W
120˚ W
100˚ W
850 mb Height (dam)
1000
800
600
400
200
0
IWV Transport (kg m-1 s-1)

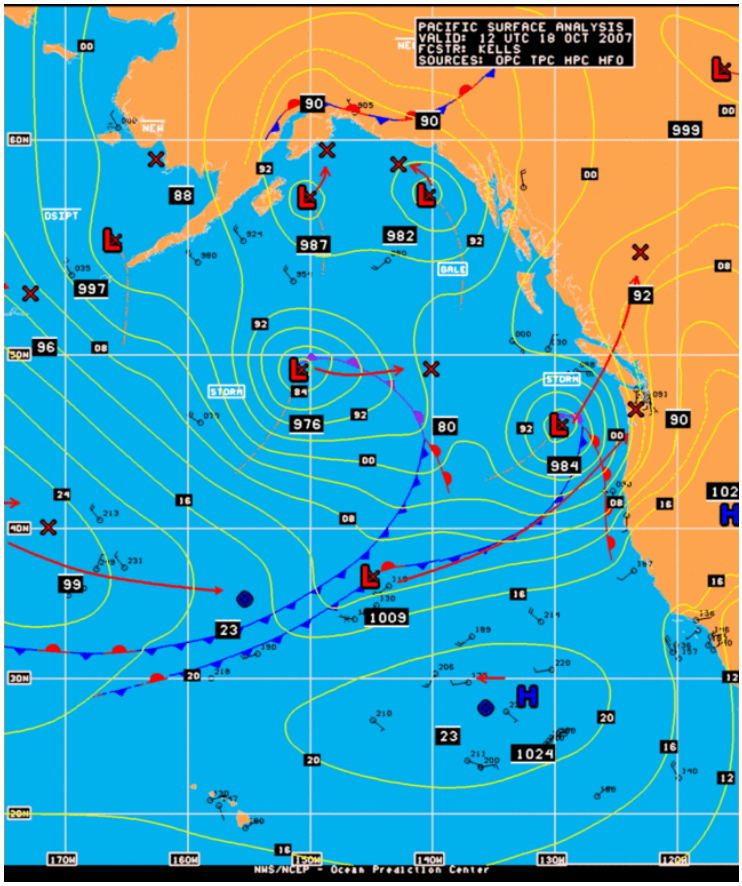
PACIFIC SURFACE ANALYSIS
VALID: 12 UTC 18 OCT 2007
FCSTR: KELLS
SOURCES: OPC TPC HPC HFO
NWS/NCEP - Ocean Prediction Center

IVT & 850 mb Height
20060111-00

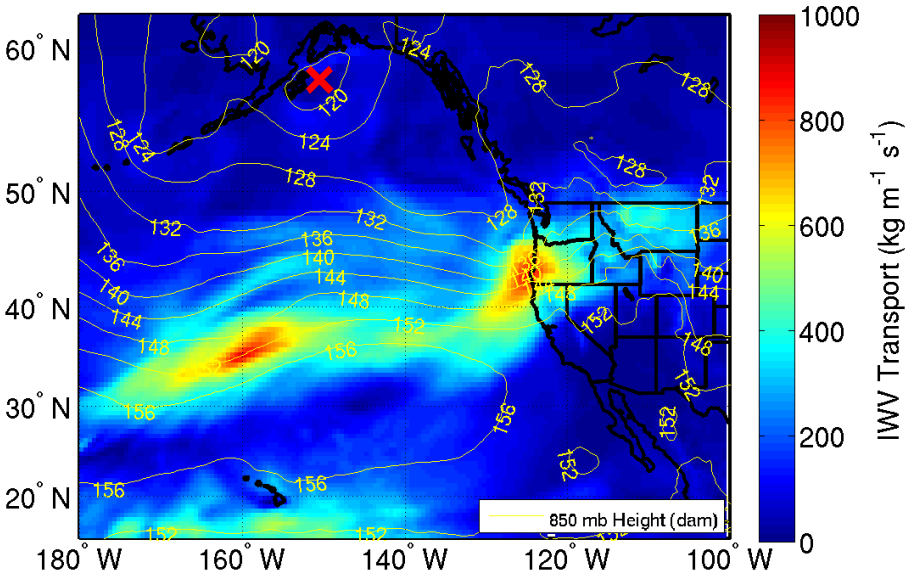

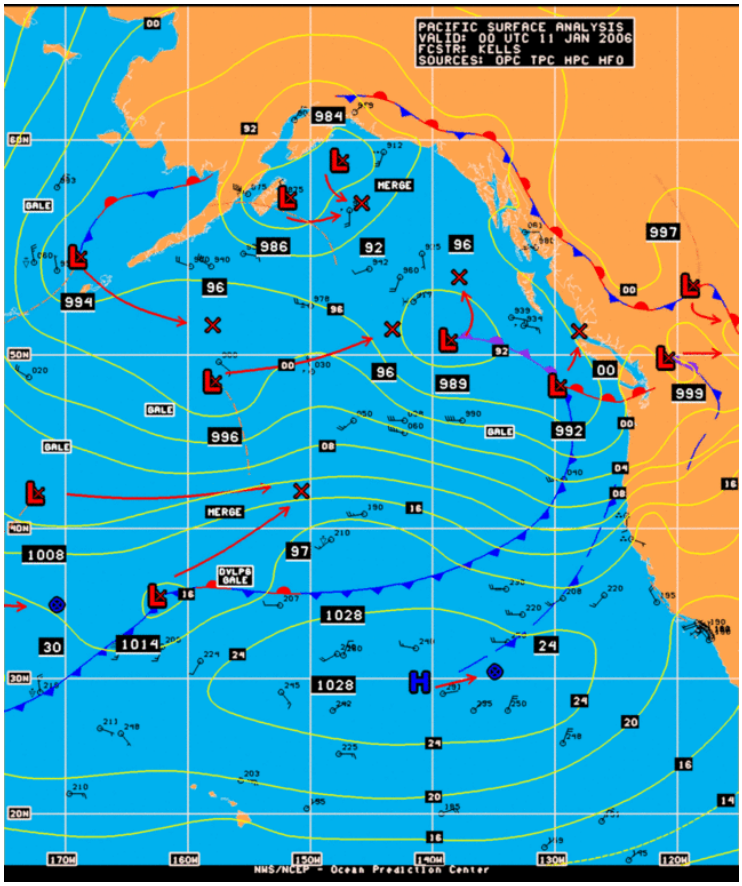

IVT & 850 mb Height
20090102-06

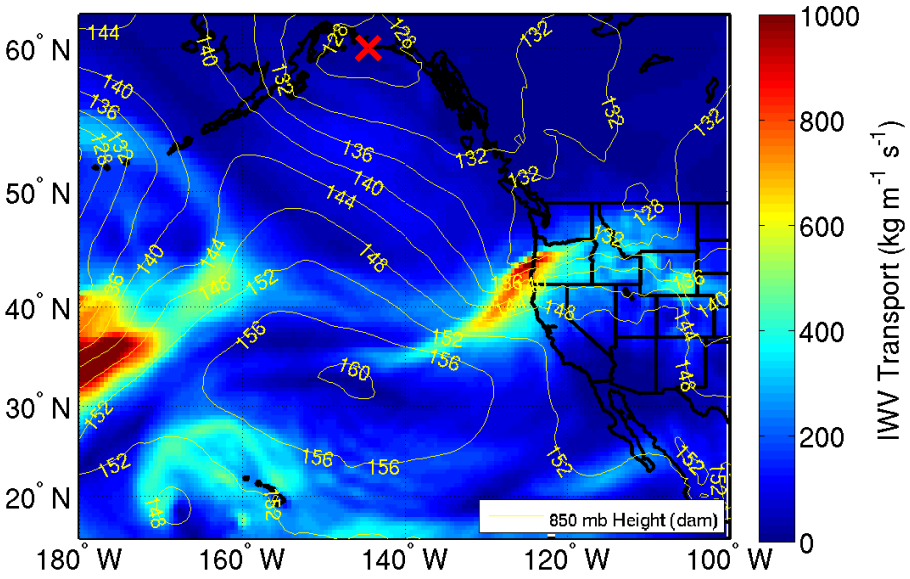

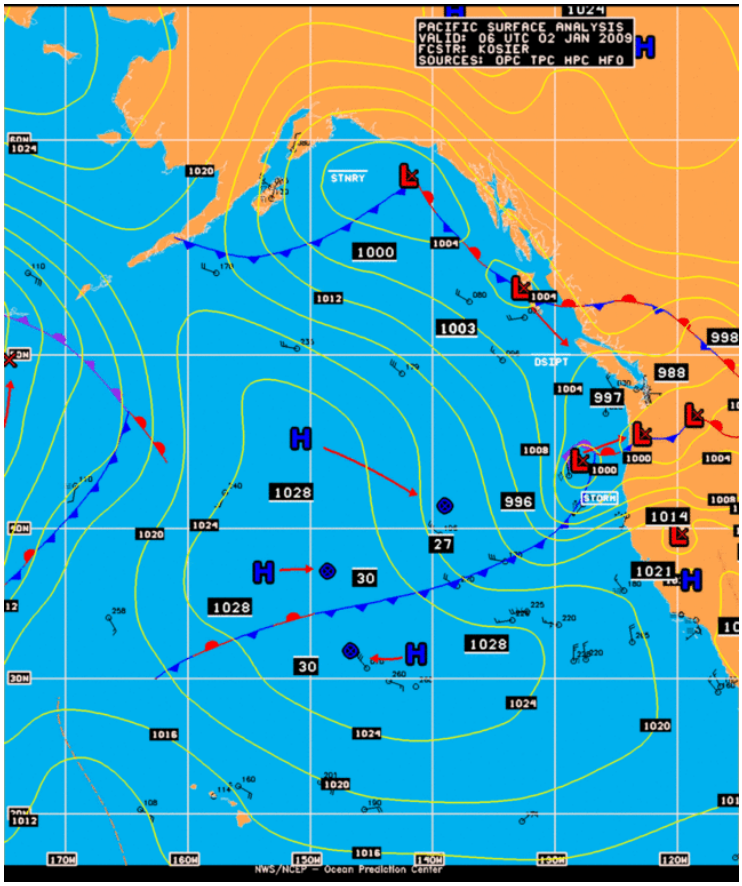

IVT & 850 mb Height
20070104-00

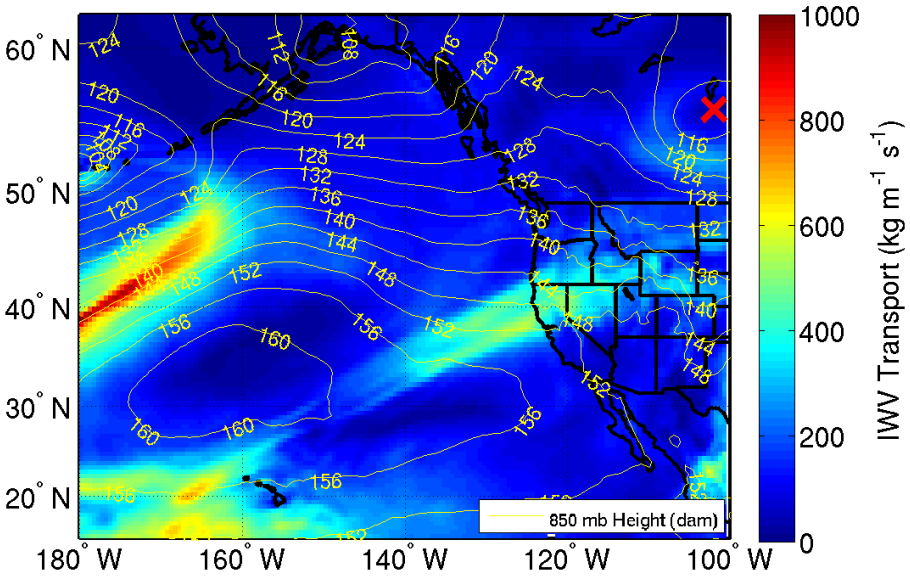

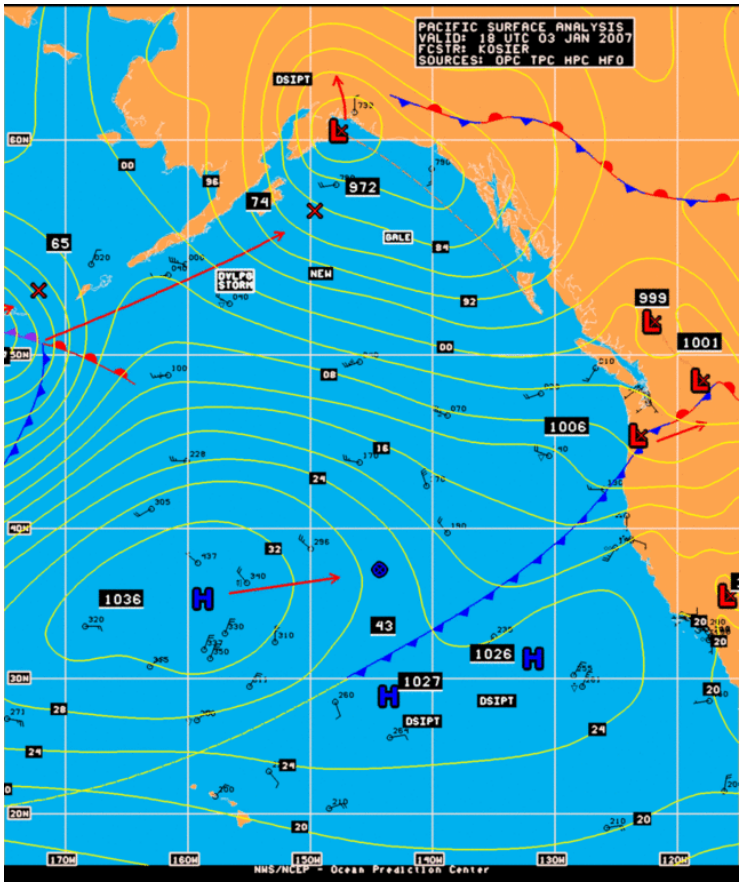

IVT & 850 mb Height
20061116-06

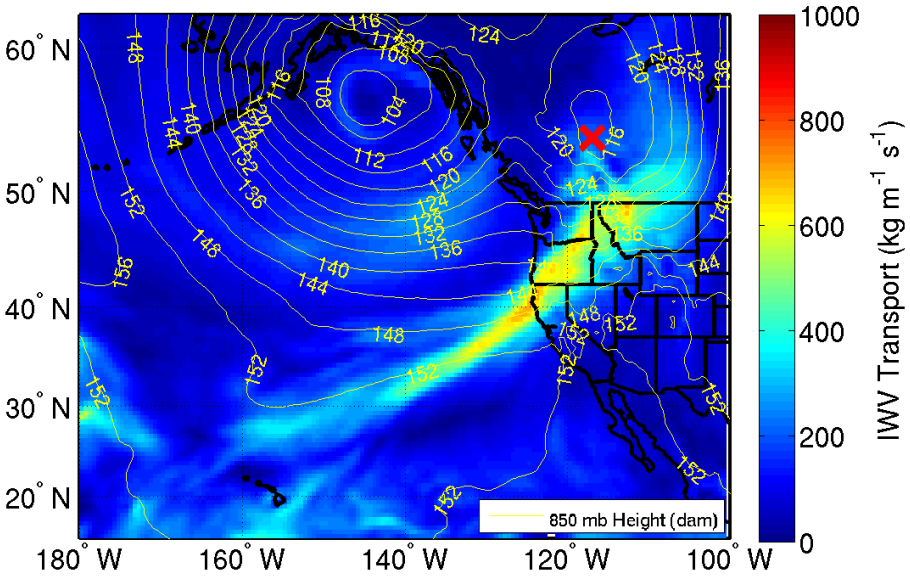

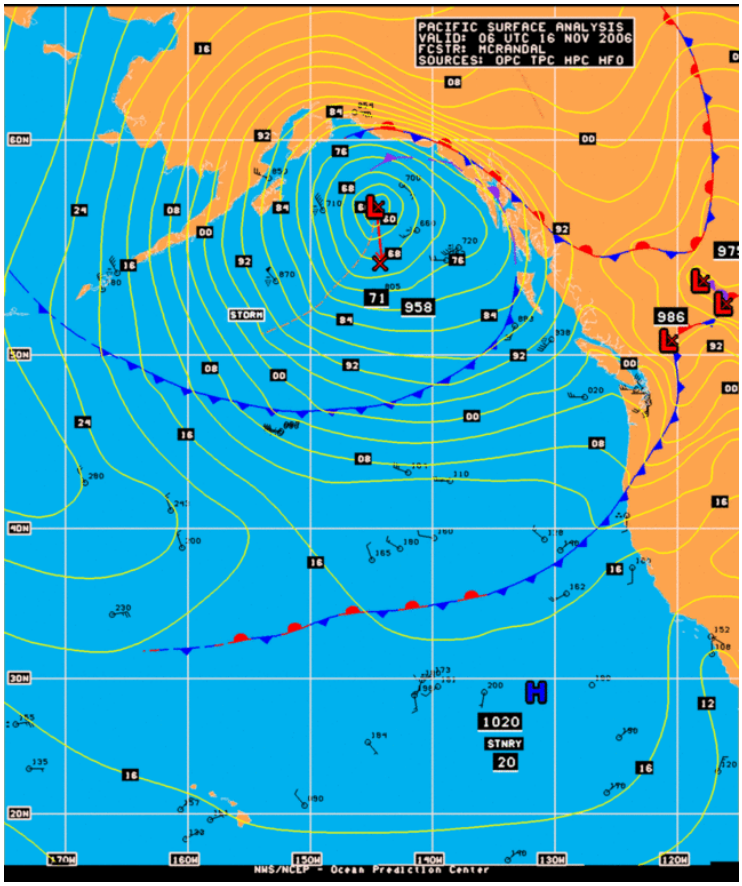

IVT & 850 mb Height
20050515-12

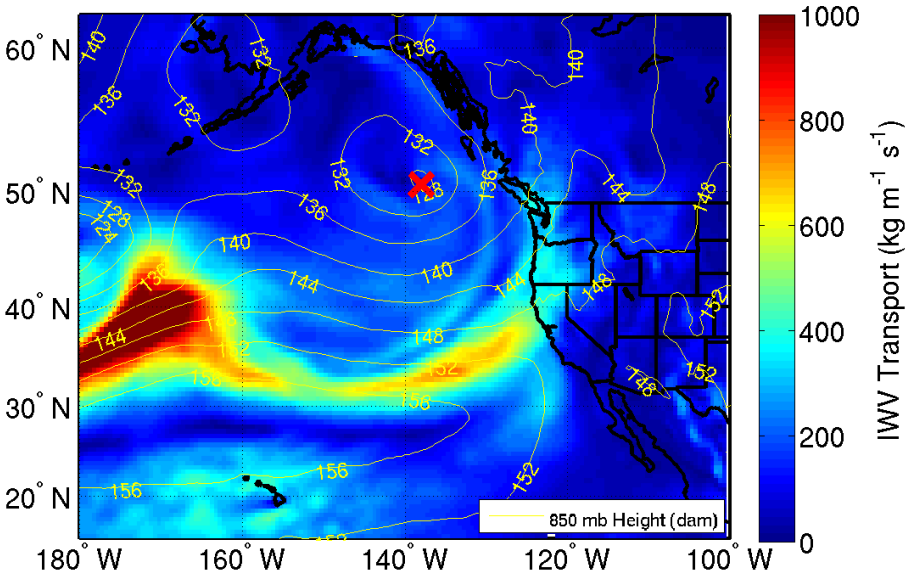

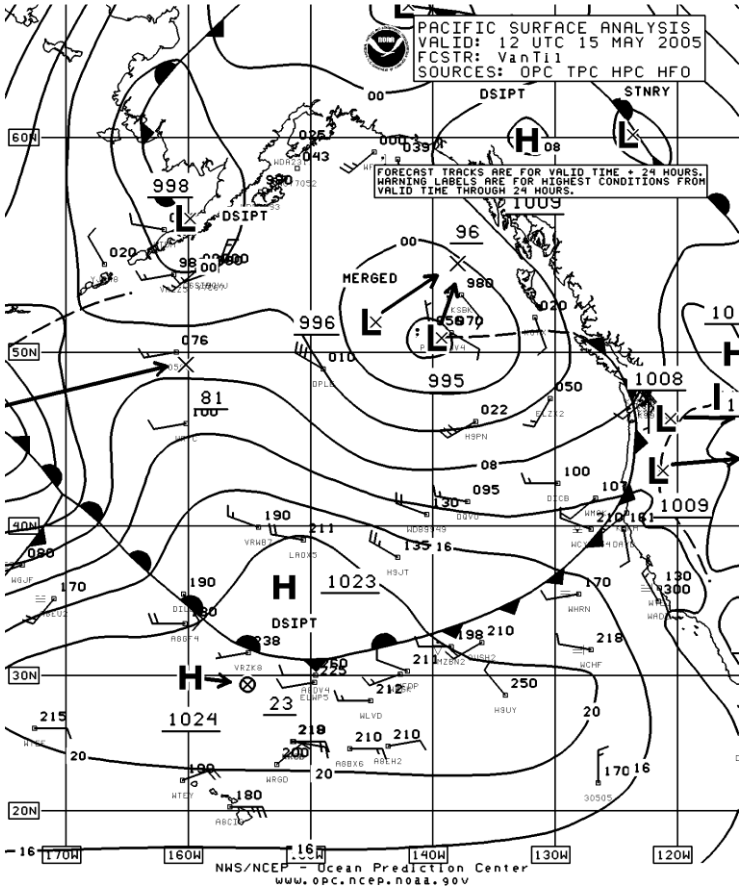

IVT & 850 mb Height
20061108-06

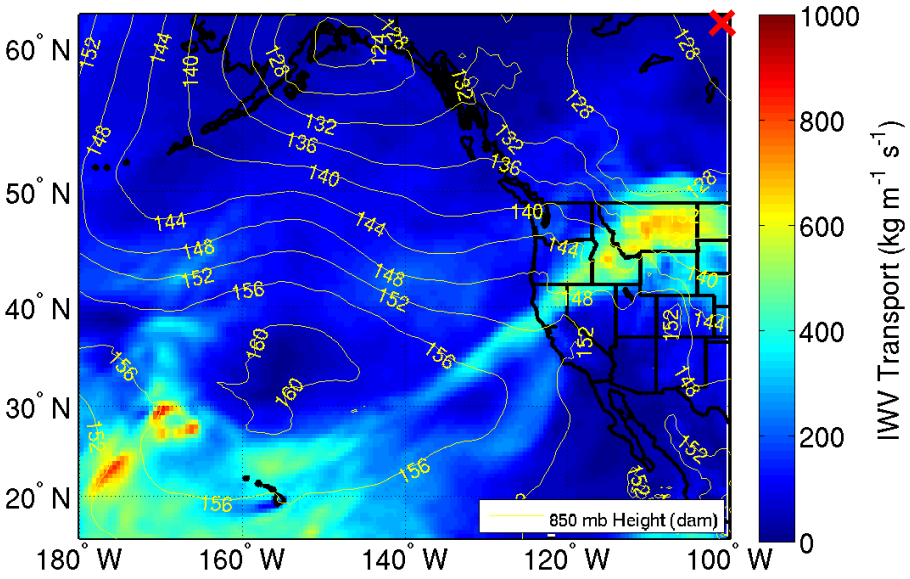

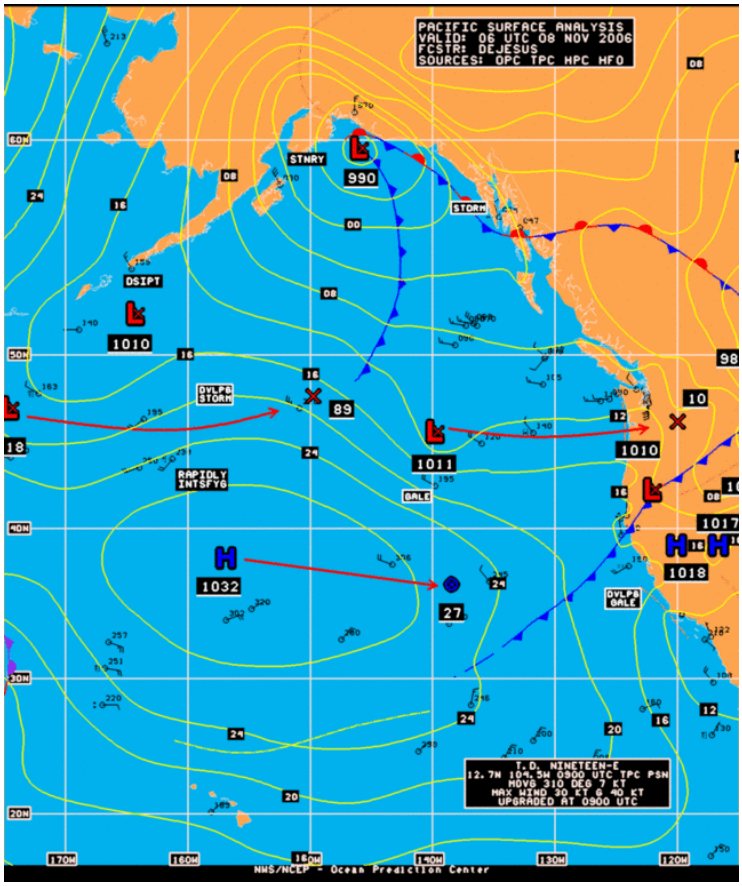

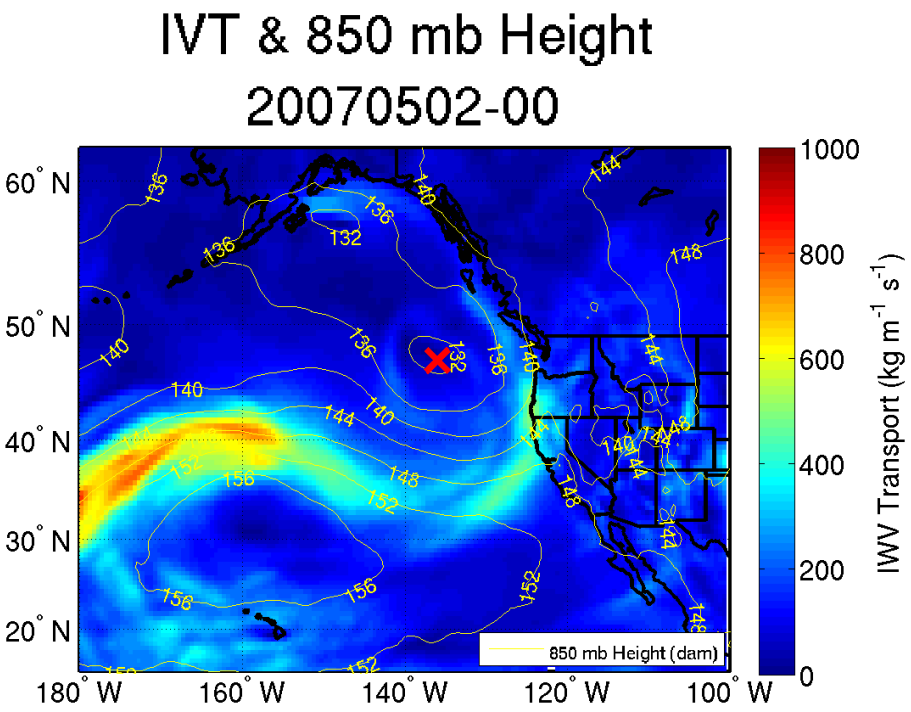
IVT & 850 mb Height
20070502-00
60° N
50° N
40° N
30° N
20° N
180° W
160° W
140° W
120° W
100° W
850 mb Height (dam)
IWV Transport (kg m-1 s-1)
1000
800
600
400
200
0

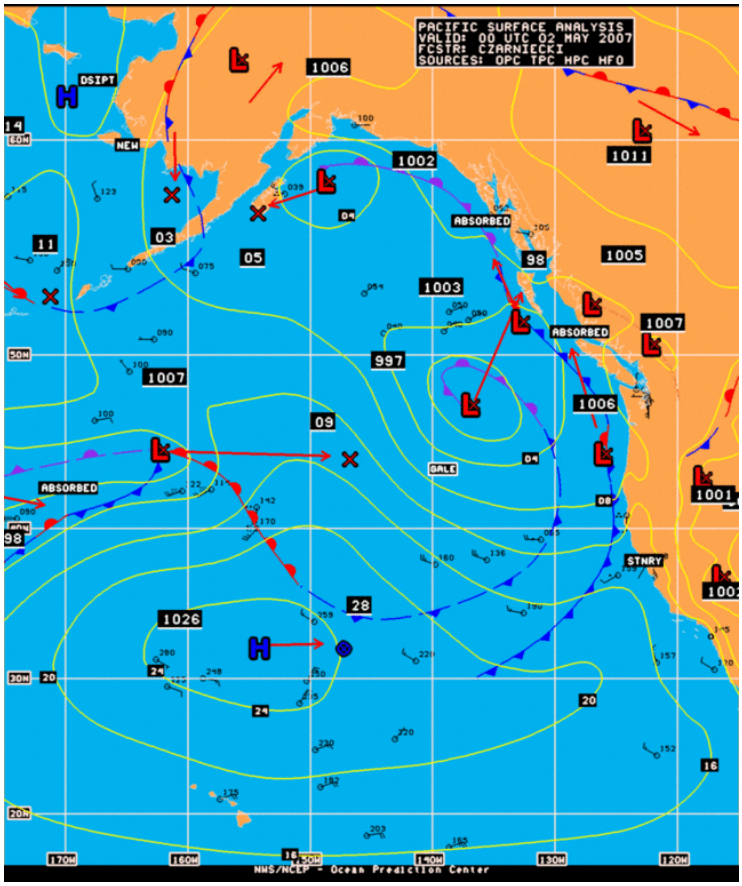
PACIFIC SURFACE ANALYSIS
VALID: 00 UTC 02 MAY 2007
FCSTR: CZARNIECKI
SOURCES: OPC TPC HPC HFO
1006
1002
1011
1005
1003
997
1007
1026
ABSORBED
STNRY
NWS/NCEP - Ocean Prediction Center

Synoptic analyses for atmospheric river events that do not have wind information at Bodega Bay are on the following slides.

IVT & 850 mb Height
20050608-06

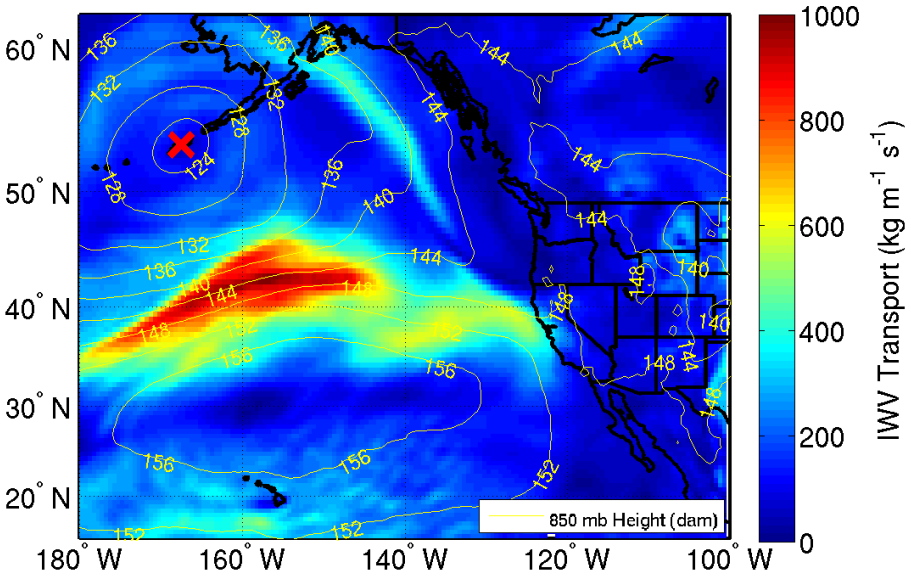

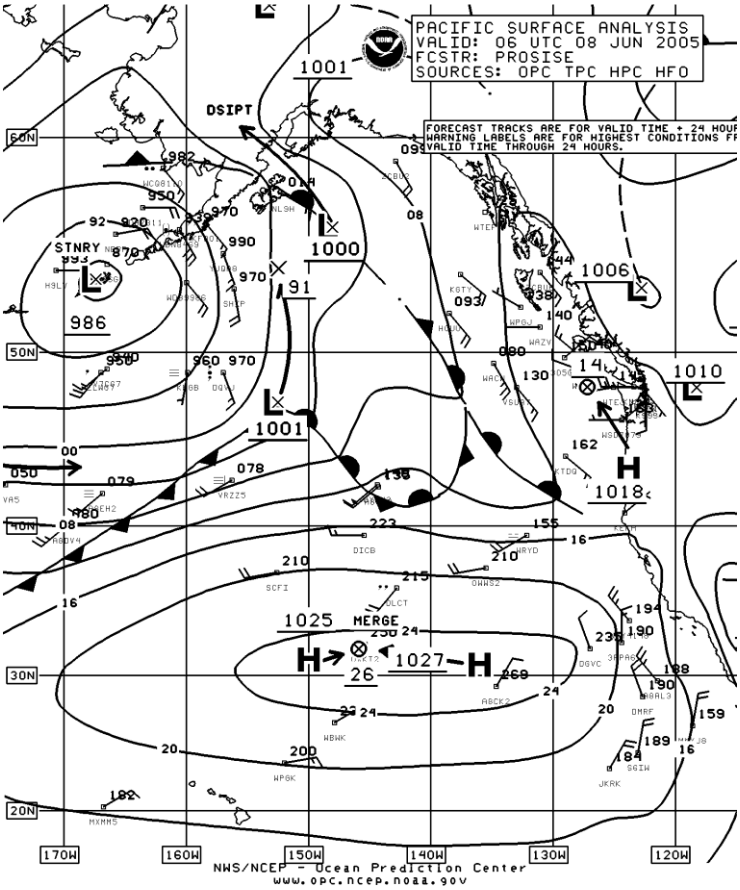

IVT & 850 mb Height
20050617-18

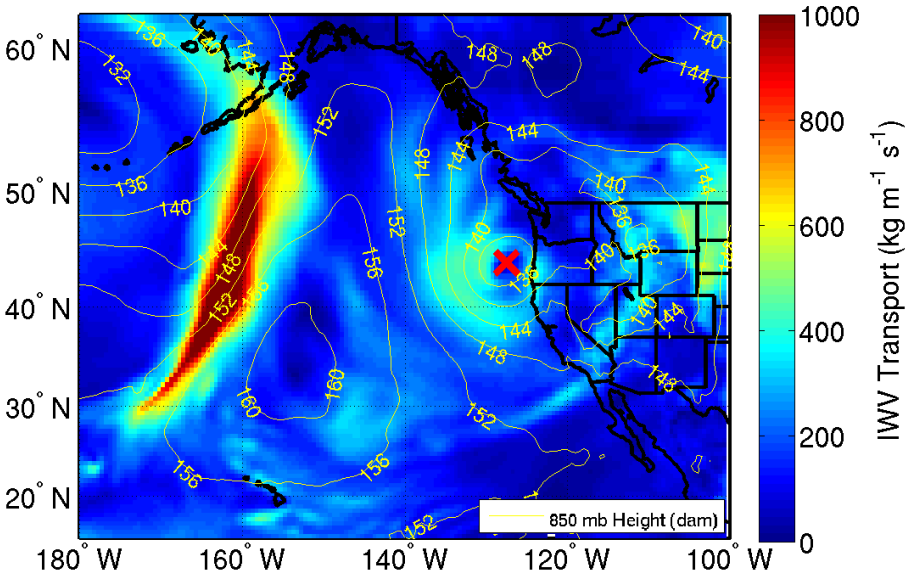

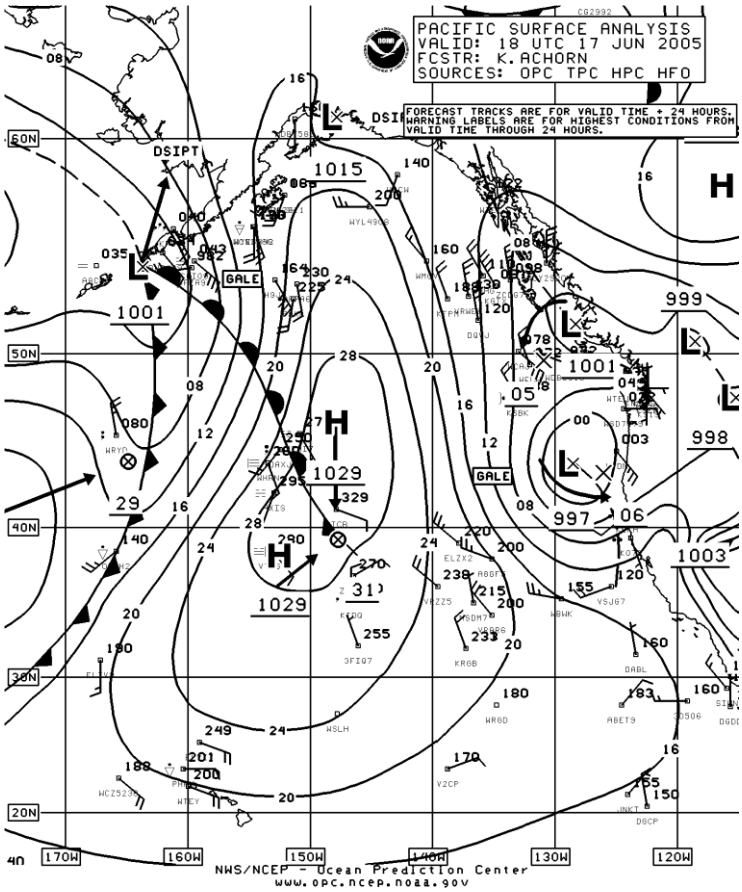

IVT & 850 mb Height
20070718-00

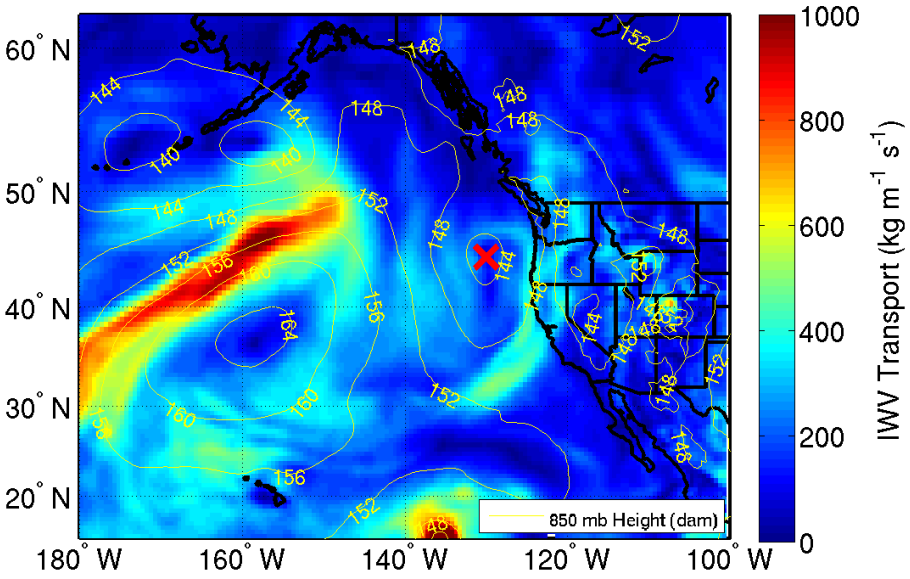

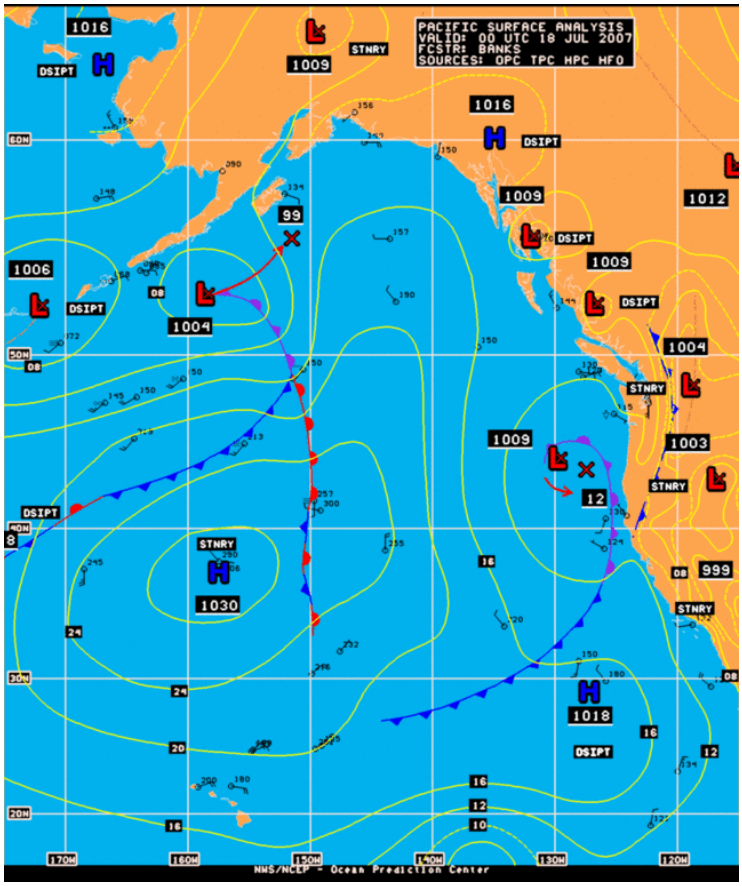

IVT & 850 mb Height
20070922-06